Probabilistic assessment of inner slope stability in dikes

Gaining insight in the difference between the semi-probabilistic and probabilistic estimates of the reliability index for inner slope stability with overtopping

Author: Casper Broman

WSP TU Delft Deltares

Probabilistic assessment of inner slope stability in dikes

Gaining insight in the difference between the semi-probabilistic and probabilistic estimates of the reliability index for inner slope stability with overtopping

By

Casper Broman

in partial fulfilment of the requirements for the degree of

Master of Science
in Civil Engineering, track Hydraulic Engineering

at the Delft University of Technology,
to be defended publicly on October 27, 2023

Student number:	5414008	
Thesis committee:	Prof. dr. ir. Matthijs Kok (chairperson)	TU Delft
	Dr. ir. Cong Mai Van	TU Delft
	Dr. ir. Mandy Korff	TU Delft
	Ir. André Broere	WSP Nederland B.V.
	Dr. ir. Mark van der Krogt	Deltares

Delft, October 2023

An electronic version of this thesis is available at http://repository.tudelft.nl/
Back cover image by WSP Nederland B.V.

Preface

The MSc thesis that you are currently reading 'Probabilistic assessment of inner slope stability in dikes' has been written as the final part of the track Hydraulic Engineering of the master Civil Engineering at the Civil Engineering and Geosciences faculty at Delft University of Technology. This research has been conducted in cooperation with WSP Nederland B.V., Deltares and TU Delft.

First of all, I would like to express my sincere appreciation to ir. André Broere of WSP Nederland B.V. and dr. ir. Mark van der Krogt of Deltares for being my company supervisors. I was always able to ask my questions to them, ask for feedback and they were always willing to help me when I was struggling. I could not have written this MSc thesis without them.

Furthermore, a very special thanks to my supervisors from the TU Delft prof. dr. ir. Matthijs Kok, dr. ir. Cong Mai Van and dr. ir. Mandy Korff. The feedback that I received from them during the committee meetings was extremely valuable. Besides, I want to thank dr. ir. Cong Mai Van of TU Delft in particular for the meetings that we had and the feedback that I received in addition to the committee meetings.

Moreover, I would like to express my gratitude to my colleagues of WSP Nederland B.V. for their support and interest in my MSc thesis, water authority Hoogheemraadschap De Stichtse Rijnlanden for the possibility to use dike trajectory Jaarsveld-Vreeswijk as case study and Deltares for providing me the profiles of the WBI calibration study and the tools for the probabilistic calculations. Finally, I would like to thank the readers of my MSc thesis for their time and interest in my research.

Casper Broman

Delft, October 2023

Abstract

After overtopping, the most common failure mechanism in the world that leads to a dike breach is the instability of the inner slope (Jonkman, Jorissen, Schweckendiek, & Van den Bos, 2021). Two stability calculations are required for the semi-probabilistic assessment of inner slope stability. One calculation is without significant overtopping and the other calculation is with significant overtopping whereby the dike is saturated. The semi-probabilistic assessment method with overtopping prescribed in the KPR factsheet 'Werkwijze macrostabiliteit i.c.m. golfoverslag' is not verified by calibration calculations or probabilistic calculations (Rijneveld, 2020). After performing semi-probabilistic and probabilistic calculations at Jaarsveld-Vreeswijk (JAV) in the Netherlands, there is an inconsistency between the estimates of the reliability index for inner slope stability with overtopping. Not only did this inconsistency arise for JAV, but also at the project Neder Betuwe of Waterschap Rivierenland (Rijneveld, 2020). If the semi-probabilistic estimates of the reliability index are too optimistic, then it can be concluded that inner slope stability is not a problem at a dike section, while it might actually be a problem.

The main objective of this MSc thesis is to gain insight in the difference between the semi-probabilistic and probabilistic estimates of the reliability index for inner slope stability with overtopping. The following research question is formulated: 'How can the inconsistency be reduced between the semi-probabilistic and probabilistic estimates of the reliability index for inner slope stability with overtopping?'.

A consistent comparison has been made between the semi-probabilistic and probabilistic estimates of the reliability index to know to what extent there is an inconsistency. There is quite a large difference between the semi-probabilistic and probabilistic estimates of the reliability index for inner slope stability for the six considered dike sections of JAV. The sample standard deviation of the results of JAV without overtopping is a factor two larger than the sample standard deviation of WBI used for the calibration line (the calibration line shows a relation between the semi-probabilistic and probabilistic results based on the WBI calibration study), due to the larger differences between the estimates of the reliability index of JAV than for the results of WBI used for the calibration line. The sample standard deviation increases by including the effects of overtopping for JAV.

It is investigated whether using additional stochastic variables instead of conservative deterministic variables influences the estimate of the failure probability based on probabilistic calculations to make sure that the inconsistency between the results of JAV is not caused by an inadequate schematization of the situation. Modelling the cohesion and the internal friction angle of the clay cover stochastic in the probabilistic calculations have an effect on the estimates of the reliability index when one is dealing with relatively small slip planes. Taking into account the uncertainty in the pore water pressure distribution through the dike with overtopping influence the estimates of the reliability index given overtopping for dike sections with both relatively small and large slip planes. However, there is still an inconsistency between the semi-probabilistic and probabilistic estimates of the reliability index after modelling the strength of the clay cover stochastic and taking into account the uncertainty of the pore water pressure distribution with overtopping.

The influence of the steepness of the inner slope on the difference between the semi-probabilistic and probabilistic estimates of the reliability index for inner slope stability has been investigated to find out whether there is a certain steepness from which the current instructions described in the

KPR factsheet are not applicable anymore. The semi-probabilistic estimates of the reliability index are too optimistic for inner slope stability given overtopping with an inner slope steepness of 1:3, while they are too conservative with an inner slope steepness of 1:5 for JAV. Therefore, the inner slope steepness has a larger influence on the estimate of the reliability index of the probabilistic calculations than the semi-probabilistic calculations for the six considered dike sections of JAV.

It is investigated to what extent the calibrated WBI damage factor line of 2016 is applicable for inner slope stability. The effects of overtopping were not considered in the calibration study of inner slope stability (Kanning, Teixeira, Van der Krogt, & Rippi, 2017). The semi-probabilistic estimates of the reliability index for inner slope stability without overtopping are all too conservative for JAV when the coefficients of variation of the variables with a large influence factor are relatively low, while this is not the case after increasing the coefficients of variation. For this reason, the applicability of the WBI calibration line of 2016 is dependent on the used coefficients of variation in the calculations of inner slope stability without overtopping. On the other hand, the WBI calibration line of 2016 is not suitable to estimate the failure probability for inner slope stability given overtopping based on the semi-probabilistic calculations, while the used coefficients of variation of the variables with a large influence factor in the calculations of inner slope stability with overtopping are reasonable.

The answer to the research question is that the inconsistency between the semi-probabilistic and probabilistic estimates of the reliability index can be reduced by using a different calibration line for inner slope stability given overtopping than for inner slope stability without overtopping. The current WBI calibration line can be used for the assessment of inner slope stability without overtopping dependent on the used coefficients of variation for the variables with a relatively large influence factor, while a calibration study is necessary to obtain a suitable calibration line for inner slope stability given overtopping.

It is possible that a dike section could not meet the required failure probability for a cross-section for inner slope stability given overtopping even if the crest level is higher than the HBN for the failure mechanism GEKB. The reason for this is that the required failure probability for a cross-section for the failure mechanism GEKB is larger than the required failure probability for a cross-section for inner slope stability. It is recommended to assess whether a dike section meets the required failure probability for inner slope stability given overtopping always, even if the crest level is higher than the HBN for the failure mechanism GEKB. Besides, it is advised to model the strength of the clay cover stochastic in the probabilistic assessment when one is dealing with relatively small slip planes and it is advised to do more research to the pore water pressure distribution with overtopping by doing tests in practice.

Most importantly, it is recommended to perform a calibration study for inner slope stability given overtopping to obtain a better estimate of the failure probability based on semi-probabilistic calculations. It is important that the calibration study for inner slope stability given overtopping is representative for the Netherlands by using cases at different locations with different conditions. After performing the calibration study for inner slope stability given overtopping, it is advised to use the obtained relation between the semi-probabilistic and probabilistic results for the semi-probabilistic assessment of inner slope stability given overtopping. The current WBI calibration line of 2016 can still be used for inner slope stability without overtopping dependent on the used coefficients of variation in the calculations for the variables with a relatively large influence factor. For this reason, it is recommended to use a different calibration line for inner slope stability given overtopping, than for inner slope stability without overtopping.

Table of Contents

List of abbreviations

Abbreviation	Meaning
AHN3	Actueel Hoogtebestand Nederland versie 3 (English: Topical surface level in the Netherlands version 3)
CoV	Coefficient of variation
CSSM	Critical State Soil Mechanics
DP	Dike pole
GEKB	Gras Erosie Kruin en binnentalud (English: Grass Erosion Crest and inner slope)
HBN	Hydraulisch belastingniveau (crest level that will lead to a given overtopping discharge with a given probability for a cross-section)
HDSR	Hoogheemraadschap De Stichtse Rijnlanden
JAV	Jaarsveld-Vreeswijk
KPR	Kennisplatform Risicobenadering (English: Knowledge platform risk approach)
MSc	Master of Science
n/a	Not applicable
OCR	Over consolidation ratio
POP	Pre overburden pressure
SAFE	Streefkerk-Ameide-Fort Everdingen
SHANSEP	Stress History And Normalized Soil Engineering Properties
TRGS	Technisch Rapport Grondmechanisch Schematiseren bij Dijken (English: Technical report soil mechanical schematization at dikes)
TRWD	Technisch Rapport Waterspanningen bij Dijken (English: Technical report pore water pressures at dikes)
TRWG	Technisch Rapport Waterkerende Grondconstructies (English: Technical report water retaining soil structures)
VNK	Veiligheid Nederland in Kaart (English: Flood risk in the Netherlands)
WBI 2017	Wettelijk Beoordelingsinstrumentarium 2017 (English: Legal assessment tools 2017)
WBN	Waterstand bij norm (English: Water level at the norm)

1. Introduction

A large part of the Netherlands is located below sea level and large rivers find their way to the sea through the Netherlands. Approximately 60% of the Netherlands is susceptible to flooding. The Netherlands has approximately 3500 km of primary flood defenses to prevent flooding. Floods have often taken place in the Netherlands in the past. Since the storm surge in 1953, the requirements of the flood defenses have become stricter. The current statutory instruments are risk-based (risk is a combination between probability and consequences). These days, the flood defenses are assessed with the statutory instruments of 2017. The strictest standards hold for the areas where the consequences of flooding are the largest (Vergouwe, 2014).

Failure of a flood defense can occur based on different failure mechanisms. The failure probabilities of the main failure mechanisms have been calculated in the project VNK. One of the main failure mechanisms is shearing of the inner slope (Vergouwe, 2014).

The maximum allowed failure probability is related to the probability of a flooding that has substantial consequences. It is related to the exceedance of the ultimate limit state (the event at which flooding occurs) and not to an event where instability occurs. For this reason, a relatively large overtopping discharge (larger than 5 or 10 l/s/m) is allowed with regard to failure due to erosion of the inner slope. There were questions about the consequences of this on the assessment of macro stability of the inner slope. The current instructions for the schematization of macro stability are developed for situations without overtopping. They are only valid for situations with a maximum overtopping discharge of approximately 0.1 to 1 l/s/m (De Visser & Jongejan, 2018). A larger overtopping discharge leads to more infiltration. This leads to saturation of the dike body and a reduced stability.

A method has been presented in a factsheet by KPR ‘Werkwijze macrostabiliteit i.c.m. golfoverslag’ to deal with the interaction between macro stability and overtopping for the assessment and the design of primary flood defenses (De Visser & Jongejan, 2018). There are no calibration calculations or probabilistic verification calculations performed for the semi-probabilistic assessment described in the KPR factsheet (Rijneveld, 2020).

1.1 Problem description

After performing the semi-probabilistic assessment of inner slope stability, it turned out that sections of dike trajectory Jaarsveld-Vreeswijk (JAV) do not meet the required failure probability. WSP Nederland B.V expected that the number of dike sections that did not meet the required failure probability could have been reduced by performing probabilistic calculations. For this reason, six dike sections were assessed probabilistic for inner slope stability. These dike sections meet the required failure probability after the semi-probabilistic assessment of inner slope stability with overtopping, but they do not meet the required failure probability based on the semi-probabilistic assessment of inner slope stability without overtopping. Deltares has supported WSP Nederland B.V with performing the probabilistic calculations and performed a verification of the results (Broere, 2022).

Normally, the semi-probabilistic assessment is conservative in eighty percent of the cases (Kanning, Teixeira, Van der Krogt, & Rippi, 2017). Therefore, the number of dike section that do not meet the required failure probability based on the semi-probabilistic assessment is expected to be reduced based on the probabilistic assessment.

After performing the probabilistic calculations, it turned out that the reliability indexes of two dike sections for inner slope stability with overtopping are extremely low (i.e., the failure probabilities are extremely high). Given that these dike sections meet the safety requirements for inner slope stability with overtopping after the semi-probabilistic assessment, it is unexpected that their reliability indexes from the probabilistic assessment are extremely low for inner slope stability with overtopping. For this reason, there is an inconsistency between the semi-probabilistic and the probabilistic estimates of the reliability index for inner slope stability with overtopping. Not only did this inconsistency arise for JAV, but also at the project Neder Betuwe of Waterschap Rivierenland (Rijneveld, 2020).

1.2 Objectives

The main objective of this MSc thesis is to gain insight in the inconsistency between the semi-probabilistic and probabilistic estimates of the reliability index for inner slope stability with overtopping. It is an objective to investigate what causes the inconsistency between the semi-probabilistic and probabilistic estimates of the reliability index for JAV. Furthermore, it is an objective to gain insight in the influence of the schematization of the dike profile on the inconsistency. An objective is to give recommendations about how the inconsistency could be reduced based on the obtained insights in this MSc thesis.

1.3 Research question and sub-questions

This MSc thesis addresses the following research question:

How can the inconsistency be reduced between the semi-probabilistic and probabilistic estimates of the reliability index for inner slope stability with overtopping?

A few sub-questions were composed to answer the research question. The following sub-questions are answered in this MSc thesis.

1. What is the difference between the semi-probabilistic and probabilistic estimates of the reliability index of inner slope stability for the six dike sections that are calculated probabilistic of JAV?
2. How incorporate additional stochastic variables in the probabilistic calculations to get a more precise estimate of the failure probability of inner slope stability?
3. What is the influence of the dike slope steepness on the difference between the semi-probabilistic and probabilistic estimates of the reliability index of inner slope stability?
4. To what extent is the calibrated WBI damage factor line of 2016 applicable for inner slope stability?

The objective behind sub-question one is to make a consistent comparison between the results of the semi-probabilistic and probabilistic calculations. An objective of this sub-question is to make clear what the inconsistency is using the current instructions and how large this inconsistency is between the semi-probabilistic and probabilistic estimates of the reliability index.

The objective of sub-question two is to investigate whether using stochastic variables instead of conservative deterministic variables influences the estimate of the failure probability based on probabilistic calculations. The hypothesis behind this sub-question is that using stochastic variables instead of conservative deterministic variables in the probabilistic calculations reduces the inconsistency. An objective is to make sure that the inconsistency between the semi-

probabilistic and probabilistic estimates of the reliability index is not caused by an inadequate schematization of the situation.

The hypothesis behind sub-question three is that the inconsistency between the semi-probabilistic and probabilistic estimates of the reliability index increases if the steepness of the inner slope increases. The objective of this sub-question is to investigate whether there is a certain steepness from which the current instructions are not applicable anymore.

The hypothesis behind sub-question four is that the calibrated WBI damage factor line of 2016 is not fully applicable for inner slope stability with overtopping. According to the report 'Derivation of the semi-probabilistic safety assessment rule for inner slope stability' are the effects of overtopping not considered in the calibration study (Kanning, Teixeira, Van der Krogt, & Rippi, 2017). The objective of this sub-question is to investigate under which conditions the calibrated WBI damage factor line of 2016 is applicable for inner slope stability.

1.4 Thesis outline

A review of the available information in literature is given in chapter two. The methodology to answer the sub-questions is discussed in chapter three. Chapter four contains the results of the sub-questions. Each paragraph in chapter three and four deals with one of the sub-questions. Paragraphs 3.1 and 4.1 deal with sub-question one, paragraphs 3.2 and 4.2 deal with sub-question two etc. Chapter five includes the discussions of the results. Finally, the conclusions and recommendations are given in chapter six.

2. Literature review

In this chapter is a review given of the available relevant information in literature. Relevant information about the case study is given in paragraph 2.1. In paragraph 2.2 are the relevant failure mechanisms explained. Probabilistic concepts are explained in paragraph 2.3. The assessment of inner slope stability is described in paragraph 2.4. Finally, some important input variables for the analysis of inner slope stability are described in paragraph 2.5.

2.1 Jaarsveld-Vreeswijk (JAV)

Jaarsveld-Vreeswijk (JAV) is a part of dike trajectory 15-1. JAV has a total length of 12.6 km and is located along the Lek river (see Figure 1). Besides, JAV is a part of the program 'Sterke Lekdijk' and water authority Hoogheemraadschap De Stichtse Rijnlanden (HDSR) is responsible for it (Barendsen, Bartels, Kriebel, Broere, & Perez Gomez, 2021). JAV is located in the province Utrecht in the Netherlands.

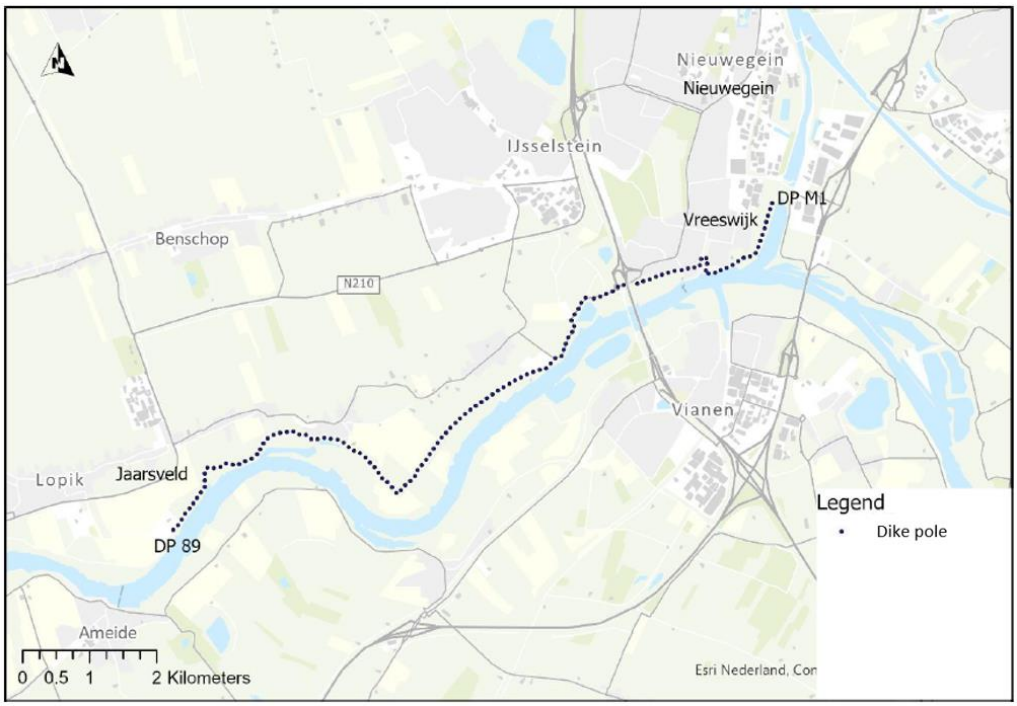

Figure 1: Overview dike trajectory Jaarsveld-Vreeswijk (JAV) (Broere, 2022)

The norm of dike trajectory 15-1 is equal to 1/30000 per year and the signal level is equal to 1/10000 per year (Waterwet, 2021). The total damage in case of flooding of dike trajectory 15-1 is approximately 90000 million euro in 2050 (Slootjes & Wagenaar, 2016).

Dike trajectory 15-1 has a length of 23.0 km. The required failure probability to determine the minimum necessary crest level is 1/41667 per year and the required reliability index for macro stability is 5.03 (Rijkswaterstaat Water, Verkeer en Leefomgeving, 2017). For the schematization factor of macro stability is a value of 1.1 assumed. The required reliability index for the probabilistic assessment of macro stability becomes 5.81 (i.e., a required failure probability of 3.23E-09 per year) after including the schematization factor of 1.1 (Broere, 2022).

2.2 Failure mechanisms

The failure mechanisms that are relevant for this research are discussed in this paragraph. First, macro stability is discussed. After this, overtopping and inner slope stability with overtopping are discussed.

2.2.1 Macro stability

After overtopping, the most common failure mechanism in the world that leads to a dike breach is the instability of the inner slope. Due to infiltration of water into the dike, the pore water pressures increase. Therefore, the effective stresses and the resistance of the soil to shear decreases. This can lead to a failure of the inner slope during floods (Jonkman, Jorissen, Schweckendiek, & Van den Bos, 2021). A sketch showing instability of the inner slope is given in Figure 2.

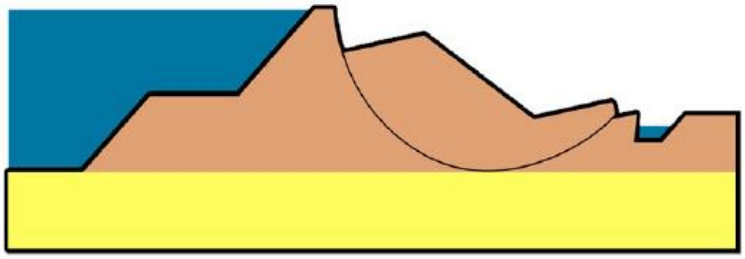

Figure 2: Schematic representation of instability of the inner slope (Jonkman, Jorissen, Schweckendiek, & Van den Bos, 2021)

Besides, a dike can also fail due to instability of the outer slope. If a dike is saturated during high water levels and is able to withstand this load, then a sudden drawdown of the water level could lead to instability of the outer slope. In case of instability of the outer slope, the pore water pressures at the base of the slide plane are still high, while the horizontal pressure from the river is reduced due to the sudden drawdown of the water level (Jonkman, Jorissen, Schweckendiek, & Van den Bos, 2021).

2.2.2 Overtopping

Waves can run-up the outer slope when they approach a dike. The run-up level is the highest point that is reached by the waves. When the crest of the dike is lower than the run-up level, then the waves will result in a flow over the dike onto the inner slope. The difference between overtopping and overflow is that with overflow the crest level is below the design water level, while with overtopping the crest level is between the design water level and the run-up level. Due to overtopping, erosion of the inner slope could occur. This can lead to progressive damage and to dike failure in the end. The overtopping rate is the volume of water that passes the crest of the dike during a certain time interval divided by the duration of the interval that water passes the crest (Jonkman, Jorissen, Schweckendiek, & Van den Bos, 2021).

2.2.3 Inner slope stability with overtopping

The current instructions for the schematization of macro stability are developed for situations without overtopping. For this reason, the instructions are only valid for situations with a maximum overtopping discharge of approximately 0.1 to 1 l/s/m (De Visser & Jongejan, 2018).

A dike could fail when there is erosion that keeps going on, as a consequence of a small slip circle and infiltration through overtopping. It is important to take this into account in the safety assessment of macro stability or the safety assessment of erosion of the crest or the inner slope of the dike. The KPR memo ‘Voorstel t.a.v. beoordeling macrostabiliteit incl. golfoverslag’ advises to take the failure of the dike through a combination of overtopping and inner slope stability into account in the

assessment of inner slope stability (Jongejan & De Visser, 2017). A schematic representation of inner slope stability with overtopping is given in Figure 3.

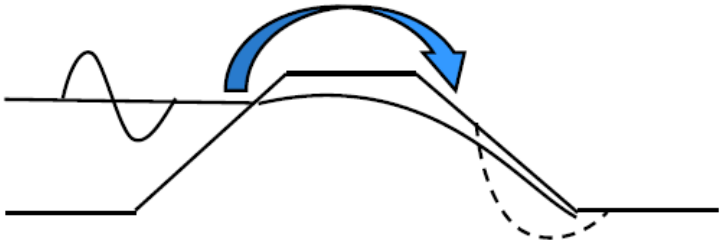

Figure 3: Schematic representation of inner slope stability with overtopping (De Visser & Jongejan, 2018)

2.3 Reliability analysis

Some basic concepts about probability theory are explained in this paragraph. In this paragraph are also the fragility curves, influence coefficients, the lognormal distribution and the sample standard deviation explained.

2.3.1 Basic concepts

In general, the failure probability is the probability that the load S is larger than the strength R. The limit state Z is the difference between the strength and the load, see the formula below (Schweckendiek, Van der Krogt, Rijneveld, & Teixeira, 2017).

$$Z = R - S$$

The failure probability is the probability that $Z < 0$, so when $R < S$ (see the equation below).

$$P_f = P(Z < 0) = P(R < S)$$

When the limit state function $Z(\underline{X})$ becomes smaller than zero, in which $\underline{X}$ represents the vector of all stochastic variables and $f_{\underline{X}}(\underline{x})$ their joint probability density function, then the equation for the failure probability becomes (Schweckendiek, Van der Krogt, Rijneveld, & Teixeira, 2017):

$$P\big(Z(\underline{X}) < 0\big) = \int_{Z(\underline{X})<0} f_{\underline{X}}(\underline{x}) d\underline{x}$$

The failure probability should be determined by the probability density of all stochastic variables in the failure domain (so where $Z(\underline{X}) < 0$). In other words, the failure probability should be determined by all parameter combinations that will lead to failure (Schweckendiek, Van der Krogt, Rijneveld, & Teixeira, 2017). An illustration of this is given in Figure 4.

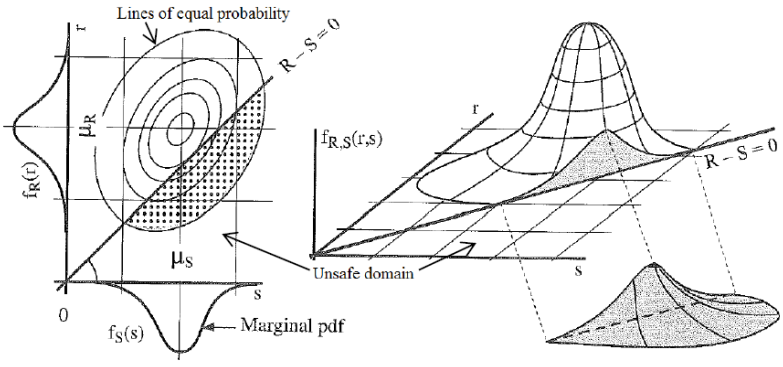

Figure 4: Illustration probability of failure (Jonkman, R.D.J.M., Morales-Nápoles, Vrouwenvelder, & Vrijling, 2017)

There are different methods to do a failure probability analysis. The methods given below are explained in more detail.

- Level 3 (exact)
- Level 2 (approximation)
- Level 1 (semi-probabilistic)

Level 3 (exact)

Exact calculation methods should be used to determine the failure probability in level three. The most common method within this level is performing a Monte Carlo simulation. A Monte Carlo simulation uses a large number of random values for the stochastic variables, based on their probability distribution. The failure probability can be determined based on the ratio between the number of simulations that resulted in a failure divided by the total number of simulations. The required number of calculations for a 95% reliable answer is four hundred divided by the failure probability. There are variants on the classic Monte Carlo simulation in order to reduce the number of calculations. An example of this is Importance Sampling (Schweckendiek, Van der Krogt, Rijneveld, & Teixeira, 2017).

The aim of Importance Sampling is to increase the number of realizations N of a random vector $\underline{X}$ that can be considered as a failure. A sampling function is chosen in such a way that its maximum is positioned on a place where it contributes most to the failure probability. When one locates the sampling function at the design point (this is the point on the line where $Z = 0$ ($g(\underline{x}) < 0$) with the largest probability of occurrence), then the failure probability should be approximately 50%. By using the ratio between the real joint probability density function $f_{\underline{X}}(\underline{x})$ and the sampling distribution function $f_S(\underline{x})$ for each sample pair, the failure probability P_f can be calculated with the formula below (Jonkman, R.D.J.M., Morales-Nápoles, Vrouwenvelder, & Vrijling, 2017).

$$P_f = \frac{1}{N}\sum_{j=1}^{N} I\left[g(\underline{x}) < 0\right]\frac{f_{\underline{X}}(\underline{x})}{f_S(\underline{x})}$$

An illustration of the Importance Sampling technique is given in Figure 5.

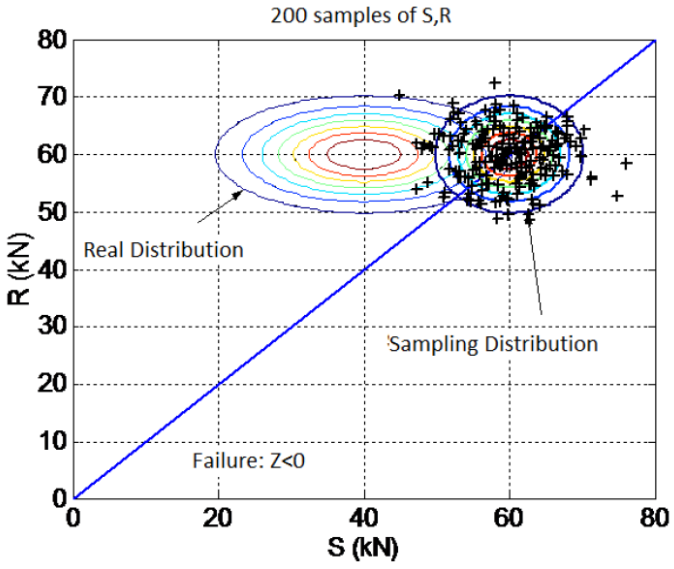

Figure 5: Example Importance Sampling (Jonkman, R.D.J.M., Morales-Nápoles, Vrouwenvelder, & Vrijling, 2017)

Level 2 (approximation)

Level two methods involve techniques that include an approximation. The most common level two method is the First-Order Reliability Method (FORM). The design point is determined in an iterative manner by FORM. FORM is exact when one is dealing with limit state functions with linear combinations of normal distributed variables. However, the limit state function is not linear and contains not normal distributed variables for most failure mechanisms. Nevertheless, FORM is usually sufficient accurate for failure mechanisms such as macro stability. An advantage of FORM is that less calculations are required and that the number of calculations is in principle not strongly dependent on the number of stochastic variables. Disadvantages are that convergence problems may arise, and that FORM might find local instead of global minima (Schweckendiek, Van der Krogt, Rijneveld, & Teixeira, 2017).

Level 1 (semi-probabilistic)

The results of level one analyses are not explicitly failure probability estimates, but they are related to the failure probability. For this reason, level one analyses are referred to as semi-probabilistic. Whether a construction or failure mechanism meets the required failure probability based on design values can be determined by the semi-probabilistic assessment. The semi-probabilistic assessment can be written in the form shown below (Schweckendiek, Van der Krogt, Rijneveld, & Teixeira, 2017).

$$\frac{R_d}{S_d} > requirement$$

The requirement is generally a damage factor, R_d is a design value for the strength and S_d is a design value for the load. The design values for the strength and the load are generally determined by their characteristic value and partial factor, see the formulas below (Schweckendiek, Van der Krogt, Rijneveld, & Teixeira, 2017).

$R_d = R_k/\gamma_R$ and $S_d = S_k \cdot \gamma_S$

The 5% quantile is often used for the characteristic values of the strength parameters for the Dutch flood defenses. The design values of the load parameters are often determined directly for a specific probability of exceedance without using a partial factor (Schweckendiek, Van der Krogt, Rijneveld, & Teixeira, 2017). An illustration of a design value for a strength and a resistance parameter is given in Figure 6.

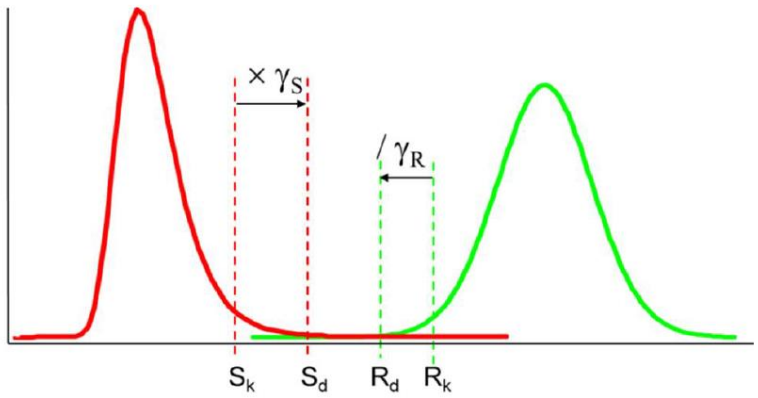

Figure 6: Illustration of design values (Schweckendiek, Van der Krogt, Rijneveld, & Teixeira, 2017)

2.3.2 Fragility curves

A fragility curve illustrates the (conditional) failure probability as a function of the load. Generally, the water level h is used as the load for inner slope stability. The reliability index can also be used as an alternative for the failure probability on the vertical axis. Only a few points of the fragility curve (fragility points) are determined for inner slope stability. Linear interpolation is used between the fragility points (Schweckendiek, Van der Krogt, Rijneveld, & Teixeira, 2017). A schematization of a fragility curve is given in Figure 7.

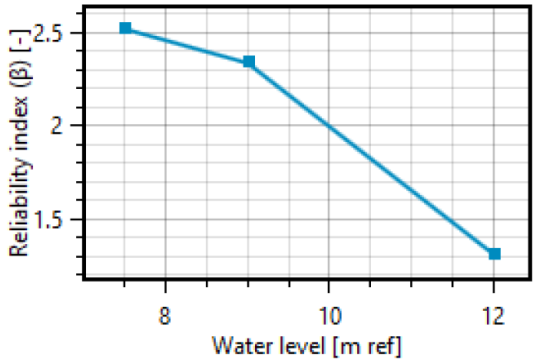

Figure 7: Fragility curve (Deltares, 2021)

A stability model can be created per fragility point for a certain water level and its corresponding pore water pressure schematization. The water level in the calculations is the highest water level during a high-water situation. In the end, the failure probability can be determined by combining the conditional failure probability (the fragility curve) and the statistics of the water level. The failure probability can be determined by solving the integral given below (Schweckendiek, Van der Krogt, Rijneveld, & Teixeira, 2017).

$$P_f = \int P(Z < 0|h) f_h(h) dh$$

In the formula above is the probability density function of the water level represented by $f_h(h)$. When the probability density function of the water level is in terms of yearly maxima, then the failure probability is calculated per year. This is convenient, since the required failure probability is also formulated per year. In case of multiple scenarios, it is advisable to calculate the failure probability per scenario and determine the total failure probability by using the probability of a scenario (Schweckendiek, Van der Krogt, Rijneveld, & Teixeira, 2017).

2.3.3 Influence coefficient

The influence coefficient is an indicator of the relative importance of a stochastic variable to the failure probability in comparison to the other stochastic variables. The influence coefficient has a value between minus one and one. The sum of the squared influence coefficients (the influence factors) is always equal to one. The influence coefficients can be determined for every fragility point in a fragility curve. Besides, the influence coefficient of the water level and the other variables can be determined for the (total) failure probability after the integration of the fragility curve with the water level statistics (Schweckendiek, Van der Krogt, Rijneveld, & Teixeira, 2017).

2.3.4 Lognormal distribution

The lognormal distribution needs to be used to determine some of the characteristic values for the semi-probabilistic assessment, according to 'Schematiseringshandleiding macrostabiliteit' (Rijkswaterstaat, Water Verkeer en Leefomgeving, 2021). The lognormal distribution is suited for most parameters with a natural spread of which a negative value is physically impossible

(Schweckendiek, Van der Krogt, Rijneveld, & Teixeira, 2017). The characteristic values of the median, with considering averaging of the uncertainties along the slip plane, for a lognormal distribution can be determined with the following formula (Rijkswaterstaat, Water Verkeer en Leefomgeving, 2021):

$$X_{med,char} = e^{\mu_{\ln(X)} \pm t_{n-1} \cdot \sigma_{\ln(X)} \cdot \sqrt{(1-a)+\frac{1}{n}}}$$

The following two equations can be used, when one assumes a perfect lognormal distribution (Rijkswaterstaat, Water Verkeer en Leefomgeving, 2021).

$$\sigma^2_{\ln(X)} = \ln\left\{1 + \left(\frac{\sigma_X}{\mu_X}\right)^2\right\}$$

$$\mu_{\ln(X)} = \ln \mu_X - \frac{1}{2}\sigma^2_{\ln(X)}$$

X	=	Observation of the sample
$X_{med,char}$	=	Characteristic value of the median of a sample for a lognormal distribution
t_{n-1}	=	Student t-factor corresponding to the 5% characteristic lower limit value and n-1
a	=	The relation between the local and regional variation. Default value is 0.75
n	=	Number of observations
μ_X	=	Mean value of the sample
$\mu_{\ln(X)}$	=	Mean value of the logarithm of the sample
σ_X	=	Standard deviation of the sample
$\sigma_{\ln(X)}$	=	Standard deviation of the logarithm of the sample

The probability density function of the lognormal distribution is given below (Jonkman, R.D.J.M., Morales-Nápoles, Vrouwenvelder, & Vrijling, 2017).

$$f_X(x) = \frac{1}{\sigma_{\ln(X)} x\sqrt{2\pi}} e^{\left\{-\frac{(\ln(x)-\mu_{\ln(X)})^2}{2\sigma^2_{\ln(X)}}\right\}}$$

2.3.5 Sample standard deviation

The amount of variability of a dataset can be expressed by the sample standard deviation. Outliners can have a very large influence on the sample standard deviation. The formula to calculate the sample standard deviation is given below (Dekking, Kraaikamp, Lopuhaä, & Meester, 2005).

$$s_n = \sqrt{\frac{1}{n-1}\sum_{i=1}^{n}(x_i - \bar{x}_n)^2}$$

s_n	=	Sample standard deviation
n	=	Number of samples
x_i	=	Individual sample value
$\bar{x}_n$	=	Sample mean

The sum of the squared differences between the individual sample value and the sample mean should be divided by a factor $n-1$ in the formula of the sample standard deviation, because the

sample standard deviation is then an unbiased estimator for the 'real' variance (Dekking, Kraaikamp, Lopuhaä, & Meester, 2005).

2.4 Assessment of inner slope stability

The assessment of inner slope stability is described in this paragraph. First, the safety requirements are described. Next, the analysis of inner slope stability and the probabilistic assessment is explained. Finally, a description of the limit equilibrium models is given.

2.4.1 Safety requirements

In this paragraph is the formula for the safety requirement of macro stability given. After this, the safety requirement for inner slope stability with overtopping is discussed.

Macro stability

The required failure probability for macro stability can be determined based on the norm of the dike trajectory, the length of the dike trajectory and the maximum contribution to the target probability. The formula to determine the required failure probability for inner slope stability is given below (Rijkswaterstaat, Water Verkeer en Leefomgeving, 2021).

$$P_{req,cross} = \frac{f \cdot P_{norm}}{\left(1 + \frac{a \cdot L}{b}\right) P_{f|inst}}$$

$P_{req,cross}$	=	Required failure probability per section for macro stability [per year]
P_{norm}	=	Probability of flooding for the dike trajectory, which is laid down in the Waterwet [per year]
f	=	Maximum contribution to the target probability [-]. For macro stability 0.04
a	=	Fraction of the length of the dike trajectory that is sensitive to the considered failure mechanism [-]. For macro stability it is 0.033
L	=	Length of the dike trajectory, according to the Waterwet [m]
b	=	Representative length for the analysis of a section [m]. For macro stability it is 50 m
$P_{f\|inst}$	=	Probability of failure given instability. For inner slope stability it is 1.0

Inner slope stability with overtopping

The probability of exceedance of an overtopping discharge of 1 l/s/m is necessary to determine the required failure probability of inner slope stability with overtopping (see paragraph 2.5.4 for a description of how this can be determined). The required failure probability of inner slope stability with overtopping can be determined with the following formula (De Visser & Jongejan, 2018):

$$P_{T,q} = \frac{P_{req,cross}}{P(q \geq 1 l/s/m)}$$

$P_{T,q}$	=	Required failure probability for inner slope stability, given significant overtopping
$P(q \geq 1 l/s/m)$	=	The probability of exceedance of an overtopping discharge of 1 l/s/m

Relation between the safety factor and the reliability index

Deltares performed a calibration study regarding the overall safety factor for inner slope stability in 2016. The goal of the calibration study was to find a relation between the overall safety factor and the reliability index. The relation between the overall safety factor and the reliability index is fitted to the twenty percent quantiles of the betas (Kanning, Teixeira, Van der Krogt, & Rippi, 2017). This

means that the reliability index, obtained from the overall safety factor and the reliability index relation, is too conservative in eighty percent of the cases.

The relation between the safety factor and the failure probability is given below (Rijkswaterstaat, Water Verkeer en Leefomgeving, 2021).

$$\beta_i = \frac{\left(\frac{F_{d;i}}{\gamma_d} - 0.41\right)}{0.15} \qquad \text{and} \qquad P_{f;i} = \Phi(-\beta_i)$$

The damage factor can be calculated from the required failure probability with the formula given below (Rijkswaterstaat, Water Verkeer en Leefomgeving, 2021).

$$\gamma_n = 0.15 \cdot \beta_{req,cross} + 0.41 \quad \text{and} \quad \beta_{req,cross} = \Phi^{-1}(P_{req,cross})$$

γ_n	=	Damage factor for macro stability [-]
$\beta_{req,cross}$	=	Required reliability index for a section [-]
$P_{req,cross}$	=	Required failure probability per section for macro stability [per year]
β_i	=	Reliability index for a section per scenario [-]
$F_{d;i}$	=	Safety factor for a section per scenario [-]
γ_d	=	Model factor [-]
$P_{f;i}$	=	Failure probability for the section per scenario [per year]

The results of the considered cases during the calibration study and the WBI calibration line are shown in Figure 8. The sample standard deviation of the calibration study is equal to 0.90 in terms of reliability index, when one assumes that the calibration line represents the sample mean of the reliability indexes. This sample standard deviation has been determined with the formula given in paragraph 2.3.5.

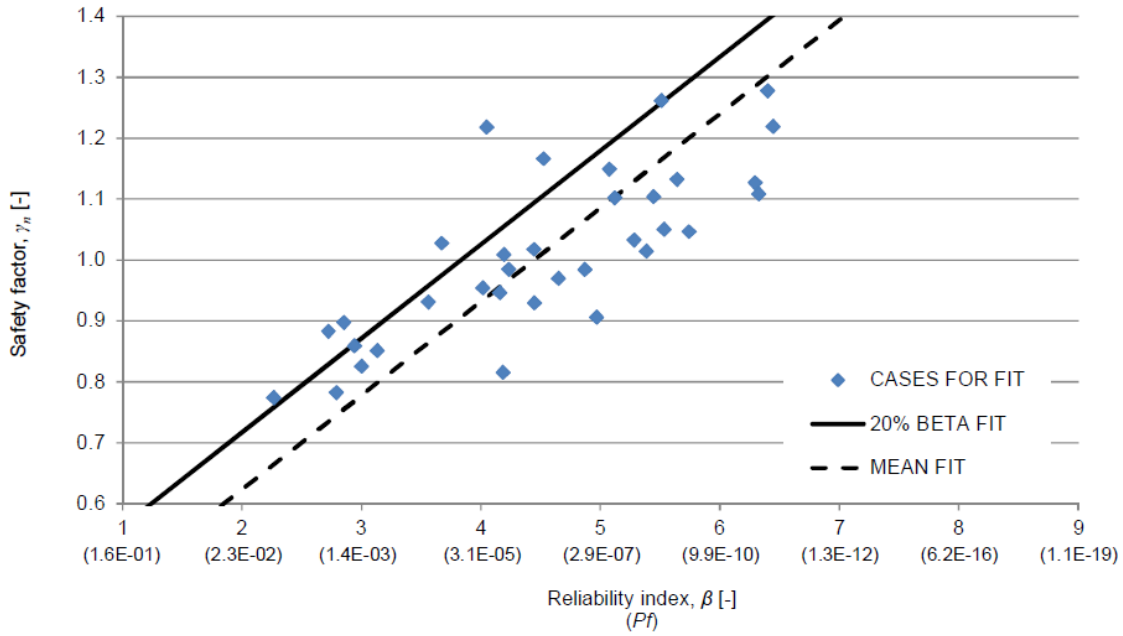

Figure 8: Calibration fit between the safety factor and the reliability index (Kanning, Teixeira, Van der Krogt, & Rippi, 2017)

According to the derivation of the semi-probabilistic assessment rule are the effects of overtopping not considered in the calibration study of inner slope stability. Therefore, dikes should be covered by a separate rule for which the pore water pressures are affected significantly by overtopping (Kanning, Teixeira, Van der Krogt, & Rippi, 2017).

The required safety factors for inner slope stability with overtopping comes from some assumptions. As a consequence, the KPR memo 'Voorstel t.a.v. beoordeling macrostabiliteit incl. golfoverslag' advises to verify the assumptions with probabilistic calculations or performing a calibration study (Jongejan & De Visser, 2017).

Whether the calibration line suits the situation where is only looked at inner slope stability with overtopping, can be verified by assessing a number of dikes semi-probabilistic and probabilistic for inner slope stability with overtopping, according to Adviesteam Dijkontwerp. After this, the relation between the results can be determined (Rijneveld, 2020).

It could certainly be possible that the damage factor line for macro stability with overtopping is different than the damage factor line for macro stability without overtopping, according to Adviesteam Dijkontwerp (Rijneveld, 2020). A calibration study has not been performed for the situation with significant overtopping. Therefore, the effects of differences from the rules of the safety format for the situation without significant overtopping are unknown. One of the aspects that deserve further research is the applicability of the WBI calibration line (Rijneveld, 2020).

2.4.2 Analysis of inner slope stability

The analysis of inner slope stability for the situation with overtopping and without overtopping is explained in this paragraph.

Without overtopping

The assessment of inner slope stability takes place by the regulations that are described in the 'Schematiseringshandleiding macrostabiliteit' of the 'Wettelijk Beoordelingsinstrumentarium 2017' (WBI 2017). One can perform the assessment of inner slope stability with Riskeer or D-Stability. Riskeer uses the limit equilibrium model Uplift-Van. First, inner slope stability should be assessed by the 'simple assessment'. When the dike section does not meet the required failure probability based on the 'simple assessment', then a 'detailed assessment' is required. When the dike section does not meet the required failure probability based on the 'detailed assessment', then there are a few options, namely (Rijkswaterstaat, Water Verkeer en Leefomgeving, 2021):

- Improving the schematization
- Accepting the calculated failure probability
- Further assessment

The 'simple assessment' and the 'detailed assessment' are explained below.

Simple assessment

General characteristics of the dike section (such as the geometry and soil composition) should be checked during the 'simple assessment'. This assessment is meant for dikes with mild slopes and wide crests. Separate graphs for the 'simple assessment' for sand and clay dikes can be found in 'WBI 2017 Bijlage III Sterkte en veiligheid' (Rijkswaterstaat, Water Verkeer en Leefomgeving, 2021). When the dike section is characterized by a point that is above the contour line belonging to that dike section, then the failure probability is negligible (Rijkswaterstaat, Water Verkeer en Leefomgeving, 2019).

Detailed assessment

The 'detailed assessment' can be performed semi-probabilistic or probabilistic per dike section. The probabilistic assessment is not possible with Riskeer. However, it is possible to perform a

probabilistic assessment with D-Stability. A limit equilibrium model is used to perform the stability analysis during the 'detailed assessment'. The failure probability can be determined based on the distribution functions of the input parameters with the probabilistic calculations. A safety factor can be calculated with the semi-probabilistic assessment, based on characteristic values for the input parameters (Rijkswaterstaat, Water Verkeer en Leefomgeving, 2021).

With overtopping

The KPR factsheet 'Werkwijze macrostabiliteit i.c.m. golfoverslag' can be used for the assessment of macro stability with an overtopping discharge larger than 1 l/s/m (Rijkswaterstaat, Water Verkeer en Leefomgeving, 2021). According to the KPR factsheet, two stability calculations are required for the semi-probabilistic assessment of inner slope stability. One calculation is without significant overtopping and one calculation is with significant overtopping. The following points are important for the semi-probabilistic assessment of inner slope stability with significant overtopping (De Visser & Jongejan, 2018):

- Infiltration needs to be considered for the schematization of the phreatic line
- The water level needs to be determined for the situation with 1 l/s/m overtopping
- Reduced partial safety factors should be used (the required failure probability per section for inner slope stability should be divided by the probability of exceedance of an overtopping discharge of 1 l/s/m)
- Not only are large slip planes important, but also small slip planes

Both the assessment of inner slope stability with significant overtopping and without significant overtopping need to meet the required failure probability (De Visser & Jongejan, 2018).

For different water levels should the failure probability be determined with the probabilistic assessment for inner slope stability. These conditional failure probabilities should be combined with the probability density function of the water level to get the (total) failure probability. When the schematizations are based on the expected amount of overtopping at a certain water level, then the interaction between macro stability and overtopping can be accounted for in the probabilistic assessment (Jongejan & De Visser, 2017).

It is probable that overtopping and infiltration of water at the inner slope occurs at many dikes from a certain water level. Since it is hard to determine the exact effects of overtopping and infiltration on the saturation of the dike body, a scenario without infiltration through overtopping and a scenario with full saturation through overtopping need to be calculated. A fragility curve needs to be created for both scenarios. After this, the fragility curves need to be combined. The combined fragility curve from the two scenarios can be determined with the equation given below (Schweckendiek, Van der Krogt, Rijneveld, & Teixeira, 2017).

$$P(failure|h) = P(failure|h, q \leq q_{crit})P(q \leq q_{crit}) + P(failure|h, q > q_{crit})P(q > q_{crit})$$

2.4.3 Probabilistic assessment

The probabilistic assessment can be performed with two different reliability analyses. The reliability index based on FORM and on Monte Carlo Importance Sampling are discussed in this paragraph.

Reliability index based on FORM

A FORM analysis can be performed per water level with D-Stability. Unfortunately, this method has a few limitations. It is often advised to use not more than ten stochastic variables in a FORM analysis.

Usually, D-Stability converges with more than twenty stochastic variables. However, it is advised to only define stochastic values for the variables with a significant influence on the safety factor (Van der Meij, 2020).

Another disadvantage is that a fixed slip circle is used in the FORM analysis. In the FORM analysis of D-Stability is assumed that the critical slip plane with the design values for the stochastic variables correspond with the slip plane with the largest failure probability. Due to the uncertainties that play a role, the critical slip plane in the semi-probabilistic calculation is not necessarily resulting in the largest failure probability (see for example the results in the document 'Aan de slag met D-Stability en Fragility curves'). For this reason, it is advised to consider multiple slip planes (Deltares, 2021).

The probabilistic calculations with FORM in D-Stability have been validated for a simplified case with calculations by using the Probabilistic Toolkit in 'Derivation of the semi-probabilistic safety assessment rule for inner slope stability'. The obtained reliability index for the simplified case with FORM is comparable to the reliability index with Probabilistic Toolkit. Unfortunately, this cannot be generalized to all possible cases (Kanning, Teixeira, Van der Krogt, & Rippi, 2017).

Reliability index based on Monte Carlo Importance Sampling

Deltares created a repository to develop tools to automate the probabilistic assessment of inner slope stability in January 2021. The tools consist of Python scripts that are used to fill a Probabilistic Toolkit file with the stochastic variables and model data to run probabilistic calculations. A D-Stability file and some Excel sheets are required as input to run the probabilistic calculations. Besides, there are some scripts to visualize and postprocess the results (Deltares, 2023).

Deltares has developed the tools in cooperation with RHDHV for Waterschap Rivierenland for the dike reinforcement project Neder Betuwe. The results are not fully validated. Cases are only tested from the project Neder Betuwe. The tools can be used for other projects, but it is completely on the users' own risk (Deltares, 2023). Deltares has developed the tools to overcome the disadvantages of the FORM analysis in D-Stability. The tools of Deltares make use of Monte Carlo Importance Sampling. Due to differences in the schematization method between Neder Betuwe and JAV, some adjustments are made by Deltares to make the tools suitable for JAV. The relatively large computation time is a disadvantage of the tools of Deltares (Broere, 2022).

2.4.4 Limit equilibrium models

Limit equilibrium models compare the loads and the resistances for force and moment equilibria at the maximum mobilizable capacity. Failure occurs when the loads are larger than the resistance for either the horizontal force, vertical force or moment equilibrium of a slip plane. The most relevant limit equilibrium models in the Netherlands are Bishop, Uplift-Van and Spencer (Jonkman, Jorissen, Schweckendiek, & Van den Bos, 2021). These models are described in this paragraph.

Bishop

Bishop is applicable to a slip plane that is circular. When the slip plane is in the limit state of equilibrium, then the safety factor is found. The safety factor can be calculated by dividing the resisting moment by the driving moment. Bishop assumes that the forces that are acting on the sides of a slice are in vertical equilibrium (Van der Meij, 2020). Bishop has a characteristic value for the model factor of 1.11 (Rijkswaterstaat, Water Verkeer en Leefomgeving, 2021). The mean value of the model factor is 1.025 and the standard deviation is 0.050 (Van Duinen, Modelonzekerheidsfactoren Spencer-Van der Meij model en ongedraineerde schuifsterkte, 2015).

Uplift-Van

Uplift-Van is applicable to a slip plane that is dual circular. Two circles (an active one and a passive one) and a horizontal bar between them form the slip circle of the Uplift-Van method. Failure due to uplift is incorporated in the Uplift-Van method. Uplift can occur when one is dealing with high pore pressures at the horizontal interface between weak layers and a permeable sand layer underneath it (Van der Meij, 2020). Uplift-Van has a characteristic value for the model factor of 1.06 (Rijkswaterstaat, Water Verkeer en Leefomgeving, 2021). The distribution of the model factor is lognormal, the mean value of the model factor is 1.005 and the standard deviation is 0.033 (Diermanse, 2016).

Spencer

The Spencer method is applicable to a non-constrained slip plane. The plane consists of an entrance point, exit point and some traversal points in between. There is a straight connection between the points. This method is not constrained to a certain shape for the slip plane. For this reason, the Spencer method can be used to freely find the slip plane that has the least resistance (Van der Meij, 2020). Spencer has a characteristic value for the model factor of 1.07 (Rijkswaterstaat, Water Verkeer en Leefomgeving, 2021). The distribution of the model factor is lognormal, the mean value of the model factor is 1.008 and the standard deviation is 0.035 (Diermanse, 2016).

2.5 Input for the analysis of inner slope stability

A few important input variables for the analysis of inner slope stability are described in this paragraph. The shear strength, the strength of the clay cover, pore water pressures and the HBN are described in this paragraph.

2.5.1 Shear strength

Not only is the shear strength of the soil dependent on the soil type and the effective stress sate of it, but also on the loading and the way that the soil responses. A distinction can be made between a drained and an undrained response of the soil (Jonkman, Jorissen, Schweckendiek, & Van den Bos, 2021).

Drained

The soil response is considered as drained when generation of excess pore pressures and the rate of deformation during sliding is small in comparison with the drainage capacity of the soil. The Mohr-Coulomb shear strength model is commonly used for drained soil response (Jonkman, Jorissen, Schweckendiek, & Van den Bos, 2021). A drained soil response is typically the case for gravel and sand with the speed of loading that is relevant for slope stability. The Mohr-Coulomb strength model is given below.

$$\tau = \sigma' \tan \varphi' + c'$$

τ	=	Shear strength [kN/m²]
σ'	=	Effective stress [kN/m²]
φ'	=	Effective internal friction angle [°]
c'	=	Effective cohesion [kN/m²]

Undrained

Undrained soil response is the case when there is no time for outflow of water, because the permeability is low and the load is applied quickly (Verruijt, 2012). The significant excess pore pressures are built up and can't drain away fast enough in the deformation process. The soil

response is typically undrained for soils with a low permeability, for example clay. The undrained shear strength based on Critical State Soil Mechanics (CSSM) is typically used for undrained soil response (Jonkman, Jorissen, Schweckendiek, & Van den Bos, 2021).

The 'Schematiseringshandleiding macrostabiliteit' uses the SHANSEP (Stress History And Normalized Soil Engineering Properties) method to determine the undrained shear strength. The SHANSEP method is connected to the CSSM model (Rijkswaterstaat, Water Verkeer en Leefomgeving, 2021). The equation for the undrained shear strength of the SHANSEP method is given below. The POP value can be used as input in D-Stability.

$s_u = \sigma'_{vi} \cdot S \cdot OCR^m$ with $OCR = \frac{\sigma'_{vy}}{\sigma'_{vi}}$ and $POP = \sigma'_{vy} - \sigma'_{vi}$

s_u	=	Undrained shear strength [kN/m²]
σ'_{vi}	=	Effective vertical stress in place [kN/m²]
S	=	Normal consolidated undrained shear strength ratio [-]
OCR	=	Over consolidation ratio [-]
m	=	Strength increase exponent [-]
σ'_{vy}	=	Effective vertical yield stress [kN/m²]
POP	=	Pre overburden pressure [kN/m²]

2.5.2 Strength of the clay cover

According to the memo 'Veiligheidsfilosofie STBI bij overslag' can the results be influenced by considering the uncertainty of the clay cover, dependent on the influence of the assumed strength of the clay cover (Rijneveld, 2020). For this reason, information about the cohesion and the internal friction angle of the clay cover has been gathered and is shown in this paragraph.

Cohesion

According to table 2-1 of 'Schematiseringshandleiding macrostabiliteit', the cohesion should be taken into account as a stochastic variable. However, according to table 2-2 of 'Schematiseringshandleiding macrostabiliteit', regarding the values that should be used during the semi-probabilistic assessment, the cohesion does not play a role in the WBI 2017 (Rijkswaterstaat, Water Verkeer en Leefomgeving, 2021).

According to appendix two of 'Notitie Omgang met GABI bij Sterke Lekdijk', which contains a guide that has been made during two sessions based on a casus at Salmsteke (Salmsteke is part of the project 'Sterke Lekdijk' like JAV), a cohesion of 5 kPa is reasonable to assume when one is dealing with saturation. For the clay cover should a design value (lower limit) for the thickness of 1 meter, cohesion of 3 kPa and an internal friction angle of 24 degrees be used for the failure mechanism GABI at the project 'Sterke Lekdijk', according to an expert session about the 'Sterke Lekdijk' on 16 December 2021 (Sluiter & Van der Kraan, 2022). These design values from the expert session are used as deterministic values during the probabilistic assessment of inner slope stability for JAV (Broere, 2022).

According to 'Handelingsperspectief schuifsterkte onverzadigde zone', an undrained shear strength of 20 kPa could be assumed for the (initial) unsaturated zone. In case that the clay of the dike is well compacted, then an undrained shear strength of 40 kPa could be assumed. When there are cracks in the (initial) undrained zone, then 25% of these values could be used, whereby the shear strength increases from the surface to the full shear strength of the clay without cracks at 1.0-1.5 m depth.

When it can be assumed that the clay has a few cracks, then a reduction of 50% of the shear strength could be assumed. These values are not meant to be used as default values, since they are based on experiences at Oijen and Westervoort and literature (Van Duinen, Handelingsperspectief schuifsterkte onverzadigde zone, 2021).

The cohesion of clay is equal to 1-10 kPa, according to the global soil characteristics of 'Technisch Rapport Waterkerende Grondconstructies' (TRWG). However, the global soil characteristics of TRWG are conservative and only meant informative (Technische Adviescommissie voor de Waterkeringen, 2001). The memo 'Modellering dijksmateriaal' advices to use a fixed strength for the cover layer of 5 kPa with a thickness of 0.8 m. Diverse research and experts agree that there is always a minimum strength, although this is not explicitly described in the current guidelines (Lodder & Kames, 2019). According to the 'Derivation of the semi-probabilistic safety assessment rule for inner slope stability', the lognormal distribution is used for the cohesion during the slope stability analyses in the macro stability kernel. The 5% value of the distribution of the cohesion is considered as the representative value for the cohesion in the semi-probabilistic calculations (Kanning, Teixeira, Van der Krogt, & Rippi, 2017). Besides, it is also according to the document 'WBI-onzekerheden' that the 5% value of the lognormal distribution should be used for the cohesion in the semi-probabilistic calculations. Furthermore, the coefficient of variation of the cohesion for macro stability is estimated to be between 0.275 and 0.4 (Diermanse, 2016). On the other hand, the coefficient of variation of the cohesion of clay is estimated to be equal to 0.45 based on samples, according to 'Technisch Rapport Grondmechanisch Schematiseren bij Dijken' (TRGS) (Deltares; Fugro Ingenieursbureau BV; HKV_Lijn in Water; Arcadis Nederland BV; Rijkswaterstaat Water, Verkeer en Leefomgeving; www.enwinfo.nl, 2012).

Internal friction angle

According to table 2-1 of 'Schematiseringshandleiding macrostabiliteit', the internal friction angle should be taken into account as a stochastic variable. Furthermore, the lognormal distribution should be used for the internal friction angle and the 5% value should be used for the semi-probabilistic calculations, according to table 2-2 of 'Schematiseringshandleiding macrostabiliteit' (Rijkswaterstaat, Water Verkeer en Leefomgeving, 2021).

A critical state angle of the internal friction of 32 degrees is an expected value for dike material, sandy clay and silty clay. The coefficient of variation is 0.10 for dike material and 0.07 for sandy clay and silty clay. This leads to a characteristic value of 29.0 degrees for dike material and 29.9 degrees for sandy clay and silty clay (Rijkswaterstaat, Water Verkeer en Leefomgeving, 2021). On the other hand, the internal friction angle of clay is equal to 20-30 degrees, according to the global soil characteristics of 'Technisch Rapport Waterkerende Grondconstructies' (TRWG). However, the global soil characteristics of TRWG are conservative and only meant informative (Technische Adviescommissie voor de Waterkeringen, 2001). A shear strength of 5 kPa is found in the clay cover at a depth of 0.8 m with an internal friction angle of approximately 30 degrees, according to the memo 'Modellering dijksmateriaal' (Lodder & Kames, 2019).

A design value (lower limit) for the thickness of 1 meter, cohesion of 3 kPa and an internal friction angle of 24 degrees should be used for the clay cover for the failure mechanism GABI at the project 'Sterke Lekdijk', according to an expert session about the 'Sterke Lekdijk' on 16 December 2021 (Sluiter & Van der Kraan, 2022). These design values from the expert session are used as deterministic values during the probabilistic assessment of inner slope stability for JAV (Broere, 2022).

The lognormal distribution is used for the tangent of the effective friction angle during the slope stability analyses in the macro stability kernel, according to the 'Derivation of the semi-probabilistic safety assessment rule for inner slope stability'. The 5% value of the distribution of the tangent of the effective friction angle is considered as the representative value for the tangent of the effective friction angle in the semi-probabilistic calculations and a coefficient of variation of 0.05-0.15 has been used during the calibration study (Kanning, Teixeira, Van der Krogt, & Rippi, 2017). Besides, it is also according to the document 'WBI-onzekerheden' that the 5% value of the lognormal distribution should be used for the tangent of the effective friction angle. Moreover, the coefficient of variation of the tangent of the effective friction angle for macro stability is estimated to be equal to 0.15 (Diermanse, 2016). The coefficient of variation of the tangent of the internal friction angle of clay is, on the other hand, estimated to be equal to 0.20 based on samples, according to 'Technisch Rapport Grondmechanisch Schematiseren bij Dijken' (TRGS) (Deltares; Fugro Ingenieursbureau BV; HKV_Lijn in Water; Arcadis Nederland BV; Rijkswaterstaat Water, Verkeer en Leefomgeving; www.enwinfo.nl, 2012).

2.5.3 Pore water pressures

The pore water pressures should be determined by the phreatic surface and the hydraulic head in the aquifer. The Waternet Creator can be used to determine the pore water pressures for the mean normal water level and the situation with the water level at the norm (Rijkswaterstaat, Water Verkeer en Leefomgeving, 2021).

Hydraulic head in the aquifer

The hydraulic head is the height that the water would reach in a monitoring well. The hydraulic head in the aquifer rises when the water level rises. Important are the thickness and the permeability of the aquifer and the resistance of the foreshore. The methods to measure and analyze the measurements of the pore water pressures and the hydraulic head in the aquifer are described in 'Technisch Rapport Waterspanningen bij Dijken' (TRWD). The conservative schematization of the TRWD can at first instance be used for the pore water pressures and the hydraulic head in the aquifer and the implementation of it in the Waternet Creator. Local research can be used to optimize the first conservative schematization (Rijkswaterstaat, Water Verkeer en Leefomgeving, 2021).

Phreatic line without overtopping

The phreatic surface is the (hypothetical) position where the pore water pressure is equal to the atmospheric pressure. Generally, the phreatic surface for the mean daily ground water level should be determined first. After this, the influence of the increased outside water level should be determined. The effects of infiltration should be accounted for in the position of the phreatic surface, when the outside water level has increased. This should be added to the mean daily ground water level. When the outside water level has increased relatively small, then it could have no influence on the level of the phreatic surface (Rijkswaterstaat, Water Verkeer en Leefomgeving, 2021).

Measuring the pore water pressures during mean circumstances is the best way to determine the initial ground water level. Otherwise, the methods described in TRWD can be used to get an estimate of the level of the phreatic surface. The phreatic surface can be schematized with the Waternet Creator. The Waternet Creator determines the schematization of the phreatic surface based on TRWD. The soil composition of the dike (clay on clay, clay on sand, sand on clay or sand on sand) is required to schematize the phreatic surface. There should be accounted for the initial ground water level. The phreatic surface should be determined for the situation with the normal mean water level and for the situation with the water level at the norm with the Waternet Creator. The nonstationary

effects of the high water on the position of the phreatic surface can be accounted for with the TRWD (Rijkswaterstaat, Water Verkeer en Leefomgeving, 2021).

According to the memo 'Pore water pressure uncertainties for slope stability' does the phreatic line uncertainty have limited effect on the reliability. Large slip circles and uplift were considered during this research. For this reason, it is recommended to evaluate the phreatic line uncertainties for cases with small slip circles and no uplift (Kanning & Van der krogt, 2016). The effects of overtopping were not considered during this research.

Phreatic line with overtopping

One must consider the infiltration with the schematization of the phreatic line. Currently, there are no general guidelines for the schematization of the phreatic line for inner slope stability with overtopping according to the KPR factsheet 'Werkwijze macrostabiliteit i.c.m. golfoverslag'. A very conservative assumption is to assume that the dike is completely saturated. The KPR factsheet advises to do a sensitivity analysis to the position of the phreatic line (De Visser & Jongejan, 2018).

The schematization of the phreatic surface in the dike is a crucial element in modelling the stability with overtopping and infiltration. Important aspects are the duration of overtopping and the characteristics of the clay cover. There is limited information available about this. As a consequence, the dike is generally modelled with the very conservative assumption of fully saturation (Rosenbrand & Rozing, 2020).

It turned out that an overtopping discharge of 1 l/s/m could lead to a saturated dike in case of a clay dike during the infiltration tests at the 'IJsseldijk'. For this reason, the scenario in which the dike is fully saturated is not always conservative (Van Hoven & Noordam, 2018).

The schematization of the phreatic line is a point of interest for assessing the inner slope stability with significant overtopping (Jongejan & De Visser, 2017). Not knowing accurately what the pore water pressures are and the strength of clay dikes is the most important knowledge gap, according to the expert session 'fragility curves conditioneel aan overslagdebiet'. The reason for this is that groundwater models do not fit the situation in practice where clay is structured and there is a large influence of the heterogeneity in permeability (Deltares, 2021). There is a lack of a validated calculation model to quantify the effects of overtopping (TAW, 2004).

2.5.4 HBN

The overtopping discharge needs to be determined after the 'detailed assessment' of 'Gras Erosie Kruin en binnentalud' (GEKB) (English: Grass Erosion Crest and inner slope) (Rijkswaterstaat, Water Verkeer en Leefomgeving, 2021). The 'Hydraulisch belastingniveau' (HBN) is the crest level that will lead to a given overtopping discharge with a given probability for a cross-section. The required failure probability for a cross-section for the failure mechanism GEKB can be determined with the formula given below (Rijkswaterstaat Water, Verkeer en Leefomgeving, 2021).

$$P_{req,cross} = \frac{\omega \cdot P_{req}}{N_{cross}}$$

$P_{req,cross}$	=	Required failure probability for a cross-section [per year]
P_{req}	=	Required failure probability belonging to the norm of the dike trajectory [per year]
ω	=	Maximum contribution to the target probability [-]. For GEKB it is 0.24
N_{cross}	=	Length effect factor for a cross-section [-]

In order to determine the HBN, a schematization of the cross-section needs to be imported. The HBN can be determined based on the overtopping discharge and the required failure probability for a cross-section (Rijkswaterstaat Water, Verkeer en Leefomgeving, 2021). The probability of exceedance of a certain overtopping discharge can be determined with a HBN calculation in Hydra-NL based on the critical overtopping discharge and the dike profile (De Visser & Jongejan, 2018).

3. Methodology

This chapter deals with the methodology that has been used to obtain the results that are shown in chapter 4. Each paragraph in this chapter deals with one of the sub-questions in paragraph 1.3. Paragraph 3.1 deals with sub-question one, paragraph 3.2 deals with sub-question two etc.

3.1 Basis semi-probabilistic and probabilistic calculations schematization

This paragraph deals with the software that has been used, number of realizations of the probabilistic calculations, slip planes, the way that the reliability indexes and sample standard deviations are estimated, the considered dike sections, the soil characteristics, pore water pressures and the traffic load for the basis semi-probabilistic and probabilistic calculations.

3.1.1 Software

D-Stability version 2020.03 has been used for the semi-probabilistic and probabilistic calculations of inner slope stability. Probabilistic Toolkit version 2.4.2 has been used for the probabilistic calculations. Besides, the latest versions of the tools to automate the probabilistic assessment of inner stability based on Monte Carlo Importance Sampling from Deltares have been used for the probabilistic calculations. Python 3.8 has been used for the probabilistic calculations, since this was required for the tools of Deltares. Furthermore, Hydra-NL version 2.7.1 has been used to determine the water level statistics in the Lek river at Jaarsveld-Vreeswijk.

3.1.2 Number of realizations probabilistic calculations

The computation time for five different water levels for one dike section takes approximately 8 hours with a maximum number of 1000 realizations. When the maximum number of realizations would be increased to 2000, then the computation time becomes approximately 13.5 hours. Besides, for a maximum number of 5000 realizations, the computation time for five different water levels for one dike section takes approximately 20 hours. The reliability index needs to be determined for some water levels with traffic load, for some water levels without traffic load and the reliability index needs to be determined with including the effects of overtopping for three water levels for most dike sections. As a consequence, it is substantial to choose an adequate maximum number of realizations to have a reasonable computation time. The computation time and the required accuracy of the results are important to determine the maximum number of realizations. Test runs have been performed with different maximum number of realizations, which can be seen in appendix A.

A maximum number of 1000 realizations leads to a reasonable difference between the expected reliability index and the 5% confidence bound of the reliability index, because the maximum difference between the expected reliability index and the 5% confidence bound of the reliability index is 0.11 with a coefficient of variation of the failure probability of 0.518 (see appendix A for the results of the test runs). It is expected that the coefficient of variation of the failure probability has a small influence on the reliability index, due to the non-linear relation between the failure probability and the reliability index (the reliability index is equal to minus the inverse standard normal distribution of the failure probability). For this reason, the probabilistic calculations are performed with a maximum number of 1000 realizations.

3.1.3 Slip plane

The Uplift-Van limit equilibrium model has been used for the analysis of inner slope stability. A minimum depth of one meter for the slip plane has been assumed. Besides, it is assumed that the beginning of the slip plane should not be located at the inner slope of the dike, but at the crest or the outer slope of the dike.

3.1.4 Estimating the reliability index and the sample standard deviation

In this paragraph is described how the reliability index is determined based on the semi-probabilistic and probabilistic calculations. Not only is the reliability index determined based on the probabilistic calculations, but also based on the semi-probabilistic calculations to make a fair comparison between the results. The sample standard deviations of the results of the basis calculations have been determined with the formula given in paragraph 2.3.5. It is assumed that the calibration line in paragraph 2.4.1 represents the sample mean of the reliability indexes to determine the sample standard deviation. To semi-probabilistic results without overtopping are used to determine the sample standard deviations for the probabilistic estimates of the reliability index from the combined fragility curves.

Semi-probabilistic

Two semi-probabilistic calculations are performed per dike section for inner slope stability. One calculation includes the effects of overtopping, and one calculation excludes the effects of overtopping. A safety factor is obtained for both calculations. The damage factor is determined by dividing the safety factor by the model factor. The estimated reliability index is determined based on the damage factor and the formula of the calibrated WBI damage factor line of 2016 in paragraph 2.4.1.

Probabilistic

A fragility curve including the effects of overtopping and a fragility curve excluding the effects of overtopping are composed. Linear interpolation has been assumed between the fragility points and linear extrapolation has been assumed outside the fragility points to compose the fragility curves (with the exception of the beginning of the fragility curve given overtopping, for which it has been assumed that the reliability index is constant). The two fragility curves are combined to one fragility curve, based on the probability of the exceedance of 1 l/s/m overtopping. An example of the fragility curves is shown in Figure 9.

The upper blue dotted line with crosses in Figure 9 represents the fragility curve without overtopping, the lower blue dotted line in Figure 9 represents the fragility curve given overtopping and the solid light blue line in between represents the combined fragility curve. The reliability index is given on the blue vertical axis on the left and the water level is given on the horizontal axis. The probability of the exceedance of 1 l/s/m overtopping given the water level is shown with the dotted green line, for which the value can be read from the green vertical axis on the right. The probability density function of the water level is given with the solid black line. One can see from Figure 9 that the reliability index decreases (blue fragility curves and the left vertical axis) if the water level increases (horizontal axis), while the probability of the exceedance of 1 l/s/m overtopping given the water level increases (dotted green line and the right vertical axis) if the water level increases (horizontal axis). Besides, one can also see from Figure 9 that the combined fragility curve is equal to the fragility curve without overtopping for relatively low water levels (the reason for this is that the probability of the exceedance of 1 l/s/m overtopping given the water level is approximately zero), while the combined fragility curve is equal to the fragility curve given overtopping when the probability of the exceedance of 1 l/s/m overtopping given the water level becomes one.

Furthermore, the reliability index after integrating the combined fragility curve with the water level statistics is given with the red square in Figure 9. The water level belonging to the red square is the design point of the water level for the combined fragility curve. It is undesirable that this point is further to the right than the upper right fragility points belonging to the water level WBN+0.3 m

(which is 7.07 m +NAP for the example in Figure 9), because the reliability index would otherwise be considerably determined based on the part of the fragility curve that is composed based on extrapolation. As a consequence, the results would be less credible, which is not the case for the example given in Figure 9.

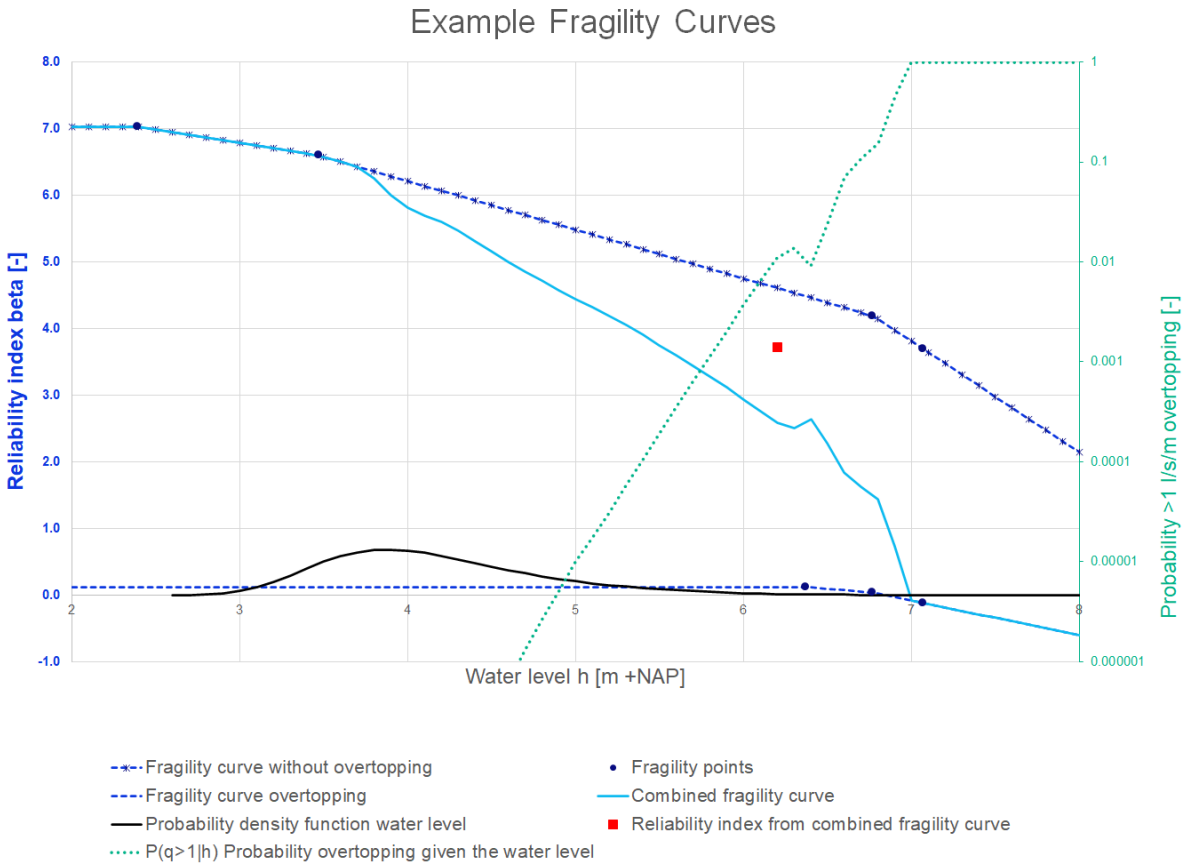

Figure 9: Example fragility curves

The reliability index from the combined fragility curve and the fragility curve without overtopping are determined based on combining the conditional reliability index (the fragility curves) and the statistics of the water level between a water level of two and eight m +NAP for JAV, according to paragraph 2.3.2. Please note that the estimated reliability index from the combined fragility curve is the reliability index for inner slope stability in general and that the estimated reliability index from the fragility curve without overtopping is the reliability index for inner slope stability given no overtopping. The reliability index for inner slope stability given overtopping has not been determined by integrating the fragility curve given overtopping with the statistics of the water level, because the reliability index would otherwise be considerably determined based on the part of the fragility curve for which it is unlikely that overtopping occurs. For this reason, it is assumed that the reliability index for inner slope stability given overtopping is equal to the conditional reliability index at the water levels that have the largest contribution to the probability of 1 l/s/m overtopping in 2073 (see Table 6 for these water levels). These water levels for the probabilistic calculations for inner slope stability given overtopping are the same water levels that are used for the semi-probabilistic calculations given overtopping.

3.1.5 Dike sections

WSP Nederland B.V. has agreed with water authority 'Hoogheemraadschap De Stichtse Rijnlanden' (HDSR) to make probabilistic calculations for inner slope stability for six dike sections with a relatively

small difference between the obtained safety factors and the required safety factors, based on the semi-probabilistic assessment. The profiles of the dike sections are obtained from AHN3 (Broere, 2022). A short description of the six considered dike sections is given in this paragraph.

Dike section 10C

Dike section 10C consists of a dike that is made of clay. The steepness of the inner slope is equal to 1:4.4 excluding the berm and the crest level is expected to be 7.04 m +NAP in 2073. Dike section 10C has a thick blanket layer (approximately 7.8 m). This dike section is located between DP12+20 m and DP14 and has a length of 180 m. During the assessment of this dike section were deep slip planes found for inner slope stability with and without overtopping (Broere, 2022). A schematization of dike section 10C is given in Figure 10.

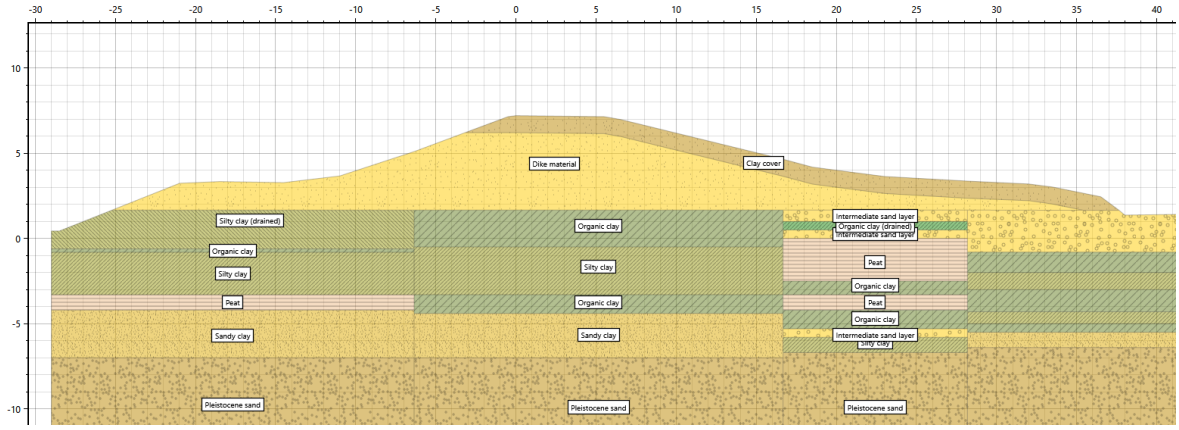

Figure 10: Schematization of dike section 10C

Dike section 11E

The dike of dike section 11E is made of clay. The steepness of the inner slope is equal to 1:3.2 over a height of approximately 4.5 m and the crest level is expected to be 6.90 m +NAP in 2073. Furthermore, the blanket layer is approximately 3 m thick. Dike section 11E is located between DP32+70 m and DP34+90 m and has a length of 220 m. Shallow slip planes were found during the assessment of inner slope stability (Broere, 2022). A schematization of dike section 11E is given in Figure 11.

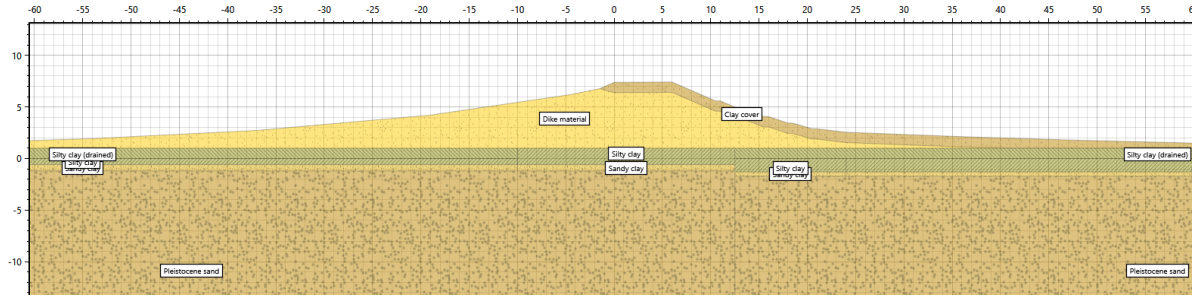

Figure 11: Schematization of dike section 11E

Dike section 11F(11D)

Dike section 11F(11D) consists of a dike that is made of clay. The steepness of the inner slope is equal to 1:3.3 over a height of 3.5 m and the crest level is expected to be 6.81 m +NAP in 2073. Dike section 11F is located between DP34+90 m and DP40 and has a total length of 510 m. Shallow slip planes were found with overtopping and deep slip planes were found without overtopping during

the assessment of inner slope stability (Broere, 2022). A schematization of dike section 11F(11D) is given in Figure 12.

The crest level of dike section 11D has been used to determine the probability of the exceedance of 1 l/s/m overtopping for dike section 11F(11D). Apart from the crest level of dike section 11D in the Hydra-NL calculations, the characteristics belonging to dike section 11F are used for dike section 11F(11D). These two dike sections were combined by WSP Nederland B.V. during the probabilistic assessment, because they are comparable to each other and it reduced the amount of work.

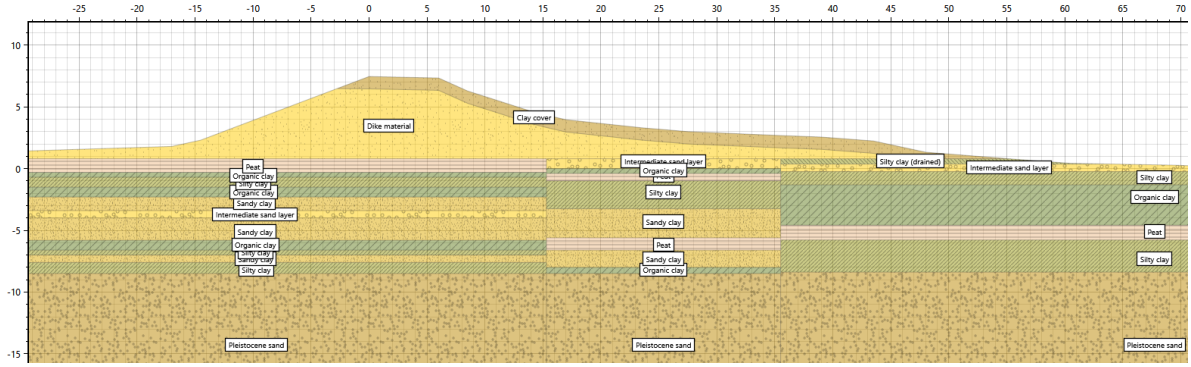

Figure 12: Schematization of dike section 11F(11D)

Dike section 13A

The dike of dike section 13A is made of clay. The steepness of the upper 1.5 m of the inner slope is equal to 1:3.4 and the average slope including the berm is equal to 1:4.8. The crest level is expected to be 6.78 m +NAP in 2073. Besides, dike section 13A consists of a blanket layer with an intermediate sand layer. This dike section is located between DP70 and DP74 and has a length of 400 m. Deep slip planes were found during the assessment of inner slope stability with and without overtopping (Broere, 2022). A schematization of dike section 13A is given in Figure 13.

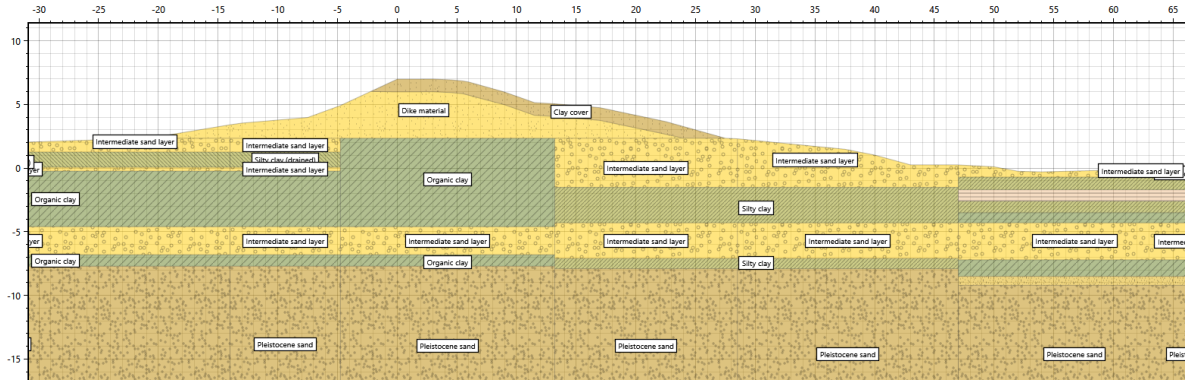

Figure 13: Schematization of dike section 13A

Dike section 13E1

Dike section 13E1 consists of a dike that is made of clay. The steepness of the upper 1.5 m of the inner slope is equal to 1:3.4 and the average slope including the berm is equal to 1:4.8. The crest level is expected to be 6.64 m +NAP in 2073. Dike section 13E1 is located between DP67+50 m and DP70 and has a length of 250 m. Deep slip planes were found during the assessment of inner slope stability (Broere, 2022). A schematization of dike section 13E1 is given in Figure 14.

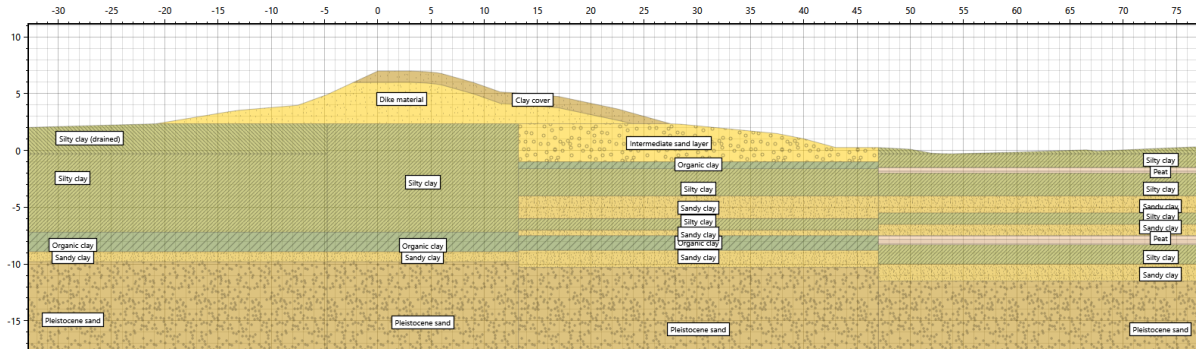

Figure 14: Schematization of dike section 13E1 and 13E2

Dike section 13E2

The dike of dike section 13E2 is made of clay. The steepness of the upper 1.5 m of the inner slope is equal to 1:3.4 and the average slope including the berm is equal to 1:4.8. The crest level is expected to be 6.34 m +NAP in 2073. Dike section 13E2 is located between DP74 and DP75+50 m and has a length of 150 m. Deep slip planes were found during the assessment of inner slope stability (Broere, 2022). For dike section 13E1 and 13E2 are the same schematization of the dike profile used. A schematization of dike section 13E2 is given in Figure 14. The difference between dike section 13E1 and 13E2 lies in the loads from the water levels in the Lek river. Dike section 13E1 and 13E2 have a different orientation, which leads to different water level statistics.

3.1.6 Soil characteristics

Characteristic values of the soil parameters are used for the semi-probabilistic calculations. For the probabilistic calculations are the mean values and the standard deviations of the soil parameters used to determine the reliability index. The unit weight (γ) is modelled as a deterministic value in both the semi-probabilistic and probabilistic calculations. The effective internal friction angle (φ'), undrained shear strength ratio (S), strength increase exponent (m) and the Pre Overburden Pressure (POP) have a lognormal distribution and are modelled as stochastic parameters in the probabilistic calculations. The used unit weights in the calculations are shown in Table 1. Please note that the saturated unit weight of sand is different than the unsaturated unit weight of sand.

Table 1: Unit weight (γ) per soil type

Soil type	Saturated unit weight γ_{sat} [kN/m^3]	Unsaturated unit weight γ_{unsat} [kN/m^3]
Dike material	18.9	18.9
Intermediate sand layer	19.0	17.0
Pleistocene sand	20.0	18.0
Sandy clay	18.4	18.4
Silty clay	16.1	16.1
Organic clay	13.2	13.2
Peat	10.9	10.9

The effective internal friction angle is used for the drained soil layers. An overview of the critical state angle of the internal friction is given in Table 2 per soil type. Please note that some of these soil types, for example silty clay, can be both an undrained soil layer and a drained soil layer, depending on the location of the soil layer and the phreatic surface at normal conditions.

Table 2: Critical state angle of the internal friction (φ') per soil type

Soil type	φ'_{char} [°]	φ'_{mean} [°]	$\varphi'_{std.dev}$ [°]
Dike material	26.1	30.01	2.50
Intermediate sand layer	29.9	31.95	1.29
Pleistocene sand layer	32.4	33.97	0.98
Sandy clay	29.6	32.79	2.01
Silty clay	28.3	34.23	3.85
Organic clay	33.5	42.22	5.76
Peat	27.4	33.38	3.89

For the clay cover is a thickness of 1 m, unit weight of 18.9 kN/m^3, cohesion of 3 kPa and an effective internal friction angle of 24 degrees assumed at the crest and on the inner slope of the dike. These characteristics of the clay cover are modelled deterministic in both the semi-probabilistic and probabilistic calculations.

For the soil types that could be considered as undrained, depending on the location of the soil layer and the phreatic surface at normal conditions, are the used values of the undrained shear strength ratio (S) and the strength increase exponent (m) given in Table 3. Besides, the POP values of the soil types that could be considered as undrained are given in Table 4.

Table 3: Undrained shear strength ratio (S) and strength increase exponent (m) for the undrained soil types

Soil type	S_{char} [-]	S_{mean} [-]	$S_{std.dev}$ [-]	m_{char} [-]	m_{mean} [-]	$m_{std.dev}$ [-]
Sandy clay	0.38	0.40	0.013	0.76	0.8	0.025
Silty clay	0.26	0.28	0.009	0.76	0.8	0.025
Organic clay	0.20	0.24	0.023	0.69	0.8	0.066
Peat	0.38	0.39	0.006	0.88	0.9	0.012

Table 4: POP values for the undrained soil types

Soil type	POP_{char} [-]	POP_{mean} [-]	$POP_{std.dev}$ [-]
Sandy clay	29.55	43.43	9.649
Silty clay	43.99	49.78	3.661
Organic clay	41.45	49.65	5.294
Peat	9.02	17.09	6.186

3.1.7 Pore water pressures

First, it needs to be determined whether inner slope stability with overtopping needs to be taken into account at a dike section, before doing the assessment. The HBN for an overtopping discharge of 1 l/s/m and a probability of 1/41667 per year (which is the required failure probability to determine the minimum necessary crest level (Rijkswaterstaat Water, Verkeer en Leefomgeving, 2017)) in 2073 has been determined with Hydra-NL version 2.7.1. Climate scenario KNMI 2006W+, years 2050 and 2100, maximum discharge of 16000 m^3/s and database WBI2017_Benedenrijn_15-1_v04 have been used to determine the HBN. Linear interpolation between 2050 and 2100 has been used to determine the HBN in 2073. The HBN has been determined with taking into account the model uncertainty and the statistic uncertainty. The HBN in 2073 for the six considered dike sections are shown in Table 5. One can see from Table 5 that the crest level is 11 cm higher than HBN for dike

section 13E1 and that the crest level of dike sections 10C and 11E are only 8 cm lower than HBN in 2073. For this reason, the probability of the exceedance of an overtopping discharge of 1 l/s/m for dike section 13E1 is relatively small. However, inner slope stability with overtopping might still be an issue at dike section 13E1, so calculations for inner slope stability with overtopping are made for all the six considered dike sections during this research.

The local water levels in 2073, including subsidence, are used in the semi-probabilistic and probabilistic calculations for inner slope stability with overtopping. The subsidence has been added to the water level, instead of lowering the dike profile, to incorporate the effects of subsidence in the calculations. The required failure probability has been determined for inner slope stability with overtopping per dike section by dividing the required failure probability of inner slope stability without overtopping by the probability of 1 l/s/m overtopping in 2073. The schematization factor has been multiplied to the required safety factor and has been transformed to determine the required reliability index for inner slope stability with overtopping including the schematization factor. The values per dike section for the different parameters are shown in Table 5.

Table 5: The local water levels, probability of 1 l/s/m overtopping and required reliability index for inner slope stability with overtopping

Parameter	10C	11E	11F(11D)	13A	13E1	13E2
HBN (1 l/s/m, 1/41667 per year, 2073) [m]	7.12	6.98	7.03	7.17	6.53	6.91
Subsidence [m]	0.236	0.413	0.413	0.236	0.236	0.236
Crest level after subsidence 2073 [m +NAP]	7.04	6.90	6.81	6.78	6.64	6.34
Difference crest level and HBN (1 l/s/m, 1/41667 per year, 2073) [m]	-0.08	-0.08	-0.22	-0.39	0.11	-0.57
Probability 1 l/s/m overtopping 2073 [-]	4.42E-05	4.98E-05	1.30E-04	1.78E-04	1.34E-05	6.87E-04
Local water level 2073 including subsidence [m +NAP]	**6.21**	**6.37**	**6.38**	**5.66**	**6.00**	**5.91**
Required failure probability for inner slope stability without overtopping [-]	2.47E-07	2.47E-07	2.47E-07	2.47E-07	2.47E-07	2.47E-07
Required failure probability for inner slope stability with overtopping [-]	5.59E-03	4.97E-03	1.91E-03	1.39E-03	1.84E-02	3.60E-04
Required reliability index for inner slope stability with overtopping [-]	2.54	2.58	2.89	2.99	2.09	3.38
Schematization factor [-]	1.1	1.1	1.1	1.1	1.1	1.1
Required reliability index for inner slope stability with overtopping including schematization factor [-]	**3.06**	**3.11**	**3.46**	**3.56**	**2.57**	**3.99**

The local water levels including subsidence in 2073 in Table 5 are considered as the 1 l/s/m overtopping water levels for the calculations with overtopping. These water levels are the water levels that have the largest contribution to the probability of 1 l/s/m overtopping in 2073.

The considered water levels in the probabilistic calculations are shown in Table 6. The WBN water levels from Table 6 are used for the semi-probabilistic calculations without overtopping. Besides, the 1 l/s/m overtopping water levels from Table 6 are used for the semi-probabilistic calculations with overtopping. The water levels in the Lek river for the uplift factors are determined based on the water head at the location where uplift would occur. Furthermore, for dike section 10C are probabilistic calculations performed with the water level a few centimeters lower than the crest

level, because the reliability index would otherwise be considerably determined based on the part of the fragility curve that is composed based on extrapolation and the results would be less credible. This situation did only occur for the basis calculations at dike section 10C, so only for this dike section are probabilistic calculations performed with the water level a few centimeters lower than the crest level.

Table 6: Water levels including subsidence in 2073 in m +NAP

Water level	10C	11E	11F(11D)	13A	13E1	13E2
Daily	0.24	-0.04	-0.04	-0.30	-0.30	-0.30
Uplift 1.2	4.37	2.39	2.63	0.87	4.69	4.69
Uplift 1.0	6.81	3.47	5.24	2.07	8.18*	8.18*
WBN	6.66	6.77	6.79	6.26	6.33	6.24
WBN+0.3 m	6.96	7.07	7.09	6.56	6.63	6.54
Overtopping, WBN	6.66	6.77	6.79	6.26	6.33	6.24
Overtopping, WBN+0.3 m	6.96	7.07	7.09	6.56	6.63	6.54
1 l/s/m overtopping water level	6.21	6.37	6.38	5.66	6.00	5.91
A few centimeters lower than the crest level	7.15	n/a	n/a	n/a	n/a	n/a
Overtopping, a few centimeters lower than the crest level	7.15	n/a	n/a	n/a	n/a	n/a

** This water level has not been used in the probabilistic calculations, since this water level is far larger than WBN*

The water head lines are determined based on the analytical formulas of model 4A/4C from TRWD. The effects of uplift are accounted for in determining the water head lines.

The phreatic surface should be 1.0 m lower at the outer crest line and 1.5 m lower at the inner crest line than the water level in the Lek river for WBN without overtopping, according to the report 'Strategische Nota van Uitgangspunten' (Strategisch team van Sterke Lekdijk, 2021). Besides, the water level at the inner toe of the dike and in the hinterland should be equal to the surface level of the hinterland at WBN (Strategisch team van Sterke Lekdijk, 2021). A schematization of the phreatic surface for WBN without overtopping is given in Figure 15.

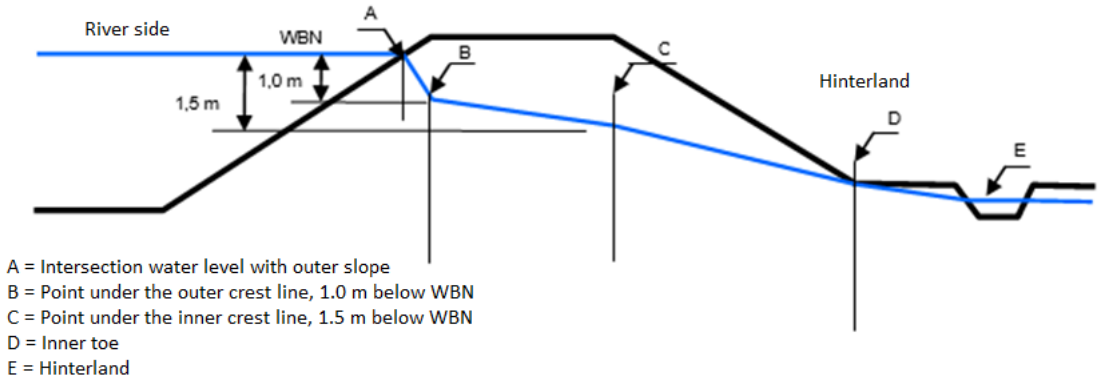

Figure 15: Schematization of the phreatic surface without overtopping for WBN (Strategisch team van Sterke Lekdijk, 2021)

The schematization of the phreatic surface for the daily situation has been determined based on measurements (Broere, 2022). Linear interpolation and extrapolation have been used for the schematization of the phreatic surface for the other water levels without overtopping in Table 6.

The upper meter of the dike has been modelled fully saturated with hydrostatic pressure gradients for the semi-probabilistic and probabilistic calculations with overtopping. Linear interpolation occurs underneath the upper meter of the dike to the top of the blanket layer (aquitard). The pore water pressures at the top of the blanket layer are assumed to be equal to the pore water pressures for the situation without overtopping. A schematization of the used pore water pressure distribution in the basis calculations with overtopping is illustrated with the green line in Figure 16 (option 2). A favorable situation is option 3 (blue line in Figure 16), with interpolation from the surface level of the dike until the top of the blanket layer, where the pore water pressures are assumed to be equal to the pore water pressures for the situation without overtopping. An unfavorable situation is option 1 (red line in Figure 16) with hydrostatic pressure gradients from the surface level of the dike until the top of the blanket layer. The schematization that has been used for the basis semi-probabilistic and probabilistic calculations (option 2) is between the favorable situation (option 3) and the unfavorable situation (option 1).

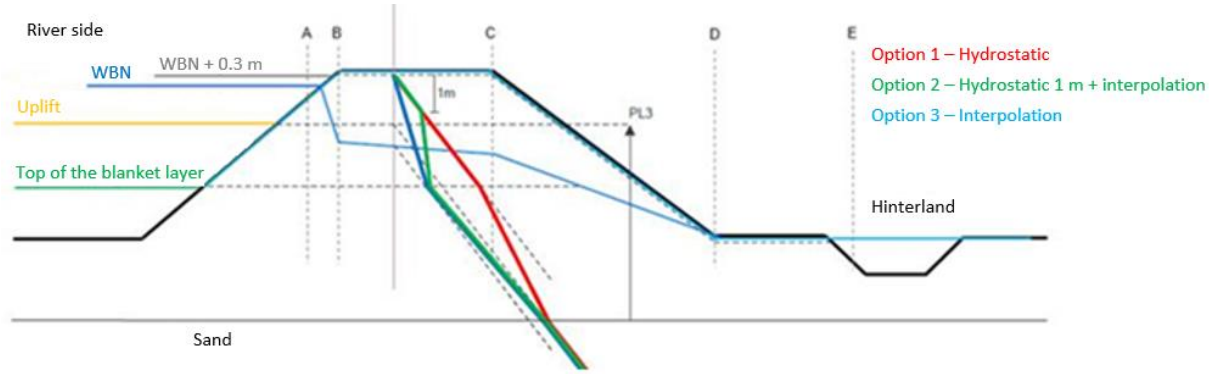

Figure 16: Schematization of the pore water pressure distribution with overtopping (Broere, 2022)

3.1.8 Traffic load

A traffic load of 15 kN/m^2 has been used for daily conditions and water levels with a probability of exceedance larger than 1/50 per year. Besides, a traffic load of 8 kN/m^2 should be used for water levels with a probability of exceedance between 1/1000 per year and 1/50 per year according to 'Strategische Nota van Uitgangspunten' (Strategisch team van Sterke Lekdijk, 2021). For this reason, a traffic load has not been modelled during the semi-probabilistic calculations, where the probability of exceedance of the water levels is far smaller than 1/1000 per year. On the other hand, the traffic load is modelled for some water levels in the probabilistic calculations. An overview of the used traffic load per water level in the probabilistic calculations is given in Table 7. The traffic load has been modelled with a spreading angle of thirty degrees over a width of 2.5 m on the inner part of the crest. A layer consolidation of zero percent has been used for the impermeable layers and a layer consolidation of one hundred percent has been used for the permeable layers.

Table 7: Traffic load per water level in kN/m²

Water level	10C	11E	11F(11D)	13A	13E1	13E2
Daily	15	15	15	15	15	15
Uplift 1.2	15	15	15	15	15	15
Uplift 1.0	0	15	15	15	0	0
WBN	0	0	0	0	0	0
WBN+0.3 m	0	0	0	0	0	0
Overtopping, WBN	0	0	0	0	0	0
Overtopping, WBN+0.3 m	0	0	0	0	0	0
1l/s/m overtopping water level	0	0	0	0	0	0
A few centimeters lower than the crest level	0	n/a	n/a	n/a	n/a	n/a
Overtopping, a few centimeters lower than the crest level	0	n/a	n/a	n/a	n/a	n/a

3.2 Incorporating additional stochastic variables in the probabilistic calculations

The methodology to incorporate additional stochastic variables is described in this paragraph. In this paragraph is explained how the cohesion and the internal friction angle of the clay cover have been modelled stochastic. Furthermore, in this paragraph is described how is dealt with the uncertainties in the pore water pressure distribution given overtopping.

3.2.1 Strength of the clay cover

It is assumed that the soil response of the clay cover is drained. For this reason, the strength of the clay cover should be modelled with a cohesion and an internal friction angle. In absence of local test data for the characteristics of the clay cover, literature has been used to model the cohesion and the internal friction angle of the clay cover stochastic. The information found in literature is shown in paragraph 2.5.2. An overview of the assumed stochastic variables of the clay cover is given in Table 8.

Cohesion

During this research is assumed that the cohesion follows a lognormal distribution, since this distribution is suited for most parameters with a natural spread of which a negative value is physically impossible (Schweckendiek, Van der Krogt, Rijneveld, & Teixeira, 2017). The coefficient of variation is fitted such that the 5% value of the cohesion of the clay cover corresponds to the design value of 3 kPa, which has been used during the basis calculations (see paragraph 3.1.6).

According to 'Notitie Omgang met GABI bij Sterke Lekdijk', a cohesion of 5 kPa is reasonable to assume when one is dealing with saturation, based on a different case at the project 'Sterke Lekdijk'. Besides, the memo 'Modellering dijksmateriaal' advices to use a fixed strength of 5 kPa for the cover layer (see paragraph 2.5.2). For this reason, a mean value of 5 kPa has been assumed for the cohesion of the clay cover. A coefficient of variation of 0.29 is necessary to obtain a 5% value of 3 kPa with a mean value of 5 kPa with the lognormal distribution (see Figure 17). Since the coefficient of variation of the cohesion is expected to be between 0.275 and 0.4 according to 'WBI-onzekerheden' (see paragraph 2.5.2), a coefficient of variation of 0.29 can be considered reasonable.

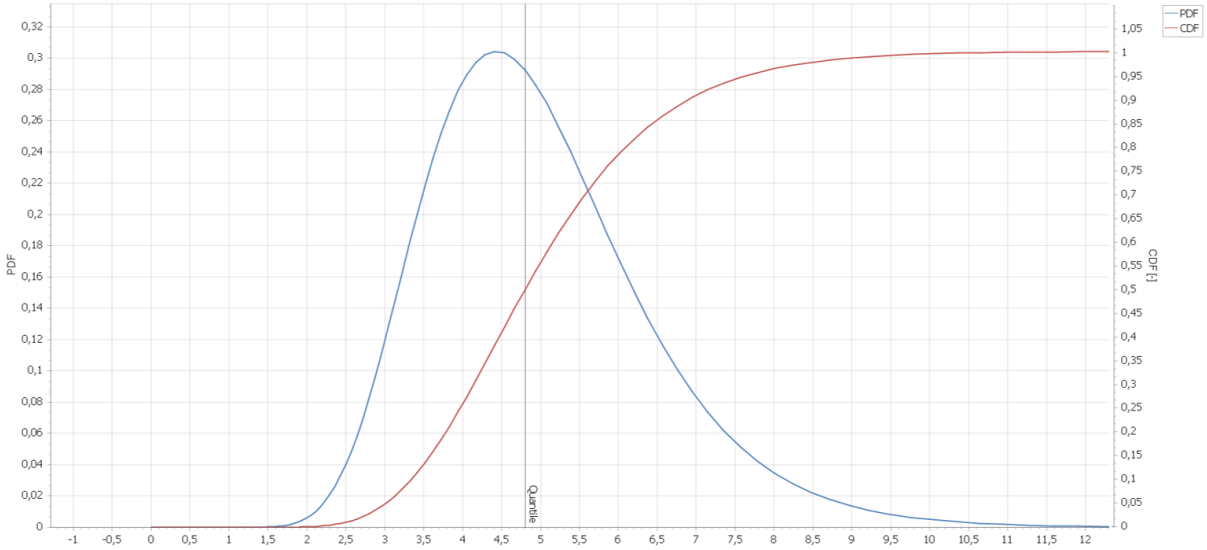

Figure 17: Lognormal distribution with mean 5 and coefficient of variation 0.29

One can see from Figure 17 that the assumed distribution of the cohesion of the clay cover is located well within the 1-10 kPa range for the cohesion of clay according to TRWG. However, the global soil characteristics of TRWG are conservative and only meant informative (Technische Adviescommissie voor de Waterkeringen, 2001). The range of 1-10 kPa for the cohesion of clay is not specifically for the clay cover, but for clay in general. The range for the cohesion of the clay cover could be different than the range for the cohesion of clay in general, due to cracks for example.

An undrained shear strength of 20 kPa could be assumed for the (initial) unsaturated zone and a value of 40 kPa could be assumed if the clay is well compacted according to 'Handelingsperspectief schuifsterkte onverzadigde zone'. When there are cracks in the (initial) undrained zone, then 25% of these values could be used and 50% could be used if the clay has a few cracks (see paragraph 2.5.2). This means that the undrained shear strength could be 10 kPa for the (initial) unsaturated zone if the clay is well compacted and there are cracks in the (initial) undrained zone. It is reasonable that the mean value of the cohesion of the clay cover is lower than 10 kPa, since the internal friction angle does also contribute to the shear strength when the soil response is considered as drained (see paragraph 2.5.1).

Internal friction angle

During this research is assumed that the internal friction angle of the clay cover follows a lognormal distribution, since this distribution is suited for most parameters with a natural spread of which a negative value is physically impossible (Schweckendiek, Van der Krogt, Rijneveld, & Teixeira, 2017). The coefficient of variation is fitted such that the 5% value of the internal friction angle of the clay cover corresponds to the design value of 24 degrees, which has been used during the basis calculations (see paragraph 3.1.6).

A critical state angle (so with a cohesion of zero) of the internal friction of 32 degrees is an expected value for dike material, sandy clay and silty clay according to the 'Schematiseringshandleiding macrostabiliteit' (Rijkswaterstaat, Water Verkeer en Leefomgeving, 2021). The mean value of the internal friction angle of dike material is equal to 30.01 degrees, for sandy clay 32.79 degrees and for silty clay 34.23 degrees for JAV according to Table 2 (these soil types have a cohesion of zero).

According to paragraph 3.1.5 are the dikes of the considered dike sections made of clay. For this reason, it is assumed that the mean value of the internal friction angle of the clay cover is equal to 30 degrees, so that it is approximately equal to the mean internal friction angle of dike material for JAV. It is reasonable to use a mean for the internal friction angle lower than the critical state value of 32 degrees based on 'Schematiseringshandleiding macrostabiliteit', because the clay cover has been modelled with a cohesion for JAV. Besides, according to 'Notitie Omgang met GABI bij Sterke Lekdijk' is the effect of the formation of structures of the clay unknown (Sluiter & Van der Kraan, 2022). For this reason, it is reasonable to use a mean value for the internal friction angle of the clay cover lower than 32 degrees.

A lognormal distribution with a mean value of 30 degrees and a coefficient of variation of 0.13, leads to a standard deviation of 3.9 degrees and a 5% value of 24 degrees (see Figure 18). Since the coefficient of variation of the tangent of the effective friction angle is expected to be equal to 0.15 according to 'WBI-onzekerheden' (see paragraph 2.5.2), a coefficient of variation of 0.13 can be considered reasonable. This coefficient of variation is within the range of used coefficients of variation in the calibration study of 0.05-0.15 (Kanning, Teixeira, Van der Krogt, & Rippi, 2017). Besides, the used coefficients of variation for the internal friction angle are between 0.03 and 0.14 for JAV based on Table 2. The coefficient of variation for the internal friction angle of dike material is approximately equal to 0.08 for JAV based on Table 2. It can be considered reasonable that the coefficient of variation of the internal friction angle is larger for the clay cover than for the dike material of JAV, due to the uncertainty of the formation of structures of the clay. For this reason, a lognormal distribution with a mean value of 30 degrees and a coefficient of variation of 0.13 (which gives a 5% value of 24 degrees) is assumed for the internal friction angle of the clay cover.

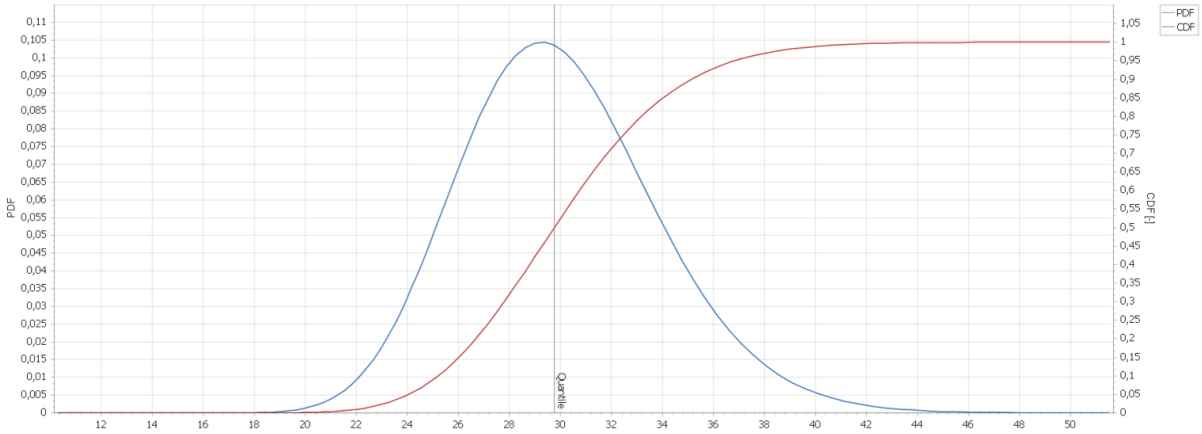

Figure 18: Lognormal distribution with mean 30 and coefficient of variation 0.13

Table 8: Assumed stochastic variables of the clay cover

Parameter	Mean value	Coefficient of variation [-]	Distribution	Design value
Cohesion	5 kPa	0.29	Lognormal	3 kPa
Internal friction angle	30 degrees	0.13	Lognormal	24 degrees

3.2.2 Pore water pressure distribution with overtopping

There is a large uncertainty about the position of the phreatic line given overtopping, based on the found literature in paragraph 2.5.3. In Figure 16 in paragraph 3.1.7 is with the green line (option 2) shown how the pore water pressure distribution with overtopping is modelled in the basis calculations of JAV. The used pore water pressure distribution with overtopping in the basis calculations is assumed between the favorable situation (option 3, interpolation, blue line in Figure 16) and the unfavorable situation (option 1, hydrostatic, red line in Figure 16). Calculations have been performed with the three options for the pore water pressure distribution with overtopping shown in Figure 16 in order to investigate the effects of the uncertainty of the pore water pressure distribution with overtopping on the results. The failure probability is determined by taking into account the weight of the different options for the pore water pressure distribution after performing the calculations with the three different options for the pore water pressure distribution with overtopping.

Infiltration tests are performed on sea dikes made of clay and sand on different locations. The results of these tests are shown in 'Sliding stability of landward slope clay cover layers of sea dikes subject to wave overtopping'. The pore pressures were compared with the calculated parallel pressure during these tests. When the pore pressure of the clay dikes was lower than the calculated parallel pressure, then there was an inward gradient or the clay cover was not fully saturated. Since the dikes at JAV are made of clay (see paragraph 3.1.5), only the results of the clay dike at Delfzijl are considered. The results of the clay dike at Delfzijl show that the assumed parallel flow condition is reached for the test with 1 l/s/m overtopping. The pore water pressure was measured at 0.8 m and 1.2 m depth. Only measurements up to approximately 1 m gave usable validation data, due to 3D effects (Van Hoven, Hardeman, Van der Meer, & Steendam, 2010). For this reason, it not possible to determine whether the pore water pressure distribution was fully hydrostatic from the surface level (option 1, hydrostatic, red line in Figure 16) or that only the first meter of the distribution was hydrostatic (option 2, green line in Figure 16) at Delfzijl.

Infiltration tests have been performed with an overtopping discharge of 1.85 l/s/m at the IJsseldijk, which can be considered as a clay dike. During the tests were the pore water pressures measured at varies depth in two rays at the crest, inner slope, inner toe and the inner berm of the dike (Van Hoven & Noordam, 2018). So, in total were the pore water pressures measured at eight locations at the IJsseldijk. The pore water pressures were measured up to a depth of approximately five meters. Since the amount of available information about the pore water pressures with overtopping is limited and not all the available results at the IJsseldijk follow the distributions in Figure 16 clearly, combinations with different probabilities of occurrence of the pore water pressure distributions, which are shown in Figure 16, have been assumed. The assumed combinations with the probability of occurrence of the pore water pressure distributions are shown in Table 9.

Due to a lack of data are the probabilities of occurrence of the 'basis', 'interpolation' and 'hydrostatic' pore water pressure distribution estimated qualitatively. Without any knowledge are the probabilities of occurrence estimated to be equal to 1/3 for combination 1. The probabilities of occurrence for combination 2, 3 and 4 are estimated based on the results of the infiltration test at the IJsseldijk.

Table 9: Probability of occurrence different pore water pressure distribution scenarios with overtopping per combination

Scenario	Combination 1	Combination 2	Combination 3	Combination 4
Probability of occurrence 'basis' schematization [-]	1/3	7/8	1/8	4/8
Probability of occurrence 'interpolation' schematization [-]	1/3	1/8	1/8	1/8
Probability of occurrence 'hydrostatic' schematization [-]	1/3	0	6/8	3/8

The failure probability is close to one for dike section 11E given overtopping for the 'hydrostatic' pore water pressure distribution (option 1, red line in Figure 16), which has as a consequence that the difference between the expected reliability index and the 5% confidence bound of the reliability index is very large. For this reason, the settings have been changed for dike section 11E given overtopping for the 'hydrostatic' pore water pressure distribution to decrease this difference (see appendix E). The settings have only been changed for dike section 11E with overtopping for the 'hydrostatic' pore water pressure distribution, where the difference between the expected reliability index and the 5% confidence bound of the reliability index was extremely large. The maximum requirement for the number of realizations has been increased to 3000 and the requirement for the coefficient of variation of the failure probability has been decreased in such a way that 3000 realizations would be obtained for dike section 11E given overtopping for the 'hydrostatic' pore water pressure distribution (option 1, red line in Figure 16), instead of a minimum of 500 and a maximum of 1000 realizations.

3.3 Steepness of the inner slope

The steepness of the inner slope has been adjusted in order to investigate the influence of it on the difference between the semi-probabilistic and probabilistic estimates of the reliability index of inner slope stability. The inner slope steepness has been adjusted between 1:3 and 1:5 to investigate how the results of JAV would change if the steepness of the inner slope changes. Since steeper slopes than 1:3 could be found in practice, it would also be interesting to investigate what the influence is on the results for inner slopes steeper than 1:3. Unfortunately, convergence problems occurred for inner slope stability with overtopping with an inner slope of 1:2.5. It is assumed that the convergence problems were caused by the relatively high failure probabilities. When the failure probability goes to one, then the reliability index would go to minus infinity. As a consequence, no calculations are performed with an inner slope steeper than 1:3. The inner slope of the six dike sections of JAV are adjusted to a steepness of 1:3, 1:3.5, 1:4, 1:4.5 and 1:5 to investigate what the influence of the dike slope steepness is on the difference between the semi-probabilistic and probabilistic estimates of the reliability index of inner slope stability.

For some dike sections are probabilistic calculations performed with an extra water level. This extra water level is for these dike sections a few centimeters lower than the crest level, because the reliability index would otherwise be considerably determined based on the part of the fragility curve that is composed based on extrapolation. As a consequence, the results would be less credible. This situation did occur for dike section 11E with an inner slope of 1:3.5, 1:4.5 and 1:5, dike section 13E1 with an inner slope of 1:3.5 and 1:4.5 and dike section 13E2 with an inner slope of 1:4. For dike section 10C are for every slope calculations performed with the water level a few centimeters lower

than the crest level, since this situation did already occur for the basis calculations of dike section 10C (see paragraph 3.1.7).

The failure probability is close to one for dike section 13A with an inner slope of 1:3 given overtopping, which has as a consequence that the difference between the estimated reliability index and the 5% confidence bound of the reliability index is very large. For this reason, the settings have been changed for dike section 13A with an inner slope of 1:3 given overtopping to decrease this difference (see appendix J). The settings have only been changed for dike section 13A with an inner slope of 1:3 given overtopping, where the difference between the estimated reliability index and the 5% confidence bound of the reliability index was extremely large. The maximum requirement for the number of realizations has been increased to 10000 and the requirement for the coefficient of variation of the failure probability has been decreased in such a way that 10000 realizations would be obtained for dike section 13A with an inner slope of 1:3 given overtopping, instead of a minimum of 500 and a maximum of 1000 realizations.

3.4 Applicability of the calibrated WBI damage factor line of 2016

The results with a steepness of the inner slope of 1:3, 1:3.5, 1:4, 1:4.5 and 1:5 are shown for JAV without overtopping, for JAV based on the combined fragility curve and for JAV given overtopping to investigate whether the WBI calibration line is applicable for inner slope stability. Besides, the applicability of the calibration line from dike trajectory SAFE and different coefficients of variation for the undrained shear strength ratio of organic clay and silty clay are considered.

In Figure 19 is the inner slope steepness shown for the profiles that have been used for the WBI calibration line. Please note that only the profiles that are actually used for the calibration line are shown in Figure 19. Most profiles that have been used for the WBI calibration line have an inner slope steeper than 1:3. One would expect that the internal friction angle of dike material has the largest influence factor for the profiles that have been used for the WBI calibration line, based on the influence factors of JAV with an inner slope steepness of 1:3 in Figure 28. However, the undrained shear strength ratio (S), the yield stress and the model uncertainty have the largest influence factors for the profiles that have been used for the WBI calibration line (Kanning, Teixeira, Van der Krogt, & Rippi, 2017). Especially the undrained shear strength ratio has a large influence factor based on Figure 6.2 in the document 'Derivation of the semi-probabilistic safety assessment rule for inner slope stability'. The undrained shear strength of organic clay and silty clay have a relatively large influence factor for most dike sections of JAV based on Figure 20.

An indication is given of expected values for the normal consolidated undrained shear strength ratio in Table 7.5 in the document 'Schematiseringshandleiding macrostabiliteit'. According to this table, the coefficient of variation of the undrained shear strength ratio of organic clay is expected to be 0.20 and for silty clay 0.10 (Rijkswaterstaat, Water Verkeer en Leefomgeving, 2021). The expected coefficient of variation of the undrained shear strength ratio of silty clay from 'Schematiseringshandleiding macrostabiliteit' is approximately a factor three larger than for JAV. Furthermore, the expected coefficient of variation of the undrained shear strength ratio of organic clay from 'Schematiseringshandleiding macrostabiliteit' is approximately a factor two larger than for JAV. It is expected that when the coefficient of variation increases that the obtained reliability index decreases for the relatively large reliability indexes in Figure 21 if the characteristic values keep the same. The coefficients of variation of the undrained shear strength ratio of organic clay and silty clay have been changed for the basis calculations of JAV to investigate whether the results of the basis calculations of JAV far at the right of the WBI calibration line (see Figure 21) would shift towards the

calibration line. The mean and standard deviations are fitted such that the coefficients of variation are equal to the values in 'Schematiseringshandleiding macrostabiliteit' and the 5% values correspond to the design values that have been used during the semi-probabilistic calculations (see Table 3 and Table 10). The assumed stochastic variables of the undrained shear strength ratio of silty clay and organic clay are shown in Table 10 with the used values in the basis calculations.

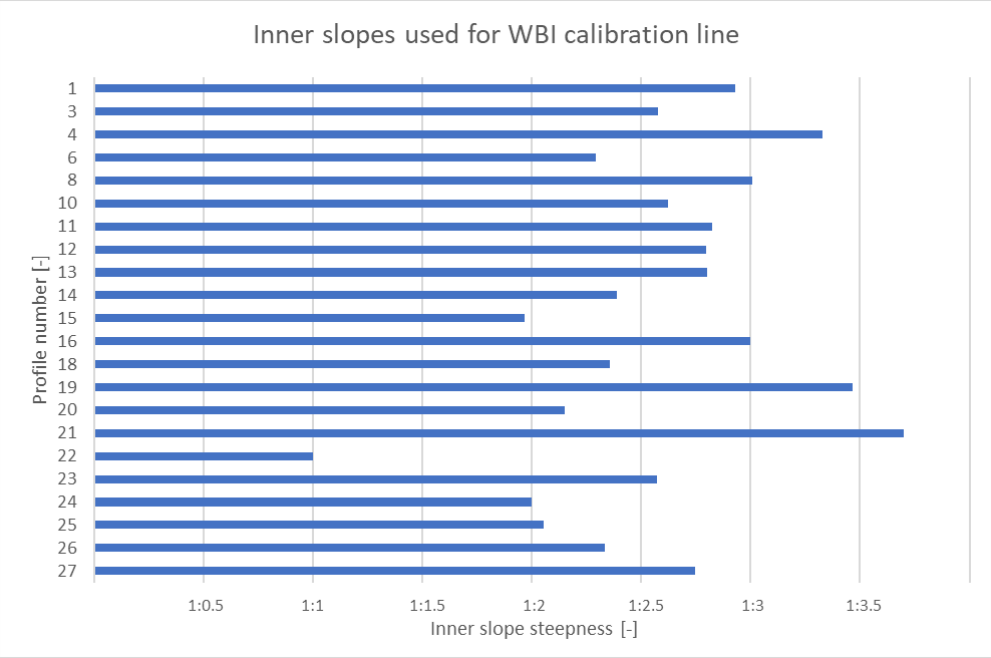

Figure 19: Inner slope steepness used during WBI calibration study

Table 10: Assumed undrained shear strength ratio (S) for silty clay and organic clay

Parameter	Mean value basis calculations [-]	Coefficient of variation basis calculations [-]	Assumed mean value [-]	Assumed coefficient of variation [-]	Distribution	Design value [-]
Silty clay S	0.28	0.03	0.31	0.10	Lognormal	0.26
Organic clay S	0.24	0.10	0.29	0.20	Lognormal	0.20

Since the results of inner slope stability with overtopping for which the internal friction angle of dike material has the largest influence factor are far at the left of the WBI calibration line (see the influence factors of 11E and 11F(11D) in Figure 20 and see Figure 21), it would be interesting to investigate whether these results would go towards the WBI calibration line after changing the coefficient of variation of the internal friction angle of dike material in the calculations. The coefficient of variation of the internal friction angle of dike material of JAV is approximately 0.08 based on Table 2. A coefficient of variation of 0.05-0.15 has been used for the tangent of the effective friction angle during the calibration study (Kanning, Teixeira, Van der Krogt, & Rippi, 2017) and a coefficient of variation of 0.10 is an expected value for the critical state angle of the internal friction of dike material according to 'Schematiseringshandleiding macrostabiliteit' (Rijkswaterstaat, Water Verkeer en Leefomgeving, 2021). For this reason, the coefficient of variation of approximately 0.08 for the internal friction angle of dike material of JAV can be considered reasonable and has not been changed.

4. Results

The obtained results are given in this chapter. Each paragraph in this chapter deals with one of the sub-questions in paragraph 1.3. Paragraph 4.1 deals with sub-question one, paragraph 4.2 deals with sub-question two etc.

4.1 Inconsistency between the basis semi-probabilistic and probabilistic estimates of the reliability index

The results of the basis semi-probabilistic and probabilistic calculations of JAV are shown in this paragraph. Besides, a comparison has been made between the results of the basis semi-probabilistic and probabilistic calculations in this paragraph. The results of the fragility points and the fragility curves can be found in appendix B.

4.1.1 Basis semi-probabilistic calculations inner slope stability

The obtained safety factors of the basis semi-probabilistic calculations without overtopping are given in Table 11. The damage factor has been determined by dividing the safety factor by the model factor. The reliability index has been estimated based on the damage factor and the calibration equation given in paragraph 2.4.1. The reliability indexes of the basis semi-probabilistic calculations given overtopping are also estimated based on the damage factors and they are shown in Table 12.

Table 11: Reliability index basis semi-probabilistic calculations without overtopping

Dike section	Safety factor [-]	Damage factor γ_n [-]	Reliability index β [-]
10C	1.34	1.26	5.68
11E	1.30	1.23	5.45
11F(11D)	1.31	1.23	5.48
13A	1.27	1.20	5.27
13E1	1.31	1.23	5.48
13E2	1.31	1.24	5.53

Table 12: Reliability index basis semi-probabilistic calculations given overtopping

Dike section	Safety factor [-]	Damage factor γ_n [-]	Reliability index β [-]
10C	1.30	1.22	5.41
11E	0.92	0.87	3.05
11F(11D)	0.99	0.94	3.52
13A	1.31	1.24	5.52
13E1	1.32	1.25	5.59
13E2	1.33	1.25	5.61

4.1.2 Basis probabilistic calculations inner slope stability

The reliability indexes of the basis probabilistic calculations have been estimated per dike section from the combined fragility curve, fragility curve without overtopping and the fragility point with the largest contribution to 1 l/s/m overtopping. The probabilistic reliability indexes are shown in Table 13. The fragility curves and the conditional reliability indexes per water level for the six dike sections are shown in appendix B.

Table 13: Reliability index basis probabilistic calculations

Dike section	Reliability index β combined fragility curve [-]	Reliability index β without overtopping [-]	Reliability index β given overtopping [-]
10C	6.29	6.38	5.61
11E	3.72	5.34	0.12
11F(11D)	4.50	8.35	1.06
13A	8.36*	8.43*	8.46*
13E1	7.14	7.19	6.81
13E2	7.27**	7.27**	6.66

** The reliability index of inner slope stability given overtopping is a little bit larger than the reliability index of inner slope stability from the combined fragility curve and without overtopping. The reason for this is that the reliability index of inner slope stability given overtopping is not estimated from the fragility curve, but it is conditional on the 1 l/s/m overtopping water level and that overtopping occurs at that water level. The design point of the water level is higher for the reliability index of inner slope stability from the combined fragility curve and without overtopping than the 1 l/s/m overtopping water level*

*** For relatively high water levels is the fragility curve for inner slope stability without overtopping almost equal to the fragility curve for inner slope stability given overtopping (see appendix B). For this reason, the reliability index of inner slope stability from the combined fragility curve is approximately equal to the reliability index of inner slope stability without overtopping*

One can see from Table 13 that there is an enormous difference between the reliability index without overtopping and the reliability index given overtopping for dike section 11E and 11F(11D). Therefore, overtopping has a large effect on the estimated failure probability when one is dealing with small slip planes (which is the case for dike section 11E and 11F(11D) with overtopping).

In Figure 20 are the influence factors shown. One can see from Figure 20 that the undrained organic clay properties have the largest influence on the failure probability for many dike sections. The internal friction angle of dike material has the largest influence factor for dike section 11E with and without overtopping and dike section 11F(11D) with overtopping, because small slip planes that are mostly situated in the dike material are found for these cases.

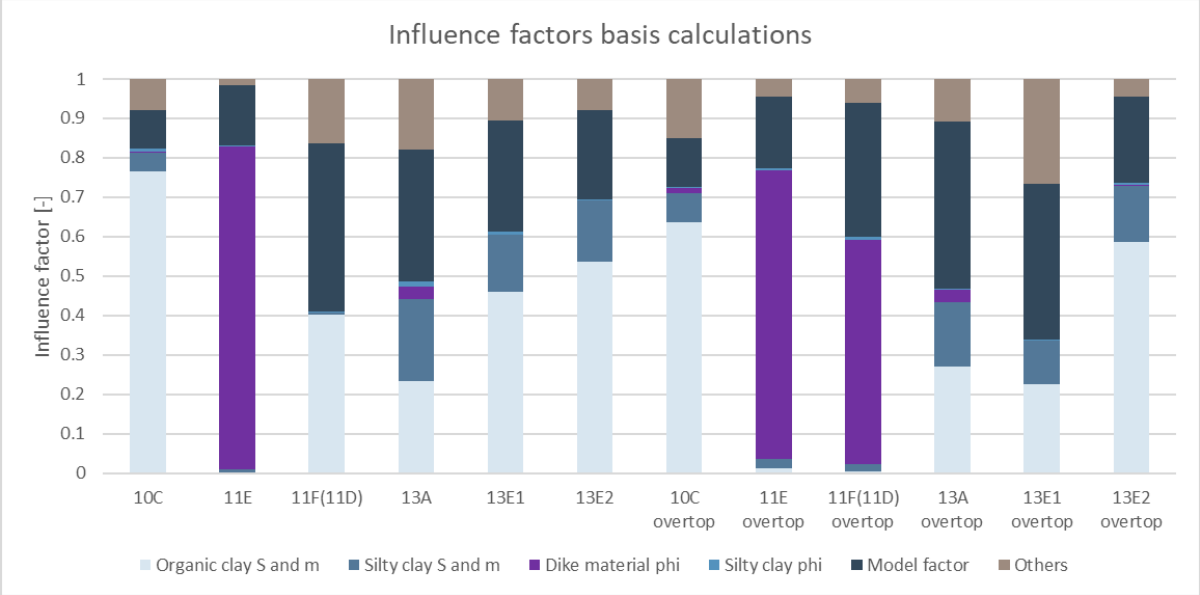

Figure 20: Influence factors basis calculations at WBN without overtopping and at the 1 l/s/m overtopping water level with overtopping

4.1.3 Comparison of the basis semi-probabilistic and probabilistic results

A comparison between the estimates of the reliability index per dike section can be found in appendix B. In Figure 21 are the results of the basis calculations of JAV plotted with the results of the WBI calibration study. It is unwanted that results are far away from the WBI calibration line (this would mean a large inconsistency between the estimated reliability index based on the semi-probabilistic calculations and the reliability index based on the probabilistic calculations) and it is also unwanted that too many results are on the left of the WBI calibration line (in this case are the semi-probabilistic results too optimistic). One can see from Figure 21 that two yellow diamond shapes (which correspond to dike section 11E and 11F(11D) given overtopping) are far on the left from the WBI calibration line, which means that these semi-probabilistic results are too optimistic. Besides, there are also points far at the right of the calibration line, which means that these semi-probabilistic results are too conservative.

The sample standard deviation of the cases of JAV without overtopping (red dots in Figure 21) is in terms of reliability index 1.80, while the sample standard deviation of the cases of WBI used for calibration line in Figure 21 is in terms of reliability index equal to 0.90, when one assumes that the calibration line represents the sample mean of the reliability indexes. So, the sample standard deviation is a factor two larger for JAV without overtopping than for the cases used for the WBI calibration line. For both situations are the effects of overtopping not included. The inconsistency increases when the effects of overtopping are included, because the sample standard deviation of the cases of JAV based on the combined fragility curve (blue squares in Figure 21) is in terms of reliability index 1.98 and the sample standard deviation of the cases of JAV given overtopping (yellow diamond shapes in Figure 21) is in terms of reliability index 2.28. Overall, there is a large inconsistency between the semi-probabilistic and probabilistic estimates of the reliability index when one compares the results of JAV with the results of WBI used for calibration line.

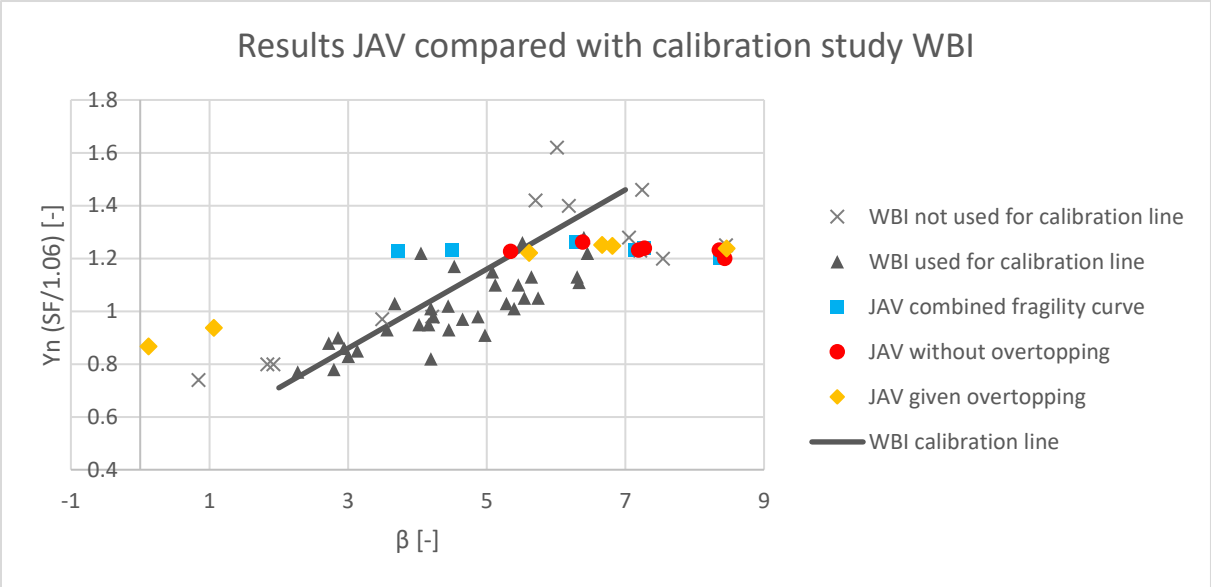

Figure 21: Results of the basis calculations of JAV compared with the calibration study of WBI. The vertical position of the results of JAV from the combined fragility curves (blue squares) are determined based on the semi-probabilistic results without overtopping

4.2 Incorporating additional stochastic variables in the probabilistic calculations

The results of incorporating additional stochastic variables are shown in this paragraph. The effects of the cohesion of the clay cover stochastic, internal friction angle of the clay cover stochastic, a combination of the cohesion and internal friction angle of the clay cover stochastic and different pore water pressure distribution scenarios with overtopping are shown in this paragraph. Please note that the semi-probabilistic results with the cohesion and the internal friction angle of the clay cover stochastic are the same as for the basis calculations, because the design values are not changed.

4.2.1 Cohesion of the clay cover

The fragility points, the fragility curves, the reliability indexes, a comparison between the results per dike section and the influence factors can be found in appendix C. In Figure 22 are the results shown of the calculations of JAV with the cohesion of the clay cover modelled as a stochastic variable and the results of the basis calculations of JAV. The differences shown in Figure 22 are the horizontal differences between the results of JAV and the WBI calibration line in terms of reliability index when one plots the results like it was done in Figure 21 for example. If a difference is negative, then the results of JAV are on the left of the WBI calibration line (so in that case are the semi-probabilistic results too optimistic). One can see from Figure 22 that the differences become less negative for dike section 11E and 11F(11D) given overtopping after modelling the cohesion of the clay cover stochastic. However, the differences are still negative and the results of these two dike sections given overtopping are still quite far from the WBI calibration line. So, the results of the semi-probabilistic calculations are for these two cases still too optimistic. Besides, the effect of modelling the cohesion of the clay cover stochastic is limited for the results of the other dike sections. Please note that the differences shown in Figure 22 for 11F(11D) without overtopping are far larger than for 11F(11D) given overtopping. The reason for this is that for those two cases are different slip planes and influence factors found (a large slip plane is found for 11F(11D) without overtopping and a small slip plane is found for 11F(11D) given overtopping).

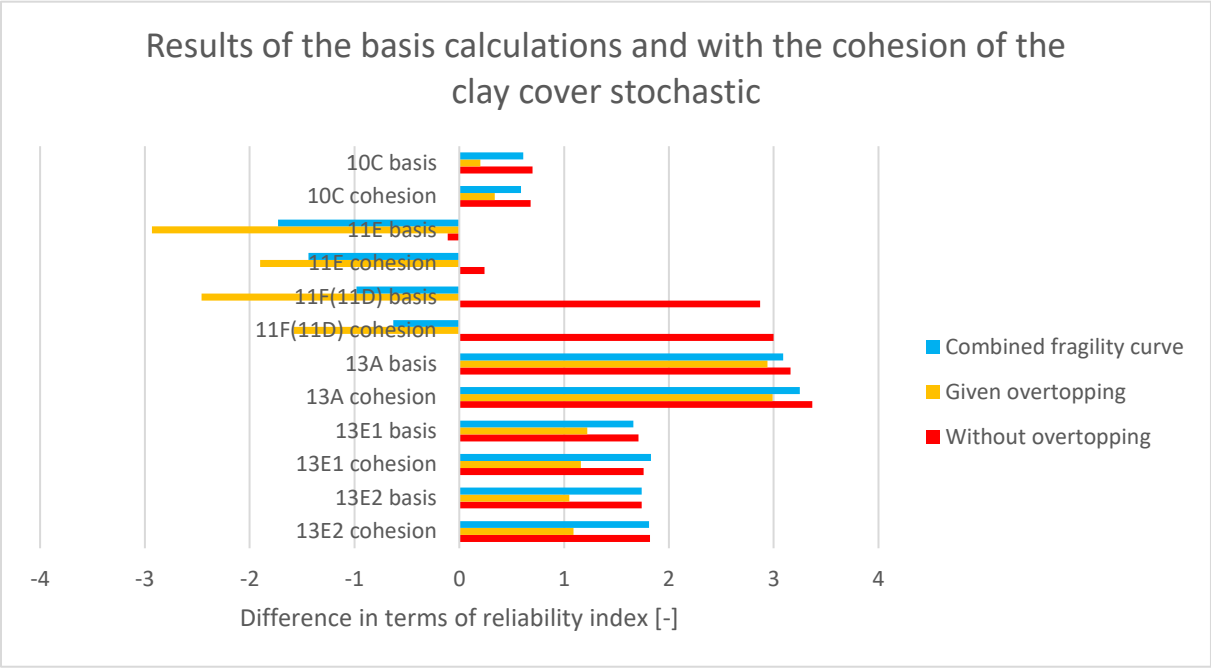

Figure 22: The results of the basis calculations of JAV and with the cohesion stochastic compared with the calibration study of WBI. The semi-probabilistic results without overtopping are used to determine the difference in terms of reliability index for the combined fragility curves

4.2.2 Internal friction angle of the clay cover

The fragility points, the fragility curves, the reliability indexes, a comparison between the results per dike section and the influence factors can be found in appendix D. In Figure 23 are the results shown of the calculations of JAV with the internal friction angle of the clay cover modelled as a stochastic variable and the results of the basis calculations of JAV. The results are less affected after modelling the internal friction angle of the clay cover stochastic in Figure 23, than after modelling the cohesion of the clay cover stochastic in Figure 22 (see for example the effects on dike section 11E and 11F(11D) given overtopping).

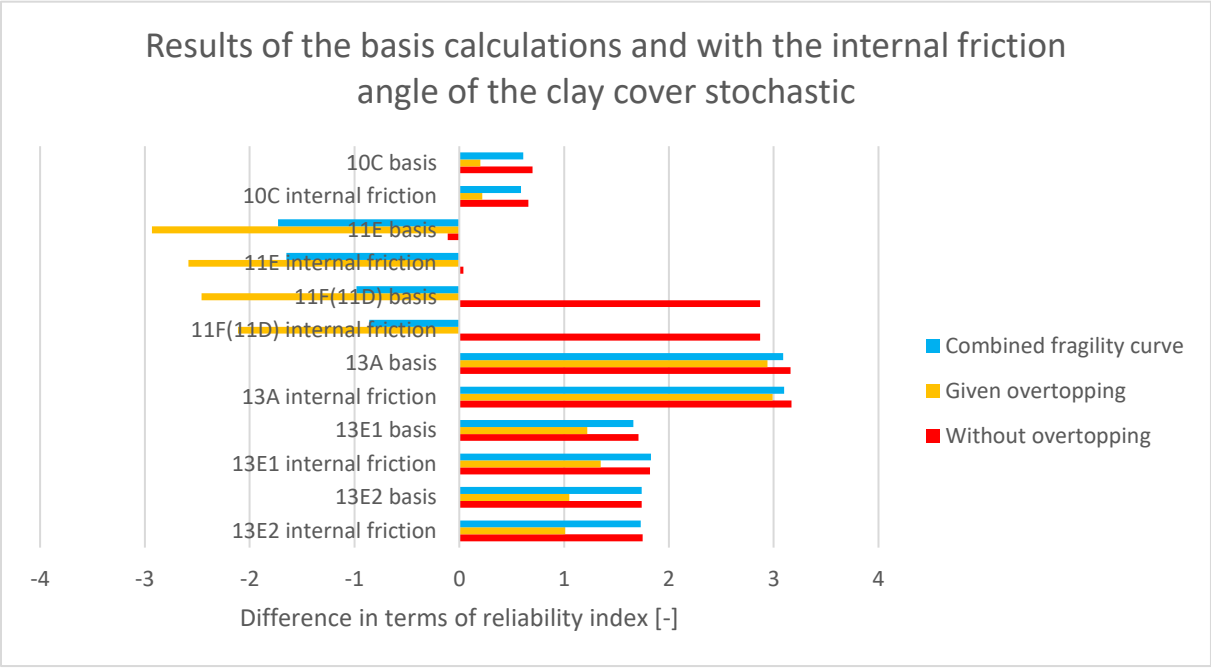

Figure 23: The results of the basis calculations of JAV and with the internal friction angle of the clay cover stochastic compared with the calibration study of WBI. The semi-probabilistic results without overtopping are used to determine the difference in terms of reliability index for the combined fragility curves

4.2.3 The cohesion and the internal friction angle of the clay cover

The fragility points, the fragility curves, the reliability indexes and a comparison between the results per dike section can be found in appendix E. In Figure 24 are the results shown of the calculations of JAV with the cohesion and the internal friction angle of the clay cover modelled stochastic and the results of the basis calculations of JAV. In Figure 25 are the influence factors shown. One can see from Figure 24 and Figure 25 that modelling the cohesion and the internal friction angle of the clay cover stochastic has an effect on the failure probability when one is dealing with relatively small slip planes (the dike sections with relatively small slip plane are 11E with and without overtopping and 11F(11D) with overtopping).

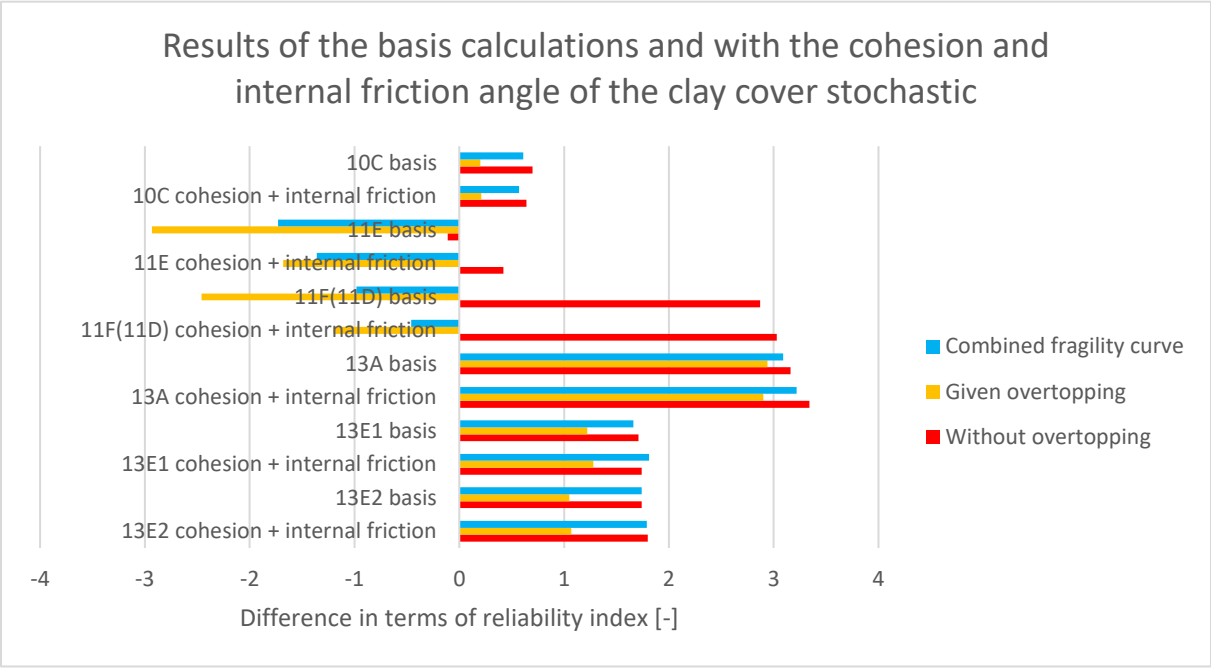

Figure 24: The results of the calculations of JAV with the cohesion and internal friction angle of the clay cover stochastic compared with the calibration study of WBI. The semi-probabilistic results without overtopping are used to determine the difference in terms of reliability index for the combined fragility curves

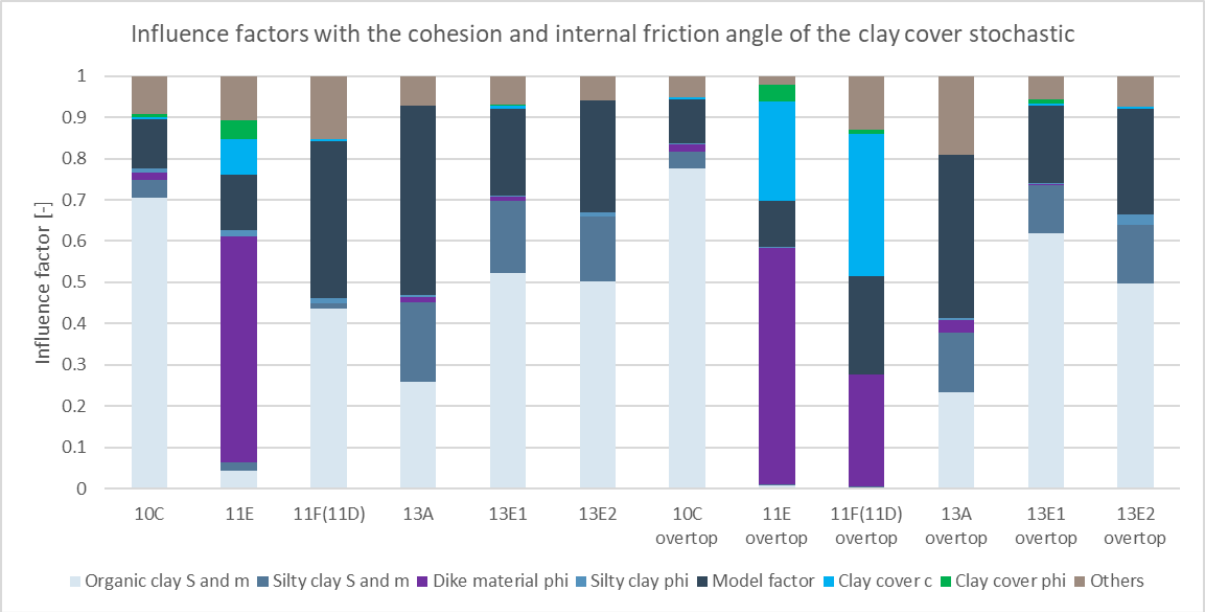

Figure 25: Influence factors with the cohesion and internal friction angle of the clay cover stochastic at WBN without overtopping and at the 1 l/s/m overtopping water level with overtopping

4.2.4 Overview results with the strength of the clay cover stochastic

The sample standard deviations for the cohesion and the internal friction angle of the clay cover stochastic are shown in Table 14. Please note that a large sample standard deviation means that the amount of variability of the results are large when one assumes that the calibration line represents the sample mean of the reliability indexes. The sample standard deviations are quite large after modelling the cohesion and the internal friction angle of the clay cover stochastic for JAV, when one

considers that the sample standard deviation of the calibration study is equal to 0.90 in terms of reliability index. However, one could see from Figure 22, Figure 23 and Figure 24 that the results with a negative difference (the results on the left of the calibration line) are becoming less negative (the difference of 11E without overtopping becomes even positive). This means that the semi-probabilistic results become less optimistic after modelling the cohesion and the internal friction angle of the clay cover stochastic in the probabilistic calculation. Even though the sample standard deviations in Table 14 are still quite large, the sample standard deviation given overtopping decreases with 0.52 after modelling the cohesion and the internal friction angle of the clay cover stochastic in comparison with the basis calculations. The reason for this is that the results of 11E and 11F(11D) given overtopping (which are located far away from the calibration line) are shifted towards the calibration line. Modelling the cohesion and the internal friction angle of the clay cover stochastic has the largest effect on the reliability index for the dike sections with a relatively small slip plane of JAV (see appendix E).

Table 14: Sample standard deviations for the cohesion and the internal friction angle of the clay cover stochastic in terms of reliability index, when one assumes that the calibration line represents the sample mean of the reliability indexes

	Basis calculations	Cohesion stochastic	Internal friction angle stochastic	Cohesion and internal friction angle stochastic
Sample standard deviation combined fragility curve [-]	1.98	2.00	1.99	1.96
Sample standard deviation without overtopping [-]	1.80	1.90	1.81	1.89
Sample standard deviation given overtopping [-]	2.28	1.88	2.14	1.76

4.2.5 Pore water pressure distribution with overtopping

The fragility points, the fragility curves and the influence factors for the 'hydrostatic' pore water pressure distribution with overtopping can be found in appendix F and for the 'interpolation' pore water pressure distribution with overtopping in appendix G. A comparison between the results of the different pore water pressure distributions with overtopping can be found in appendix H. In Table 15 are the probabilistic estimates of the reliability index based on the combined fragility curves shown for different combinations of the pore water pressure distribution with overtopping. Besides, in Table 16 are the probabilistic estimates of the reliability index given overtopping shown for different combinations of the pore water pressure distribution with overtopping.

It can be seen from Table 16 that the uncertainty in the pore water pressure distribution with overtopping has an influence on the results. Not only is this the case for dike sections with relatively small slip planes (see for example the reliability indexes of dike section 11E), but also for dike sections with relatively large slip planes (see for example the reliability indexes of dike section 13A). According to the memo 'Pore water pressure uncertainties for slope stability' has the phreatic line uncertainty limited effect on the reliability. Changing the phreatic surface at the outer crest line and the inner crest line with 0.9 m for two cases, leaded to a difference of 0.01 and 0.077 on the reliability index (Kanning & Van der krogt, 2016). During that research were the effects of overtopping not included and were large slip planes considered. Taking into account the uncertainty

of the pore water pressure distribution with overtopping has an influence on the estimates of the reliability index for small and large slip planes based on Table 16.

Table 15: Probabilistic reliability index based on the combined fragility curve with different combinations for the pore water pressure distribution given overtopping

Dike section	Probabilistic reliability index combination 1 β [-]	Probabilistic reliability index combination 2 β [-]	Probabilistic reliability index combination 3 β [-]	Probabilistic reliability index combination 4 β [-]
10C	6.15	6.29	6.07	6.14
11E	3.73	3.75	3.61	3.67
11F(11D)	4.40	4.53	4.27	4.36
13A	7.79	8.36	7.69	7.77
13E1	7.03	7.15	6.95	7.02
13E2	6.88	7.27	6.77	6.87

Table 16: Probabilistic reliability index given overtopping with different combinations for the pore water pressure distribution

Dike section	Probabilistic reliability index combination 1 β [-]	Probabilistic reliability index combination 2 β [-]	Probabilistic reliability index combination 3 β [-]	Probabilistic reliability index combination 4 β [-]
10C	5.39	5.63	5.26	5.36
11E	0.11	0.26	-0.61	-0.16
11F(11D)	0.73	1.14	0.16	0.58
13A	7.16	8.46	7.05	7.15
13E1	5.39	6.81	5.24	5.37
13E2	5.83	6.67	5.69	5.81

In appendix I are the results of the calculations of JAV with different combinations of the pore water pressure distribution with overtopping plotted with the results of the WBI calibration study. The sample standard deviations for the different combinations of the pore water pressure distribution with overtopping are shown in Table 17. The results of the 'basis' pore water pressure distribution are used for the semi-probabilistic results in the plots in appendix I and to determine the sample standard deviations in Table 17. The sample standard deviations are large for every combination, when one considers that the sample standard deviation of the calibration study is equal to 0.90 in terms of reliability index. Besides, it can be seen from Table 17 that the used combination of the pore water pressure distribution influences the sample standard deviation of the results. For this reason, taking into account the uncertainty of the pore water pressure distribution with overtopping has an influence on the results, but despite the influence of it, there is still an inconsistency between the semi-probabilistic and probabilistic estimates of the reliability index with overtopping, based on the used combinations.

Table 17: Sample standard deviations for the different combinations of the pore water pressure distribution given overtopping in terms of reliability index, when one assumes that the calibration line represents the sample mean of the reliability indexes

	'Basis' pore water pressure distribution	Combination 1	Combination 2	Combination 3	Combination 4
Sample standard deviation combined fragility curve [-]	1.98	1.73	1.98	1.70	1.73
Sample standard deviation given overtopping [-]	2.28	1.96	2.23	2.33	2.08

4.3 The influence of the steepness of the inner slope on the inconsistency

The results of the semi-probabilistic and probabilistic calculations with different slopes are shown in this paragraph. The fragility points, the fragility curves and the reliability indexes can be seen in appendix J for an inner slope steepness of 1:3, appendix K for 1:3.5, appendix L for 1:4, appendix M for 1:4.5 and appendix N for 1:5.

In Figure 26 are the results of the calculations of JAV with an inner slope steepness of 1:3 plotted with the results of the WBI calibration study. The results with an inner slope steepness of 1:3.5 are plotted in appendix K, for 1:4 in appendix L, for 1:4.5 in appendix M and for 1:5 in Figure 27. In Figure 26 are the results grouped for the different types of results with an inner slope steepness of 1:3. The results of JAV given overtopping in Figure 26 (yellow diamond shapes) are all located far on the left of the WBI calibration line. This means that the semi-probabilistic results are all far too optimistic for JAV given overtopping with an inner slope steepness of 1:3. The semi-probabilistic results are also too optimistic for JAV based on the combined fragility curve in Figure 26 (blue squares). On the other hand, the results of JAV without overtopping are all on the right of the WBI calibration line in Figure 26 (red dots). The results of JAV without overtopping with an inner slope steepness of 1:3 are quite close to the calibration line and are positioned quite well between the results of WBI used for calibration line.

An interesting result from Figure 26 is that the probabilistic reliability indexes for JAV given overtopping are all lower than the required reliability indexes for these dike sections given overtopping (see Table 5 for the required reliability indexes given overtopping), while for one dike section (13E1) the crest level is higher than the HBN in 2073 (see Table 5). For this reason, it is possible that a dike section could not meet the required failure probability for inner slope stability given overtopping, even if the crest level is higher than the HBN.

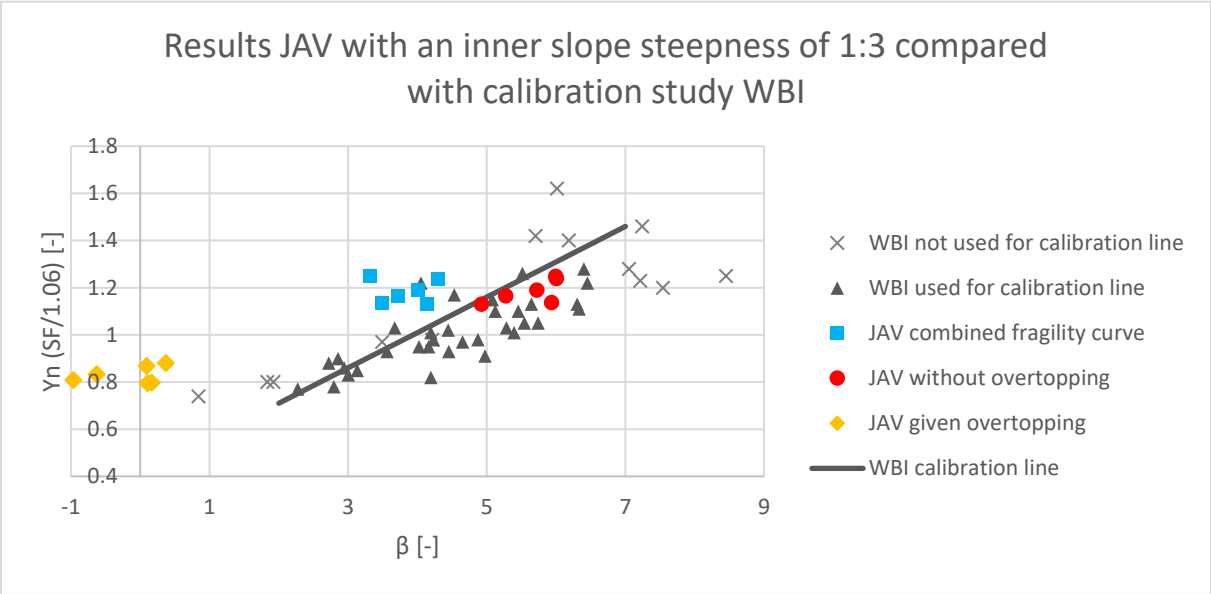

Figure 26: The results of the calculations of JAV with an inner slope steepness of 1:3 compared with the calibration study of WBI. The vertical position of the results of JAV from the combined fragility curves (blue squares) are determined based on the semi-probabilistic results without overtopping

It can be seen from Figure 27 that the results are shifted towards the right in comparison with Figure 26 after the steepness of the slope has been decreased. Besides, the results are shifted upwards after the slope steepness has been decreased. It is reasonable that the reliability index and the safety factor increases if the slope steepness decreases. However, the results of JAV are shifted more horizontally than vertically in comparison with the WBI calibration line. This can be seen from the number of results on the left of the calibration line in Figure 26 (all the results of JAV given overtopping and all the results based on the combined fragility curve) compared to the number of results on the left of the calibration line in Figure 27 (zero results).

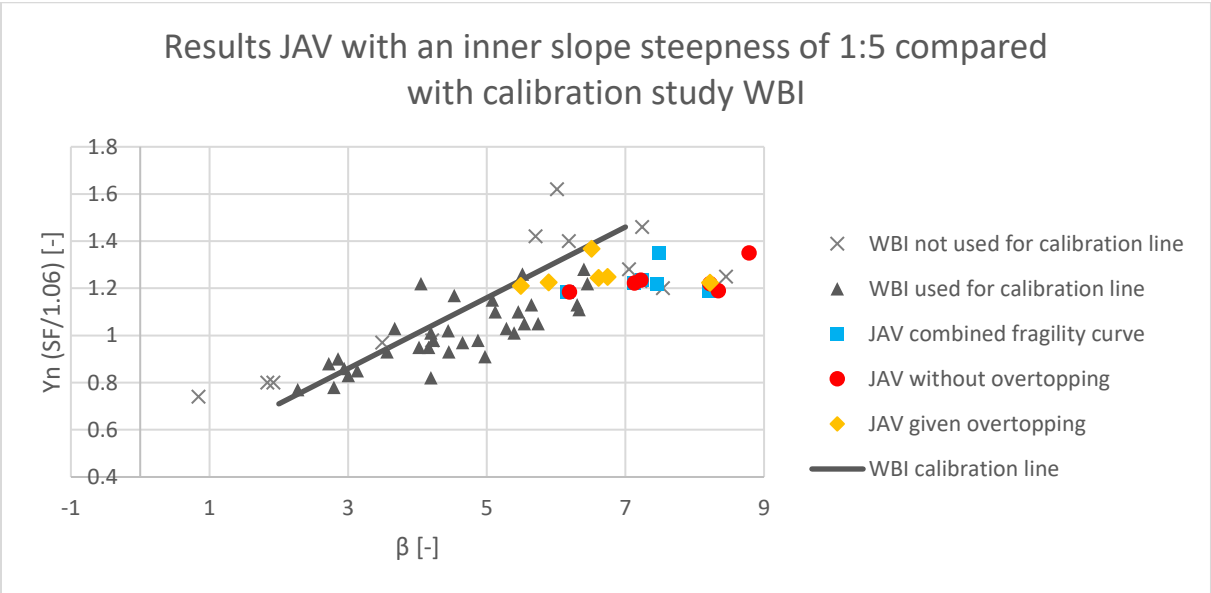

Figure 27: The results of the calculations of JAV with an inner slope steepness of 1:5 compared with the calibration study of WBI. The vertical position of the results of JAV from the combined fragility curves (blue squares) are determined based on the semi-probabilistic results without overtopping

The influence factors with an inner slope steepness of 1:3 are shown in Figure 28, for 1:3.5 in appendix K, for 1:4 in appendix L, for 1:4.5 in appendix M and for 1:5 in Figure 29. One can see from Figure 28 that for most cases the internal friction angle of the dike material has the largest influence factor. On the other hand, one can see from Figure 29 that the undrained soil characteristics of organic clay and silty clay have a larger influence factor for most cases with an inner slope steepness of 1:5, than the drained soil characteristic dike material phi. The influence factors are dependent on the position of the slip plane, which can change if the inner slope steepness changes.

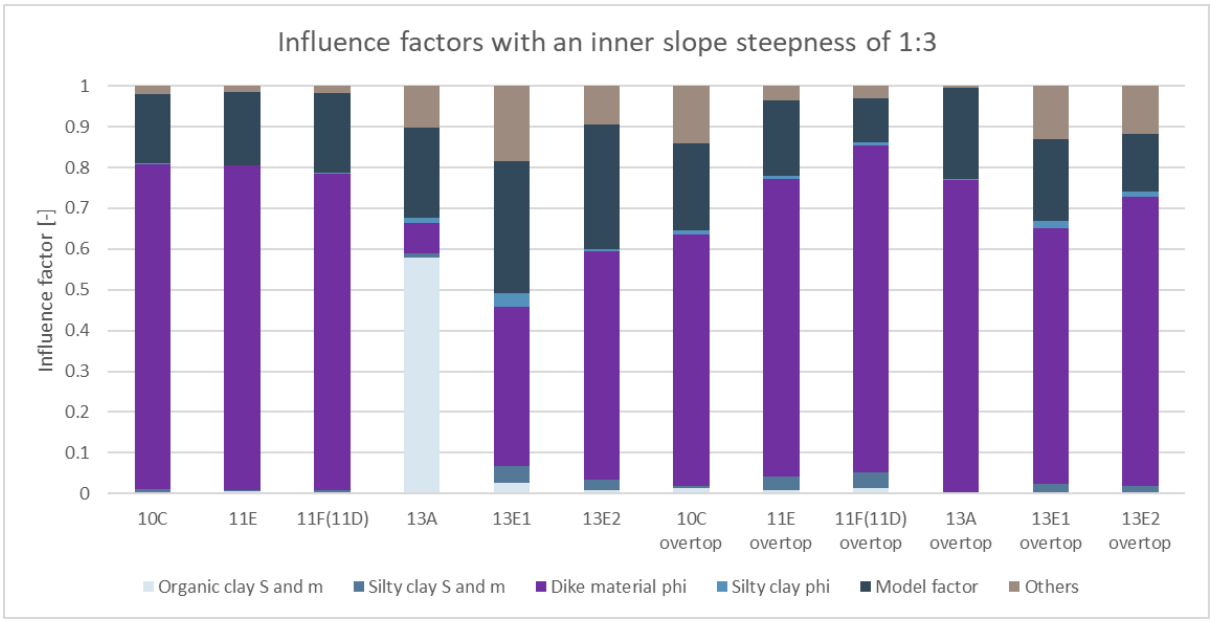

Figure 28: Influence factors with an inner slope steepness of 1:3 at WBN without overtopping and at the 1 l/s/m overtopping water level with overtopping

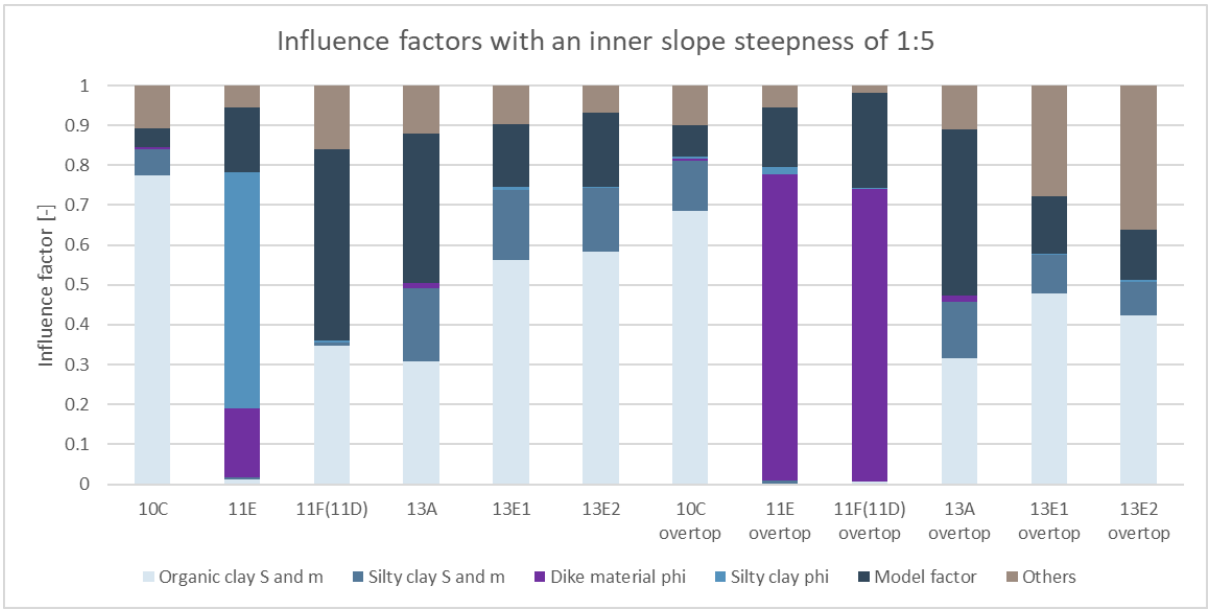

Figure 29: Influence factors with an inner slope steepness of 1:5 at WBN without overtopping and at the 1 l/s/m overtopping water level with overtopping

The sample standard deviations of JAV for different steepness of the inner slope are shown in Table 18 in terms of reliability index. The steepness of the inner slope has a large effect on the sample standard deviation, based on the sample standard deviations in Table 18. The sample standard deviation is for the combined fragility curve minimum with an inner slope steepness of 1:4, while this is minimum without overtopping with an inner slope steepness of 1:3 and for the results given overtopping with an inner slope steepness of 1:4.5. The largest sample standard deviation is found for the results given overtopping with an inner slope steepness of 1:3. The largest sample standard deviation of 3.27 is far larger than the sample standard deviation of 0.90 for the results of WBI used for calibration line.

Table 18: Sample standard deviations for the results of JAV with different inner slope steepness in terms of reliability index, when one assumes that the calibration line represents the sample mean of the reliability indexes

	Basis calculations	Slope 1:3	Slope 1:3.5	Slope 1:4	Slope 1:4.5	Slope 1:5
Sample standard deviation combined fragility curve [-]	1.98	1.56	0.96	0.87	1.59	2.08
Sample standard deviation without overtopping [-]	1.80	0.34	1.47	1.68	1.91	1.99
Sample standard deviation given overtopping [-]	2.28	3.27	1.86	1.15	0.86	1.45

According to the MSc thesis 'Revision of the calibration equation for a river dike on macro stability' of Melvin Prins, the influence of the gradient and width of the inner slope is not remarkable on the horizontal differences between the calibration line and the results of dike trajectory Streefkerk-Ameide-Fort Everdingen (SAFE). The effect of the geometry of the inner slope is negligible (Prins, 2021). In Figure 30 can the results of SAFE without overtopping be seen. One can see from the dotted line in Figure 30 that the influence of the gradient and width of the inner slope is not remarkable. Profiles where reinforcements are implemented are meant with design profiles in Figure 30. The difference on the horizontal axis in Figure 30 represents the horizontal differences between the calibration line and the results of SAFE in terms of reliability index. Most profiles of SAFE have a gradient of the inner slope between 20 and 25 degrees based on Figure 30. This corresponds to an inner slope steepness between approximately 1:2.1 and 1:2.7, while the influence of the inner slope steepness is investigated between 1:3 and 1:5 for JAV. For this reason, flatter slopes and a wider range of the steepness of the inner slope has been investigated for JAV. This could be the reason why different observations are found between JAV and SAFE.

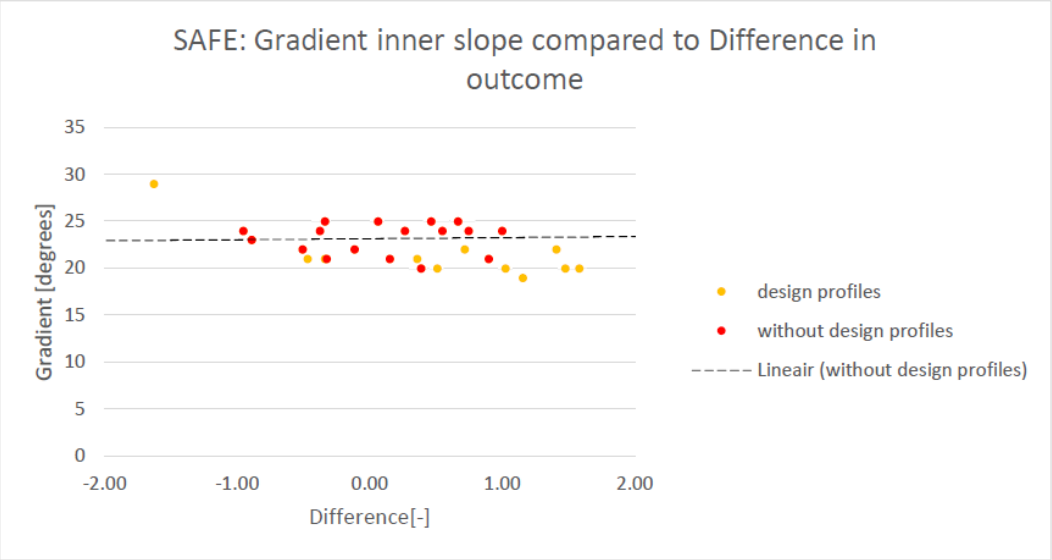

Figure 30: Effect gradient of the inner slope on the difference in reliability index without overtopping for SAFE (Prins, 2021)

4.4 Applicability of the calibrated WBI damage factor line of 2016

The results of the semi-probabilistic and probabilistic calculations with different slopes, the results with different coefficients of variation and the calibration line from dike trajectory SAFE are shown in this paragraph. The results of the fragility points, the fragility curves and the reliability indexes can be found in appendix O for the calculations of JAV with different coefficients of variation.

4.4.1 All the results of JAV with different slopes

One can see in Figure 31 that all the results of JAV without overtopping with different slopes are on the right of the calibration line. For this reason, the semi-probabilistic results of JAV without overtopping with different slopes are too conservative. Since the relation between the overall safety factor and the reliability index is fitted to the twenty percent quantiles of the betas during the calibration study (Kanning, Teixeira, Van der Krogt, & Rippi, 2017), it is unexpected that all the results of JAV without overtopping with different slopes are on the right of the calibration line. Most results of JAV without overtopping have a reliability index larger than seven, which were not considered for the calibration fit. The results of JAV without overtopping with a reliability index lower than seven are located between the results of WBI used for calibration line. It is unexpected that results are far at the right of the calibration line, which was also the case for some of the results of the basis calculations (see Figure 21).

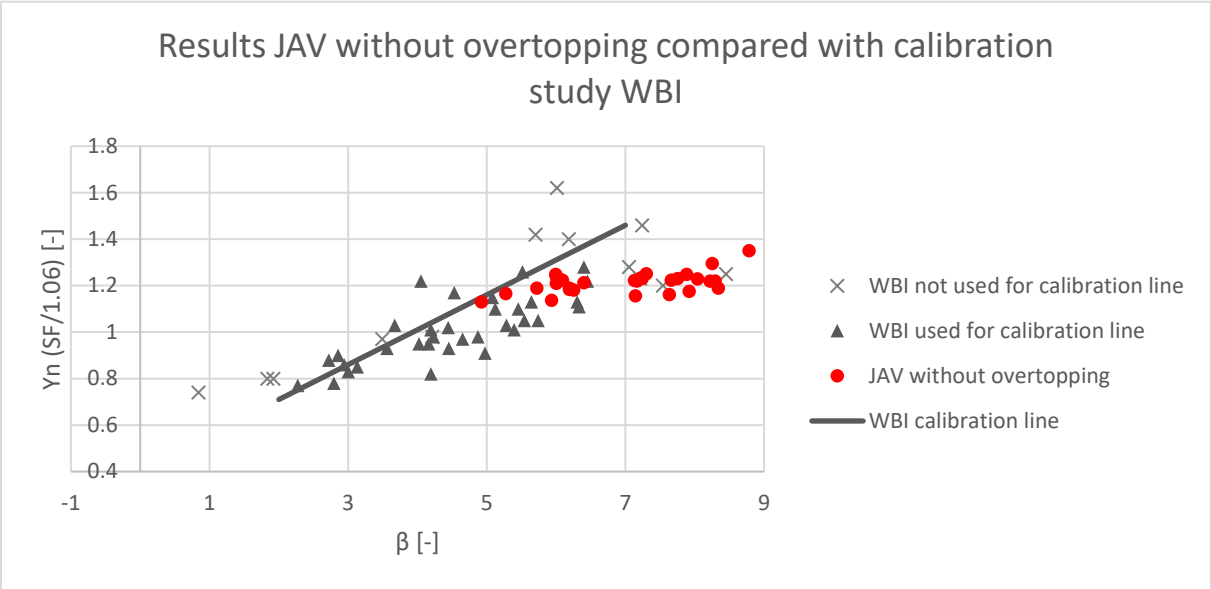

Figure 31: The results of the calculations of JAV without overtopping with different slopes compared with the calibration study of WBI.

The results of JAV from the combined fragility curves in Figure 32 are located further to the left than the results of JAV without overtopping in Figure 31, due to the effects of overtopping on the probabilistic estimates of the reliability index. The WBI calibration line is not applicable to compare the semi-probabilistic damage factor without overtopping with the probabilistic reliability index from the combined fragility curve based on the results of JAV in Figure 32. Since the effects of overtopping were not included in the probabilistic calculations of the WBI used for calibration line, it is reasonable that the calibration line cannot be used to compare the semi-probabilistic damage factor without overtopping with the probabilistic reliability index from the combined fragility curve. Nevertheless, the results of JAV show that taking into account the effects of overtopping by using the probability that 1 l/s/m overtopping occurs decreases the estimates of the reliability index from the probabilistic calculations considerably.

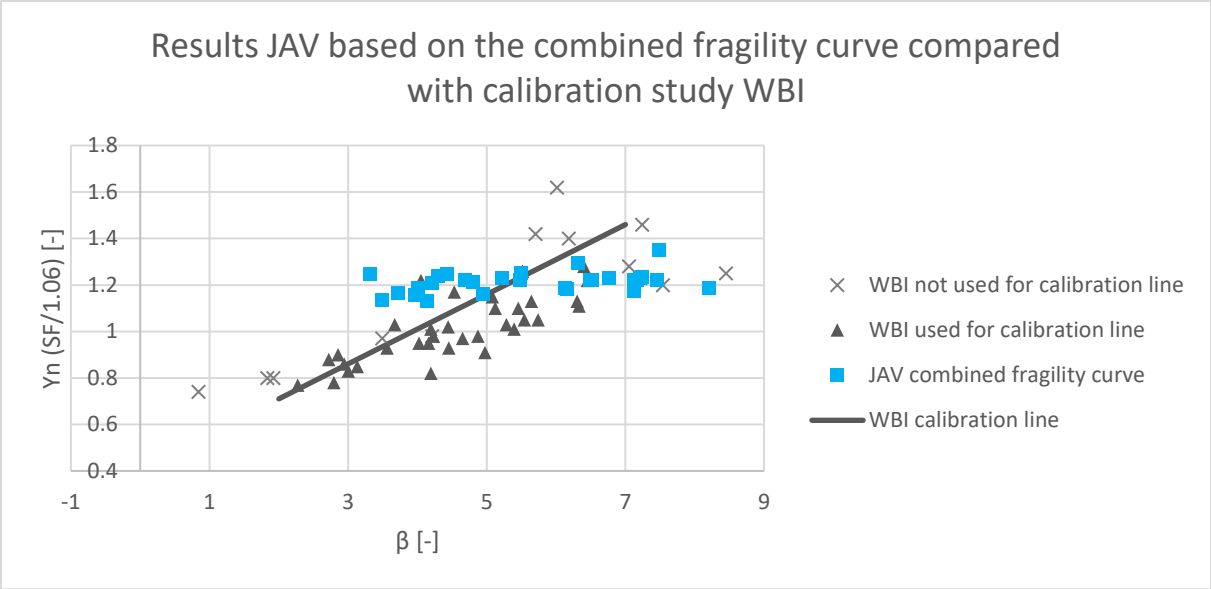

Figure 32: The results of the calculations of JAV based on the combined fragility curves with different slopes compared with the calibration study of WBI. The vertical position of the results of JAV from the combined fragility curves (blue squares) are determined based on the semi-probabilistic results without overtopping

The results of JAV given overtopping with different steepness of the inner slope are plotted in Figure 33. One can see from Figure 33 that there are many results of JAV given overtopping on the left of the calibration line, for which the semi-probabilistic results are too optimistic. One would expect a less steep relation between the damage factor and the reliability index for JAV given overtopping than the WBI calibration line, based on the results in Figure 33. The calibration line should be located higher at the beginning of the line at a reliability index of 2 based on the results of JAV. Since the required reliability index for JAV given overtopping is between 2.57 and 3.99 for the six considered dike sections in this research (see Table 5), the required safety factor should be larger for the semi-probabilistic assessment based on the results in Figure 33. Less dike sections would probably meet the required safety factor if the required safety factor becomes stricter.

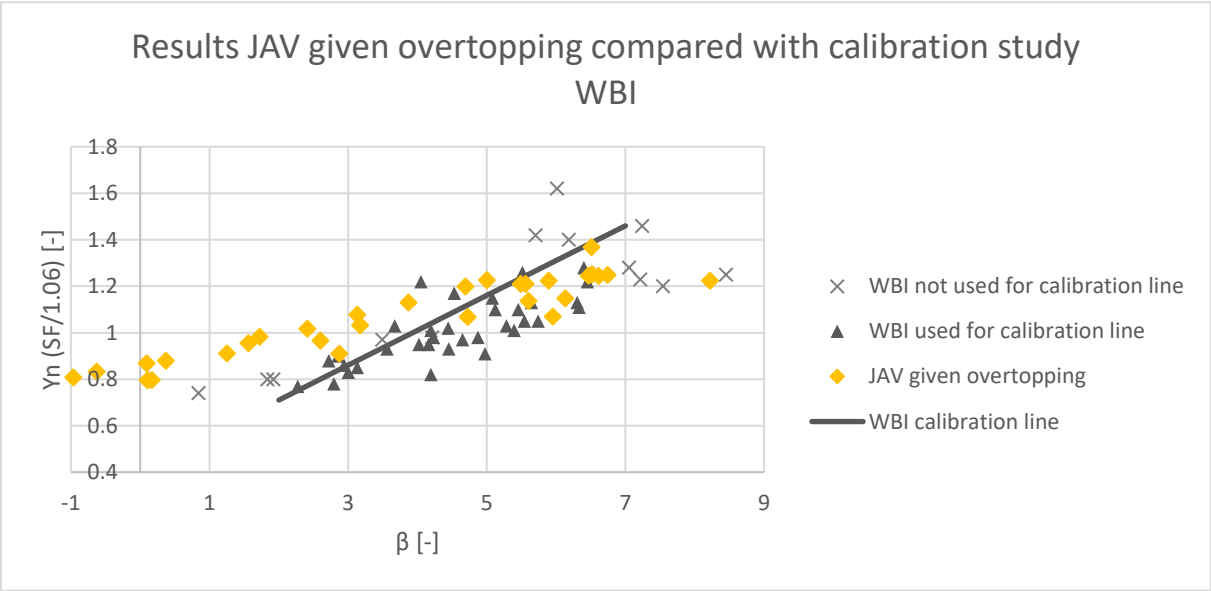

Figure 33: The results of the calculations of JAV given overtopping with different slopes compared with the calibration study of WBI

4.4.2 Calibration line from dike trajectory SAFE

A new calibration line is given in the MSc thesis 'Revision of the calibration equation for a river dike on macro stability' based on the results from dike trajectory SAFE. The WBI calibration line and the new calibration line based on the results of SAFE are shown in Figure 34. For both calibration lines are the effects of overtopping not considered. The calibration line of SAFE is a bit flatter than the WBI calibration line. Besides, the calibration line of SAFE is a bit higher at a reliability index of 2 than the WBI calibration line. The two calibration lines have almost the same damage factor for a reliability index of 7. Since the calibration line of SAFE is located higher than the WBI calibration line for reliability indexes lower than 7, it does not seem useful for JAV without overtopping based on the results in Figure 31. Unfortunately, the calibration line of SAFE is, just like the WBI calibration line, still too low for relatively low reliability indexes for JAV given overtopping based on the results in Figure 33.

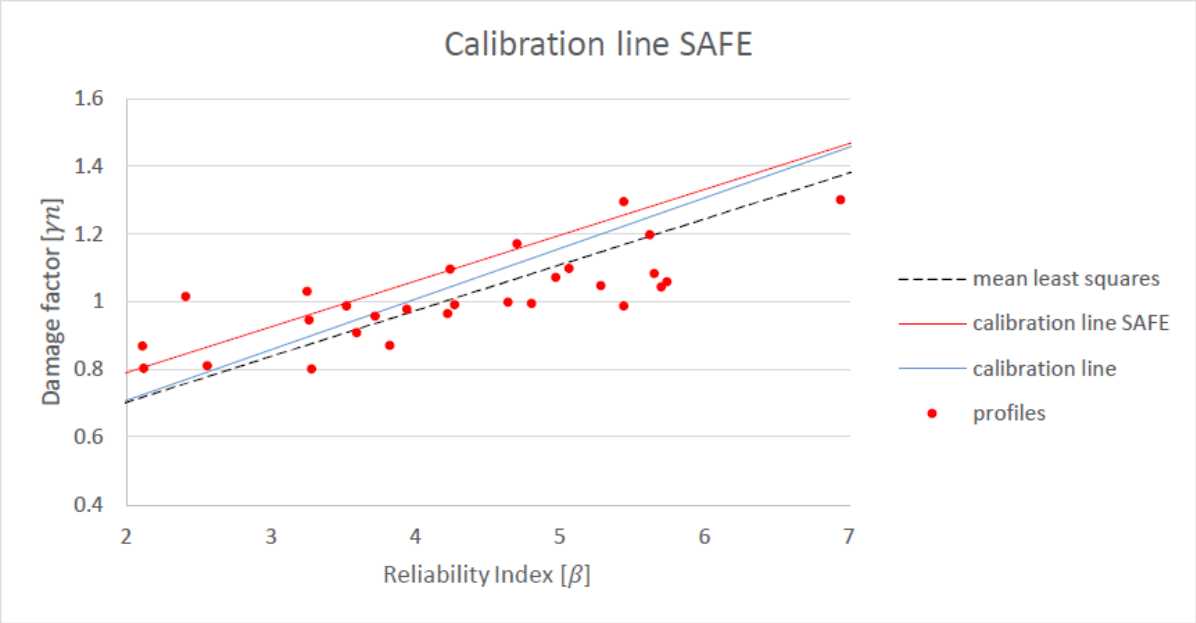

Figure 34: Calibration lines from the WBI calibration study (blue) and SAFE (red) (Prins, 2021)

4.4.3 Different coefficients of variation for the undrained shear strength ratio

The results with different coefficients of variation for the undrained shear strength ratio are shown in Figure 35. The reliability index decreases for most dike sections after increasing the coefficients of variation of the undrained shear strength ratio of organic clay and silty clay. When the coefficient of variation increases, then the probability density function of that variable becomes wider. It is reasonable that the reliability index decreases when the uncertainty increases. Based on the results in Figure 35, it turned out that some results of the basis calculations of JAV were relative far at the right of the WBI calibration line, due to the relatively small coefficients of variation used in the calculations for the undrained shear strength ratio of organic clay and silty clay.

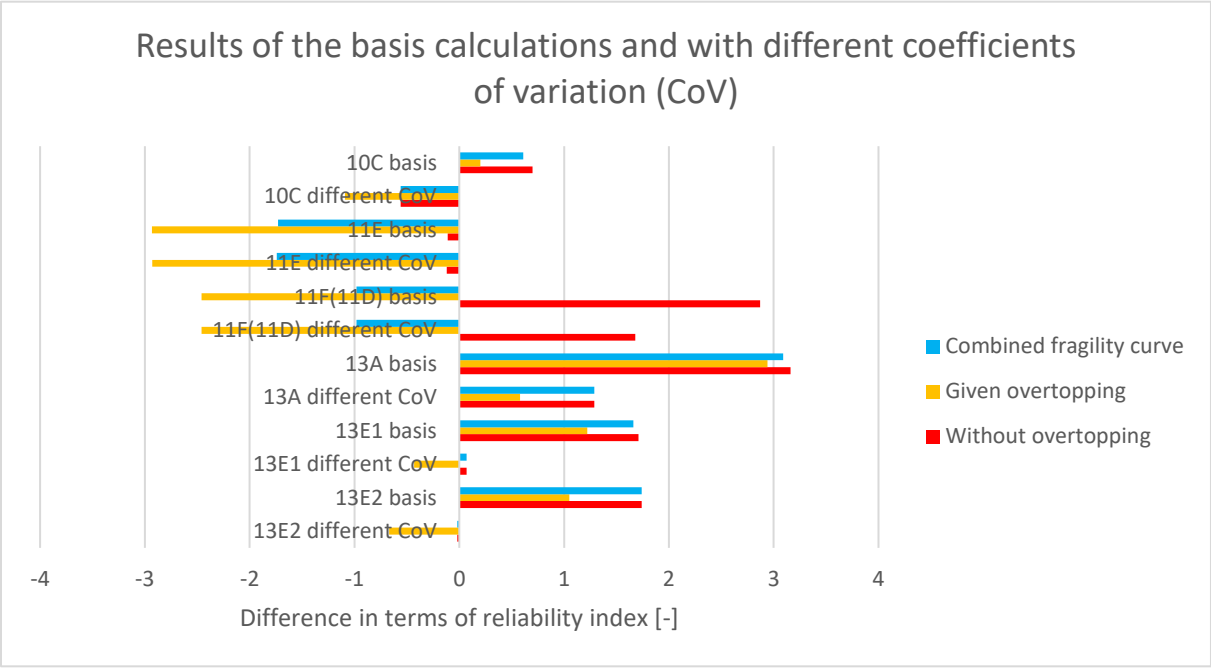

Figure 35: The results of the basis calculations of JAV and with different coefficients of variation compared with the calibration study of WBI. The semi-probabilistic results without overtopping are used to determine the difference in terms of reliability index for the combined fragility curves

In Table 19 are the sample standard deviations with different coefficients of variation shown. One can see from Table 19 that the sample standard deviations decrease after increasing the coefficients of variation for the undrained shear strength ratio of organic clay and silty clay. The sample standard deviation of JAV without overtopping is after increasing the coefficients of variation even the same as the sample standard deviation of the calibration study of 0.90 in terms of reliability index. However, it is a bit unexpected that three of the six dike sections of JAV in Figure 35 have a negative difference in terms of reliability index for the results without overtopping after increasing the coefficients of variation, since the relation between the overall safety factor and the reliability index is fitted to the twenty percent quantiles of the betas for the calibrated WBI damage factor line of 2016 (Kanning, Teixeira, Van der Krogt, & Rippi, 2017). On the other hand, the negative differences of dike section 11E and 13E2 without overtopping with different coefficients of variation are relatively small (see Figure 35).

Table 19: Sample standard deviations for the basis calculations of JAV and with different coefficients of variation in terms of reliability index, when one assumes that the calibration line represents the sample mean of the reliability indexes

	Basis calculations	Different coefficients of variation (CoV)
Sample standard deviation combined fragility curve [-]	1.98	1.09
Sample standard deviation without overtopping [-]	1.80	0.90
Sample standard deviation given overtopping [-]	2.28	1.83

5. Discussions

The assumptions and limitations are discussed in paragraph 5.1. After this, the implications for assessing inner slope stability are discussed in paragraph 5.2.

5.1 Assumptions and limitations

The reliability indexes of the probabilistic calculations without overtopping have been determined under the assumption that 1 l/s/m overtopping never occurs. As a consequence, conditional failure probabilities have been calculated after combining the fragility curves without overtopping with the statistics of the water level, based on the condition that overtopping never occurs. Furthermore, it is assumed that the probabilistic reliability indexes for inner slope stability given overtopping are equal to the conditional reliability indexes at the water levels that have the largest contribution to the probability of 1 l/s/m overtopping in 2073 (so for inner slope stability given overtopping are the reliability indexes estimated based on one fragility point instead of the fragility curve given overtopping). The reliability indexes for inner slope stability given overtopping have not been determined by integrating the fragility curve given overtopping with the statistics of the water level, because the reliability indexes would otherwise be considerably determined based on the part of the fragility curve for which it is unlikely that overtopping occurs. For this reason, the reliability indexes of inner slope stability given overtopping are conditional on the water level and that overtopping occurs at that water level.

Two semi-probabilistic calculations are performed for inner slope stability for the six considered dike sections of JAV. One calculation is without significant overtopping and the other calculation is with significant overtopping whereby the dike is saturated. For the probabilistic assessment are two fragility curves composed (one fragility curve including the effects of overtopping and one fragility curve excluding the effects of overtopping), which are combined based on the probability of the exceedance of 1 l/s/m overtopping. There are no semi-probabilistic results available to make a fair comparison with the probabilistic estimates of the reliability index based on the combined fragility curves. The probabilistic estimates of the reliability index based on the combined fragility curves are compared with the semi-probabilistic results without overtopping to investigate how the probabilistic estimates of the reliability index changes after including the probability of the exceedance of 1 l/s/m overtopping.

The water levels including subsidence that have the largest contribution to the probability of 1 l/s/m overtopping in 2073, have been used during the semi-probabilistic and probabilistic calculations with overtopping. It is uncertain whether the water level from the design point of the 1 l/s/m overtopping calculation is a suitable water level for the semi-probabilistic assessment of inner slope stability with overtopping, according to the KPR memo 'Voorstel t.a.v. beoordeling macrostabiliteit incl. golfoverslag' (Jongejan & De Visser, 2017). It is not investigated in this MSc thesis whether this water level is suitable for the calculations with overtopping.

The unit weight of the different soil types has been modelled deterministic in the probabilistic calculations. Besides, also the thickness of the soil layers has been modelled deterministic in the probabilistic calculations. Taking into account the uncertainty of the unit weight and the thickness of the layers could have influenced the results, but was not investigated in this MSc thesis.

It is assumed that undrained shear strength ratio S and strength increase exponent m are fully correlated in the probabilistic calculations. For this reason, the influence factors of the undrained

shear strength ratio S and strength increase exponent m are shown together for the different soil types.

The inner slope is steeper than 1:3 for most profiles used for the WBI calibration line (see Figure 19). It is a bit strange that the internal friction angle of dike material has the largest influence factor for most cases of JAV with an inner slope steepness of 1:3, while this is not the case for the profiles used for the WBI calibration line. The used coefficients of variation for the stochastic variables of JAV could have contributed to this difference. The effects of different coefficients of variation are not investigated for JAV with an inner slope steepness of 1:3 in this research.

In absence of local test data for the strength of the clay cover, literature has been used to model the cohesion and the internal friction angle of the clay cover stochastic. For this reason, the stochastic variables of the cohesion and the internal friction angle of the clay cover could be different in practice. Besides, the amount of research performed to the pore water pressure distribution with overtopping is limited. There is also no local test data for the pore water pressure distribution with overtopping. Therefore, multiple scenarios are assumed for the pore water pressure distribution with overtopping in this research.

Different results might be found after moving the position of the search or swarm scope in D-Stability (Van der Meij, 2020). A large slip plane was sometimes found with a large swarm scope, while a small slip plane was found with a small swarm scope for the same case. For this reason, the results are sensitive to errors based on the position of the swarm scope. Besides, the FORM analysis of D-Stability converges with twenty or more stochastic parameters usually, while it is often advised to use not more than ten stochastic parameters in a FORM analysis. For this reason, it is advised in the user manual of D-Stability to only model the parameters stochastic that influence the results significantly (Van der Meij, 2020). The probabilistic calculations are performed with more than twenty stochastic variables with Monte Carlo Importance Sampling in this research.

A maximum number of 1000 realizations has been used to determine the reliability index for a fragility point for most probabilistic calculations. The results could have been more accurate if the number of realizations would have been larger. A maximum number of 1000 realizations has been used to have an acceptable accuracy of the results and a reasonable computation time. The estimates of the reliability index could have been more accurate with a larger number of realizations if the computation capacity was larger. However, the difference between the expected reliability index and the 5% confidence bound of the reliability index is small for most fragility points. For this reason, it is expected that a larger number of realizations would not have increased the accuracy of the reliability indexes remarkably.

Only six dike profiles at one dike trajectory are investigated in this MSc thesis. The six dike profiles are all clay dikes. As a consequence, it is uncertain how representative these six dike profiles are to generalize the results.

Reliability indexes lower than two and larger than seven were not considered for the calibration fit during the WBI calibration study (Kanning, Teixeira, Van der Krogt, & Rippi, 2017). Reliability indexes lower than two and larger than seven are considered in this MSc thesis, because only six dike sections at JAV are considered during this research.

For some cases of JAV with different slopes is a small slip plane found based on the semi-probabilistic calculation and large slip planes found based on the probabilistic calculations (and the other way around) (see Table 20 and Table 21). This situation did only occur after changing the steepness of the inner slope. Table 20 and Table 21 show an advantage of determining the reliability index based on Monte Carlo Importance Sampling instead of FORM. Since a fixed slip circle should be used in a FORM analysis (see paragraph 2.4.3), the slip plane with the largest failure probability would possibly not has been found for some cases in Table 20 with a FORM analysis. The reliability indexes of the probabilistic calculations are determined based on Monte Carlo Importance Sampling in this MSc thesis. It is uncertain to what extend the estimates of the reliability index of the semi-probabilistic calculations can be compared with the estimates of the reliability index of the probabilistic calculations when different slip planes are found.

Table 20: Overview of the dimensions of the slip planes with different slopes

Dike section	1:3	1:3.5	1:4	1:4.5	1:5	1:3 overtop	1:3.5 overtop	1:4 overtop	1:4.5 overtop	1:5 overtop
10C										
11E										
11F(11D)										
13A										
13E1										
13E2										

Table 21: Legend for the overview of the dimensions of the slip planes with different slopes

Semi-probabilistic	Probabilistic
Small	Small
Large	Large
Small	Large
Large	Small

5.2 Implications for assessing inner slope stability

For some cases was the design point of the water level higher than the crest level, due to the used water levels in the probabilistic calculations. When the highest water level in the analysis is a few centimeters lower than the crest level, then the part of the fragility curve that is constructed by extrapolation to higher water levels is as small as possible. Probabilistic calculations with the water level a few centimeters below the crest level were performed for the cases where the design point of the water level was higher than the crest level. Performing probabilistic calculations with the water level a few centimeters lower than the crest level was effective for all those cases in preventing that the design point of the water level was higher than the crest level. For this reason, the highest considered water level in the probabilistic assessment of inner slope stability should be a few centimeters lower than the crest level.

The influence factors of the cohesion and the internal friction angle of in the clay cover in Figure 25 show that modelling the strength of the clay cover stochastic has an influence on the probabilistic estimates of the reliability index with relatively small slip planes. Besides, the influence factors in Figure 25 show that modelling the cohesion of the clay cover stochastic has a larger effect on the failure probability than the internal friction angle of the clay cover. However, it is uncertain whether the cohesion of the clay cover has a larger effect on the failure probability than the internal friction angle of the clay cover in general. The reason for this is that the used coefficient of variation of the

cohesion of the clay cover was more than two times larger than the used coefficient of variation of the internal friction angle of the clay cover in the calculations, which could have contributed to the larger influence factors for the cohesion of the clay cover in Figure 25. The cohesion and the internal friction angle of the clay cover should both be modelled stochastic when one is dealing with relatively small slip planes in the probabilistic assessment, due to their influence on the estimates of the reliability index.

With an inner slope steepness of 1:3 are all the reliability indexes from the probabilistic calculations given overtopping lower than the required reliability indexes given overtopping for the considered dike sections of JAV (see Figure 26 for the probabilistic estimates of the reliability index with an inner slope steepness of 1:3 and see Table 5 for the required reliability indexes given overtopping). For dike section 13E1 is the crest level higher than the HBN for an overtopping discharge of 1 l/s/m and a probability of 1/41667 per year in 2073 (see Table 5). This is possible, because the required failure probability for a cross-section for the failure mechanism GEKB (which is 1/41667 per year for JAV (Rijkswaterstaat Water, Verkeer en Leefomgeving, 2017)) is approximately a factor 10^4 larger than the required failure probability for a cross-section for inner slope stability (which is 3.23E-09 per year for JAV including the schematization factor of 1.1 (Broere, 2022)). A possibility would be to make a HBN calculation with the required failure probability for a cross-section for inner slope stability to check whether inner slope stability with overtopping could be a problem (if the HBN with the required failure probability for a cross-section for inner slope stability is smaller than the crest level after subsidence, then the estimated failure probability should be larger than one to not meet the required failure probability for inner slope stability with overtopping, which is physically impossible). However, it is not expected that the crest level after subsidence would be larger than the HBN with the required failure probability for a cross-section for inner slope stability, because the dike section would then be considerably overdesigned for the failure mechanism GEKB. For this reason, it should always be assessed whether a dike section meets the required failure probability for inner slope stability given overtopping based on the results of JAV.

The amount of available information in literature about the pore water pressures with overtopping is limited. The results of the infiltration tests with an overtopping discharge of 1.85 l/s/m at the IJsseldijk are used during this research. Since not all the results of the infiltration tests at the IJsseldijk follow the pore water pressure distributions in Figure 16 clearly, combinations with different probabilities of occurrence for the pore water pressure distributions are assumed. Taking into account the probability of occurrence for different pore water pressure distributions with overtopping has an influence on the estimates of the reliability index with overtopping based on the results of JAV in paragraph 4.2.5. The estimates of the reliability index for inner slope stability with overtopping can be improved by doing tests in practice to the pore water pressure distribution with overtopping.

Different mean values and coefficients of variation could lead to the same design value. The semi-probabilistic results are the same when the design values are equal with different mean values and coefficients of variation, while the probabilistic results would not be the same with different mean values and coefficients of variation. The coefficients of variation of the soil characteristics are not compared for every soil layer with the used coefficients of variation in the WBI calibration study. Different soil types are used during the WBI calibration study and it is unknown which soil types have the largest influence factors for the failure probability per case. For this reason, it was not possible to compare the coefficients of variation of JAV thoroughly with the coefficients of variation of the WBI calibration study, while the used coefficients of variation influence the estimates of the reliability

index based on Figure 35. Based on the results of JAV, the applicability of the WBI calibration line for the semi-probabilistic assessment of inner slope stability without overtopping is dependent on the used coefficients of variation in the calculations. The WBI calibration line is not suitable to estimate the failure probability for inner slope stability given overtopping based on the results of JAV, while the used coefficients of variation for the largest influence factors are reasonable.

The inner slope steepness of the six dike profiles of JAV has been adjusted between 1:3 and 1:5 to answer sub-question 3, while steeper slopes than 1:3 could be found in practice. Unfortunately, convergence problems occurred for inner slope stability given overtopping with an inner slope steepness of 1:2.5 for JAV. The failure probability is too close to one for inner slope stability given overtopping with an inner slope steepness of 1:2.5 for JAV. The reliability index would go to minus infinity if the failure probability goes to one. For this reason, inner slopes steeper than 1:3 are not investigated in this MSc thesis. The convergence problems are a point of interest for the probabilistic assessment with relatively steep slopes and when a calibration study for inner slope stability with overtopping would be performed to obtain a suitable calibration line for inner slope stability given overtopping.

6. Conclusions and recommendations

The findings of this research allow to draw the concluding remarks described in this chapter. First, the sub-questions and the research question are answered. After this, the recommendations are given.

6.1 Conclusions

Sub-question 1: 'What is the difference between the semi-probabilistic and probabilistic estimates of the reliability index of inner slope stability for the six dike sections that are calculated probabilistic of JAV?'

There is quite a large difference between the semi-probabilistic and probabilistic estimates of the reliability index of inner slope stability for the six considered dike sections of JAV. The sample standard deviation of JAV without overtopping is a factor two larger than the sample standard deviation of WBI used for the calibration line. A large sample standard deviation means that the amount of variability of the results are large when one assumes that the calibration line represents the sample mean of the reliability indexes. The sample standard deviation increases by including the effects of overtopping for JAV and therefore decreases the applicability of the WBI calibration line.

Sub-question 2: 'How incorporate additional stochastic variables in the probabilistic calculations to get a more precise estimate of the failure probability of inner slope stability?'

Modelling the cohesion and the internal friction angle of the clay cover stochastic in the probabilistic calculations have an effect on the estimates of the reliability index when one is dealing with relatively small slip planes. The uncertainty in the pore water pressure distribution with overtopping has an influence on the estimates of the reliability index given overtopping for dike sections with both relatively small and large slip planes. Although modelling the strength of the clay cover stochastic and taking into account the uncertainty of the pore water pressure distribution with overtopping have an influence on the estimates of the reliability index, there is still an inconsistency between the semi-probabilistic and probabilistic estimates of the reliability index. Nevertheless, a more credible estimate of the failure probability is obtained after modelling the strength of the clay cover stochastic and taking into account the uncertainty of the pore water pressure distribution with overtopping.

Sub-question 3: 'What is the influence of the dike slope steepness on the difference between the semi-probabilistic and probabilistic estimates of the reliability index of inner slope stability?'

With an inner slope steepness of 1:3 are the semi-probabilistic estimates of the reliability index far too optimistic for inner slope stability given overtopping for JAV, for which relatively small slip planes are found. The internal friction angle of dike material has a large influence factor with relatively small slip planes, while the undrained soil characteristics of organic clay and silty clay have a relatively large influence factor for most cases with a large slip plane of JAV. With an inner slope steepness of 1:5 are the semi-probabilistic estimates of the reliability index too conservative for JAV, for which generally large slip planes are found. Therefore, the inner slope steepness has a larger influence on the estimates of the reliability index of the probabilistic calculations than the semi-probabilistic calculations for the six dike sections of JAV.

Sub-question 4: 'To what extent is the calibrated WBI damage factor line of 2016 applicable for inner slope stability?'

The semi-probabilistic estimates of the reliability index for inner slope stability without overtopping are all too conservative for JAV when the coefficients of variation of the variables with a large

influence factor are relatively low, while this is not the case after increasing the coefficients of variation. For this reason, the applicability of the WBI calibration line of 2016 for inner slope stability without overtopping is dependent on the used coefficients of variation in the calculations. The calibration line is not suitable for the estimates of the reliability index based on the combined fragility curves when one is dealing with relatively small slip planes, because small slip planes for inner slope stability given overtopping have a too negative impact on the estimates of the reliability index from the combined fragility curves.

One would expect a less steep relation between the semi-probabilistic and probabilistic results and that the beginning of the calibration line should be located higher for relatively low reliability indexes for inner slope stability given overtopping based on the results of JAV (see Figure 33). As a consequence, the WBI calibration line of 2016 is not suitable to estimate the failure probability for inner slope stability given overtopping based on semi-probabilistic calculations.

Research question: 'How can the inconsistency be reduced between the semi-probabilistic and probabilistic estimates of the reliability index for inner slope stability with overtopping?'
The inconsistency between the semi-probabilistic and probabilistic estimates of the reliability index can be reduced by using a different calibration line for inner slope stability given overtopping than for inner slope stability without overtopping. The current WBI calibration line can be used for the assessment of inner slope stability without overtopping dependent on the used coefficients of variation in the calculations for the variables with a relatively large influence factor, while a calibration study is necessary to obtain a suitable calibration line for inner slope stability given overtopping.

6.2 Recommendations

It is recommended to model the strength of the clay cover stochastic in the probabilistic assessment when one is dealing with relatively small slip planes, because modelling the strength of the clay cover stochastic influences the estimates of the reliability index from the probabilistic calculations when one is dealing with relatively small slip planes. Besides, it is recommended to perform more research to the uncertainty of the pore water pressure distribution given overtopping by doing tests in practice. The reason for this is that the available amount of information in literature about the pore water pressure distribution given overtopping is limited, while it influences the results with both relatively small and large slip planes.

It is possible that a dike section could not meet the required failure probability for inner slope stability given overtopping even if the crest level is higher than the HBN for the failure mechanism GEKB. The reason for this is that the required failure probability for a cross-section for the failure mechanism GEKB is larger than the required failure probability for a cross-section for inner slope stability. When the probability of the exceedance of 1 l/s/m is relatively small and the probability of failure for inner slope stability given overtopping is relatively large, then it can be the case that the crest level is higher than the HBN for the failure mechanism GEKB and that the dike section does not meet required failure probability for inner slope stability. So, even if the probability that overtopping occurs is considered as small, it is recommended to assess whether a dike section meets the required failure probability for inner slope stability given overtopping.

Currently, one calculation including the effects of overtopping and one calculation excluding the effects of overtopping need to be performed for the semi-probabilistic assessment of inner slope stability. It is an option to do the probabilistic assessment based on the combined fragility curve

instead of the semi-probabilistic assessment. However, since the probabilistic calculations take a lot of computation time and the calculations with D-Stability are error sensitive, it is recommended to keep executing the assessment of inner slope stability based on semi-probabilistic calculations to have a reasonable computation time. It is recommended to perform a calibration study for inner slope stability given overtopping to obtain a better estimate of the failure probability based on the semi-probabilistic calculations and to reduce the inconsistency between the semi-probabilistic and probabilistic estimates of the reliability index. After performing the calibration study for inner slope stability given overtopping, it is advised to use the obtained relation between the semi-probabilistic and probabilistic results for the semi-probabilistic assessment of inner slope stability given overtopping. It is important that the calibration study for inner slope stability given overtopping is representative for the Netherlands by using cases at different locations with different conditions. Less dike sections would probably meet the required safety factor if the required safety factor becomes stricter based on the obtained relation between the semi-probabilistic and probabilistic results from the calibration study for inner slope stability given overtopping. Nevertheless, a better estimate of the failure probability would be obtained when a calibration study would be performed for inner slope stability given overtopping. The current WBI calibration line of 2016 can still be used for inner slope stability without overtopping dependent on the used coefficients of variation in the calculations for the variables with a relatively large influence factor. For this reason, it is recommended to use a different calibration line for inner slope stability given overtopping, than for inner slope stability without overtopping.

It is recommended to perform more research to the uncertainty of the pore water pressure distribution given overtopping by doing tests in practice before performing the calibration study for inner slope stability given overtopping. The results of the tests in practice to the uncertainty of the pore water pressure distribution given overtopping can then be used during the calibration study for inner slope stability given overtopping.

After the semi-probabilistic assessment, it is advised to estimate the failure probability based on the combined fragility curve of the probabilistic assessment if a dike section does not meet the required safety factor based on the semi-probabilistic assessment and when certain conditions are met. These conditions are that the difference between the required and calculated safety factor is relatively small, the slip planes are relatively large and the coefficients of variation are relatively small for the soil layers that are expected to have a relatively large influence factor. It is not recommended to perform the probabilistic assessment if a dike section does not meet the required safety factor based on the semi-probabilistic assessment when relatively small slip planes are found, because small slip planes for inner slope stability with overtopping have a too negative impact on the estimated reliability index from the combined fragility curve based on the results of JAV. It is also not recommended to perform the probabilistic assessment if a dike section does not meet the required safety factor based on the semi-probabilistic assessment when the coefficients of variation are not relatively small for the soil layers that are expected to have a relatively large influence factor, due to the influence of it on the estimates of the reliability index from the probabilistic calculations.

References

Barendsen, L., Bartels, W., Kriebel, M., Broere, A., & Perez Gomez, I. (2021). *Nota Veiligheidsopgave.* Breda: Lievense Infra B.V.

Broere, A. (2022). *Probabilistische berekeningen veiligheidsopgave STBI.* Nieuwegein: WSP Nederland B.V.

De Visser, M., & Jongejan, R. (2018). *KPR factsheet werkwijze macrostabiliteit i.c.m. golfoverslag OI2014v4.* Nieuwegein: Kennisplatform Risicobenadering.

Dekking, F., Kraaikamp, C., Lopuhaä, H., & Meester, L. (2005). *A Modern Introduction to Probability and Statistics.* Delft: Springer.

Deltares. (2021). *Aan de slag met D-Stability en Fragility curves.* Delft: Deltares.

Deltares. (2021). *Expert sessie fragility curves conditioneel aan overslagdebiet.* Delft: Deltares.

Deltares. (2022). *Probabilistic Toolkit User Manual.* Delft: Deltares.

Deltares. (2023, January 26). ptk-dike-assessment. Delft.

Deltares; Fugro Ingenieursbureau BV; HKV_Lijn in Water; Arcadis Nederland BV; Rijkswaterstaat Water, Verkeer en Leefomgeving; www.enwinfo.nl. (2012). *Technisch Rapport Grondmechanisch Schematiseren bij Dijken.* Rijkswaterstaat Water, Verkeer en Leefomgeving.

Diermanse, F. (2016). *WBI - Onzekerheden.* Delft: Deltares.

Jongejan, R., & De Visser, M. (2017). *Voorstel t.a.v. beoordeling macrostabiliteit incl. golfoverslag.* Nieuwegein: Kennisplatform Risicobenadering.

Jonkman, S., Jorissen, R., Schweckendiek, T., & Van den Bos, J. (2021). *Flood Defences.* Delft: Delft University of Technology.

Jonkman, S., R.D.J.M., S., Morales-Nápoles, O., Vrouwenvelder, A., & Vrijling, J. (2017). *Probabilistic Design: Risk and Reliability Analysis in Civil Engineering.* Delft: Delft University of Technology.

Kanning, W., & Van der krogt, M. (2016). *Memo: Pore water pressure uncertainties for slope stability.* Delft: Deltares.

Kanning, W., Teixeira, A., Van der Krogt, M., & Rippi, K. (2017). *Derivation of the semi-probabilistic safety assessment rule for inner slope stability.* Delft: Deltares.

Lodder, H.-J., & Kames, J. (2019). *Modellering dijksmateriaal.* Tiel: Waterschap Rivierenland.

Prins, M. (2021). *Revision of the calibration equation for a river dike on macro stability.* Delft: TU Delft.

Rijkswaterstaat Water, Verkeer en Leefomgeving. (2017). *Handreiking ontwerpen met overstromingskansen.* Rijkswaterstaat Water, Verkeer en Leefomgeving.

Rijkswaterstaat Water, Verkeer en Leefomgeving. (2021). *Schematiseringshandleiding grasbekleding.* The Hague: Ministerie van Infrastructuur en Waterstaat.

Rijkswaterstaat, Water Verkeer en Leefomgeving. (2019). *Regeling veiligheid primaire waterkeringen 2017, Bijlage III Sterkte en veiligheid.* The Hague: Ministerie van Infrastructuur en Milieu.

Rijkswaterstaat, Water Verkeer en Leefomgeving. (2021). *Schematiseringshandleiding macrostabiliteit.* The Hague: Ministerie van Infrastructuur en Waterstaat.

Rijneveld, B. (2020). *Veiligheidsfilosofie STBI bij overslag.* Utrecht: Adviesteam Dijkontwerp.

Rosenbrand, E., & Rozing, A. (2020). *POVM Actuele Sterkte.* Tiel: POV Macrostabiliteit.

Schweckendiek, T., Van der Krogt, M., Rijneveld, B., & Teixeira, A. M. (2017). *Handreiking Faalkansanalyse Macrostabiliteit.* Delft: Deltares.

Slootjes, N., & Wagenaar, D. (2016). *Factsheets normering primaire waterkeringen.* The Hague: Ministerie van Infrastructuur en Milieu.

Sluiter, D.-J., & Van der Kraan, A. (2022). *Notitie Omgang met GABI bij Sterke Lekdijk.* Technisch team Sterke Lekdijk.

Strategisch team van Sterke Lekdijk. (2021). *Strategische Nota van Uitgangspunten.* Hoogheemraadschap De Stichtse Rijnlanden.

TAW. (2004). *Technisch Rapport Waterspanningen bij dijken.* TAW.

Technische Adviescommissie voor de Waterkeringen. (2001). *Technisch Rapport Waterkerende Grondconstructies.* Delft: Technische Adviescommissie voor de Waterkeringen.

Van der Meij, R. (2020). *D-Stability.* Delft: Deltares.

Van Duinen, A. (2015). *Modelonzekerheidsfactoren Spencer-Van der Meij model en ongedraineerde schuifsterkte.* Delft: Deltares.

Van Duinen, A. (2021). *Handelingsperspectief schuifsterkte onverzadigde zone.* HWBP De Innovatieversneller.

Van Hoven, A., & Noordam, A. (2018). *Analyse infiltratieproef IJsseldijk.* POV Macrostabiliteit.

Van Hoven, A., Hardeman, B., Van der Meer, J., & Steendam, G. (2010). *Sliding stability of landward slope clay cover layers of sea dikes subject to wave overtopping.*

Vergouwe, R. (2014). *The National Flood Risk Analysis for the Netherlands.* Rijkswaterstaat VNK Project Office.

Verruijt, A. (2012). *Soil Mechanics.* Delft: Delft University of Technology.

Waterwet. (2021, Augustes 1). Opgehaald van Overheid.nl: https://wetten.overheid.nl/BWBR0025458/2021-07-01/0

Appendices

A. Test runs probabilistic calculations

The results of the test runs to determine the maximum number of realizations are given in this appendix. In Table 22 are the results of the test runs for dike section 10C given and in Table 23 are the results of the test runs of dike section 11E given. Please note that the estimated reliability indexes in Table 22 and Table 23 are not the same as for the basis probabilistic calculations in appendix B. The reason for this is that there have been made some small changes to the settings in Probabilistic Toolkit to find the design point more accurately. Besides, the calculations of dike section 10C are made without a traffic load for every water level and the calculations of 11E are made with a traffic load for every water level in the test runs, while this is not the case for every water level in practice. The 5% confidence bound of the reliability index is determined based on the failure probability and the coefficient of variation of the failure probability. The coefficient of variation of the failure probability is specified as the standard deviation of the probability of failure divided by the probability of failure (Deltares, 2022).

Table 22: Results test runs probabilistic calculations dike section 10C

Dike section	10C	10C	10C	10C	10C	10C	10C
Water level [m +NAP]	0.24	4.37	6.81	6.66	6.96	6.66	6.96
Overtopping	No	No	No	No	No	Yes	Yes
Traffic	No	No	No	No	No	No	No
Realizations [-]	1000	1000	1000	1000	1000	1000	1000
Reliability index [-]	**11.4**	**7.55**	**5.25**	**5.31**	**4.41**	**5.29**	**4.16**
Coefficient of variation [-]	**0.484**	**0.322**	**0.232**	**0.518**	**0.106**	**0.204**	**0.139**
Failure probability [per year]	2.09E-30	2.11E-14	7.82E-08	5.45E-08	5.07E-06	5.98E-08	1.57E-05
Standard deviation [per year]	1.01E-30	6.79E-15	1.81E-08	2.82E-08	5.37E-07	1.22E-08	2.18E-06
5% confidence bound failure probability [per year]	3.75E-30	3.23E-14	1.08E-07	1.01E-07	5.95E-06	7.99E-08	1.93E-05
5% confidence bound reliability index [-]	**11.3**	**7.50**	**5.18**	**5.20**	**4.38**	**5.24**	**4.12**
Reliability index - 5% confidence bound reliability index [-]	**0.1**	**0.05**	**0.07**	**0.11**	**0.03**	**0.05**	**0.04**
Dike section	10C	10C	10C	10C	10C	10C	10C
Water level [m +NAP]	0.24	4.37	6.81	6.66	6.96	6.66	6.96
Overtopping	No	No	No	No	No	Yes	Yes
Traffic	No	No	No	No	No	No	No
Realizations [-]	2000	2000	2000	2000	2000	2000	2000
Reliability index [-]	**11.5**	**7.55**	**5.25**	**5.35**	**4.37**	**5.21**	**4.21**
Coefficient of variation [-]	**0.405**	**0.295**	**0.132**	**0.262**	**0.0898**	**0.214**	**0.0952**
Failure probability [per year]	6.61E-31	2.19E-14	7.57E-08	4.30E-08	6.13E-06	9.50E-08	1.27E-05
Standard deviation [per year]	2.68E-31	6.46E-15	9.99E-09	1.13E-08	5.50E-07	2.03E-08	1.21E-06
5% confidence bound failure probability [per year]	1.10E-30	3.25E-14	9.21E-08	6.15E-08	7.04E-06	1.28E-07	1.47E-05
5% confidence bound reliability index [-]	**11.5**	**7.50**	**5.21**	**5.29**	**4.34**	**5.15**	**4.18**
Reliability index - 5% confidence bound reliability index [-]	**0.0**	**0.05**	**0.04**	**0.06**	**0.03**	**0.06**	**0.03**
Difference in reliability index [-]	-0.1	0.00	0.00	-0.04	0.04	0.08	-0.05
Difference in coefficient of variation [-]	0.079	0.027	0.100	0.256	0.0162	-0.010	0.0438
Difference in reliability index - 5% confidence bound reliability index [-]	0.1	0.00	0.03	0.05	0.00	-0.01	0.01

Table 23: Results test runs probabilistic calculations dike section 11E

Dike section	11E	11E	11E	11E	11E
Water level [m +NAP]	-0.04	2.39	3.47	6.77	7.07
Overtopping	No	No	No	No	No
Traffic	Yes	Yes	Yes	Yes	Yes
Realizations [-]	1000	1000	1000	1000	1000
Reliability index [-]	**7.01**	**6.94**	**6.57**	**3.49**	**3.04**
Coefficient of variation [-]	**0.341**	**0.248**	**0.196**	**0.076**	**0.0682**
Failure probability [per year]	1.23E-12	2.04E-12	2.60E-11	2.37E-04	1.17E-03
Standard deviation [per year]	4.19E-13	5.06E-13	5.10E-12	1.80E-05	7.98E-05
5% confidence bound failure probability [per year]	1.92E-12	2.87E-12	3.44E-11	2.67E-04	1.30E-03
5% confidence bound reliability index [-]	**6.94**	**6.89**	**6.52**	**3.46**	**3.01**
Reliability index - 5% confidence bound reliability index [-]	**0.07**	**0.05**	**0.05**	**0.03**	**0.03**
Dike section	11E	11E	11E	11E	11E
Water level [m +NAP]	-0.04	2.39	3.47	6.77	7.07
Overtopping	No	No	No	No	No
Traffic	Yes	Yes	Yes	Yes	Yes
Realizations [-]	5000	5000	5000	5000	5000
Reliability index [-]	**7.04**	**6.99**	**6.62**	**3.51**	**3.06**
Coefficient of variation [-]	**0.134**	**0.116**	**0.0777**	**0.05**	**0.0499**
Failure probability [per year]	9.38E-13	1.37E-12	1.82E-11	2.23E-04	1.11E-03
Standard deviation [per year]	1.26E-13	1.59E-13	1.41E-12	1.12E-05	5.54E-05
5% confidence bound failure probability [per year]	1.14E-12	1.63E-12	2.05E-11	2.41E-04	1.20E-03
5% confidence bound reliability index [-]	**7.02**	**6.97**	**6.60**	**3.49**	**3.04**
Reliability index - 5% confidence bound reliability index [-]	**0.02**	**0.02**	**0.02**	**0.02**	**0.02**
Difference in reliability index [-]	-0.03	-0.05	-0.05	-0.02	-0.02
Difference in coefficient of variation [-]	0.207	0.132	0.1183	0.026	0.0183
Difference in reliability index - 5% confidence bound reliability index [-]	0.04	0.03	0.03	0.01	0.00

B. Results basis probabilistic calculations

The results of the basis probabilistic calculations are given in this appendix. For every dike section are per water level the expected reliability index, coefficient of variation of the failure probability, 5% confidence bound of the reliability index and the difference between the expected reliability index and the 5% confidence bound of the reliability index given in the tables in this appendix. The coefficient of variation of the failure probability is specified as the standard deviation of the probability of failure divided by the probability of failure (Deltares, 2022). The 5% confidence bound of the reliability index is determined based on the failure probability and the coefficient of variation of the failure probability.

Besides, for every dike section are the fragility curves given. The fragility points, the fragility curve without overtopping, the fragility curve given overtopping, the combined fragility curve, the probability of exceedance of 1 l/s/m overtopping given the water level and the probability density function of the water level are given in the figures in this appendix. Furthermore, a comparison has been made between the semi-probabilistic and probabilistic estimates of the reliability index.

The results of the basis probabilistic calculations for dike section 10C are given in Table 24 and the fragility curves are shown in Figure 36.

Table 24: Reliability index basis probabilistic calculations per water level for dike section 10C

Water level [m +NAP]	Traffic	Overtopping	Reliability index [-]	Coefficient of variation of the failure probability [-]	5% Confidence bound reliability index [-]	Reliability index - 5% confidence bound reliability index [-]
0.24	Yes	No	11.2	0.724	11.1	0.1
4.37	Yes	No	7.26	0.271	7.21	0.05
6.81	No	No	5.24	0.242	5.18	0.06
6.66	No	No	5.65	0.188	5.60	0.05
6.96	No	No	4.21	0.322	4.11	0.10
7.15	No	No	4.12	0.264	4.03	0.09
6.66	No	Yes	5.29	0.204	5.24	0.05
6.96	No	Yes	4.15	0.192	4.09	0.06
6.21	No	Yes	5.61	0.338	5.53	0.08
7.15	No	Yes	3.86	0.195	3.79	0.07

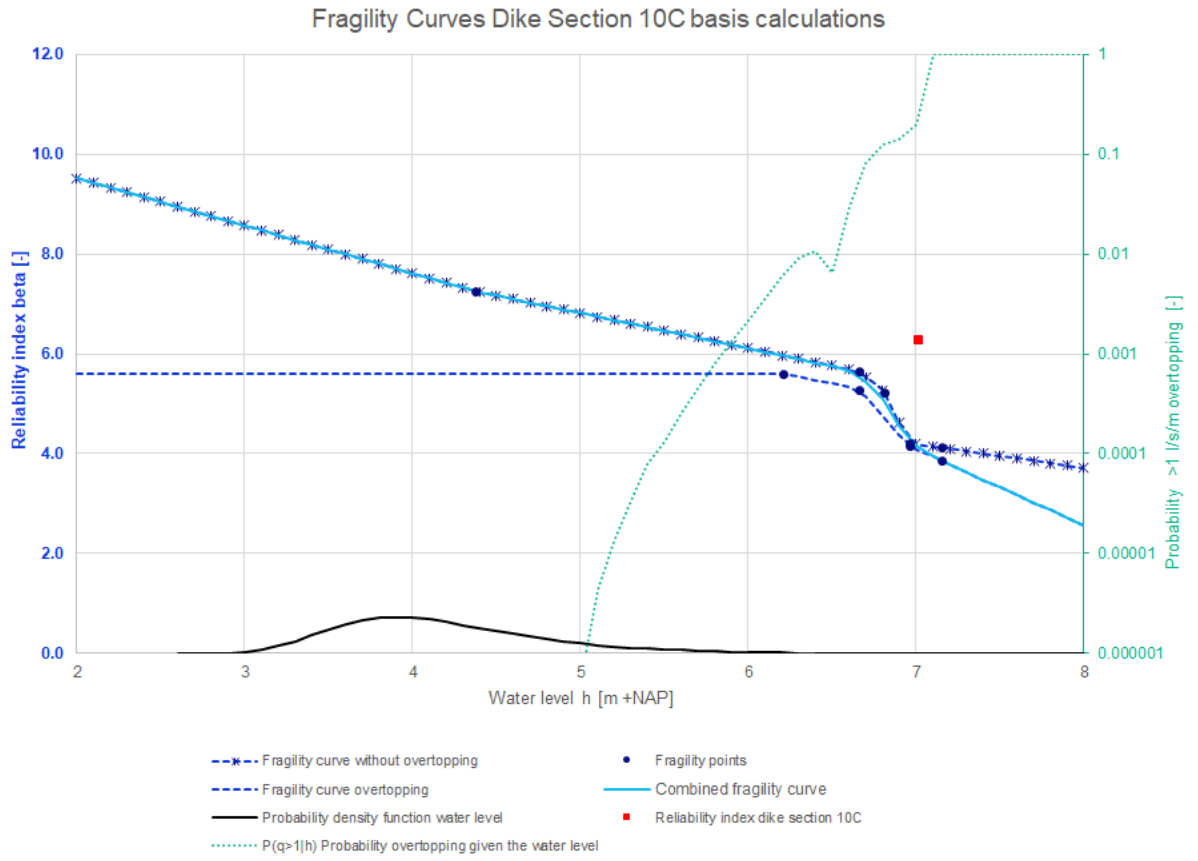

Figure 36: Fragility curves dike section 10C basis calculations

The results of the basis probabilistic calculations for dike section 11E are given in Table 25 and the fragility curves are shown in Figure 37.

Table 25: Reliability index basis probabilistic calculations per water level for dike section 11E

Water level [m +NAP]	Traffic	Overtopping	Reliability index [-]	Coefficient of variation of the failure probability [-]	5% Confidence bound reliability index [-]	Reliability index - 5% confidence bound reliability index [-]
-0.04	Yes	No	7.03	0.154	7.00	0.03
2.39	Yes	No	7.03	0.119	7.00	0.03
3.47	Yes	No	6.60	0.165	6.56	0.04
6.77	No	No	4.19	0.113	4.15	0.04
7.07	No	No	3.69	0.0854	3.65	0.04
6.77	No	Yes	0.0341	0.0405	-0.05	0.08
7.07	No	Yes	-0.121	0.0399	-0.21	0.09
6.37	No	Yes	0.118	0.045	0.03	0.08

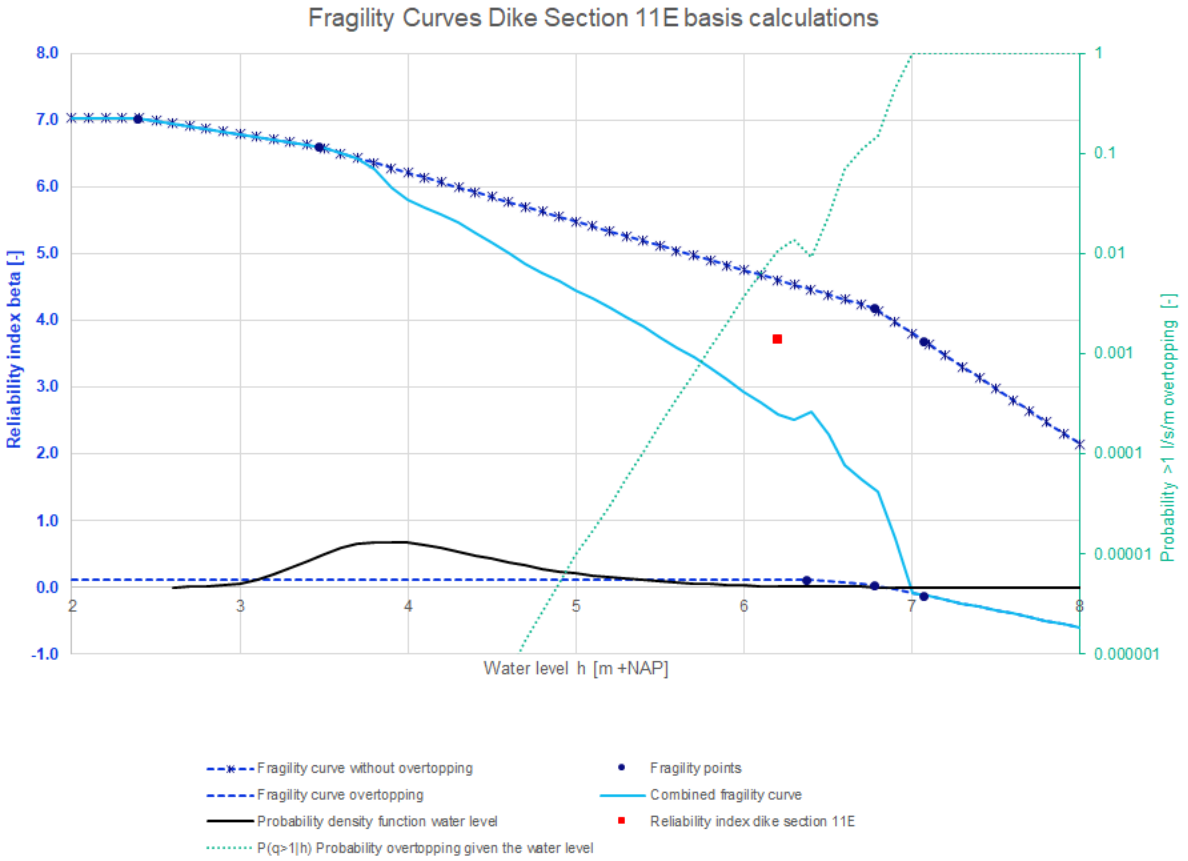

Figure 37: Fragility curves dike section 11E basis calculations

The results of the basis probabilistic calculations for dike section 11F(11D) are given in Table 26 and the fragility curves are shown in Figure 38.

Table 26: Reliability index basis probabilistic calculations per water level for dike section 11F(11D)

Water level [m +NAP]	Traffic	Overtopping	Reliability index [-]	Coefficient of variation of the failure probability [-]	5% Confidence bound reliability index [-]	Reliability index - 5% confidence bound reliability index [-]
-0.04	Yes	No	17.8	0.888	17.7	0.1
2.63	Yes	No	15.6	0.351	15.6	0.0
5.24	Yes	No	9.10	0.412	9.04	0.06
6.79	No	No	7.38	0.235	7.34	0.04
7.09	No	No	7.18	0.161	7.14	0.04
6.79	No	Yes	0.880	0.0499	0.82	0.06
7.09	No	Yes	0.766	0.0499	0.71	0.06
6.38	No	Yes	1.06	0.0559	1.00	0.06

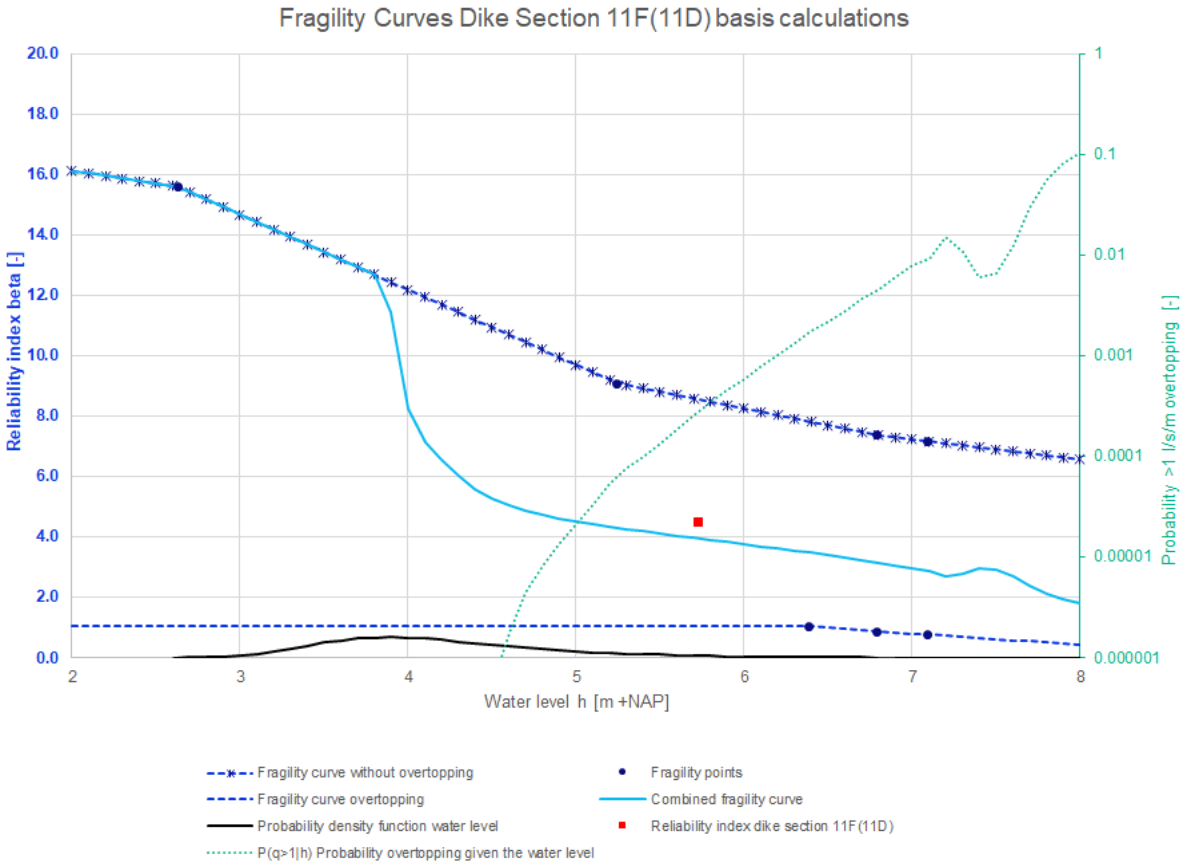

Figure 38: Fragility curves dike section 11F(11D) basis calculations

The results of the basis probabilistic calculations for dike section 13A are given in Table 27 and the fragility curves are shown in Figure 39.

Table 27: Reliability index basis probabilistic calculations per water level for dike section 13A

Water level [m +NAP]	Traffic	Overtopping	Reliability index [-]	Coefficient of variation of the failure probability [-]	5% Confidence bound reliability index [-]	Reliability index - 5% confidence bound reliability index [-]
-0.30	Yes	No	13.5	0.580	13.5	0.0
0.87	Yes	No	12.8	0.769	12.7	0.1
2.07	Yes	No	11.8	0.723	11.7	0.1
6.26	No	No	7.51	0.314	7.45	0.06
6.56	No	No	7.34	0.197	7.30	0.04
6.26	No	Yes	7.26	0.188	7.22	0.04
6.56	No	Yes	7.05	0.181	7.02	0.03
5.66	No	Yes	8.46	0.214	8.42	0.04

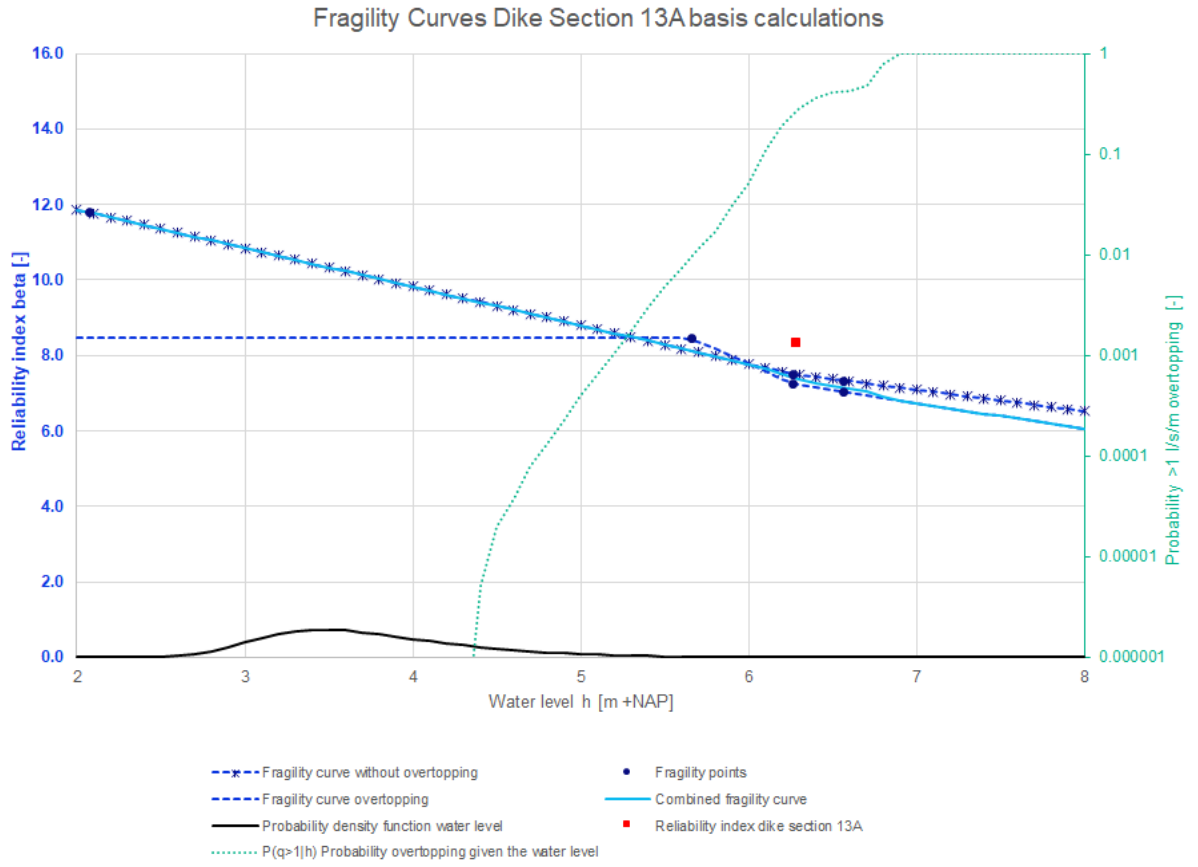

Figure 39: Fragility curves dike section 13A basis calculations

The results of the basis probabilistic calculations for dike section 13E1 are given in Table 28 and the fragility curves are shown in Figure 40.

Table 28: Reliability index basis probabilistic calculations per water level for dike section 13E1

Water level [m +NAP]	Traffic	Overtopping	Reliability index [-]	Coefficient of variation of the failure probability [-]	5% Confidence bound reliability index [-]	Reliability index - 5% confidence bound reliability index [-]
-0.30	Yes	No	10.0	0.225	10.0	0.0
4.69	Yes	No	7.59	0.371	7.53	0.06
6.33	No	No	6.19	0.432	6.11	0.08
6.63	No	No	5.85	0.193	5.81	0.04
6.33	No	Yes	6.59	0.317	6.52	0.07
6.63	No	Yes	5.82	0.152	5.79	0.03
6.00	No	Yes	6.81	0.771	6.69	0.12

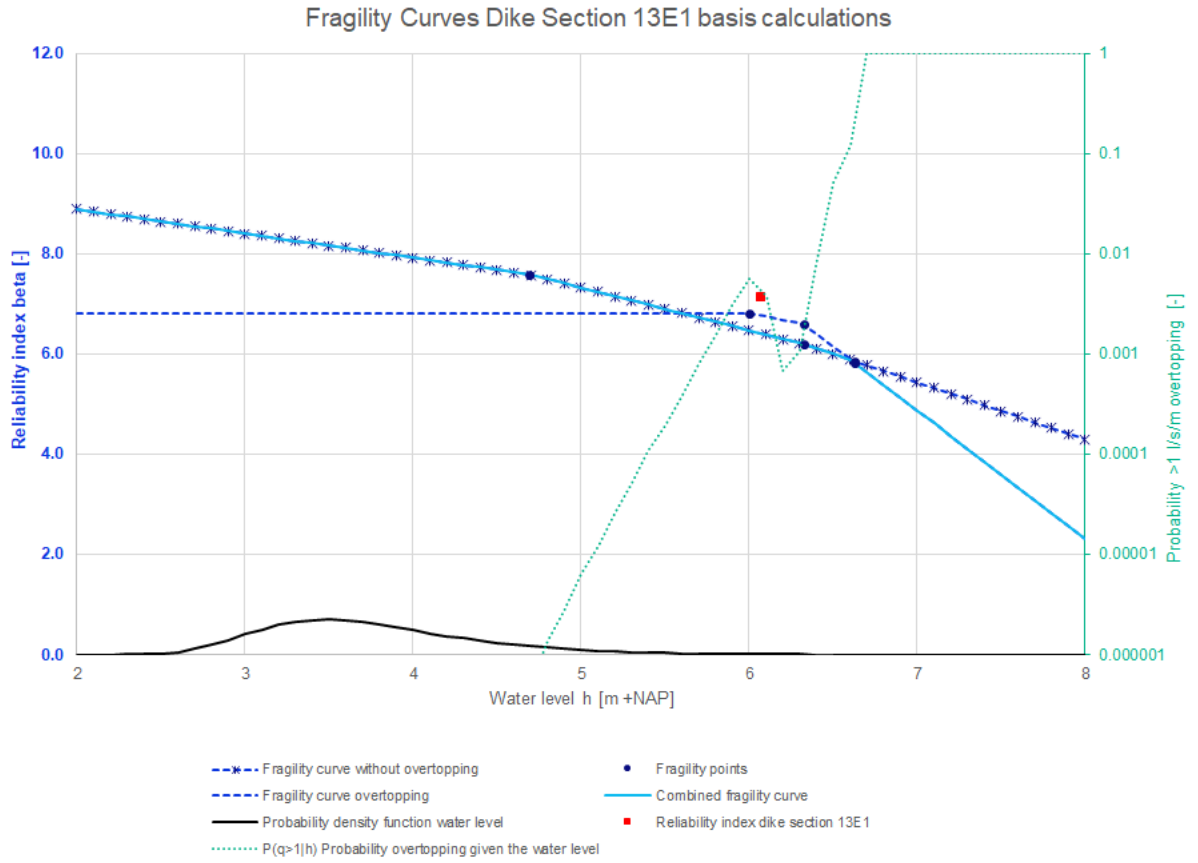

Figure 40: Fragility curves dike section 13E1 basis calculations

The results of the basis probabilistic calculations for dike section 13E2 are given in Table 29 and the fragility curves are shown in Figure 41.

Table 29: Reliability index basis probabilistic calculations per water level for dike section 13E2

Water level [m +NAP]	Traffic	Overtopping	Reliability index [-]	Coefficient of variation of the failure probability [-]	5% Confidence bound reliability index [-]	Reliability index - 5% confidence bound reliability index [-]
-0.30	Yes	No	10.2	0.262	10.2	0.0
4.69	Yes	No	7.39	0.164	7.36	0.03
6.24	No	No	6.37	0.149	6.33	0.04
6.54	No	No	6.02	0.169	5.98	0.04
6.24	No	Yes	6.42	0.391	6.34	0.08
6.54	No	Yes	6.03	0.213	5.98	0.05
5.91	No	Yes	6.66	0.204	6.62	0.04

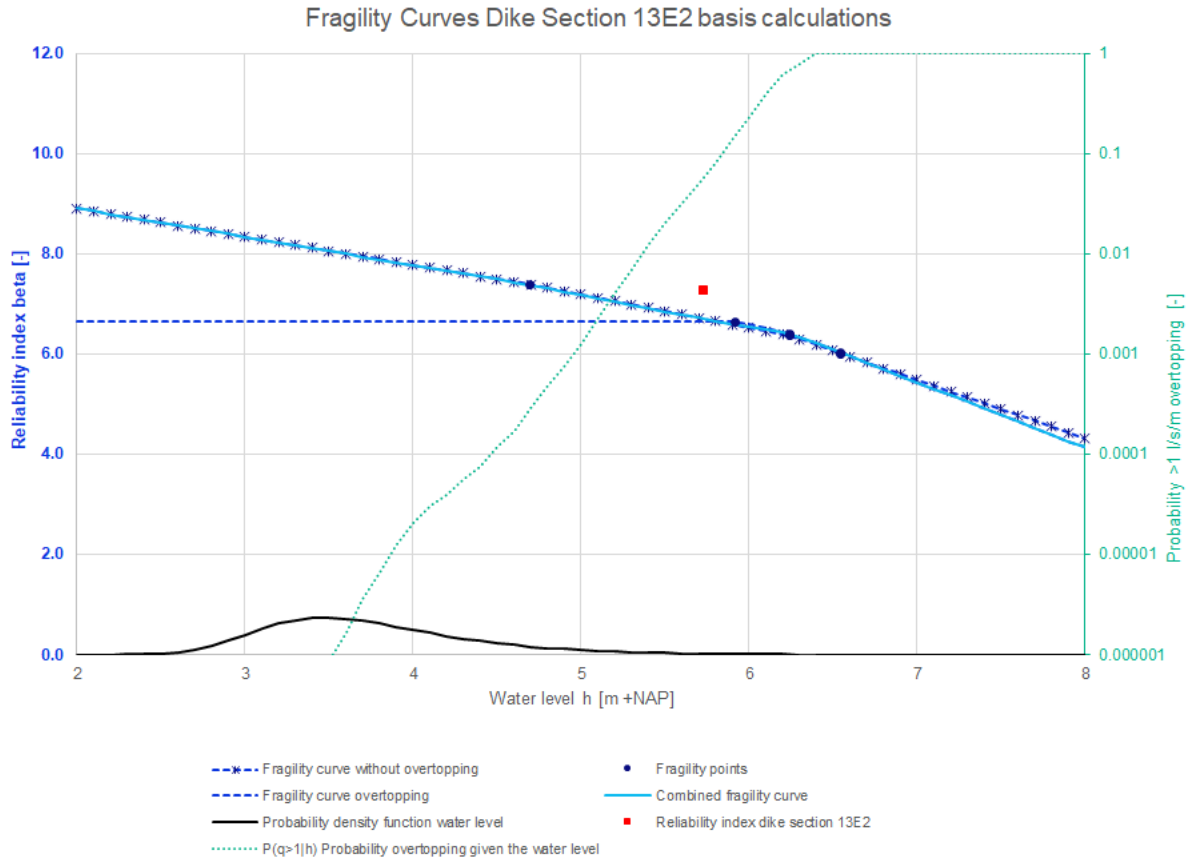

Figure 41: Fragility curves dike section 13E2 basis calculations

The estimated reliability index of the basis semi-probabilistic calculations without overtopping and the reliability index of the basis probabilistic calculations based on the combined fragility curves are compared with each other in Table 30. The relation between the overall safety factor and the reliability index is fitted to the twenty percent quantiles of the betas for the calibrated WBI damage factor line of 2016 (Kanning, Teixeira, Van der Krogt, & Rippi, 2017). For this reason, one would expect that the semi-probabilistic results are more conservative than the probabilistic results for eighty percent of the cases. Important to note is that the effects of overtopping were not accounted for in constructing the calibrated WBI damage factor line of 2016. One can see from Table 30 that the semi-probabilistic results are more conservative than the probabilistic results for most cases. However, the reliability index from the probabilistic calculation is 0.98 lower than the estimated reliability index from the semi-probabilistic calculation for dike section 11F(11D). Moreover, for dike section 11E is the reliability index from the probabilistic calculation 1.73 lower than the estimated reliability index from the semi-probabilistic calculation. It is unwanted that the estimated reliability index based on the semi-probabilistic calculation is considerably larger than the reliability index based on the probabilistic calculations. The reason for this is that if the semi-probabilistic results are too optimistic, then it could be assumed that inner slope stability is not a problem at a dike section after performing the semi-probabilistic calculations, while it might actually be a problem.

Table 30: Comparison reliability index basis semi-probabilistic calculations without overtopping and probabilistic calculations combined fragility curve

Dike section	Semi-probabilistic reliability index β [-]	Probabilistic reliability index β [-]	Difference probabilistic and semi-probabilistic reliability index β [-]
10C	5.68	6.29	0.61
11E	5.45	3.72	-1.73
11F(11D)	5.48	4.50	-0.98
13A	5.27	8.36	3.09
13E1	5.48	7.14	1.66
13E2	5.53	7.27	1.74

The estimated reliability index of the basis semi-probabilistic calculations without overtopping and the reliability index of the basis probabilistic calculations based on the fragility curve without overtopping are compared with each other in Table 31. From Table 31 one can see that there is one case for which the semi-probabilistic result is too optimistic for the basis calculations of inner slope stability without overtopping for JAV.

Table 31: Comparison reliability index basis semi-probabilistic and probabilistic calculations without overtopping

Dike section	Semi-probabilistic reliability index β [-]	Probabilistic reliability index β [-]	Difference probabilistic and semi-probabilistic reliability index β [-]
10C	5.68	6.38	0.70
11E	5.45	5.34	-0.11
11F(11D)	5.48	8.35	2.87
13A	5.27	8.43	3.16
13E1	5.48	7.19	1.71
13E2	5.53	7.27	1.74

Finally, the estimated reliability index of the basis semi-probabilistic calculations given overtopping and the reliability index of the basis probabilistic calculations based on the fragility point with the largest contribution to 1 l/s/m overtopping are compared with each other in Table 32. One can see from Table 32 that there is an extremely large difference between the estimated semi-probabilistic and probabilistic reliability index for dike section 11E and 11F(11D). The reliability index based on the probabilistic calculations is 2.93 lower than the estimated reliability index based on the semi-probabilistic calculation for dike section 11E. For this reason, there is an inconsistency between the estimated reliability index based on the semi-probabilistic and probabilistic calculations for inner slope stability given overtopping. The inconsistency between the semi-probabilistic and probabilistic results leads to too optimistic results for inner slope stability given overtopping based on the semi-probabilistic calculations.

Table 32: Comparison reliability index basis semi-probabilistic and probabilistic calculations given overtopping

Dike section	Semi-probabilistic reliability index β [-]	Probabilistic reliability index β [-]	Difference probabilistic and semi-probabilistic reliability index β [-]
10C	5.41	5.61	0.20
11E	3.05	0.12	-2.93
11F(11D)	3.52	1.06	-2.46
13A	5.52	8.46	2.94
13E1	5.59	6.81	1.22
13E2	5.61	6.66	1.05

C. Results probabilistic calculations with the cohesion of the clay cover stochastic

The results of the probabilistic calculations with the cohesion of the clay cover stochastic are given in this appendix. For every dike section are per water level the expected reliability index, coefficient of variation of the failure probability, 5% confidence bound of the reliability index and the difference between the expected reliability index and the 5% confidence bound of the reliability index given in the tables in this appendix. The coefficient of variation of the failure probability is specified as the standard deviation of the probability of failure divided by the probability of failure (Deltares, 2022). The 5% confidence bound of the reliability index is determined based on the failure probability and the coefficient of variation of the failure probability.

Besides, for every dike section are the fragility curves given. The fragility points, the fragility curve without overtopping, the fragility curve given overtopping, the combined fragility curve, the probability of exceedance of 1 l/s/m overtopping given the water level and the probability density function of the water level are given in the figures in this appendix. Furthermore, the reliability indexes are given per dike section, a comparison has been made between the semi-probabilistic and probabilistic estimates of the reliability index, the results are plotted with the results of the WBI calibration study and the influence factors are shown.

The results of the probabilistic calculations with the cohesion of the clay cover stochastic for dike section 10C are given in Table 33 and the fragility curves are shown in Figure 42.

Table 33: Reliability index probabilistic calculations with the cohesion of the clay cover stochastic per water level for dike section 10C

Water level [m +NAP]	Traffic	Overtopping	Reliability index [-]	Coefficient of variation of the failure probability [-]	5% Confidence bound reliability index [-]	Reliability index - 5% confidence bound reliability index [-]
0.24	Yes	No	10.8	0.534	10.7	0.1
4.37	Yes	No	7.43	0.203	7.39	0.04
6.81	No	No	5.20	0.227	5.14	0.06
6.66	No	No	5.55	0.169	5.50	0.05
6.96	No	No	4.29	0.300	4.20	0.09
7.15	No	No	4.03	0.121	3.99	0.04
6.66	No	Yes	5.15	0.139	5.11	0.04
6.96	No	Yes	4.08	0.168	4.02	0.06
6.21	No	Yes	5.75	0.183	5.70	0.05
7.15	No	Yes	3.81	0.101	3.77	0.04

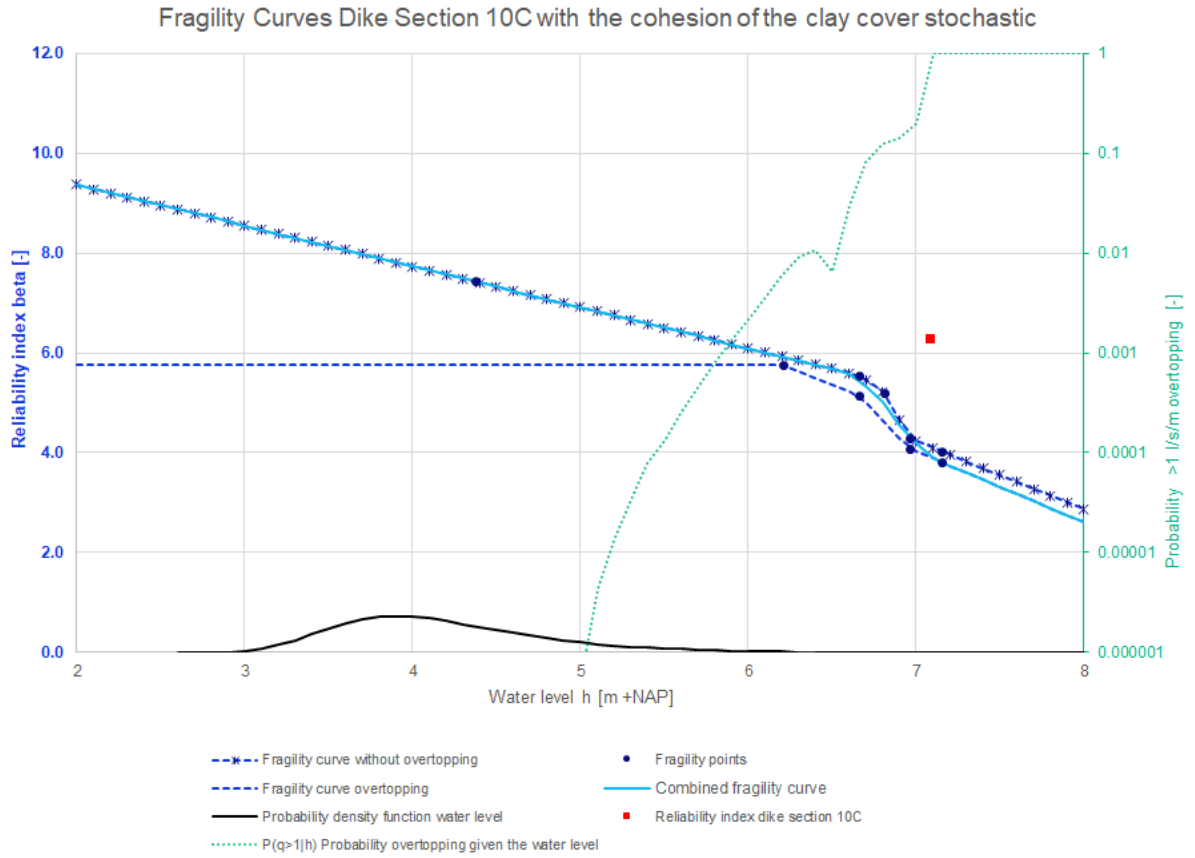

Figure 42: Fragility curves dike section 10C with the cohesion of the clay cover stochastic

The results of the probabilistic calculations with the cohesion of the clay cover stochastic for dike section 11E are given in Table 34 and the fragility curves are shown in Figure 43.

Table 34: Reliability index probabilistic calculations with the cohesion of the clay cover stochastic per water level for dike section 11E

Water level [m +NAP]	Traffic	Overtopping	Reliability index [-]	Coefficient of variation of the failure probability [-]	5% Confidence bound reliability index [-]	Reliability index - 5% confidence bound reliability index [-]
-0.04	Yes	No	7.33	0.262	7.28	0.05
2.39	Yes	No	7.38	0.218	7.34	0.04
3.47	Yes	No	7.01	0.385	6.94	0.07
6.77	No	No	4.59	0.312	4.50	0.09
7.07	No	No	4.02	0.205	3.95	0.07
6.77	No	Yes	0.926	0.0499	0.87	0.05
7.07	No	Yes	0.820	0.0499	0.76	0.06
6.37	No	Yes	1.15	0.05	1.10	0.05

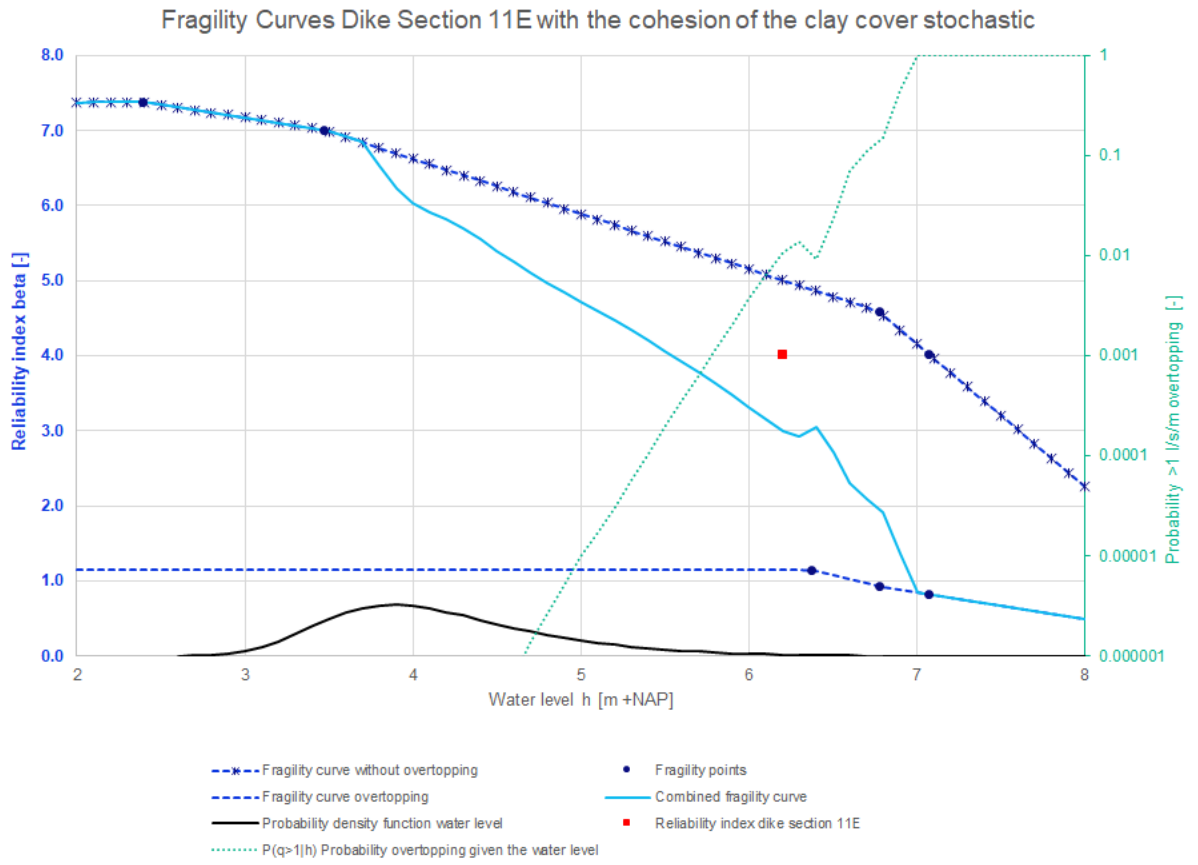

Figure 43: Fragility curves dike section 11E with the cohesion of the clay cover stochastic

The results of the probabilistic calculations with the cohesion of the clay cover stochastic for dike section 11F(11D) are given in Table 35 and the fragility curves are shown in Figure 44.

Table 35: Reliability index probabilistic calculations with the cohesion of the clay cover stochastic per water level for dike section 11F(11D)

Water level [m +NAP]	Traffic	Overtopping	Reliability index [-]	Coefficient of variation of the failure probability [-]	5% Confidence bound reliability index [-]	Reliability index - 5% confidence bound reliability index [-]
-0.04	Yes	No	17.8	0.352	17.8	0.0
2.63	Yes	No	15.8	0.366	15.8	0.0
5.24	Yes	No	9.37	0.334	9.32	0.05
6.79	No	No	7.53	0.224	7.48	0.05
7.09	No	No	7.26	0.277	7.20	0.06
6.79	No	Yes	1.79	0.0614	1.74	0.05
7.09	No	Yes	1.75	0.0729	1.70	0.05
6.38	No	Yes	1.94	0.0649	1.89	0.05

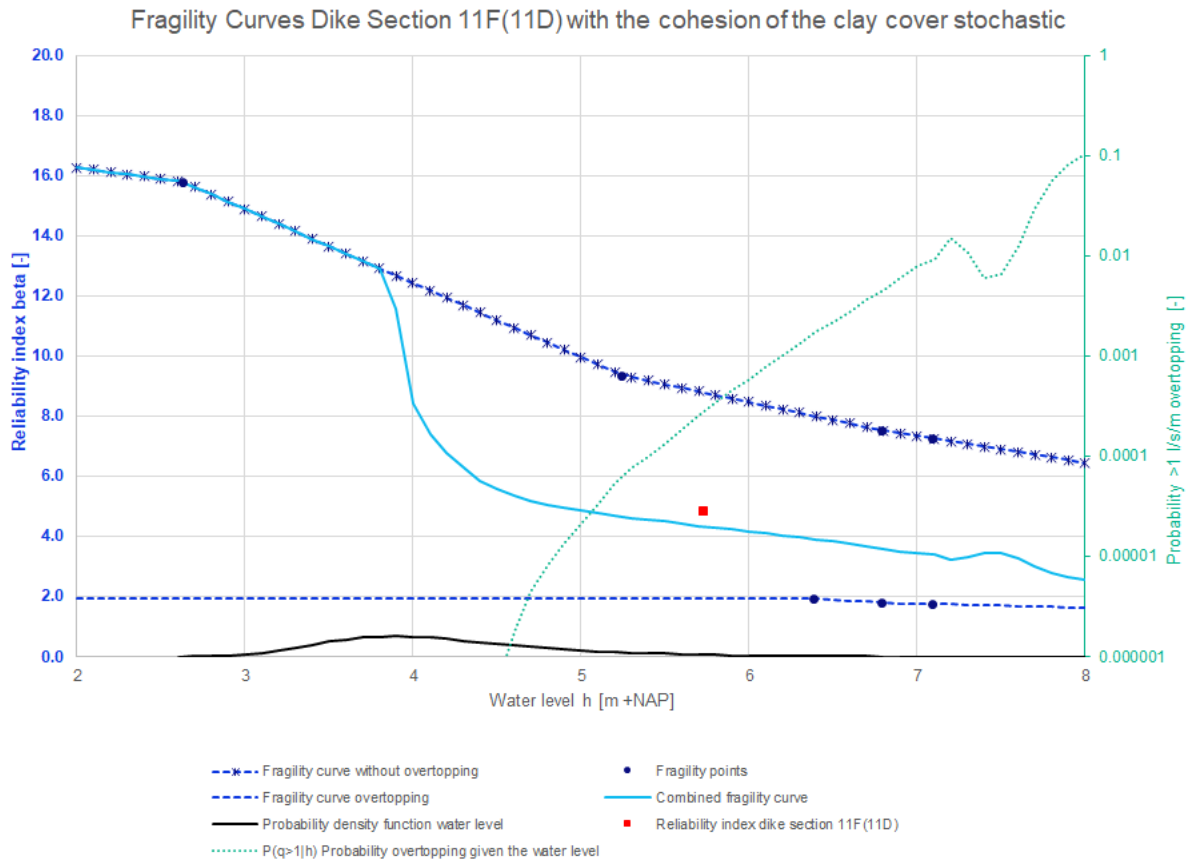

Figure 44: Fragility curves dike section 11F(11D) with the cohesion of the clay cover stochastic

The results of the probabilistic calculations with the cohesion of the clay cover stochastic for dike section 13A are given in Table 36 and the fragility curves are shown in Figure 45.

Table 36: Reliability index probabilistic calculations with the cohesion of the clay cover stochastic per water level for dike section 13A

Water level [m +NAP]	Traffic	Overtopping	Reliability index [-]	Coefficient of variation of the failure probability [-]	5% Confidence bound reliability index [-]	Reliability index - 5% confidence bound reliability index [-]
-0.30	Yes	No	13.4	0.931	13.3	0.1
0.87	Yes	No	13.0	0.398	13.0	0.0
2.07	Yes	No	12.0	0.363	12.0	0.0
6.26	No	No	7.75	0.200	7.71	0.04
6.56	No	No	7.52	0.188	7.48	0.04
6.26	No	Yes	7.41	0.183	7.37	0.04
6.56	No	Yes	7.20	0.179	7.17	0.03
5.66	No	Yes	8.51	0.329	8.46	0.05

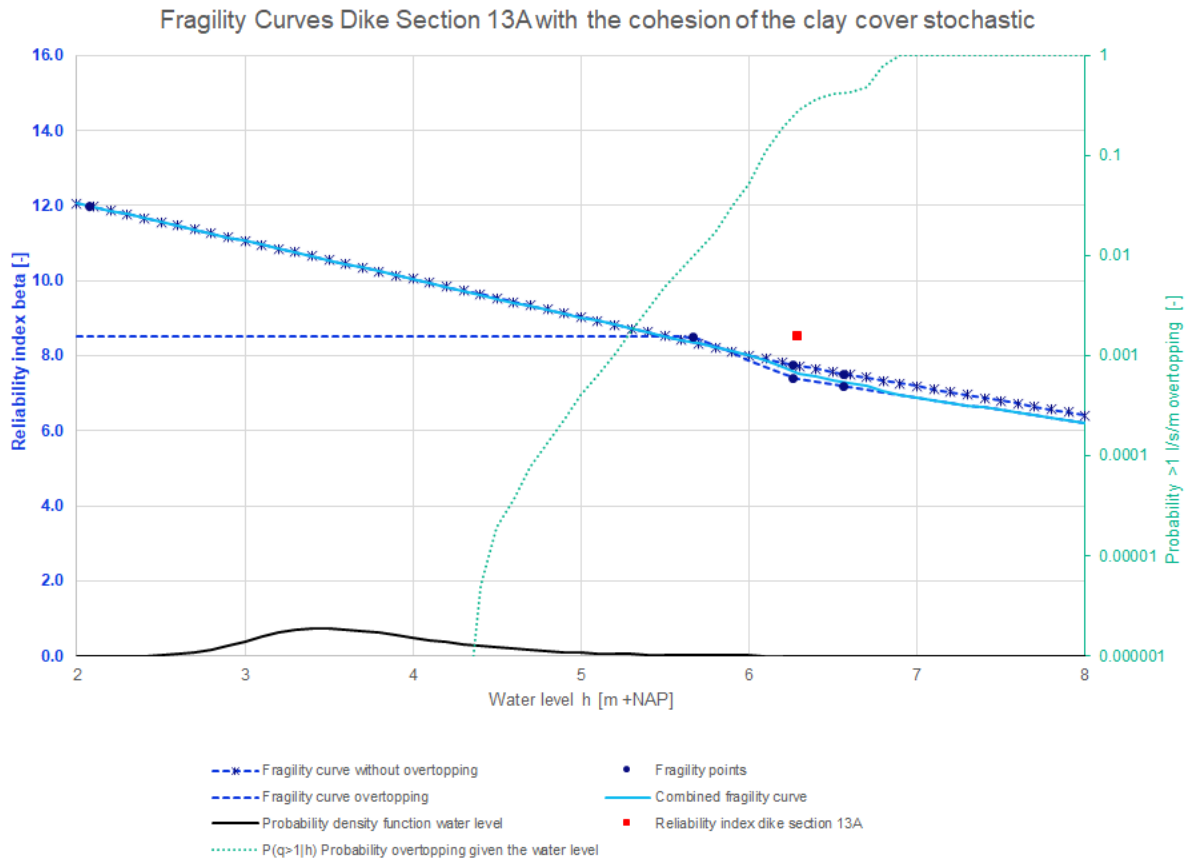

Figure 45: Fragility curves dike section 13A with the cohesion of the clay cover stochastic

The results of the probabilistic calculations with the cohesion of the clay cover stochastic for dike section 13E1 are given in Table 37 and the fragility curves are shown in Figure 46.

Table 37: Reliability index probabilistic calculations with the cohesion of the clay cover stochastic per water level for dike section 13E1

Water level [m +NAP]	Traffic	Overtopping	Reliability index [-]	Coefficient of variation of the failure probability [-]	5% Confidence bound reliability index [-]	Reliability index - 5% confidence bound reliability index [-]
-0.30	Yes	No	9.93	0.215	9.89	0.04
4.69	Yes	No	7.69	0.322	7.63	0.06
6.33	No	No	6.36	0.213	6.31	0.05
6.63	No	No	5.74	0.225	5.69	0.05
6.33	No	Yes	6.32	0.182	6.28	0.04
6.63	No	Yes	5.97	0.773	5.84	0.13
6.00	No	Yes	6.75	0.344	6.68	0.07

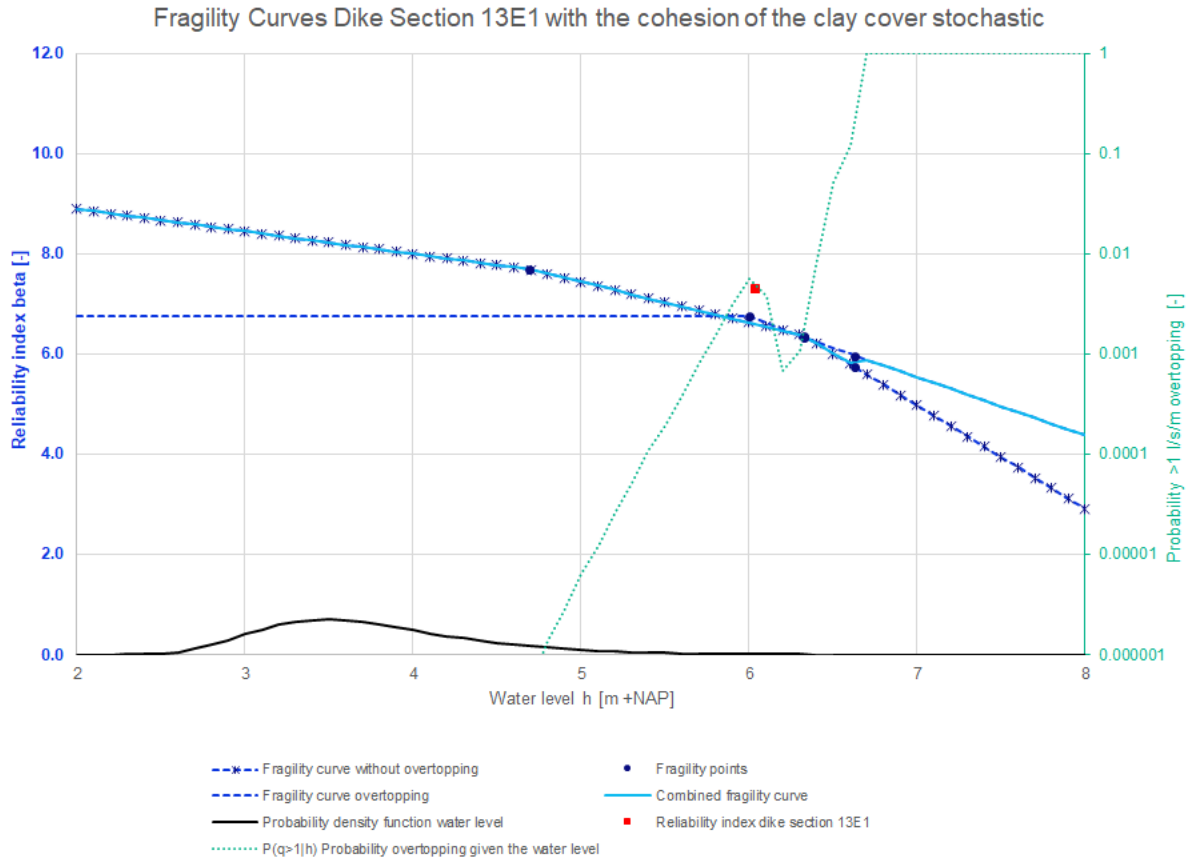

Figure 46: Fragility curves dike section 13E1 with the cohesion of the clay cover stochastic

The results of the probabilistic calculations with the cohesion of the clay cover stochastic for dike section 13E2 are given in Table 38 and the fragility curves are shown in Figure 47.

Table 38: Reliability index probabilistic calculations with the cohesion of the clay cover stochastic per water level for dike section 13E2

Water level [m +NAP]	Traffic	Overtopping	Reliability index [-]	Coefficient of variation of the failure probability [-]	5% Confidence bound reliability index [-]	Reliability index - 5% confidence bound reliability index [-]
-0.30	Yes	No	9.93	0.419	9.87	0.06
4.69	Yes	No	7.51	0.177	7.47	0.04
6.24	No	No	6.47	0.153	6.43	0.04
6.54	No	No	6.03	0.189	5.98	0.05
6.24	No	Yes	6.41	0.215	6.36	0.05
6.54	No	Yes	6.02	0.154	5.99	0.03
5.91	No	Yes	6.70	0.221	6.65	0.05

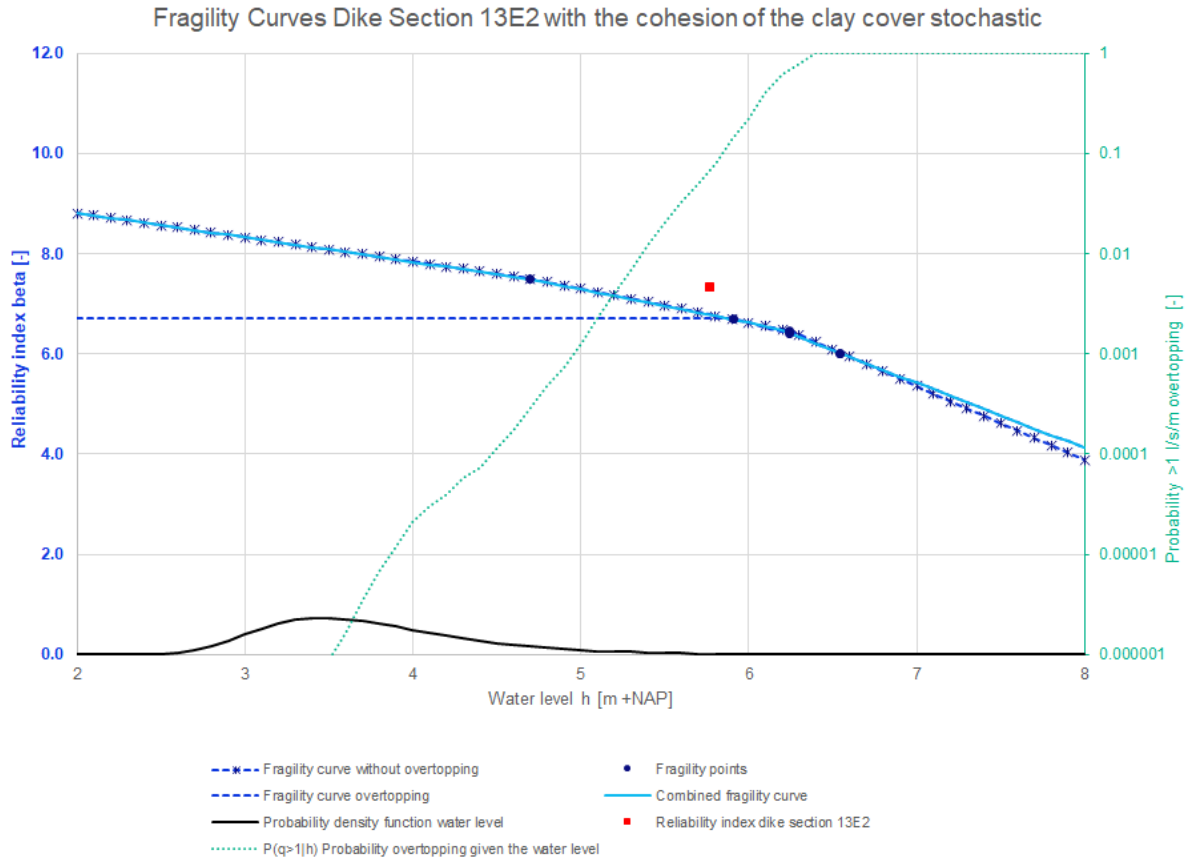

Figure 47: Fragility curves dike section 13E2 with the cohesion of the clay cover stochastic

The reliability index for the probabilistic calculations with the cohesion of the clay cover modelled as a stochastic variable are shown in Table 39.

Table 39: Reliability index probabilistic calculations with the cohesion of the clay cover stochastic

Dike section	Reliability index β combined fragility curve [-]	Reliability index β without overtopping [-]	Reliability index β given overtopping [-]
10C	6.27	6.36	5.75
11E	4.01	5.69	1.15
11F(11D)	4.85	8.48	1.94
13A	8.52	8.64	8.51
13E1	7.31*	7.24*	6.75
13E2	7.34	7.35	6.70

** The reason why the reliability index without overtopping is lower than the reliability index for the combined fragility curve is probably caused by the schematization of the dike profile*

A comparison has been made between the reliability index of the combined fragility curve with the cohesion of the clay cover modelled as a stochastic variable, the combined fragility curve of the basis probabilistic calculations and the semi-probabilistic calculations without overtopping in Table 40. One can see from Table 40 that the reliability index with the cohesion of the clay cover modelled as a stochastic variable increases for most cases compared with the reliability index of the basis probabilistic calculations (upper right column).

Table 40: Comparison reliability index semi-probabilistic calculations without overtopping, basis probabilistic calculations combined fragility curve and probabilistic calculations combined fragility curve with the cohesion of the clay cover stochastic

Dike section	Semi-probabilistic reliability index β [-]	Probabilistic reliability index basis calculations β [-]	Probabilistic reliability index with cohesion stochastic β [-]	Difference probabilistic and semi-probabilistic reliability index with cohesion stochastic β [-]	Difference between probabilistic calculation with cohesion stochastic and basis calculation β [-]
10C	5.68	6.29	6.27	0.59	-0.02*
11E	5.45	3.72	4.01	-1.44	0.29
11F(11D)	5.48	4.50	4.85	-0.63	0.35
13A	5.27	8.36	8.52	3.25	0.16
13E1	5.48	7.14	7.31	1.83	0.17
13E2	5.53	7.27	7.34	1.81	0.07

** It is unexpected that the reliability index is lower with the cohesion of the clay cover modelled as a stochastic variable. However, the difference between the reliability index of the probabilistic calculations with the cohesion stochastic and the basis probabilistic calculations is small. For this reason, this unexpected result is acceptable with taking into account the coefficients of variation of the failure probability of the fragility points*

The reliability index of the fragility curve without overtopping with the cohesion of the clay cover modelled as a stochastic variable, the fragility curve without overtopping of the basis probabilistic calculations and the semi-probabilistic calculations without overtopping are compared with each other in Table 41. One can see that the semi-probabilistic estimates of the reliability index are conservative for all dike sections from the second column from the right after modelling the cohesion of the clay cover as a stochastic variable in the probabilistic calculations. This is a bit unexpected, since the WBI damage factor line of 2016 is fitted to the twenty percent quantiles of the betas for the situation without overtopping (see paragraph 2.4.1).

Table 41: Comparison reliability index semi-probabilistic calculations without overtopping, basis probabilistic calculations without overtopping and probabilistic calculations without overtopping with the cohesion of the clay cover stochastic

Dike section	Semi-probabilistic reliability index β [-]	Probabilistic reliability index basis calculations β [-]	Probabilistic reliability index with cohesion stochastic β [-]	Difference probabilistic and semi-probabilistic reliability index with cohesion stochastic β [-]	Difference between probabilistic calculation with cohesion stochastic and basis calculation β [-]
10C	5.68	6.38	6.36	0.68	-0.02*
11E	5.45	5.34	5.69	0.24	0.35
11F(11D)	5.48	8.35	8.48	3.00	0.13
13A	5.27	8.43	8.64	3.37	0.21
13E1	5.48	7.19	7.24	1.76	0.05
13E2	5.53	7.27	7.35	1.82	0.08

** It is unexpected that the reliability index is lower with the cohesion of the clay cover modelled as a stochastic variable. However, the difference between the reliability index of the probabilistic calculations with the cohesion stochastic and the basis probabilistic calculations is small. For this reason, this unexpected result is acceptable with taking into account the coefficients of variation of the failure probability of the fragility points*

A comparison has been made between the reliability index of the fragility point with the largest contribution to 1 l/s/m overtopping with the cohesion of the clay cover modelled as a stochastic variable, the fragility point with the largest contribution to 1 l/s/m overtopping of the basis probabilistic calculations and the semi-probabilistic calculations given overtopping in Table 42. The reliability index of the probabilistic calculations given overtopping increases the most for dike section 11E and 11F(11D) after modelling the cohesion of the clay cover stochastic compared with the basis probabilistic calculations (see upper right column in Table 42), which have a relatively small slip plane compared with the other dike sections. This increase in reliability index is lower for the combined fragility curve (see Table 40) and the fragility curve without overtopping (see Table 41).

Table 42: Comparison reliability index semi-probabilistic calculations given overtopping, basis probabilistic calculations given overtopping and probabilistic calculations given overtopping with the cohesion of the clay cover stochastic

Dike section	Semi-probabilistic reliability index β [-]	Probabilistic reliability index basis calculations β [-]	Probabilistic reliability index with cohesion stochastic β [-]	Difference probabilistic and semi-probabilistic reliability index with cohesion stochastic β [-]	Difference between probabilistic calculation with cohesion stochastic and basis calculation β [-]
10C	5.41	5.61	5.75	0.34	0.14
11E	3.05	0.12	1.15	-1.90	1.03
11F(11D)	3.52	1.06	1.94	-1.58	0.88
13A	5.52	8.46	8.51	2.99	0.05
13E1	5.59	6.81	6.75	1.16	-0.06*
13E2	5.61	6.66	6.70	1.09	0.04

** It is unexpected that the reliability index is lower with the cohesion of the clay cover modelled as a stochastic variable. However, the difference between the reliability index of the probabilistic calculations with the cohesion stochastic and the basis probabilistic calculations is small. For this reason, this unexpected result is acceptable with taking into account the coefficients of variation of the failure probability of the fragility points*

In Figure 48 are the results of JAV with the cohesion of the clay cover stochastic plotted with the results of the WBI calibration study. In Figure 49 are the influence factors shown.

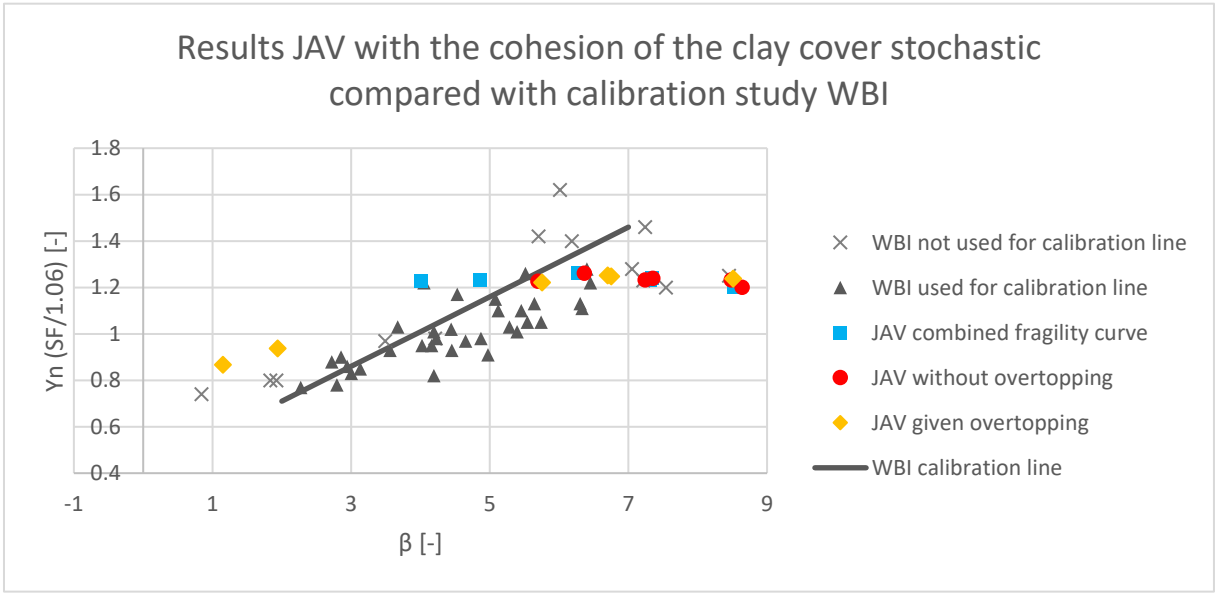

Figure 48: The results of the calculations of JAV with the cohesion of the clay cover stochastic compared with the calibration study of WBI. The vertical position of the results of JAV from the combined fragility curves (blue squares) are determined based on the semi-probabilistic results without overtopping

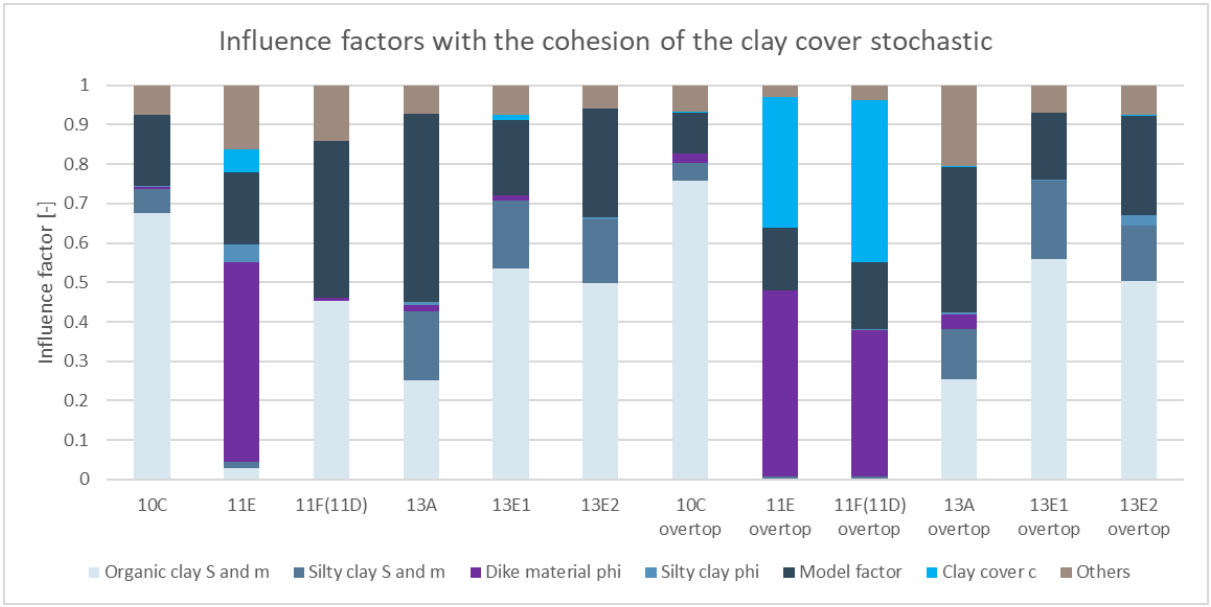

Figure 49: Influence factors with the cohesion of the clay cover stochastic at WBN without overtopping and at the 1 l/s/m overtopping water level with overtopping

D. Results probabilistic calculations with the internal friction angle of the clay cover stochastic

The results of the probabilistic calculations with the internal friction angle of the clay cover stochastic are given in this appendix. For every dike section are per water level the expected reliability index, coefficient of variation of the failure probability, 5% confidence bound of the reliability index and the difference between the expected reliability index and the 5% confidence bound of the reliability index given in the tables in this appendix. The coefficient of variation of the failure probability is specified as the standard deviation of the probability of failure divided by the probability of failure (Deltares, 2022). The 5% confidence bound of the reliability index is determined based on the failure probability and the coefficient of variation of the failure probability.

Besides, for every dike section are the fragility curves given. The fragility points, the fragility curve without overtopping, the fragility curve given overtopping, the combined fragility curve, the probability of exceedance of 1 l/s/m overtopping given the water level and the probability density function of the water level are given in the figures in this appendix. Furthermore, the reliability indexes are given per dike section, a comparison has been made between the semi-probabilistic and probabilistic estimates of the reliability index, the results are plotted with the results of the WBI calibration study and the influence factors are shown.

The results of the probabilistic calculations with the internal friction angle of the clay cover stochastic for dike section 10C are given in Table 43 and the fragility curves are shown in Figure 50.

Table 43: Reliability index probabilistic calculations with the internal friction angle of the clay cover stochastic per water level for dike section 10C

Water level [m +NAP]	Traffic	Overtopping	Reliability index [-]	Coefficient of variation of the failure probability [-]	5% Confidence bound reliability index [-]	Reliability index - 5% confidence bound reliability index [-]
0.24	Yes	No	11.2	0.749	11.1	0.1
4.37	Yes	No	7.26	0.277	7.21	0.05
6.81	No	No	5.22	0.222	5.16	0.06
6.66	No	No	5.47	0.199	5.42	0.05
6.96	No	No	4.21	0.321	4.11	0.10
7.15	No	No	4.12	0.281	4.03	0.09
6.66	No	Yes	5.29	0.203	5.24	0.05
6.96	No	Yes	4.15	0.193	4.09	0.06
6.21	No	Yes	5.63	0.327	5.55	0.08
7.15	No	Yes	3.87	0.186	3.81	0.06

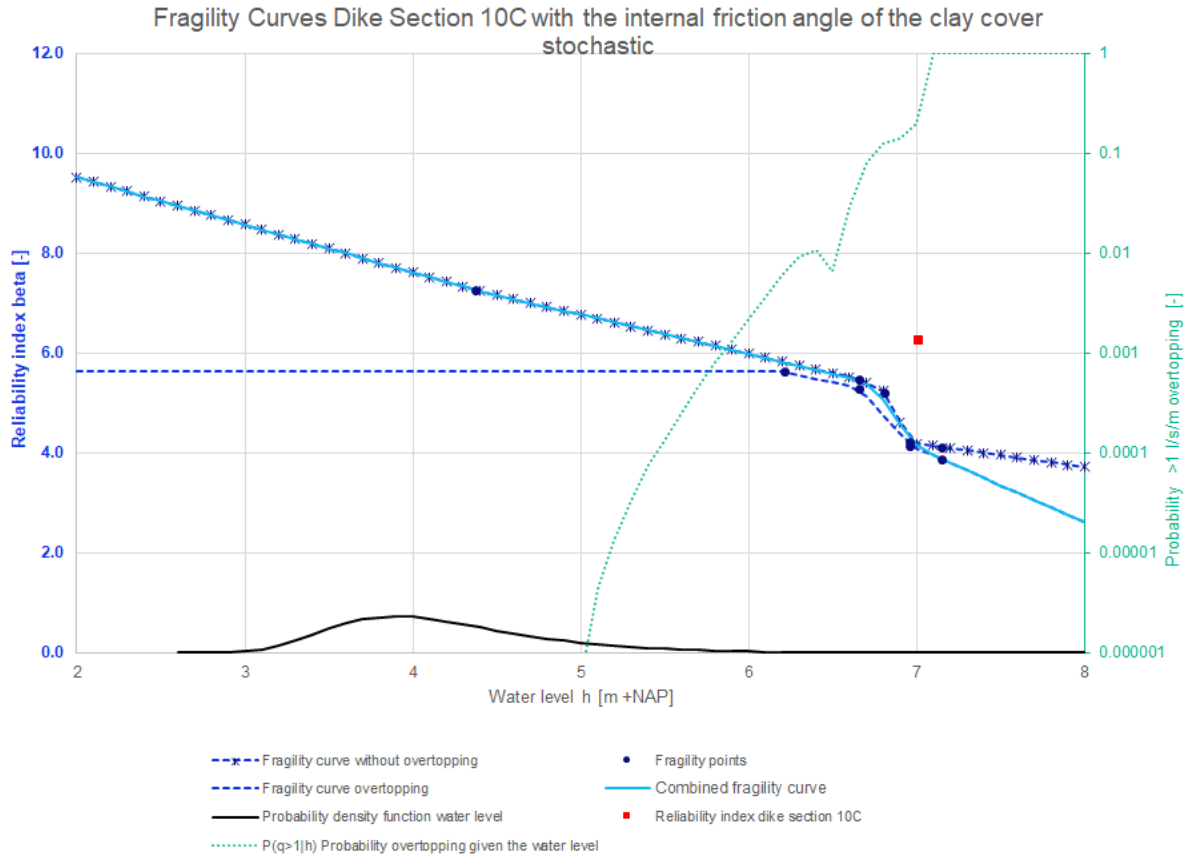

Figure 50: Fragility curves dike section 10C with the internal friction angle of the clay cover stochastic

The results of the probabilistic calculations with the internal friction angle of the clay cover stochastic for dike section 11E are given in Table 44 and the fragility curves are shown in Figure 51.

Table 44: Reliability index probabilistic calculations with the internal friction angle of the clay cover stochastic per water level for dike section 11E

Water level [m +NAP]	Traffic	Overtopping	Reliability index [-]	Coefficient of variation of the failure probability [-]	5% Confidence bound reliability index [-]	Reliability index - 5% confidence bound reliability index [-]
-0.04	Yes	No	7.23	0.155	7.20	0.03
2.39	Yes	No	7.20	0.186	7.16	0.04
3.47	Yes	No	6.98	0.325	6.92	0.06
6.77	No	No	4.31	0.119	4.27	0.04
7.07	No	No	3.82	0.0894	3.78	0.04
6.77	No	Yes	0.348	0.0489	0.27	0.08
7.07	No	Yes	0.167	0.0468	0.08	0.09
6.37	No	Yes	0.465	0.0471	0.40	0.07

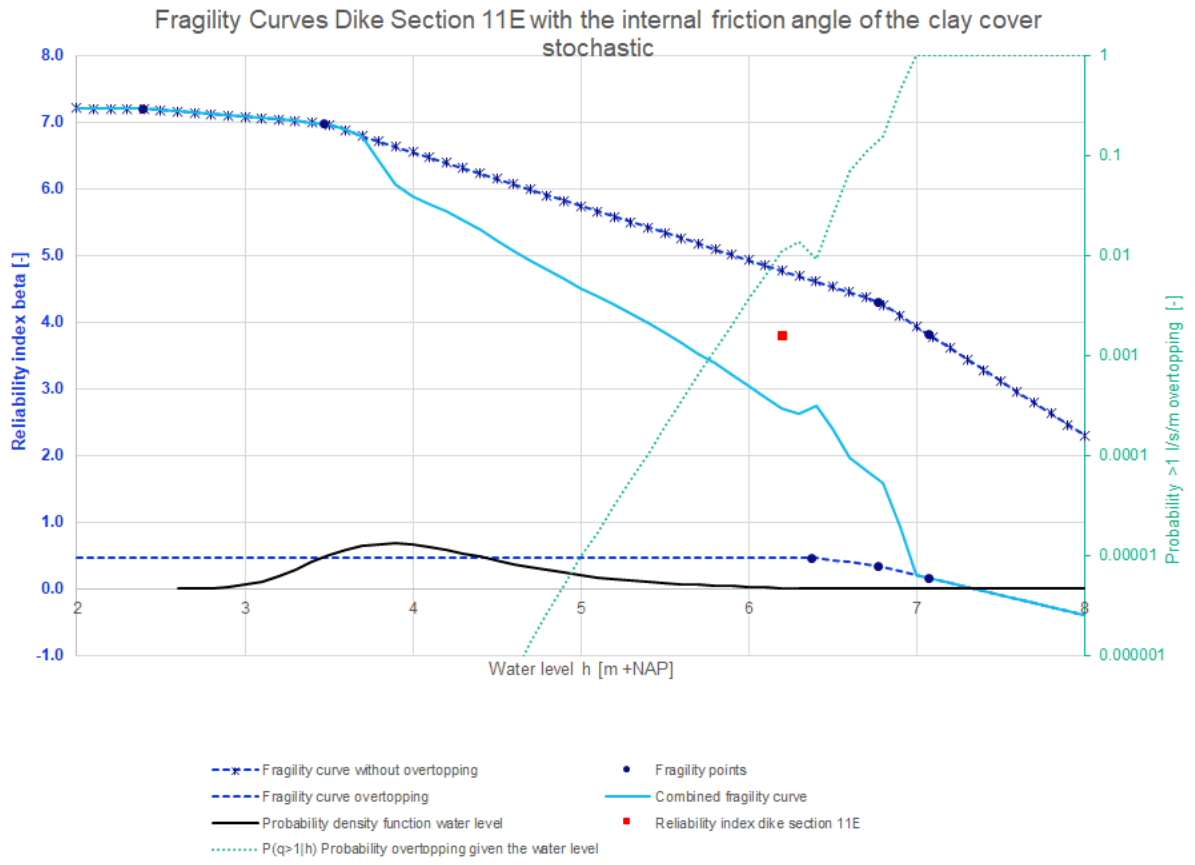

Figure 51: Fragility curves dike section 11E with the internal friction angle of the clay cover stochastic

The results of the probabilistic calculations with the internal friction angle of the clay cover stochastic for dike section 11F(11D) are given in Table 45 and the fragility curves are shown in Figure 52.

Table 45: Reliability index probabilistic calculations with the internal friction angle of the clay cover stochastic per water level for dike section 11F(11D)

Water level [m +NAP]	Traffic	Overtopping	Reliability index [-]	Coefficient of variation of the failure probability [-]	5% Confidence bound reliability index [-]	Reliability index - 5% confidence bound reliability index [-]
-0.04	Yes	No	17.7	0.949	17.6	0.1
2.63	Yes	No	15.6	0.479	15.6	0.0
5.24	Yes	No	9.20	0.326	9.15	0.05
6.79	No	No	7.37	0.254	7.32	0.05
7.09	No	No	7.18	0.163	7.14	0.04
6.79	No	Yes	1.27	0.113	1.18	0.09
7.09	No	Yes	1.18	0.0973	1.09	0.09
6.38	No	Yes	1.41	0.125	1.31	0.10

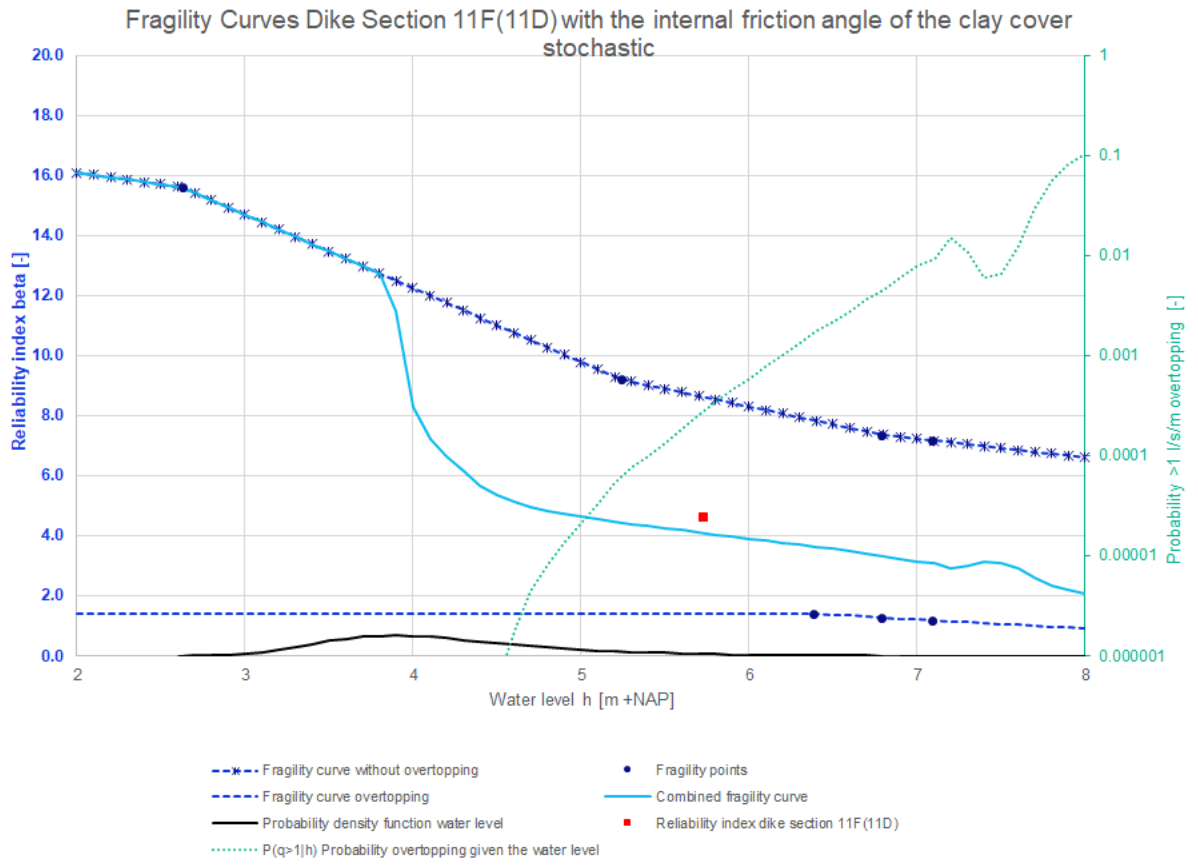

Figure 52: Fragility curves dike section 11F(11D) with the internal friction angle of the clay cover stochastic

The results of the probabilistic calculations with the internal friction angle of the clay cover stochastic for dike section 13A are given in Table 46 and the fragility curves are shown in Figure 53.

Table 46: Reliability index probabilistic calculations with the internal friction angle of the clay cover stochastic per water level for dike section 13A

Water level [m +NAP]	Traffic	Overtopping	Reliability index [-]	Coefficient of variation of the failure probability [-]	5% Confidence bound reliability index [-]	Reliability index - 5% confidence bound reliability index [-]
-0.30	Yes	No	13.6	0.778	13.5	0.1
0.87	Yes	No	12.8	0.766	12.7	0.1
2.07	Yes	No	11.8	0.732	11.7	0.1
6.26	No	No	7.52	0.302	7.47	0.05
6.56	No	No	7.35	0.186	7.31	0.04
6.26	No	Yes	7.26	0.184	7.23	0.03
6.56	No	Yes	7.06	0.178	7.02	0.04
5.66	No	Yes	8.51	0.206	8.48	0.03

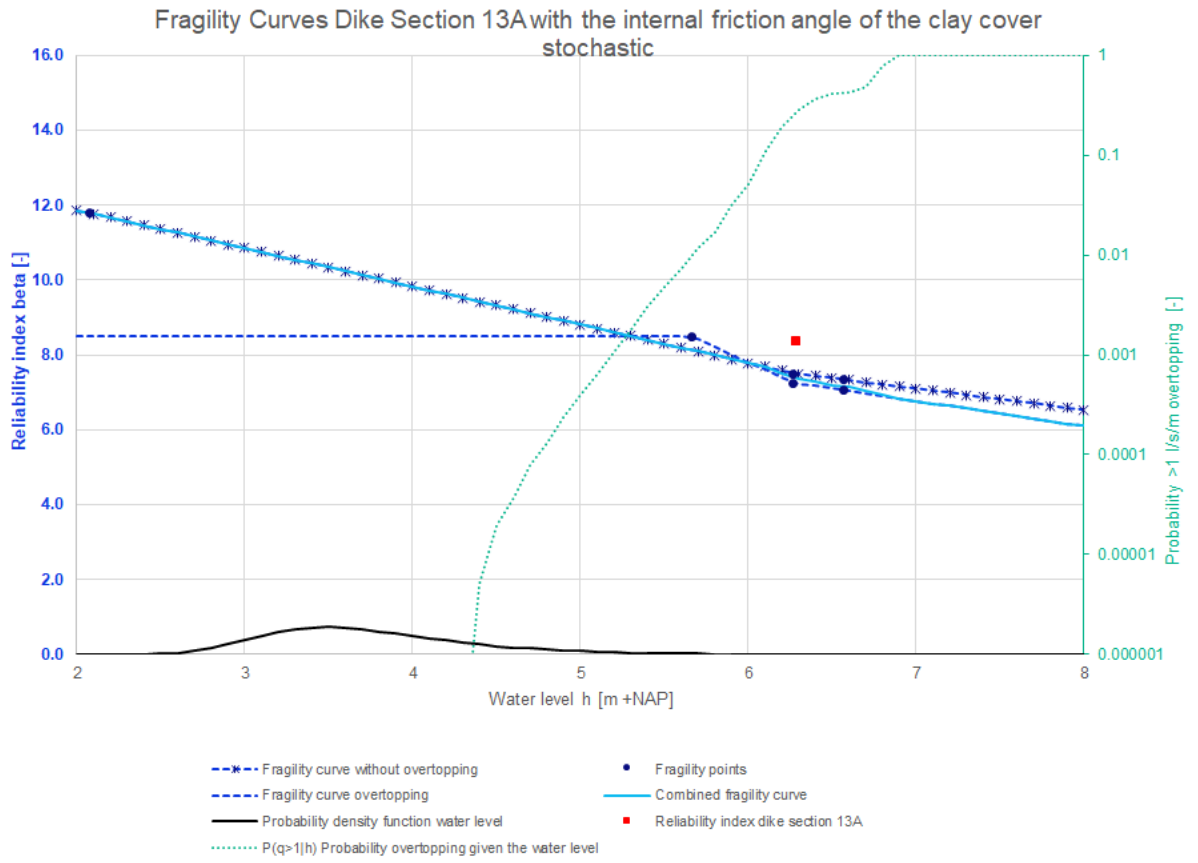

Figure 53: Fragility curves dike section 13A with the internal friction angle of the clay cover stochastic

The results of the probabilistic calculations with the internal friction angle of the clay cover stochastic for dike section 13E1 are given in Table 47 and the fragility curves are shown in Figure 54.

Table 47: Reliability index probabilistic calculations with the internal friction angle of the clay cover stochastic per water level for dike section 13E1

Water level [m +NAP]	Traffic	Overtopping	Reliability index [-]	Coefficient of variation of the failure probability [-]	5% Confidence bound reliability index [-]	Reliability index - 5% confidence bound reliability index [-]
-0.30	Yes	No	10.0	0.242	10.0	0.0
4.69	Yes	No	7.74	0.653	7.65	0.09
6.33	No	No	6.34	0.175	6.30	0.04
6.63	No	No	5.86	0.189	5.82	0.04
6.33	No	Yes	6.64	0.277	6.58	0.06
6.63	No	Yes	6.05	0.173	6.01	0.04
6.00	No	Yes	6.94	0.576	6.85	0.09

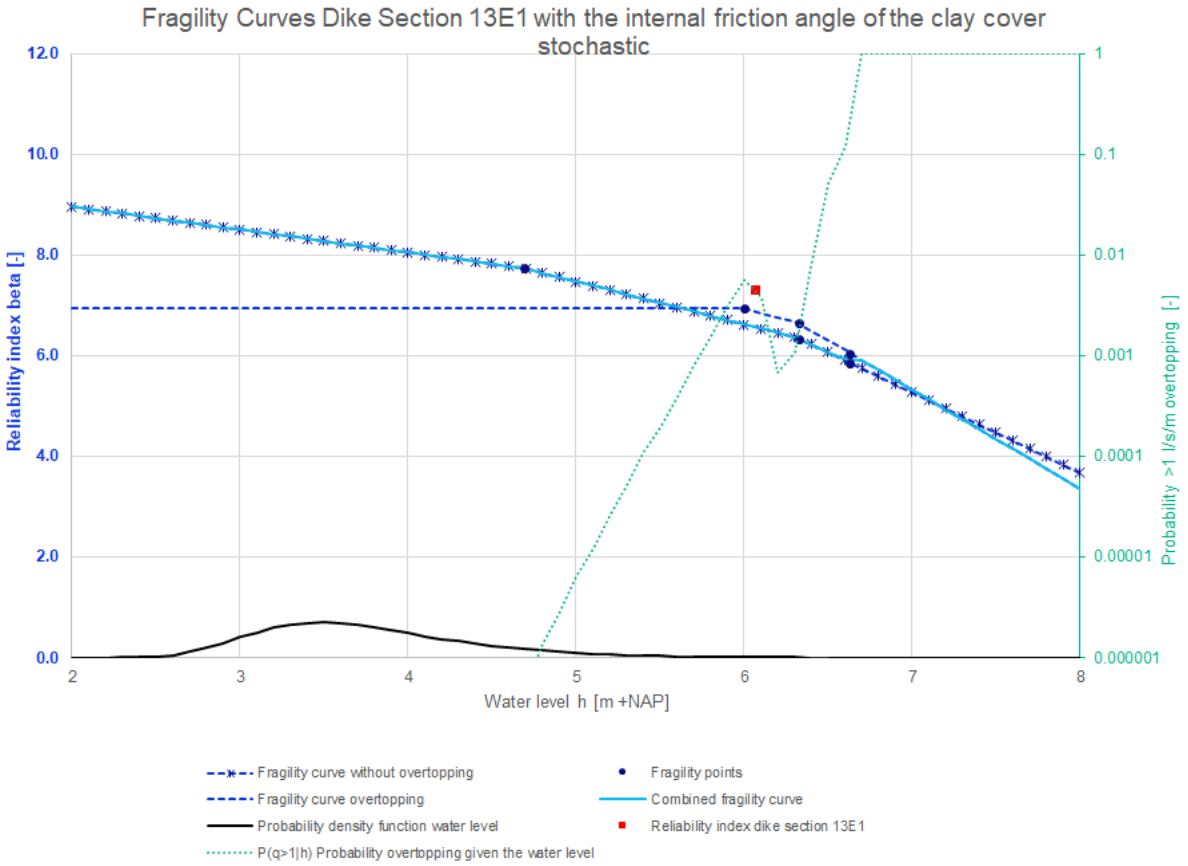

Figure 54: Fragility curves dike section 13E1 with the internal friction angle of the clay cover stochastic

The results of the probabilistic calculations with the internal friction angle of the clay cover stochastic for dike section 13E2 are given in Table 48 and the fragility curves are shown in Figure 55.

Table 48: Reliability index probabilistic calculations with the internal friction angle of the clay cover stochastic per water level for dike section 13E2

Water level [m +NAP]	Traffic	Overtopping	Reliability index [-]	Coefficient of variation of the failure probability [-]	5% Confidence bound reliability index [-]	Reliability index - 5% confidence bound reliability index [-]
-0.30	Yes	No	10.1	0.215	10.1	0.0
4.69	Yes	No	7.39	0.163	7.36	0.03
6.24	No	No	6.40	0.165	6.37	0.03
6.54	No	No	5.99	0.151	5.95	0.04
6.24	No	Yes	6.29	0.156	6.26	0.03
6.54	No	Yes	5.94	0.167	5.90	0.04
5.91	No	Yes	6.62	0.173	6.59	0.03

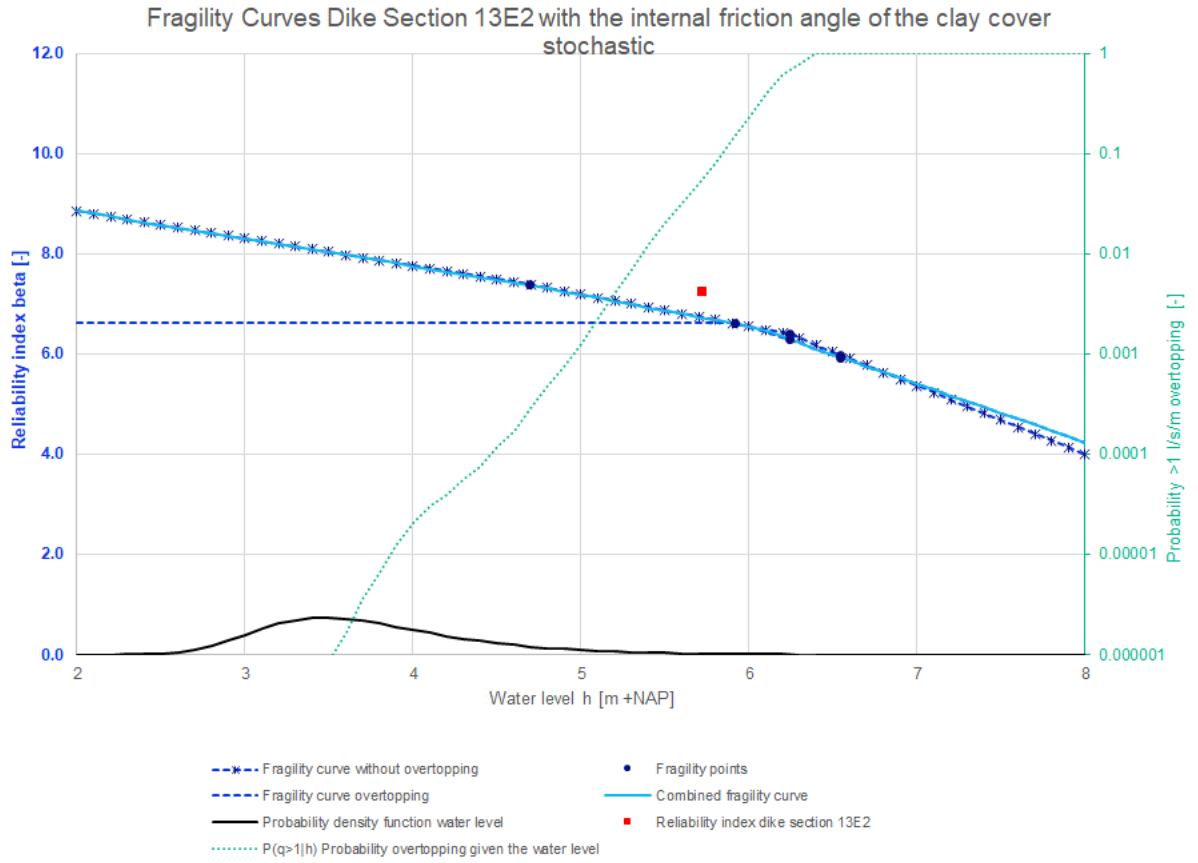

Figure 55: Fragility curves dike section 13E2 with the internal friction angle of the clay cover stochastic

The reliability index for the probabilistic calculations with the internal friction angle of the clay cover modelled as a stochastic variable are shown in Table 49.

Table 49: Reliability index probabilistic calculations with the internal friction angle of the clay cover stochastic

Dike section	Reliability index β combined fragility curve [-]	Reliability index β without overtopping [-]	Reliability index β given overtopping [-]
10C	6.27	6.34	5.63
11E	3.80	5.49	0.47
11F(11D)	4.62	8.35	1.41
13A	8.37	8.44	8.51
13E1	7.31*	7.30*	6.94
13E2	7.26	7.28	6.62

** The reason why the reliability index without overtopping is lower than the reliability index for the combined fragility curve is probably caused by the schematization of the dike profile*

A comparison has been made between the reliability index of the combined fragility curve with the internal friction angle of the clay cover modelled as a stochastic variable, the combined fragility curve of the basis probabilistic calculations and the semi-probabilistic calculations without overtopping in Table 50. Modelling the internal friction angle of the clay cover as a stochastic variable in the probabilistic calculations has a small effect on the reliability index in comparison with the basis calculations of JAV (see upper right column in Table 50).

Table 50: Comparison reliability index semi-probabilistic calculations without overtopping, basis probabilistic calculations combined fragility curve and probabilistic calculations combined fragility curve with the internal friction angle of the clay cover stochastic

Dike section	Semi-probabilistic reliability index β [-]	Probabilistic reliability index basis calculations β [-]	Probabilistic reliability index with internal friction angle stochastic β [-]	Difference probabilistic and semi-probabilistic reliability index with internal friction angle stochastic β [-]	Difference between probabilistic calculation with internal friction angle stochastic and basis calculation β [-]
10C	5.68	6.29	6.27	0.59	-0.02*
11E	5.45	3.72	3.80	-1.65	0.08
11F(11D)	5.48	4.50	4.62	-0.86	0.12
13A	5.27	8.36	8.37	3.10	0.01
13E1	5.48	7.14	7.31	1.83	0.17
13E2	5.53	7.27	7.26	1.73	-0.01*

** It is unexpected that the reliability index is lower with the internal friction angle of the clay cover modelled as a stochastic variable. However, the difference between the reliability index of the probabilistic calculations with the internal friction angle of the clay cover stochastic and the basis probabilistic calculations is small. For this reason, this unexpected result is acceptable with taking into account the coefficients of variation of the failure probability of the fragility points*

The reliability index for the fragility curve without overtopping with the internal friction angle of the clay cover modelled as a stochastic variable, the fragility curve without overtopping of the basis probabilistic calculations and the semi-probabilistic calculations without overtopping are compared with each other in Table 51. The estimated reliability index based on the semi-probabilistic calculations is for all of the six dike sections too conservative, which can be seen from the second column from the right in Table 51. This is a bit unexpected, since the WBI damage factor line of 2016

is fitted to the twenty percent quantiles of the betas for the situation without overtopping (see paragraph 2.4.1). Modelling the internal friction angle of the clay cover as a stochastic variable in the probabilistic calculations without overtopping has a relatively small effect on the reliability index in comparison with the basis calculations of JAV (see upper right column in Table 51), which was also the case for the results based on the combined fragility curves in Table 50.

Table 51: Comparison reliability index semi-probabilistic calculations without overtopping, basis probabilistic calculations without overtopping and probabilistic calculations without overtopping with the internal friction angle of the clay cover stochastic

Dike section	Semi-probabilistic reliability index β [-]	Probabilistic reliability index basis calculations β [-]	Probabilistic reliability index with internal friction angle stochastic β [-]	Difference probabilistic and semi-probabilistic reliability index with internal friction angle stochastic β [-]	Difference between probabilistic calculation with internal friction angle stochastic and basis calculation β [-]
10C	5.68	6.38	6.34	0.66	-0.04*
11E	5.45	5.34	5.49	0.04	0.15
11F(11D)	5.48	8.35	8.35	2.87	0.00
13A	5.27	8.43	8.44	3.17	0.01
13E1	5.48	7.19	7.30	1.82	0.11
13E2	5.53	7.27	7.28	1.75	0.01

** It is unexpected that the reliability index is lower with the internal friction angle of the clay cover modelled as a stochastic variable. However, the difference between the reliability index of the probabilistic calculations with the internal friction angle of the clay cover stochastic and the basis probabilistic calculations is small. For this reason, this unexpected result is acceptable with taking into account the coefficients of variation of the failure probability of the fragility points*

A comparison has been made between the reliability index of the fragility point with the largest contribution to 1 l/s/m overtopping with the internal friction angle of the clay cover modelled as a stochastic variable, the fragility point with the largest contribution to 1 l/s/m overtopping of the basis probabilistic calculations and the semi-probabilistic calculations given overtopping in Table 52. The largest increase in the reliability index in comparison with the basis probabilistic calculations given overtopping is found for the dike sections with a relatively small slip plane of JAV (dike section 11E and 11F(11D), see upper right column in Table 52). However, the increase in reliability index of dike section 11E and 11F(11D) with the internal friction angle of the clay cover modelled stochastic is lower than with the cohesion of the clay cover modelled stochastic (see Table 42).

Table 52: Comparison reliability index semi-probabilistic calculations given overtopping, basis probabilistic calculations given overtopping and probabilistic calculations given overtopping with the internal friction angle of the clay cover stochastic

Dike section	Semi-probabilistic reliability index β [-]	Probabilistic reliability index basis calculations β [-]	Probabilistic reliability index with internal friction angle stochastic β [-]	Difference probabilistic and semi-probabilistic reliability index with internal friction angle stochastic β [-]	Difference between probabilistic calculation with internal friction angle stochastic and basis calculation β [-]
10C	5.41	5.61	5.63	0.22	0.02
11E	3.05	0.12	0.47	-2.58	0.35
11F(11D)	3.52	1.06	1.41	-2.11	0.35
13A	5.52	8.46	8.51	2.99	0.05
13E1	5.59	6.81	6.94	1.35	0.13
13E2	5.61	6.66	6.62	1.01	-0.04*

** It is unexpected that the reliability index is lower with the internal friction angle of the clay cover modelled as a stochastic variable. However, the difference between the reliability index of the probabilistic calculations with the internal friction angle of the clay cover stochastic and the basis probabilistic calculations is small. For this reason, this unexpected result is acceptable with taking into account the coefficients of variation of the failure probability of the fragility points*

In Figure 56 are the results of JAV with the internal friction angle of the clay cover stochastic plotted with the results of the WBI calibration study. In Figure 57 are the influence factors shown.

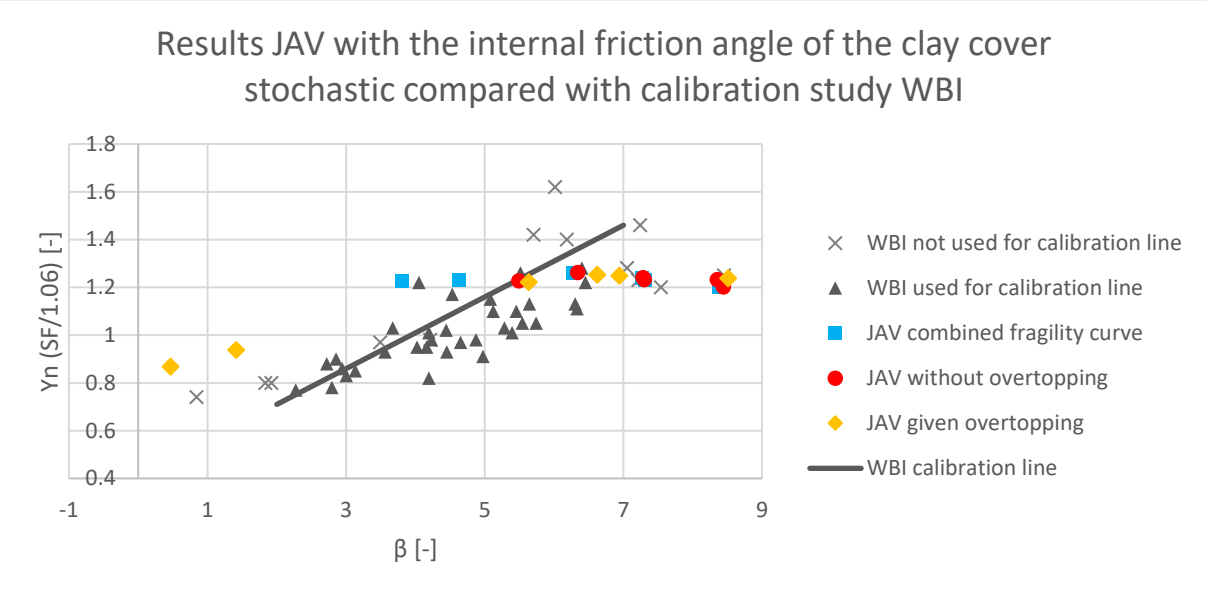

Figure 56: The results of the calculations of JAV with the internal friction angle of the clay cover stochastic compared with the calibration study of WBI. The vertical position of the results of JAV from the combined fragility curves (blue squares) are determined based on the semi-probabilistic results without overtopping

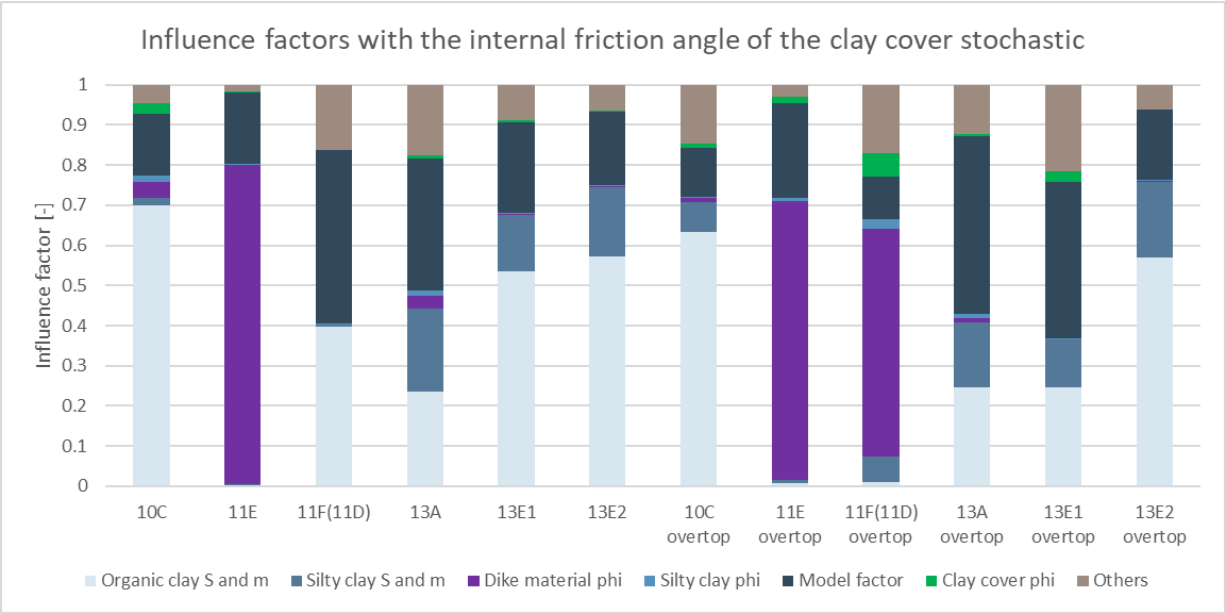

Figure 57: Influence factors with the internal friction angle of the clay cover stochastic at WBN without overtopping and at the 1 l/s/m overtopping water level with overtopping

E. Results probabilistic calculations with the cohesion and the internal friction angle of the clay cover stochastic

The results of the probabilistic calculations with the cohesion and the internal friction angle of the clay cover stochastic are given in this appendix. For every dike section are per water level the expected reliability index, coefficient of variation of the failure probability, 5% confidence bound of the reliability index and the difference between the expected reliability index and the 5% confidence bound of the reliability index given in the tables in this appendix. The coefficient of variation of the failure probability is specified as the standard deviation of the probability of failure divided by the probability of failure (Deltares, 2022). The 5% confidence bound of the reliability index is determined based on the failure probability and the coefficient of variation of the failure probability.

Besides, for every dike section are the fragility curves given. The fragility points, the fragility curve without overtopping, the fragility curve given overtopping, the combined fragility curve, the probability of exceedance of 1 l/s/m overtopping given the water level and the probability density function of the water level are given in the figures in this appendix. Furthermore, the reliability indexes are given per dike section, a comparison has been made between the semi-probabilistic and probabilistic estimates of the reliability index and the results are plotted with the results of the WBI calibration study.

The results of the probabilistic calculations with the cohesion and internal friction angle of the clay cover stochastic for dike section 10C are given in Table 53 and the fragility curves are shown in Figure 58.

Table 53: Reliability index probabilistic calculations with the cohesion and internal friction angle of the clay cover stochastic per water level for dike section 10C

Water level [m +NAP]	Traffic	Overtopping	Reliability index [-]	Coefficient of variation of the failure probability [-]	5% Confidence bound reliability index [-]	Reliability index - 5% confidence bound reliability index [-]
0.24	Yes	No	10.7	0.553	10.7	0.0
4.37	Yes	No	7.17	0.432	7.09	0.08
6.81	No	No	5.25	0.210	5.19	0.06
6.66	No	No	5.51	0.206	5.45	0.06
6.96	No	No	4.30	0.282	4.22	0.08
7.15	No	No	3.99	0.136	3.94	0.05
6.66	No	Yes	5.13	0.153	5.09	0.04
6.96	No	Yes	4.06	0.176	4.00	0.06
6.21	No	Yes	5.62	0.136	5.58	0.04
7.15	No	Yes	3.80	0.101	3.76	0.04

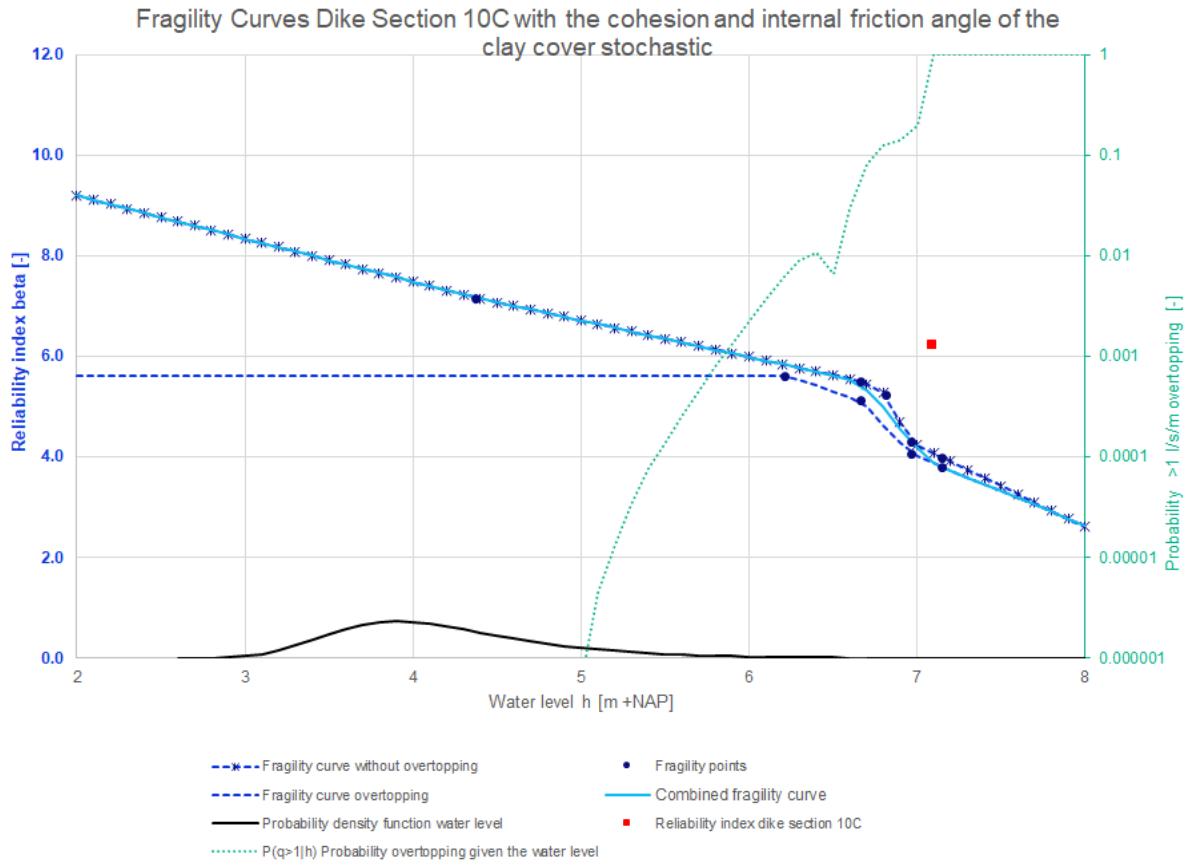

Figure 58: Fragility curves dike section 10C with the cohesion and internal friction angle of the clay cover stochastic

The results of the probabilistic calculations with the cohesion and internal friction angle of the clay cover stochastic for dike section 11E are given in Table 54 and the fragility curves are shown in Figure 59.

Table 54: Reliability index probabilistic calculations with the cohesion and internal friction angle stochastic per water level for dike section 11E

Water level [m +NAP]	Traffic	Overtopping	Reliability index [-]	Coefficient of variation of the failure probability [-]	5% Confidence bound reliability index [-]	Reliability index - 5% confidence bound reliability index [-]
-0.04	Yes	No	7.41	0.172	7.38	0.03
2.39	Yes	No	7.55	0.201	7.51	0.04
3.47	Yes	No	7.06	0.476	6.97	0.09
6.77	No	No	4.84	0.233	4.77	0.07
7.07	No	No	4.15	0.260	4.07	0.08
6.77	No	Yes	1.15	0.05	1.10	0.05
7.07	No	Yes	0.974	0.05	0.92	0.05
6.37	No	Yes	1.37	0.0512	1.33	0.04

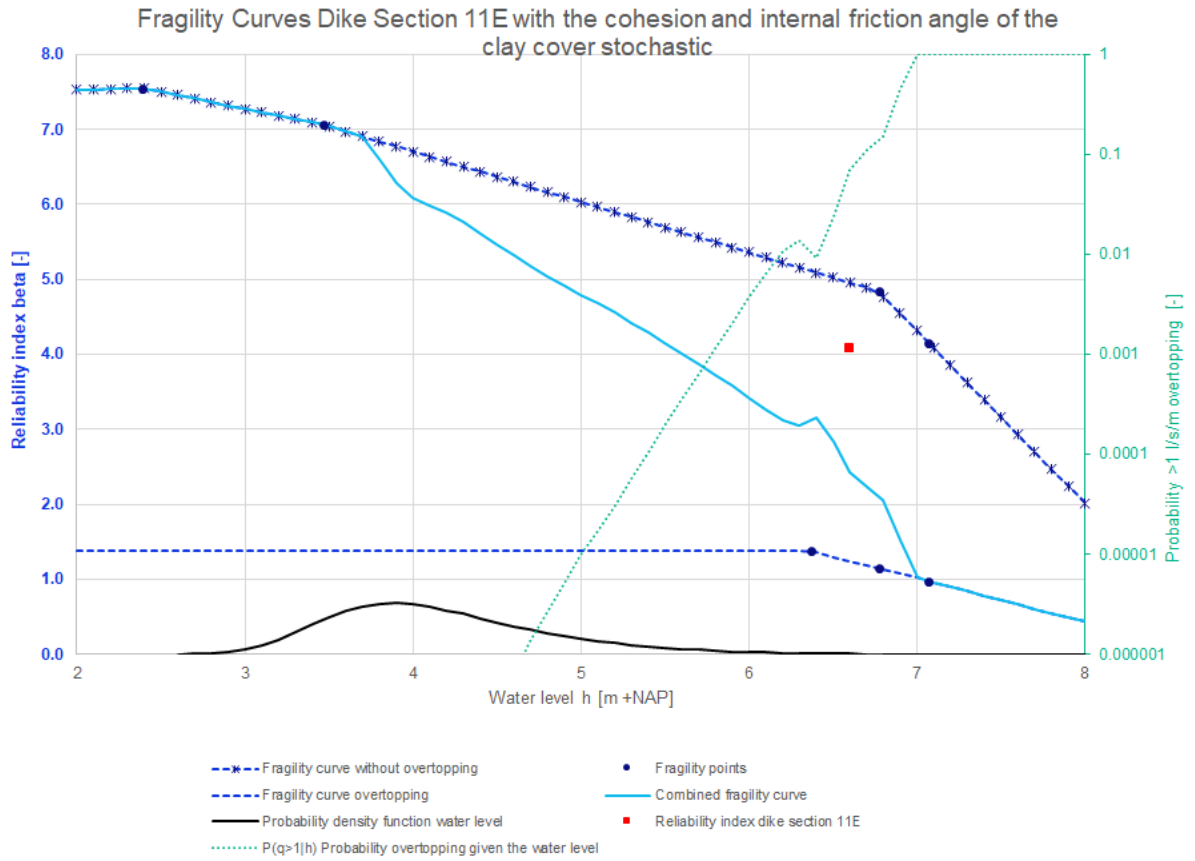

Figure 59: Fragility curves dike section 11E with the cohesion and internal friction angle of the clay cover stochastic

The results of the probabilistic calculations with the cohesion and internal friction angle of the clay cover stochastic for dike section 11F(11D) are given in Table 55 and the fragility curves are shown in Figure 60.

Table 55: Reliability index probabilistic calculations with the cohesion and internal friction angle of the clay cover stochastic per water level for dike section 11F(11D)

Water level [m +NAP]	Traffic	Overtopping	Reliability index [-]	Coefficient of variation of the failure probability [-]	5% Confidence bound reliability index [-]	Reliability index - 5% confidence bound reliability index [-]
-0.04	Yes	No	17.8	0.452	17.8	0.0
2.63	Yes	No	15.8	0.325	15.8	0.0
5.24	Yes	No	9.39	0.354	9.34	0.05
6.79	No	No	7.54	0.242	7.49	0.05
7.09	No	No	7.36	0.274	7.31	0.05
6.79	No	Yes	2.05	0.0641	2.01	0.04
7.09	No	Yes	1.90	0.0976	1.83	0.07
6.38	No	Yes	2.32	0.127	2.24	0.08

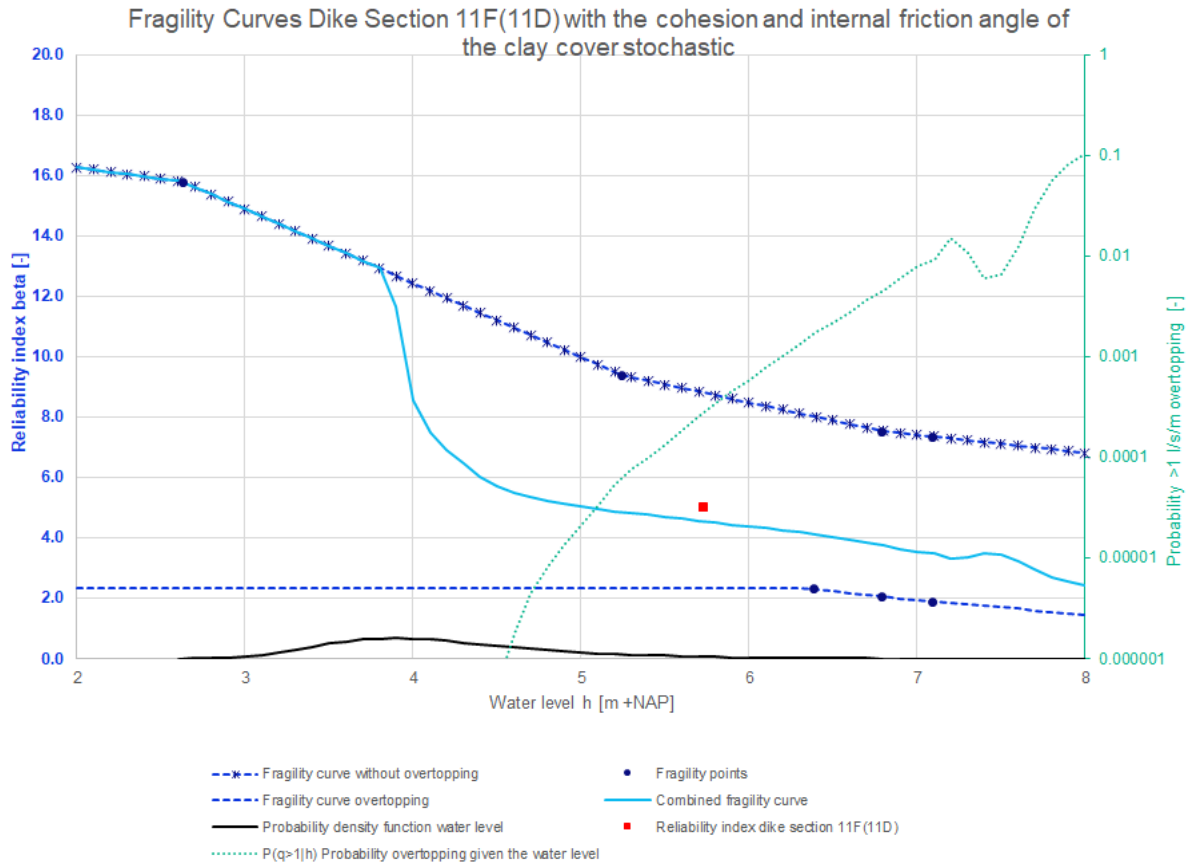

Figure 60: Fragility curves dike section 11F(11D) with the cohesion and internal friction angle of the clay cover stochastic

The results of the probabilistic calculations with the cohesion and internal friction angle of the clay cover stochastic for dike section 13A are given in Table 56 and the fragility curves are shown in Figure 61.

Table 56: Reliability index probabilistic calculations with the cohesion and internal friction angle of the clay cover stochastic per water level for dike section 13A

Water level [m +NAP]	Traffic	Overtopping	Reliability index [-]	Coefficient of variation of the failure probability [-]	5% Confidence bound reliability index [-]	Reliability index - 5% confidence bound reliability index [-]
-0.30	Yes	No	13.7	0.674	13.6	0.1
0.87	Yes	No	13.1	0.300	13.1	0.0
2.07	Yes	No	11.6	0.913	11.5	0.1
6.26	No	No	7.73	0.201	7.70	0.03
6.56	No	No	7.51	0.202	7.47	0.04
6.26	No	Yes	7.37	0.207	7.33	0.04
6.56	No	Yes	7.16	0.202	7.12	0.04
5.66	No	Yes	8.42	0.333	8.37	0.05

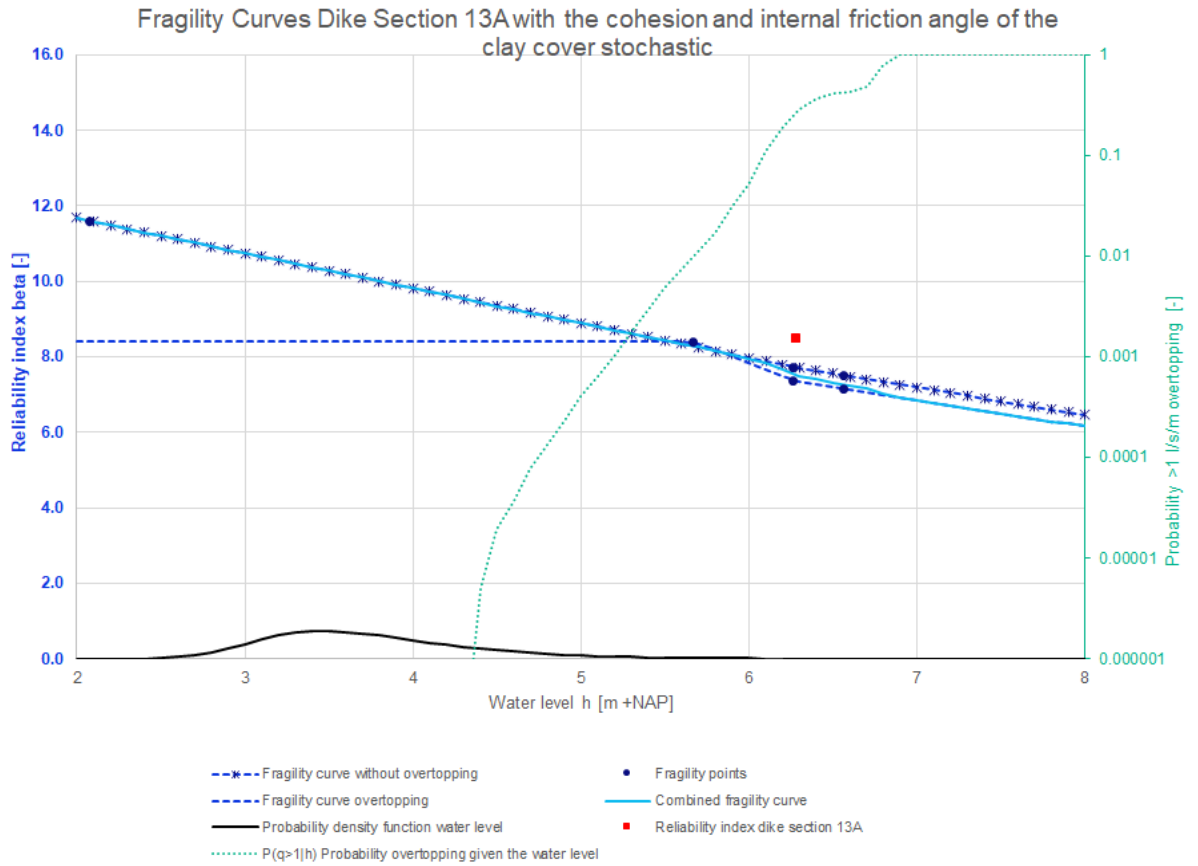

Figure 61: Fragility curves dike section 13A with the cohesion and internal friction angle of the clay cover stochastic

The results of the probabilistic calculations with the cohesion and internal friction angle of the clay cover stochastic for dike section 13E1 are given in Table 57 and the fragility curves are shown in Figure 62.

Table 57: Reliability index probabilistic calculations with the cohesion and internal friction angle of the clay cover stochastic per water level for dike section 13E1

Water level [m +NAP]	Traffic	Overtopping	Reliability index [-]	Coefficient of variation of the failure probability [-]	5% Confidence bound reliability index [-]	Reliability index - 5% confidence bound reliability index [-]
-0.30	Yes	No	9.93	0.209	9.90	0.03
4.69	Yes	No	7.58	0.452	7.51	0.07
6.33	No	No	6.37	0.188	6.33	0.04
6.63	No	No	5.73	0.234	5.67	0.06
6.33	No	Yes	6.39	0.198	6.34	0.05
6.63	No	Yes	5.98	0.758	5.85	0.13
6.00	No	Yes	6.87	0.231	6.82	0.05

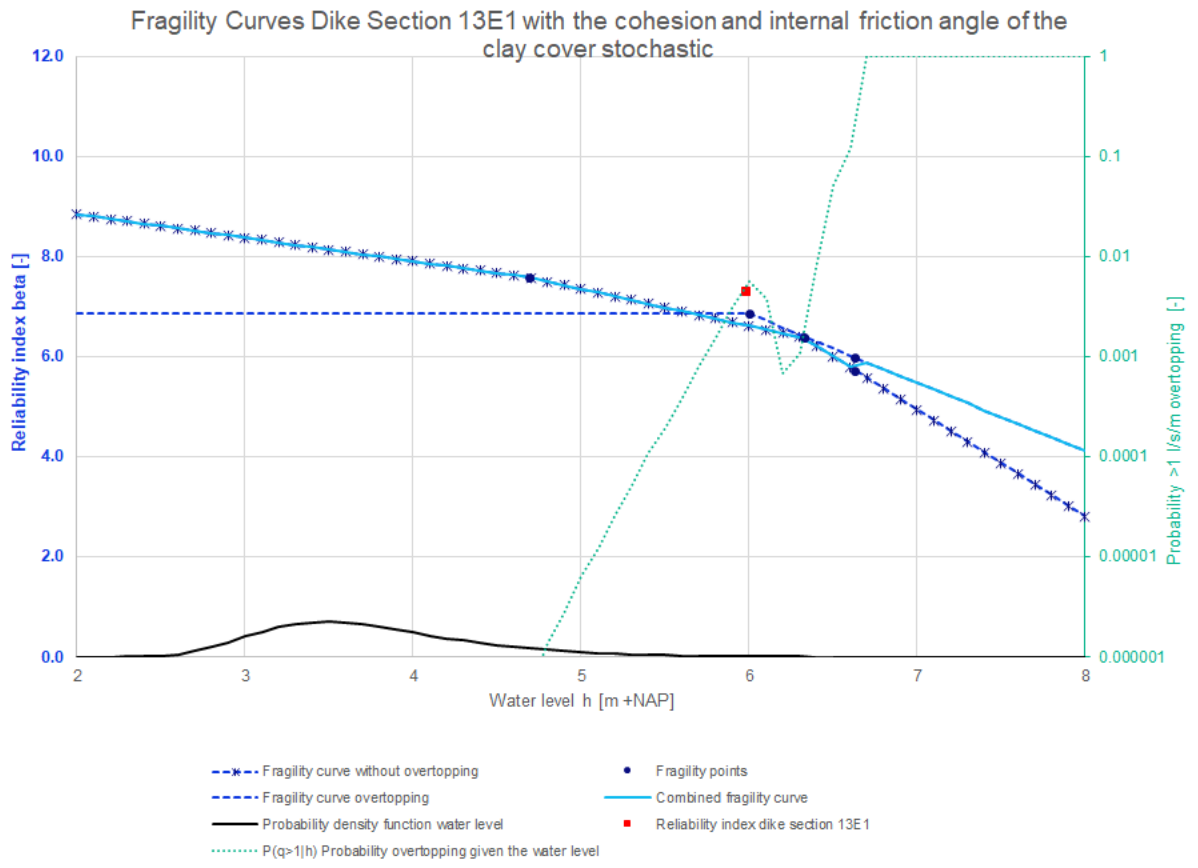

Figure 62: Fragility curves dike section 13E1 with the cohesion and internal friction angle of the clay cover stochastic

The results of the probabilistic calculations with the cohesion and internal friction angle of the clay cover stochastic for dike section 13E2 are given in Table 58 and the fragility curves are shown in Figure 63.

Table 58: Reliability index probabilistic calculations with the cohesion and internal friction angle of the clay cover stochastic per water level for dike section 13E2

Water level [m +NAP]	Traffic	Overtopping	Reliability index [-]	Coefficient of variation of the failure probability [-]	5% Confidence bound reliability index [-]	Reliability index - 5% confidence bound reliability index [-]
-0.30	Yes	No	9.94	0.420	9.88	0.06
4.69	Yes	No	7.45	0.222	7.41	0.04
6.24	No	No	6.46	0.151	6.43	0.03
6.54	No	No	6.03	0.130	6.00	0.03
6.24	No	Yes	6.39	0.223	6.35	0.04
6.54	No	Yes	6.00	0.169	5.96	0.04
5.91	No	Yes	6.68	0.277	6.63	0.05

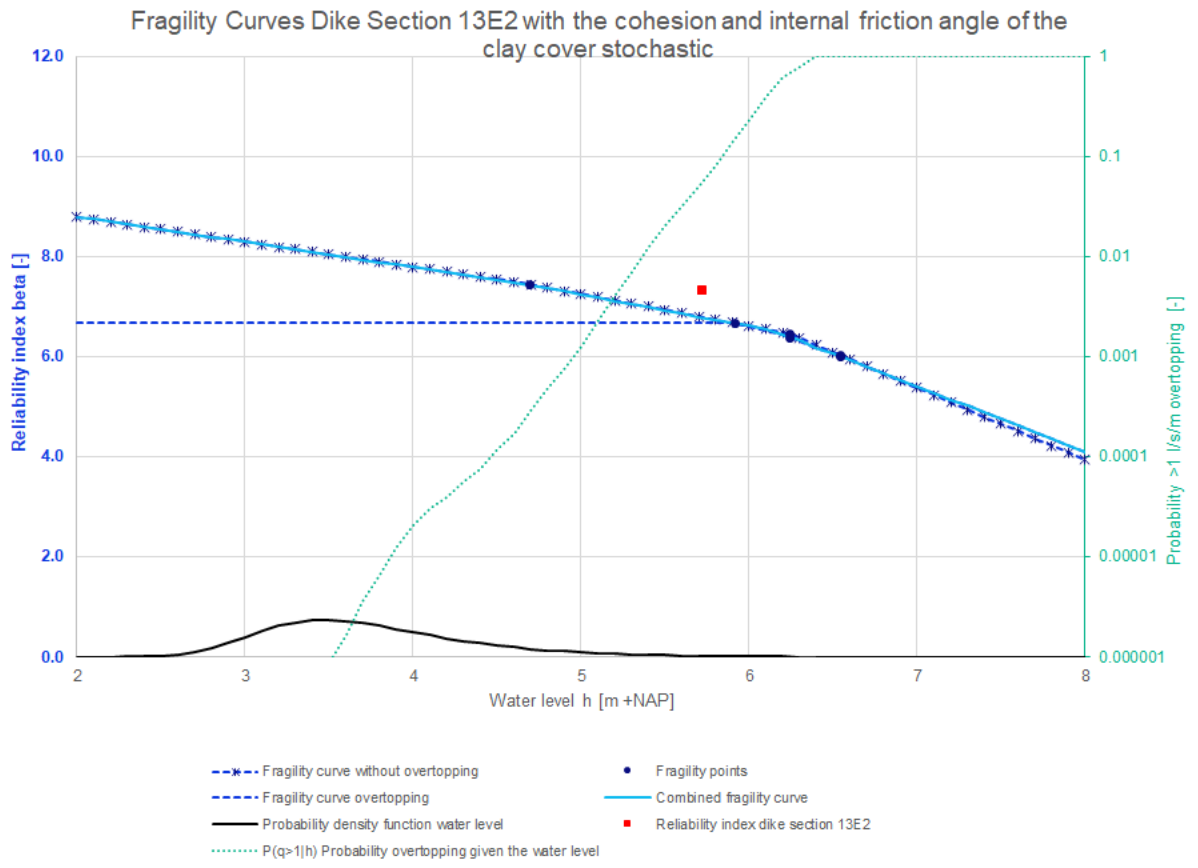

Figure 63: Fragility curves dike section 13E2 with the cohesion and internal friction angle of the clay cover stochastic

The reliability index for the probabilistic calculations with the cohesion and the internal friction angle of the clay cover modelled as a stochastic variable are shown in Table 59.

Table 59: Reliability index probabilistic calculations with the cohesion and the internal friction angle of the clay cover stochastic

Dike section	Reliability index β combined fragility curve [-]	Reliability index β without overtopping [-]	Reliability index β given overtopping [-]
10C	6.25	6.32	5.62
11E	4.09	5.87	1.37
11F(11D)	5.02	8.51	2.32
13A	8.49	8.61	8.42
13E1	7.29*	7.22*	6.87
13E2	7.32	7.33	6.68

** The reason why the reliability index without overtopping is lower than the reliability index for the combined fragility curve is probably caused by the schematization of the dike profile*

A comparison has been made between the reliability index of the combined fragility curve with the cohesion and the internal friction angle of the clay cover modelled as a stochastic variable, the combined fragility curve of the basis probabilistic calculations and the semi-probabilistic calculations without overtopping in Table 60. Modelling the cohesion and the internal friction angle of the clay cover stochastic in the probabilistic calculations has an effect on the reliability index for dike sections with a relatively small slip plane (dike section 11E and 11F(11D)) in comparison with the results of the basis calculations of JAV (see upper right column in Table 60).

Table 60: Comparison reliability index semi-probabilistic calculations without overtopping, basis probabilistic calculations combined fragility curve and probabilistic calculations combined fragility curve with the cohesion and the internal friction angle of the clay cover stochastic

Dike section	Semi-probabilistic reliability index β [-]	Probabilistic reliability index basis calculations β [-]	Probabilistic reliability index with cohesion and internal friction angle stochastic β [-]	Difference probabilistic and semi-probabilistic reliability index with cohesion and internal friction angle stochastic β [-]	Difference between probabilistic calculation with cohesion and internal friction angle stochastic and basis calculation β [-]
10C	5.68	6.29	6.25	0.57	-0.04*
11E	5.45	3.72	4.09	-1.36	0.37
11F(11D)	5.48	4.50	5.02	-0.46	0.52
13A	5.27	8.36	8.49	3.22	0.13
13E1	5.48	7.14	7.29	1.81	0.15
13E2	5.53	7.27	7.32	1.79	0.05

** It is unexpected that the reliability index is lower with the cohesion and the internal friction angle of the clay cover modelled stochastic. However, the difference between the reliability index of the probabilistic calculations with the cohesion and the internal friction angle of the clay cover stochastic and the basis probabilistic calculations is small. For this reason, this unexpected result is acceptable with taking into account the coefficients of variation of the failure probability of the fragility points*

The reliability index for the fragility curve without overtopping with the cohesion and the internal friction angle of the clay cover modelled as a stochastic variable, the fragility curve without overtopping of the basis probabilistic calculations and the semi-probabilistic calculations without

overtopping are compared with each other in Table 61. One can see that the semi-probabilistic results are conservative for all dike sections from the second column from the right after modelling the cohesion and the internal friction angle of the clay cover stochastic in the probabilistic calculations. This is a bit unexpected, since the WBI damage factor line of 2016 is fitted to the twenty percent quantiles of the betas for the situation without overtopping (see paragraph 2.4.1). Modelling the cohesion and the internal friction angle of the clay cover stochastic in the probabilistic calculations without overtopping has the largest effect on the reliability index of dike section 11E in comparison with the basis probabilistic calculations of JAV (see upper right column in Table 61).

Table 61: Comparison reliability index semi-probabilistic calculations without overtopping, basis probabilistic calculations without overtopping and probabilistic calculations without overtopping with the cohesion and the internal friction angle of the clay cover stochastic

Dike section	Semi-probabilistic reliability index β [-]	Probabilistic reliability index basis calculations β [-]	Probabilistic reliability index with cohesion and internal friction angle stochastic β [-]	Difference probabilistic and semi-probabilistic reliability index with cohesion and internal friction angle stochastic β [-]	Difference between probabilistic calculation with cohesion and internal friction angle stochastic and basis calculation β [-]
10C	5.68	6.38	6.32	0.64	-0.06*
11E	5.45	5.34	5.87	0.42	0.53
11F(11D)	5.48	8.35	8.51	3.03	0.16
13A	5.27	8.43	8.61	3.34	0.18
13E1	5.48	7.19	7.22	1.74	0.03
13E2	5.53	7.27	7.33	1.80	0.06

** It is unexpected that the reliability index is lower with the cohesion and the internal friction angle of the clay cover modelled stochastic. However, the difference between the reliability index of the probabilistic calculations with the cohesion and the internal friction angle of the clay cover stochastic and the basis probabilistic calculations is small. For this reason, this unexpected result is acceptable with taking into account the coefficients of variation of the failure probability of the fragility points*

A comparison has been made between the reliability index of the fragility point with the largest contribution to 1 l/s/m overtopping with the cohesion and the internal friction angle of the clay cover modelled as a stochastic variable, the fragility point with the largest contribution to 1 l/s/m overtopping of the basis probabilistic calculations and the semi-probabilistic calculations given overtopping in Table 62. Modelling the cohesion and the internal friction angle of the clay cover stochastic has the largest effect on the reliability index for the dike sections with a relatively small slip plane of JAV (dike section 11E and 11F(11D), see upper right column in Table 62).

Table 62: Comparison reliability index semi-probabilistic calculations given overtopping, basis probabilistic calculations given overtopping and probabilistic calculations given overtopping with the cohesion and the internal friction angle of the clay cover stochastic

Dike section	Semi-probabilistic reliability index β [-]	Probabilistic reliability index basis calculations β [-]	Probabilistic reliability index with cohesion and internal friction angle stochastic β [-]	Difference probabilistic and semi-probabilistic reliability index with cohesion and internal friction angle stochastic β [-]	Difference between probabilistic calculation with cohesion and internal friction angle stochastic and basis calculation β [-]
10C	5.41	5.61	5.62	0.21	0.01
11E	3.05	0.12	1.37	-1.68	1.25
11F(11D)	3.52	1.06	2.32	-1.20	1.26
13A	5.52	8.46	8.42	2.90	-0.04*
13E1	5.59	6.81	6.87	1.28	0.06
13E2	5.61	6.66	6.68	1.07	0.02

** It is unexpected that the reliability index is lower with the cohesion and the internal friction angle of the clay cover modelled stochastic. However, the difference between the reliability index of the probabilistic calculations with the cohesion and the internal friction angle of the clay cover stochastic and the basis probabilistic calculations is small. For this reason, this unexpected result is acceptable with taking into account the coefficients of variation of the failure probability of the fragility points*

In Figure 64 are the results of JAV with the cohesion and the internal friction angle of the clay cover stochastic plotted with the results of the WBI calibration study.

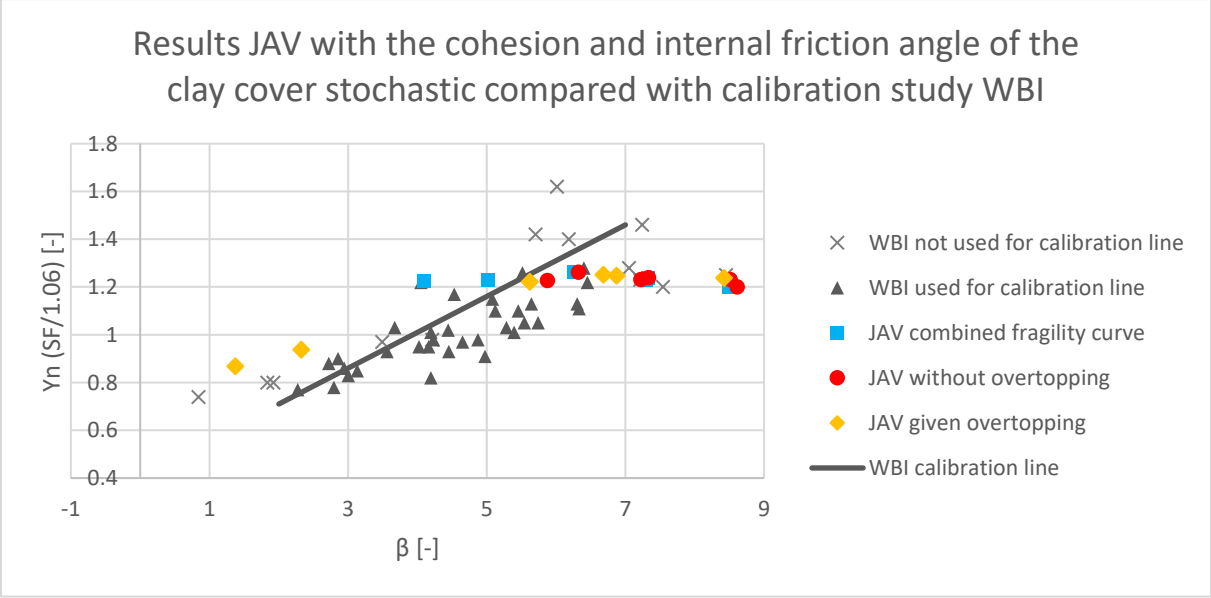

Figure 64: The results of the calculations of JAV with the cohesion and internal friction angle of the clay cover stochastic compared with the calibration study of WBI. The vertical position of the results of JAV from the combined fragility curves (blue squares) are determined based on the semi-probabilistic results without overtopping

F. Results probabilistic calculations with hydrostatic pore water pressure distribution

The results of the probabilistic calculations with the 'hydrostatic' pore water pressure distribution (option 1, red line in Figure 16) given overtopping are given in this appendix. For every dike section are per water level the expected reliability index, coefficient of variation of the failure probability, 5% confidence bound of the reliability index and the difference between the expected reliability index and the 5% confidence bound of the reliability index given in the tables in this appendix. The coefficient of variation of the failure probability is specified as the standard deviation of the probability of failure divided by the probability of failure (Deltares, 2022). The 5% confidence bound of the reliability index is determined based on the failure probability and the coefficient of variation of the failure probability.

Besides, for every dike section are the fragility curves given. The fragility points, the fragility curve without overtopping, the fragility curve given overtopping, the combined fragility curve, the probability of exceedance of 1 l/s/m overtopping given the water level and the probability density function of the water level are given in the figures in this appendix. Besides, the influence factors are shown. Please note that the results without overtopping are the same as the results of the basis probabilistic calculations, because only the pore water pressure distribution given overtopping has been changed in comparison with the basis probabilistic calculations.

The results of the probabilistic calculations with 'hydrostatic' pore water pressure distribution given overtopping for dike section 10C are given in Table 63 and the fragility curves are shown in Figure 65.

Table 63: Reliability index probabilistic calculations per water level for dike section 10C with 'hydrostatic' pore water pressure distribution given overtopping

Water level [m +NAP]	Traffic	Overtopping	Reliability index [-]	Coefficient of variation of the failure probability [-]	5% Confidence bound reliability index [-]	Reliability index - 5% confidence bound reliability index [-]
0.24	Yes	No	11.2	0.724	11.1	0.1
4.37	Yes	No	7.26	0.271	7.21	0.05
6.81	No	No	5.24	0.242	5.18	0.06
6.66	No	No	5.65	0.188	5.60	0.05
6.96	No	No	4.21	0.322	4.11	0.10
7.15	No	No	4.12	0.264	4.03	0.09
6.66	No	Yes	4.66	0.133	4.62	0.04
6.96	No	Yes	3.55	0.194	3.48	0.07
6.21	No	Yes	5.21	0.296	5.14	0.07
7.15	No	Yes	3.36	0.158	3.30	0.06

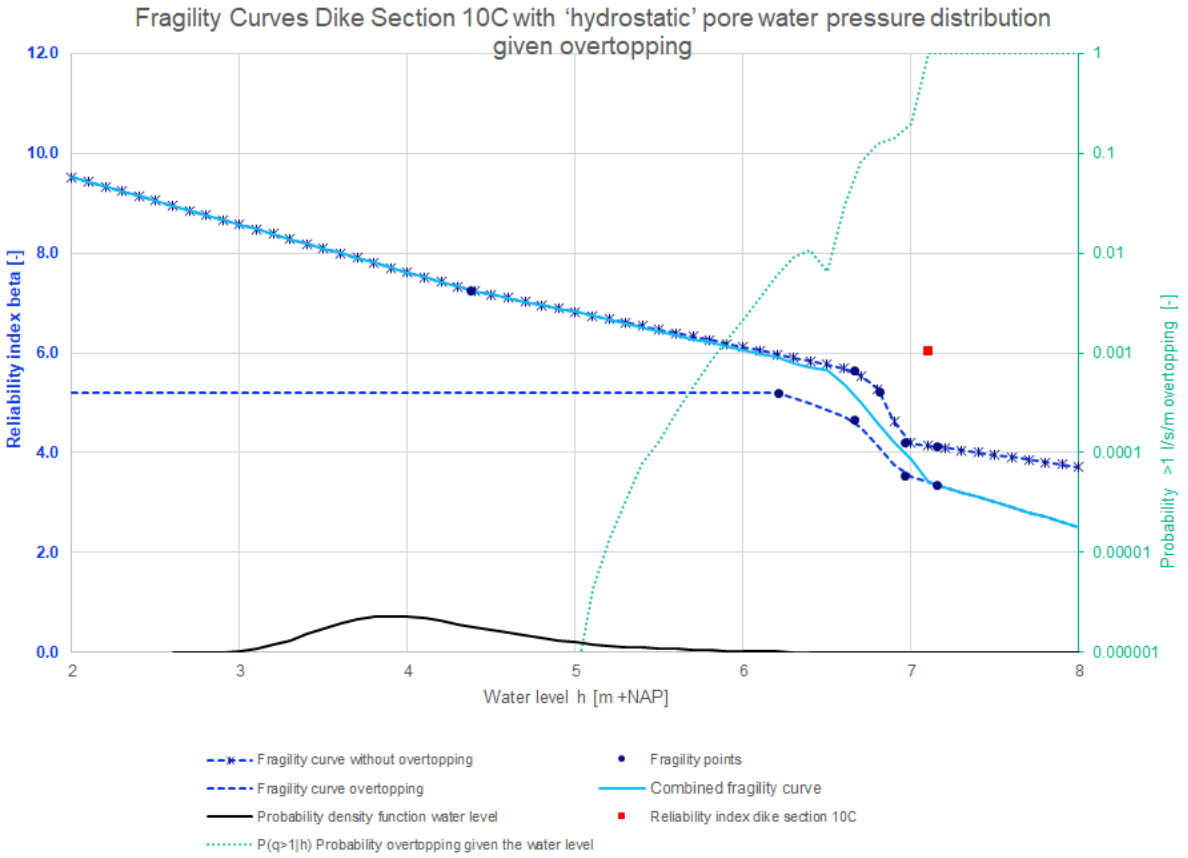

Figure 65: Fragility curves dike section 10C with 'hydrostatic' pore water pressure distribution given overtopping

The results of the probabilistic calculations with 'hydrostatic' pore water pressure distribution given overtopping for dike section 11E are given in Table 64 and the fragility curves are shown in Figure 66.

Table 64: Reliability index probabilistic calculations per water level for dike section 11E with 'hydrostatic' pore water pressure distribution given overtopping

Water level [m +NAP]	Traffic	Overtopping	Reliability index [-]	Coefficient of variation of the failure probability [-]	5% Confidence bound reliability index [-]	Reliability index - 5% confidence bound reliability index [-]
-0.04	Yes	No	7.03	0.154	7.00	0.03
2.39	Yes	No	7.03	0.119	7.00	0.03
3.47	Yes	No	6.60	0.165	6.56	0.04
6.77	No	No	4.19	0.113	4.15	0.04
7.07	No	No	3.69	0.0854	3.65	0.04
6.77	No	Yes	-1.26	0.0274	-1.52	0.26
7.07	No	Yes	-1.26	0.0274	-1.52	0.26
6.37	No	Yes	-1.25	0.0274	-1.52	0.27

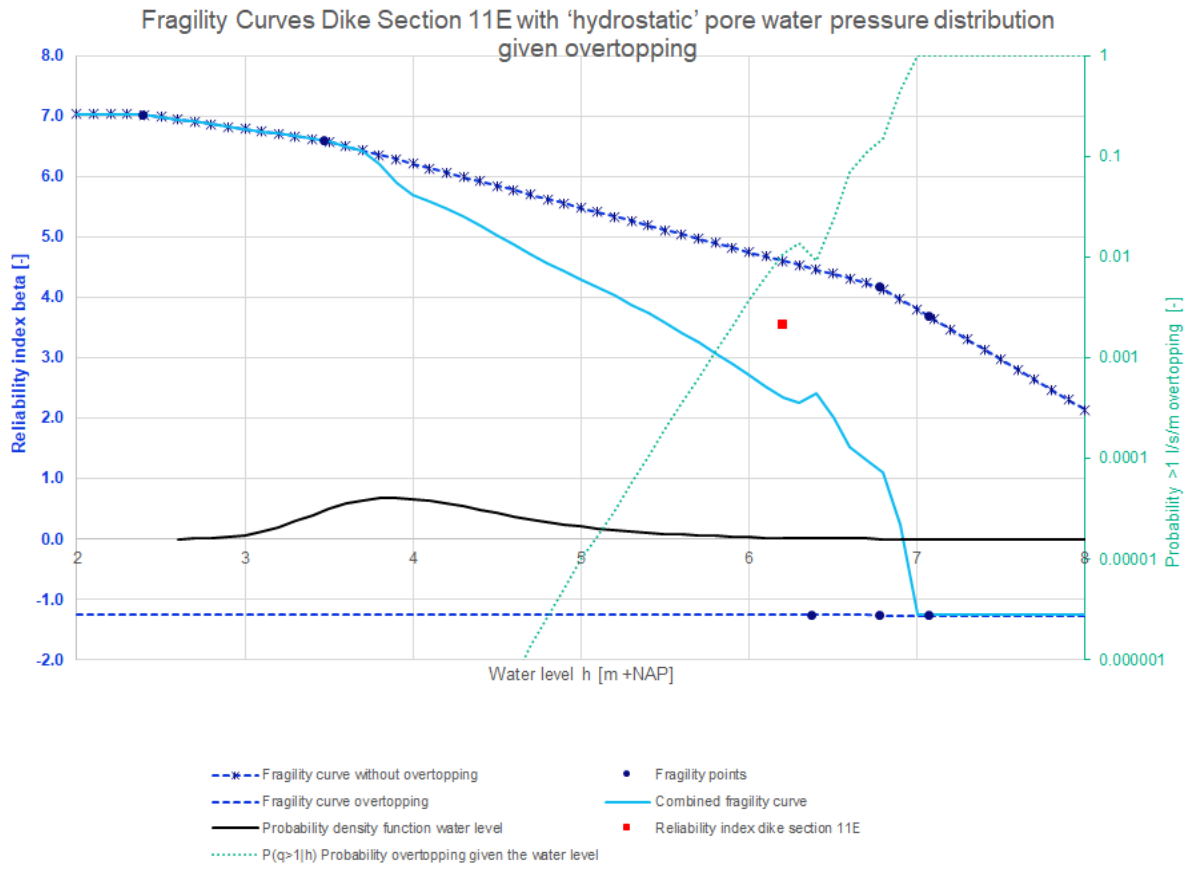

Figure 66: Fragility curves dike section 11E with 'hydrostatic' pore water pressure distribution given overtopping

The results of the probabilistic calculations with 'hydrostatic' pore water pressure distribution given overtopping for dike section 11F(11D) are given in Table 65 and the fragility curves are shown in Figure 67.

Table 65: Reliability index probabilistic calculations per water level for dike section 11F(11D) with 'hydrostatic' pore water pressure distribution given overtopping

Water level [m +NAP]	Traffic	Overtopping	Reliability index [-]	Coefficient of variation of the failure probability [-]	5% Confidence bound reliability index [-]	Reliability index - 5% confidence bound reliability index [-]
-0.04	Yes	No	17.8	0.888	17.7	0.1
2.63	Yes	No	15.6	0.351	15.6	0.0
5.24	Yes	No	9.10	0.412	9.04	0.06
6.79	No	No	7.38	0.235	7.34	0.04
7.09	No	No	7.18	0.161	7.14	0.04
6.79	No	Yes	-0.142	0.0399	-0.24	0.09
7.09	No	Yes	-0.142	0.0399	-0.24	0.09
6.38	No	Yes	-0.142	0.0399	-0.24	0.09

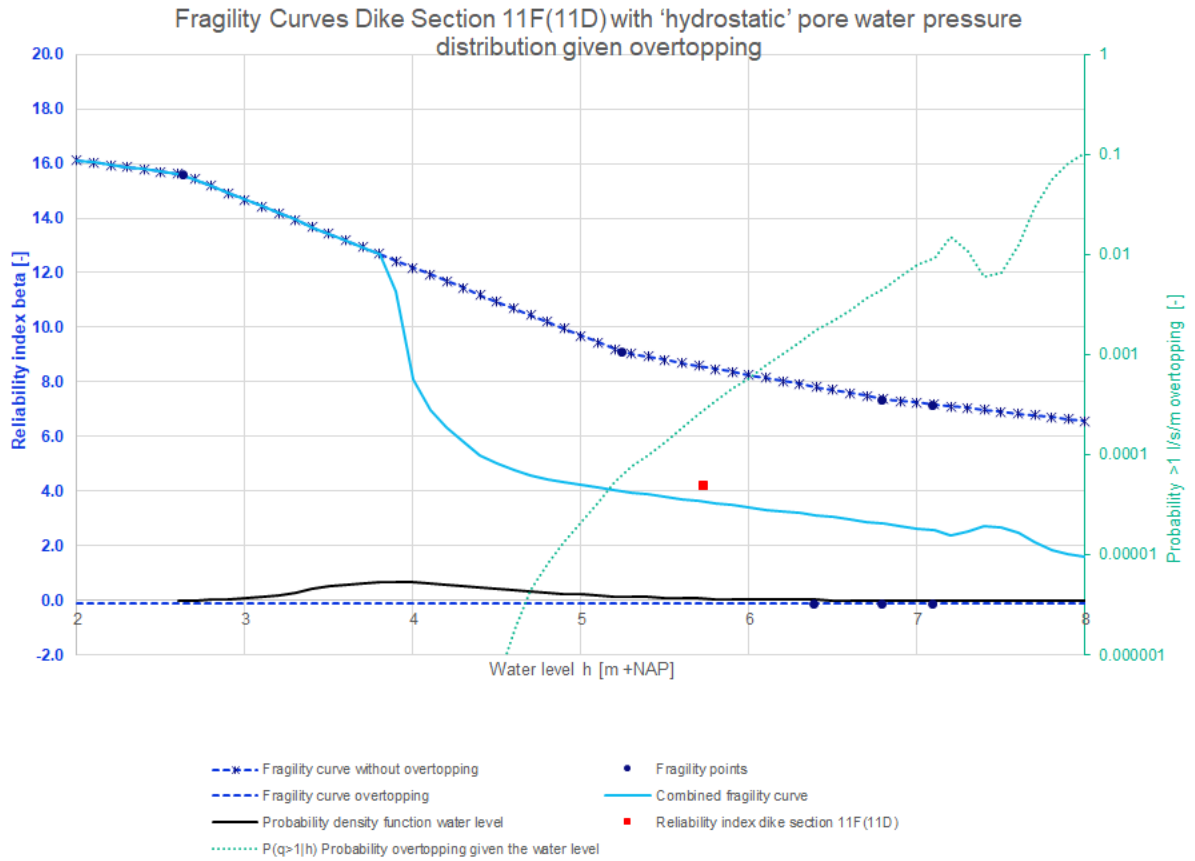

Figure 67: Fragility curves dike section 11F(11D) with 'hydrostatic' pore water pressure distribution given overtopping

The results of the probabilistic calculations with 'hydrostatic' pore water pressure distribution given overtopping for dike section 13A are given in Table 66 and the fragility curves are shown in Figure 68.

Table 66: Reliability index probabilistic calculations per water level for dike section 13A with 'hydrostatic' pore water pressure distribution given overtopping

Water level [m +NAP]	Traffic	Overtopping	Reliability index [-]	Coefficient of variation of the failure probability [-]	5% Confidence bound reliability index [-]	Reliability index - 5% confidence bound reliability index [-]
-0.30	Yes	No	13.5	0.580	13.5	0.0
0.87	Yes	No	12.8	0.769	12.7	0.1
2.07	Yes	No	11.8	0.723	11.7	0.1
6.26	No	No	7.51	0.314	7.45	0.06
6.56	No	No	7.34	0.197	7.30	0.04
6.26	No	Yes	6.34	0.124	6.31	0.03
6.56	No	Yes	6.25	0.121	6.22	0.03
5.66	No	Yes	7.01	0.140	6.98	0.03

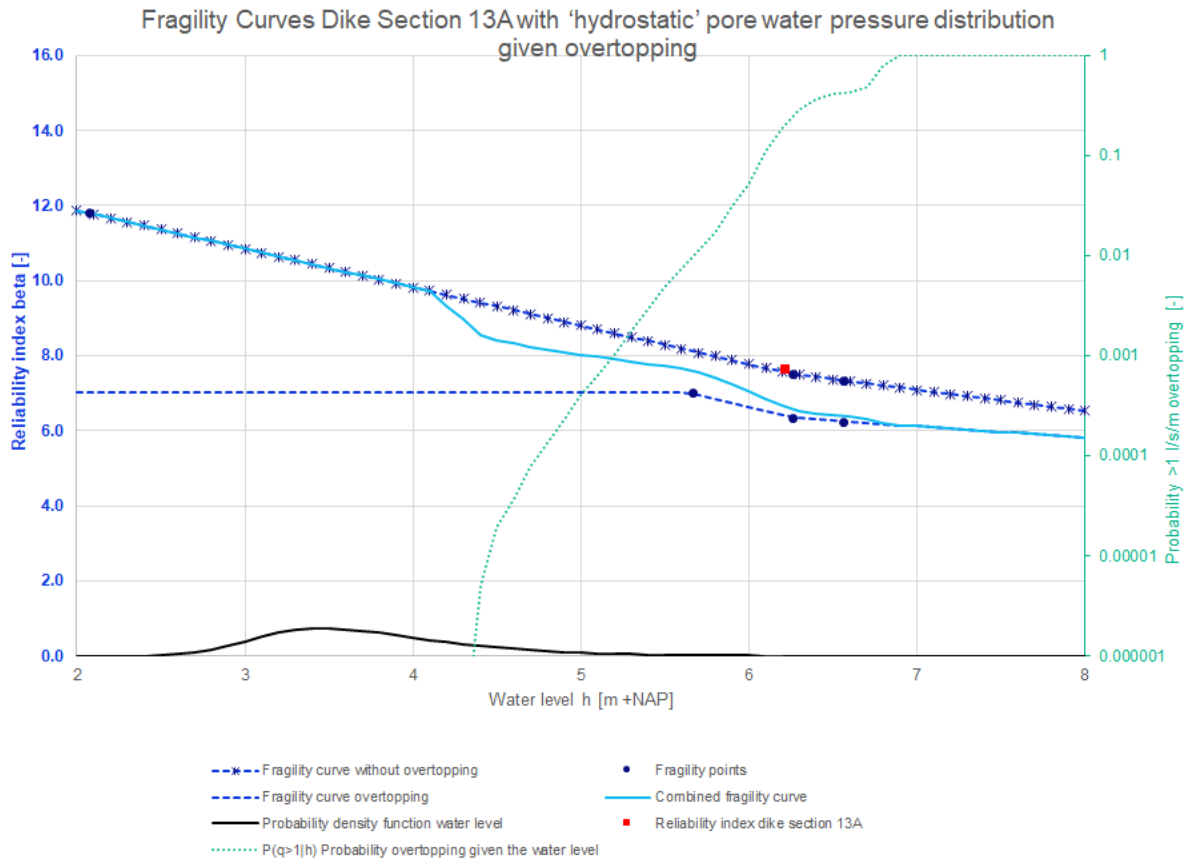

Figure 68: Fragility curves dike section 13A with 'hydrostatic' pore water pressure distribution given overtopping

The results of the probabilistic calculations with 'hydrostatic' pore water pressure distribution given overtopping for dike section 13E1 are given in Table 67 and the fragility curves are shown in Figure 69.

Table 67: Reliability index probabilistic calculations per water level for dike section 13E1 with 'hydrostatic' pore water pressure distribution given overtopping

Water level [m +NAP]	Traffic	Overtopping	Reliability index [-]	Coefficient of variation of the failure probability [-]	5% Confidence bound reliability index [-]	Reliability index - 5% confidence bound reliability index [-]
-0.30	Yes	No	10.0	0.225	10.0	0.0
4.69	Yes	No	7.59	0.371	7.53	0.06
6.33	No	No	6.19	0.432	6.11	0.08
6.63	No	No	5.85	0.193	5.81	0.04
6.33	No	Yes	5.19	0.162	5.14	0.05
6.63	No	Yes	5.19	0.162	5.14	0.05
6.00	No	Yes	5.19	0.162	5.14	0.05

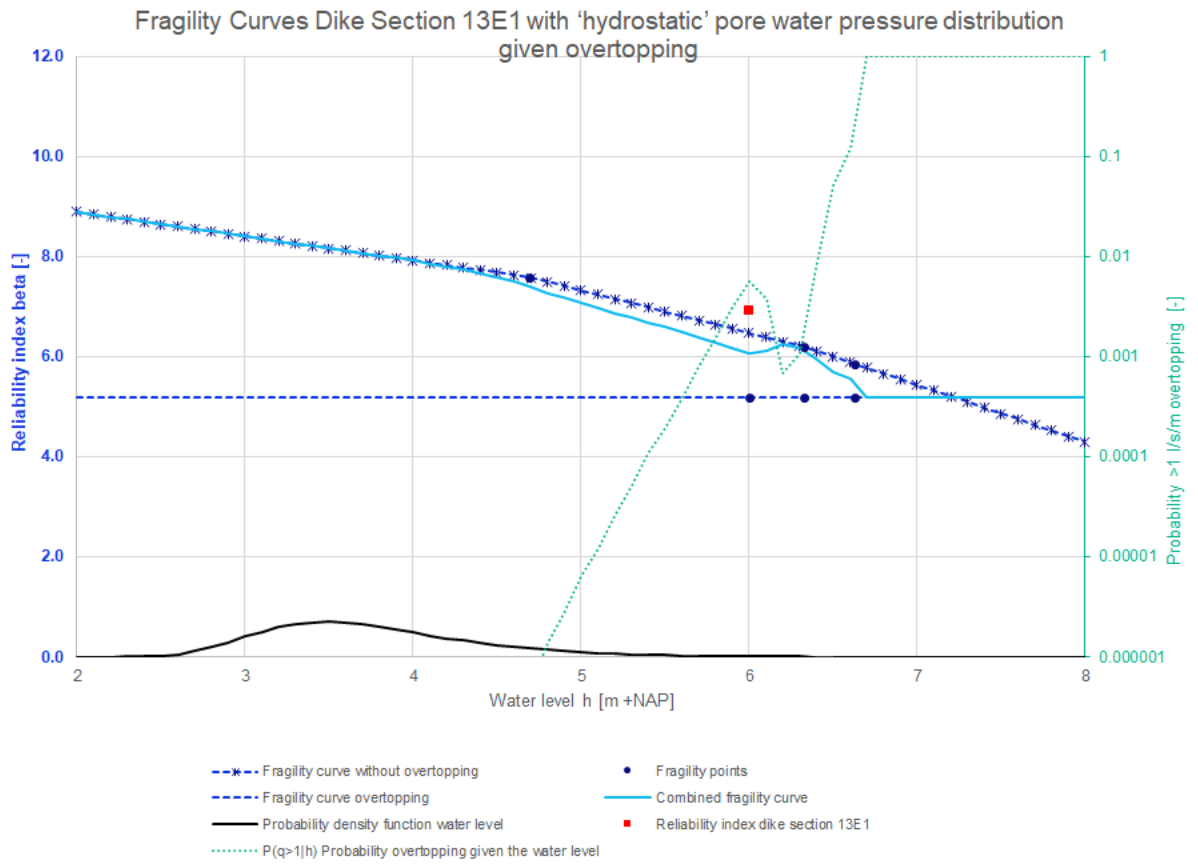

Figure 69: Fragility curves dike section 13E1 with 'hydrostatic' pore water pressure distribution given overtopping

The results of the probabilistic calculations with 'hydrostatic' pore water pressure distribution given overtopping for dike section 13E2 are given in Table 68 and the fragility curves are shown in Figure 70.

Table 68: Reliability index probabilistic calculations per water level for dike section 13E2 with 'hydrostatic' pore water pressure distribution given overtopping

Water level [m +NAP]	Traffic	Overtopping	Reliability index [-]	Coefficient of variation of the failure probability [-]	5% Confidence bound reliability index [-]	Reliability index - 5% confidence bound reliability index [-]
-0.30	Yes	No	10.2	0.262	10.2	0.0
4.69	Yes	No	7.39	0.164	7.36	0.03
6.24	No	No	6.37	0.149	6.33	0.04
6.54	No	No	6.02	0.169	5.98	0.04
6.24	No	Yes	5.64	0.160	5.60	0.04
6.54	No	Yes	5.64	0.160	5.60	0.04
5.91	No	Yes	5.64	0.160	5.60	0.04

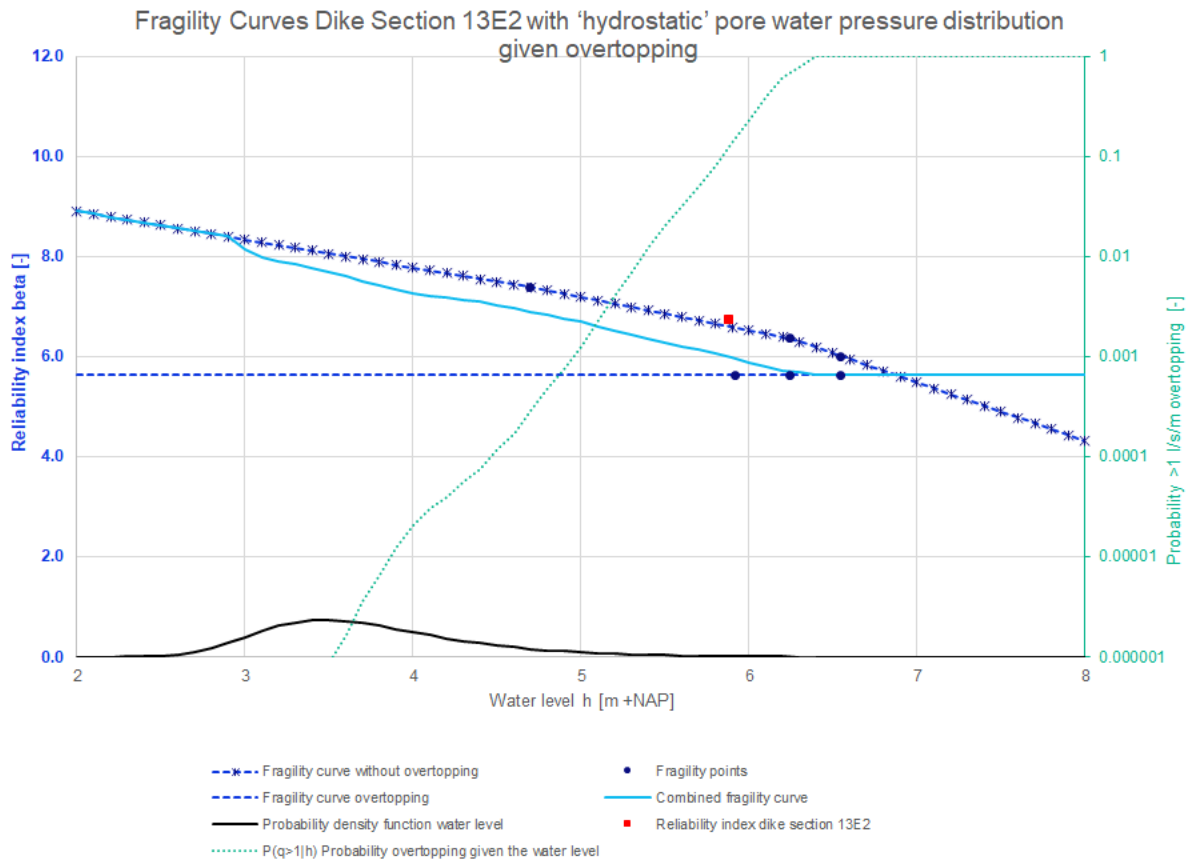

Figure 70: Fragility curves dike section 13E2 with 'hydrostatic' pore water pressure distribution given overtopping

In Figure 71 are the influence factors shown. Please note that the influence factors without overtopping are the same as the influence factors of the basis probabilistic calculations, because only the pore water distribution given overtopping has been changed in comparison with the basis probabilistic calculations.

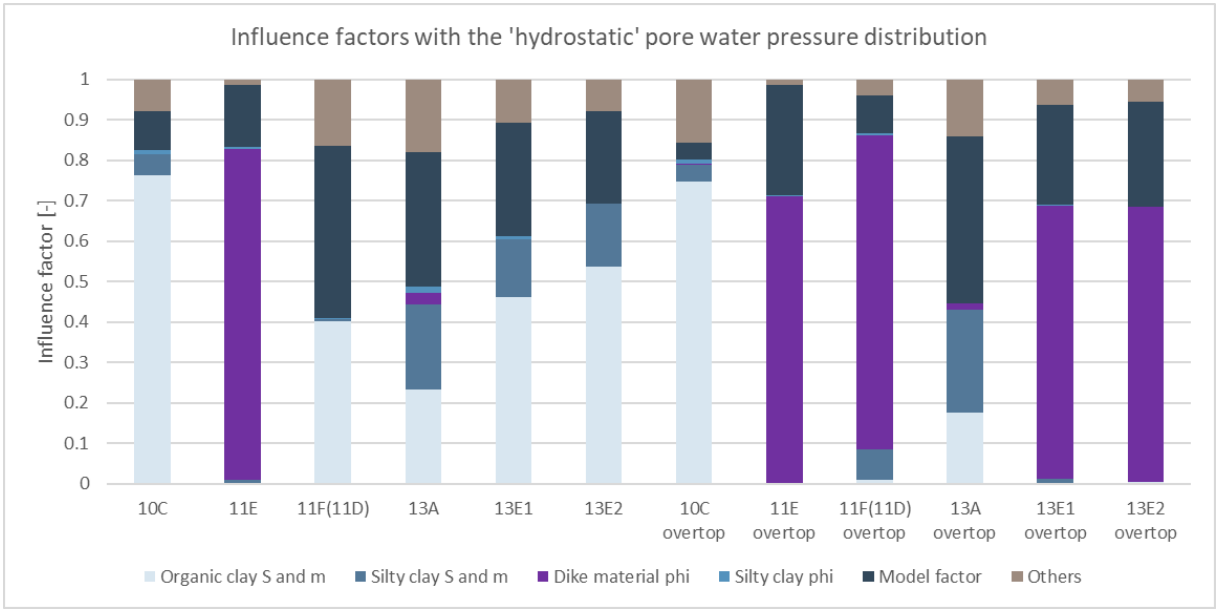

Figure 71: Influence factors with the 'hydrostatic' pore water pressure distribution at WBN without overtopping and at the 1 l/s/m overtopping water level with overtopping

G. Results probabilistic calculations with interpolation pore water pressure distribution

The results of the probabilistic calculations with the 'interpolation' pore water pressure distribution (option 3, blue line in Figure 16) given overtopping are given in this appendix. For every dike section are per water level the expected reliability index, coefficient of variation of the failure probability, 5% confidence bound of the reliability index and the difference between the expected reliability index and the 5% confidence bound of the reliability index given in the tables in this appendix. The coefficient of variation of the failure probability is specified as the standard deviation of the probability of failure divided by the probability of failure (Deltares, 2022). The 5% confidence bound of the reliability index is determined based on the failure probability and the coefficient of variation of the failure probability.

Besides, for every dike section are the fragility curves given. The fragility points, the fragility curve without overtopping, the fragility curve given overtopping, the combined fragility curve, the probability of exceedance of 1 l/s/m overtopping given the water level and the probability density function of the water level are given in the figures in this appendix. Besides, the influence factors are shown. Please note that the results without overtopping are the same as the results of the basis probabilistic calculations, because only the pore water pressure distribution given overtopping has been changed in comparison with the basis probabilistic calculations.

The results of the probabilistic calculations with 'interpolation' pore water pressure distribution given overtopping for dike section 10C are given in Table 69 and the fragility curves are shown in Figure 72.

Table 69: Reliability index probabilistic calculations per water level for dike section 10C with 'interpolation' pore water pressure distribution given overtopping

Water level [m +NAP]	Traffic	Overtopping	Reliability index [-]	Coefficient of variation of the failure probability [-]	5% Confidence bound reliability index [-]	Reliability index - 5% confidence bound reliability index [-]
0.24	Yes	No	11.2	0.724	11.1	0.1
4.37	Yes	No	7.26	0.271	7.21	0.05
6.81	No	No	5.24	0.242	5.18	0.06
6.66	No	No	5.65	0.188	5.60	0.05
6.96	No	No	4.21	0.322	4.11	0.10
7.15	No	No	4.12	0.264	4.03	0.09
6.66	No	Yes	5.37	0.174	5.33	0.04
6.96	No	Yes	4.20	0.202	4.13	0.07
6.21	No	Yes	5.96	0.168	5.92	0.04
7.15	No	Yes	3.89	0.156	3.84	0.05

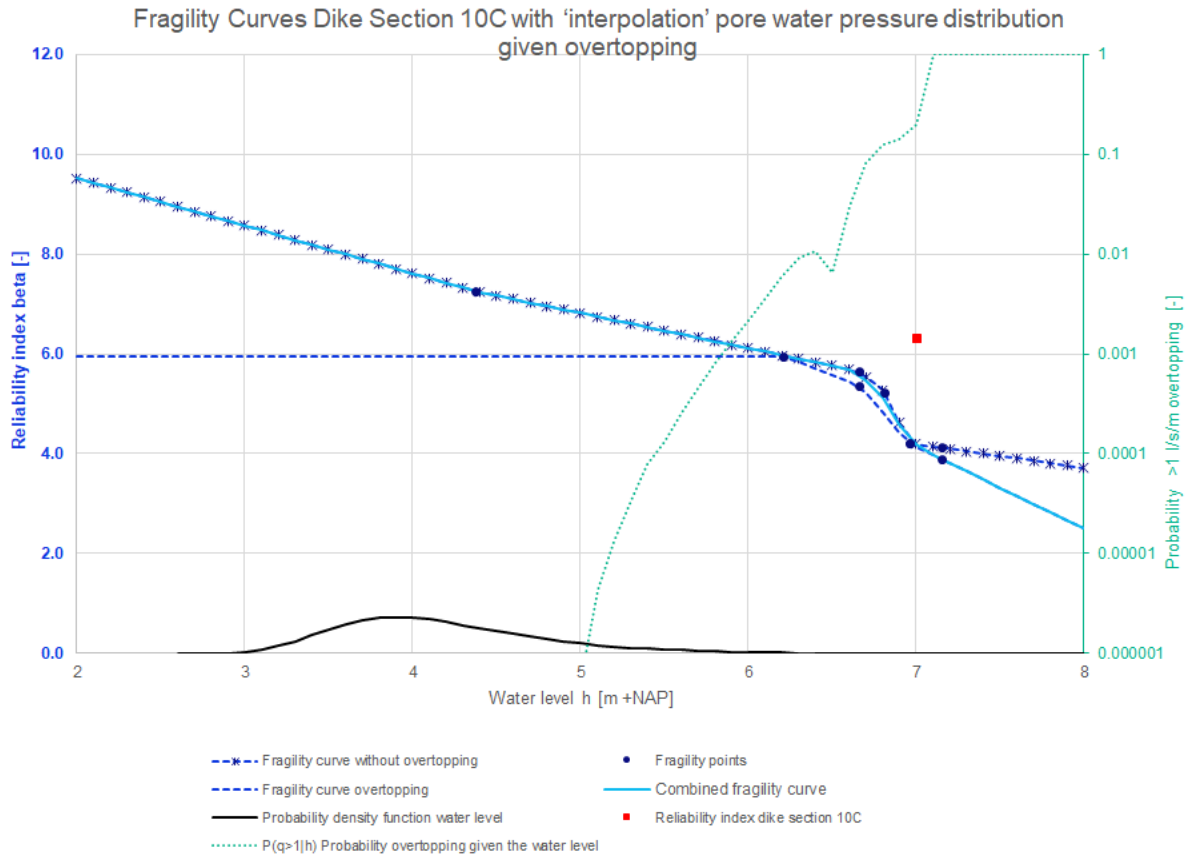

Figure 72: Fragility curves dike section 10C with 'interpolation' pore water pressure distribution given overtopping

The results of the probabilistic calculations with 'interpolation' pore water pressure distribution given overtopping for dike section 11E are given in Table 70 and the fragility curves are shown in Figure 73.

Table 70: Reliability index probabilistic calculations per water level for dike section 11E with 'interpolation' pore water pressure distribution given overtopping

Water level [m +NAP]	Traffic	Overtopping	Reliability index [-]	Coefficient of variation of the failure probability [-]	5% Confidence bound reliability index [-]	Reliability index - 5% confidence bound reliability index [-]
-0.04	Yes	No	7.03	0.154	7.00	0.03
2.39	Yes	No	7.03	0.119	7.00	0.03
3.47	Yes	No	6.60	0.165	6.56	0.04
6.77	No	No	4.19	0.113	4.15	0.04
7.07	No	No	3.69	0.0854	3.65	0.04
6.77	No	Yes	1.61	0.05	1.57	0.04
7.07	No	Yes	1.24	0.0499	1.19	0.05
6.37	No	Yes	2.13	0.057	2.10	0.03

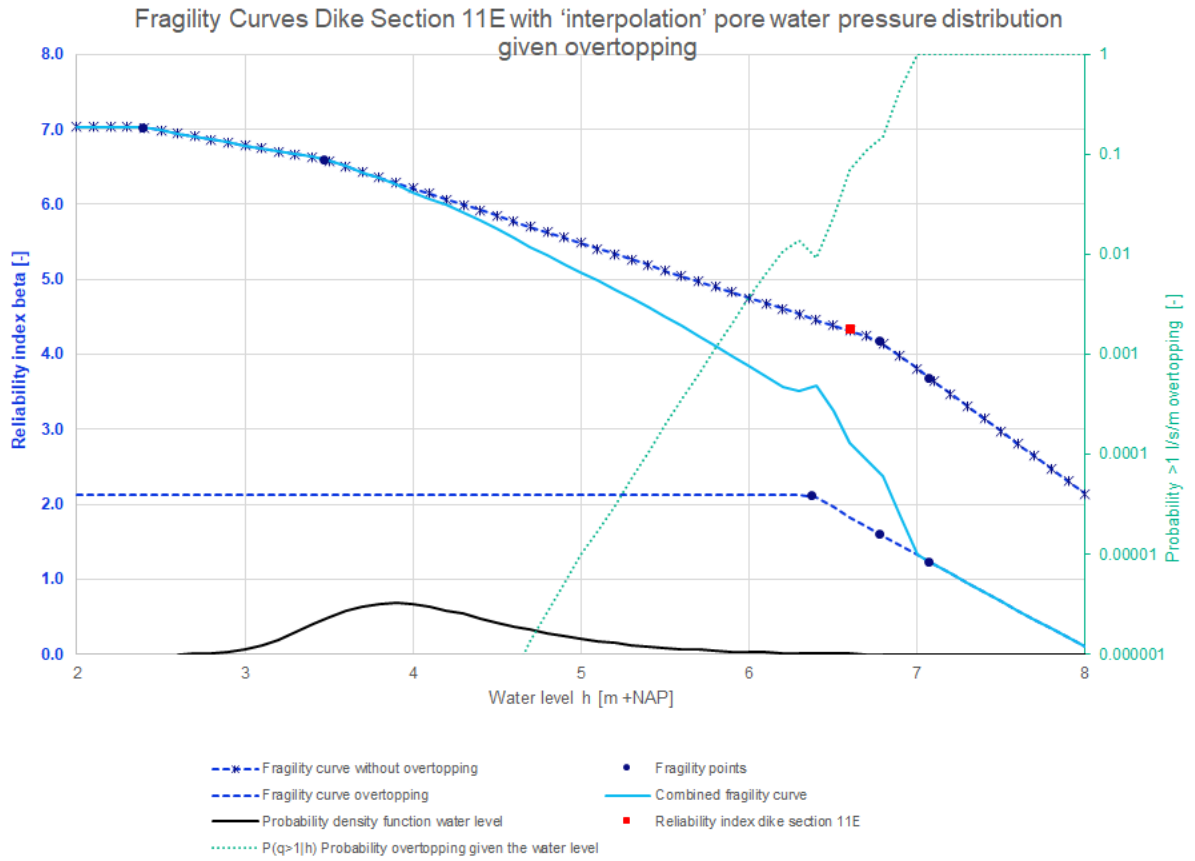

Figure 73: Fragility curves dike section 11E with 'interpolation' pore water pressure distribution given overtopping

The results of the probabilistic calculations with 'interpolation' pore water pressure distribution given overtopping for dike section 11F(11D) are given in Table 71 and the fragility curves are shown in Figure 74.

Table 71: Reliability index probabilistic calculations per water level for dike section 11F(11D) with 'interpolation' pore water pressure distribution given overtopping

Water level [m +NAP]	Traffic	Overtopping	Reliability index [-]	Coefficient of variation of the failure probability [-]	5% Confidence bound reliability index [-]	Reliability index - 5% confidence bound reliability index [-]
-0.04	Yes	No	17.8	0.888	17.7	0.1
2.63	Yes	No	15.6	0.351	15.6	0.0
5.24	Yes	No	9.10	0.412	9.04	0.06
6.79	No	No	7.38	0.235	7.34	0.04
7.09	No	No	7.18	0.161	7.14	0.04
6.79	No	Yes	2.60	0.0664	2.57	0.03
7.09	No	Yes	2.29	0.0611	2.26	0.03
6.38	No	Yes	2.94	0.0751	2.90	0.04

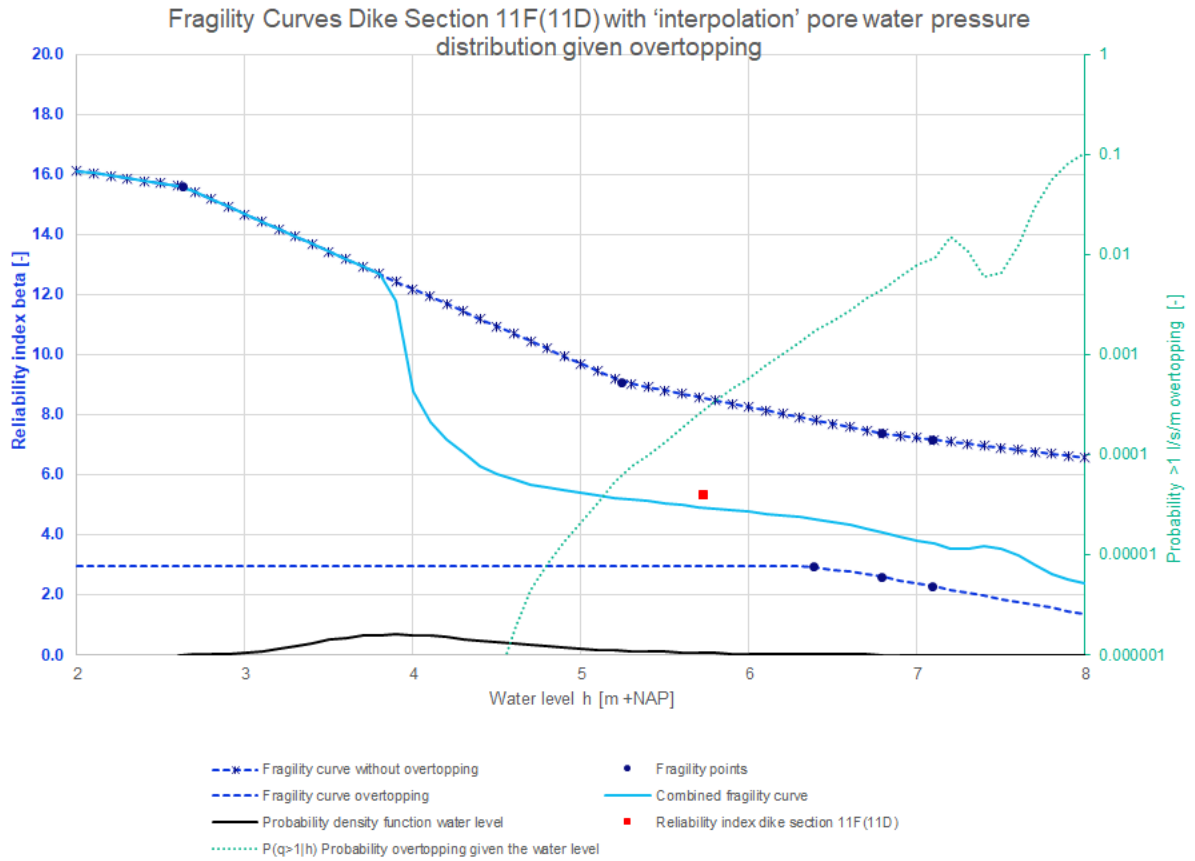

Figure 74: Fragility curves dike section 11F(11D) with 'interpolation' pore water pressure distribution given overtopping

The results of the probabilistic calculations with 'interpolation' pore water pressure distribution given overtopping for dike section 13A are given in Table 72 and the fragility curves are shown in Figure 75.

Table 72: Reliability index probabilistic calculations per water level for dike section 13A with 'interpolation' pore water pressure distribution given overtopping

Water level [m +NAP]	Traffic	Overtopping	Reliability index [-]	Coefficient of variation of the failure probability [-]	5% Confidence bound reliability index [-]	Reliability index - 5% confidence bound reliability index [-]
-0.30	Yes	No	13.5	0.580	13.5	0.0
0.87	Yes	No	12.8	0.769	12.7	0.1
2.07	Yes	No	11.8	0.723	11.7	0.1
6.26	No	No	7.51	0.314	7.45	0.06
6.56	No	No	7.34	0.197	7.30	0.04
6.26	No	Yes	7.36	0.212	7.32	0.04
6.56	No	Yes	7.15	0.191	7.11	0.04
5.66	No	Yes	8.45	0.468	8.39	0.06

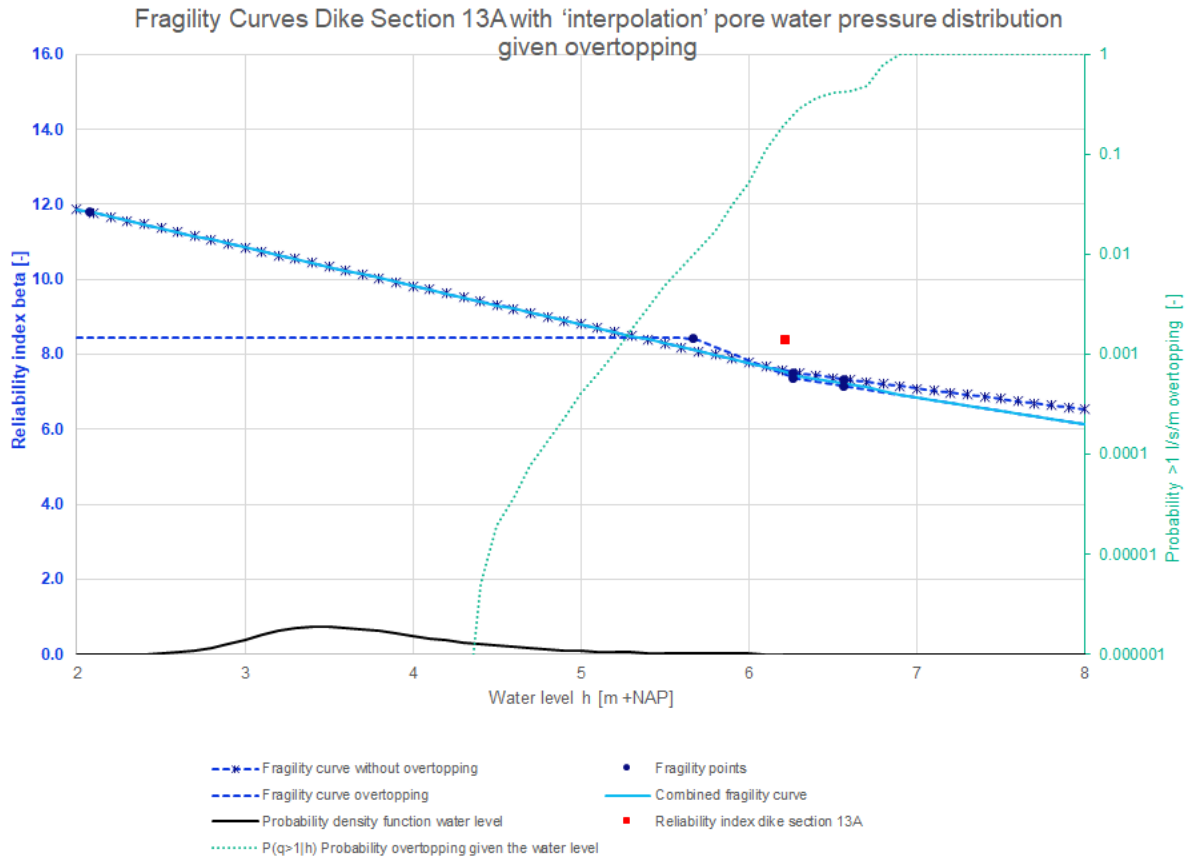

Figure 75: Fragility curves dike section 13A with 'interpolation' pore water pressure distribution given overtopping

The results of the probabilistic calculations with 'interpolation' pore water pressure distribution given overtopping for dike section 13E1 are given in Table 73 and the fragility curves are shown in Figure 76.

Table 73: Reliability index probabilistic calculations per water level for dike section 13E1 with 'interpolation' pore water pressure distribution given overtopping

Water level [m +NAP]	Traffic	Overtopping	Reliability index [-]	Coefficient of variation of the failure probability [-]	5% Confidence bound reliability index [-]	Reliability index - 5% confidence bound reliability index [-]
-0.30	Yes	No	10.0	0.225	10.0	0.0
4.69	Yes	No	7.59	0.371	7.53	0.06
6.33	No	No	6.19	0.432	6.11	0.08
6.63	No	No	5.85	0.193	5.81	0.04
6.33	No	Yes	6.53	0.199	6.49	0.04
6.63	No	Yes	6.11	0.220	6.06	0.05
6.00	No	Yes	6.83	0.611	6.73	0.10

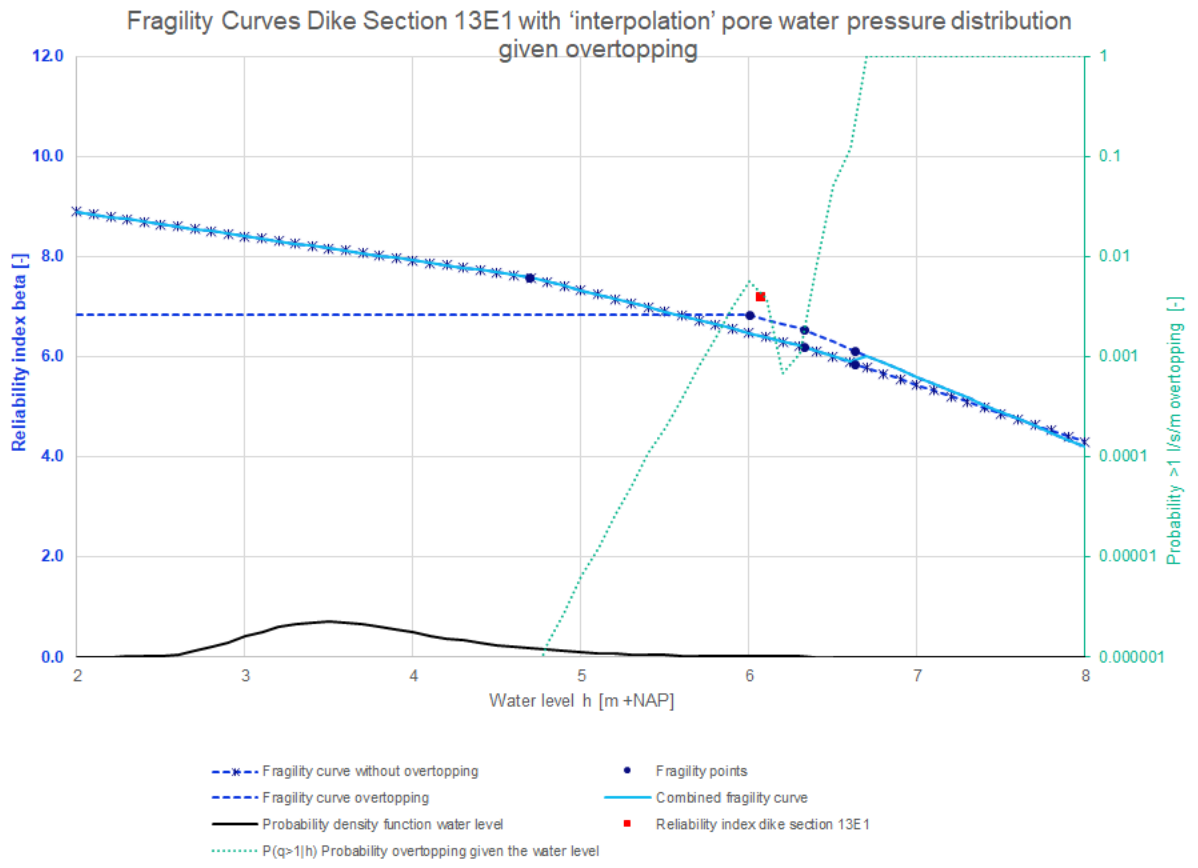

Figure 76: Fragility curves dike section 13E1 with 'interpolation' pore water pressure distribution given overtopping

The results of the probabilistic calculations with 'interpolation' pore water pressure distribution given overtopping for dike section 13E2 are given in Table 74 and the fragility curves are shown in Figure 77.

Table 74: Reliability index probabilistic calculations per water level for dike section 13E2 with 'interpolation' pore water pressure distribution given overtopping

Water level [m +NAP]	Traffic	Overtopping	Reliability index [-]	Coefficient of variation of the failure probability [-]	5% Confidence bound reliability index [-]	Reliability index - 5% confidence bound reliability index [-]
-0.30	Yes	No	10.2	0.262	10.2	0.0
4.69	Yes	No	7.39	0.164	7.36	0.03
6.24	No	No	6.37	0.149	6.33	0.04
6.54	No	No	6.02	0.169	5.98	0.04
6.24	No	Yes	6.43	0.158	6.40	0.03
6.54	No	Yes	6.09	0.166	6.05	0.04
5.91	No	Yes	6.74	0.179	6.70	0.04

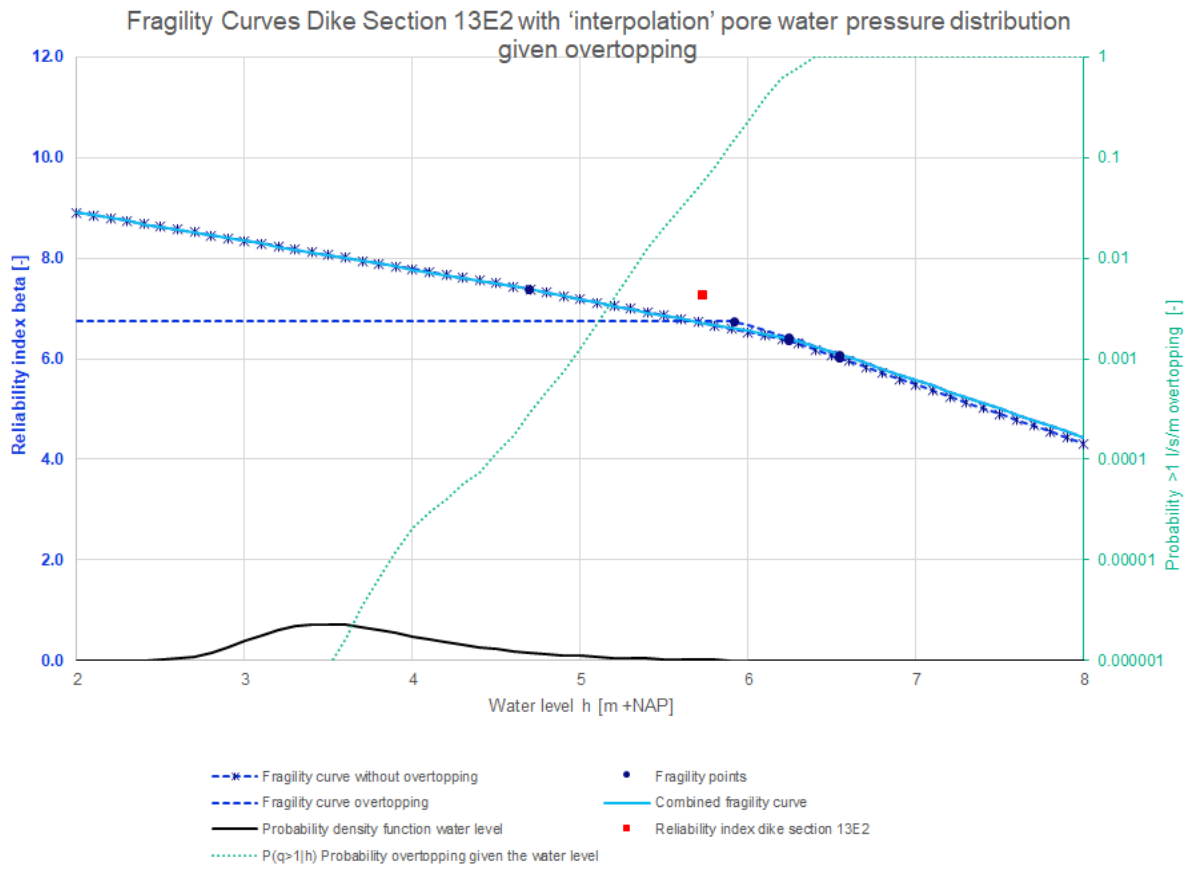

Figure 77: Fragility curves dike section 13E2 with 'interpolation' pore water pressure distribution given overtopping

In Figure 78 are the influence factors shown. Please note that the influence factors without overtopping are the same as the influence factors of the basis probabilistic calculations, because only the pore water distribution given overtopping has been changed in comparison with the basis probabilistic calculations.

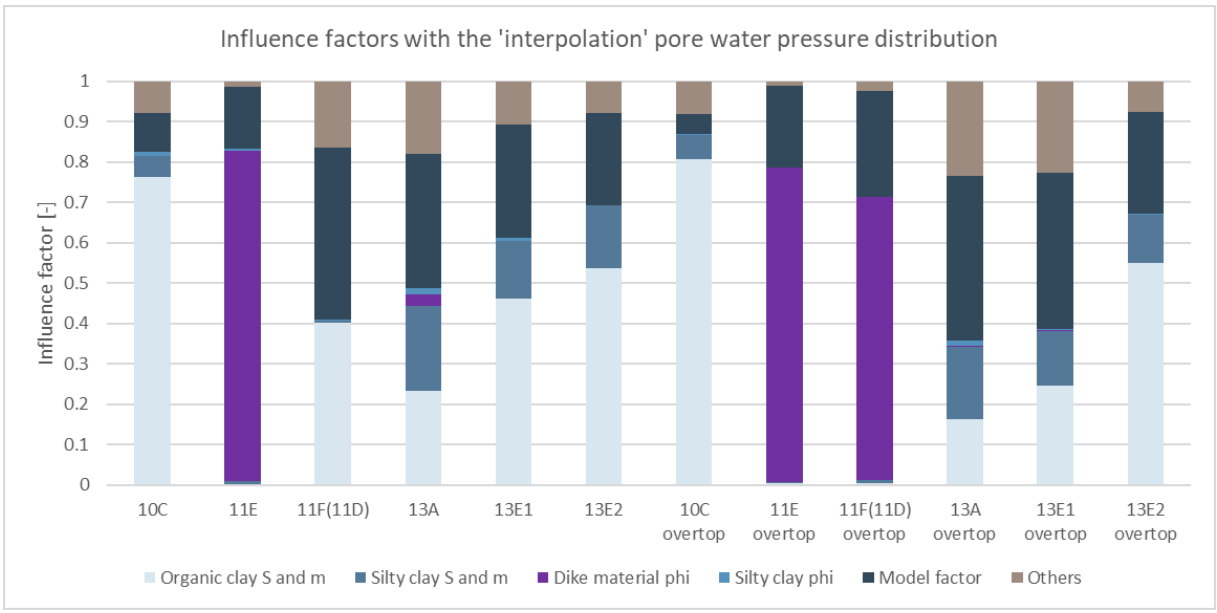

Figure 78: Influence factors with the 'interpolation' pore water pressure distribution at WBN without overtopping and at the 1 l/s/m overtopping water level with overtopping

H. Results of the different pore water pressure distribution schematizations with overtopping

The pore water pressure distribution that has been used during the basis calculations given overtopping (option 2, green line in Figure 16), is considered as the 'basis' pore water pressure distribution given overtopping. Besides, the pore water pressure distribution that has been shown with the red line in Figure 16 (option 1), is considered as the 'hydrostatic' pore water pressure distribution given overtopping. Furthermore, the pore water pressure distribution that has been shown with the blue line in Figure 16 (option 3), is considered as the 'interpolation' pore water pressure distribution given overtopping.

The estimates of the reliability index of the semi-probabilistic calculations given overtopping with the three different pore water pressure distributions are shown in Table 75 in terms of reliability index. One can see from Table 75 that the reliability indexes with the 'interpolation' pore water pressure distribution given overtopping are larger than the other pore water distributions and that the 'hydrostatic' pore water pressure distribution given overtopping leads to the lowest reliability indexes for the considered dike sections of JAV. This is reasonable, because the effective soil stresses are lower if the pore water pressures are larger.

Table 75: Reliability index semi-probabilistic calculations given overtopping with different pore water pressure distributions

Dike section	Reliability index 'basis' pore water pressure distribution β [-]	Reliability index 'hydrostatic' pore water pressure distribution β [-]	Reliability index 'interpolation' pore water pressure distribution β [-]
10C	5.41	5.00	5.46
11E	3.05	2.57	3.88
11F(11D)	3.52	3.00	4.30
13A	5.52	4.98	5.52
13E1	5.59	5.18	5.61
13E2	5.61	5.39	5.64

The estimates of the reliability index for the probabilistic calculations with different pore water pressure distributions given overtopping are shown in Table 76. One can see from Table 76 that the used pore water pressure distribution given overtopping has an influence on the probabilistic estimates of the reliability index.

Table 76: Reliability index probabilistic calculations with different pore water pressure distributions given overtopping

Dike section	Reliability index combined fragility curve β [-]			Reliability index given overtopping β [-]		
	'Basis' pore water pressure distribution	'Hydrostatic' pore water pressure distribution	'Interpolation' pore water pressure distribution	'Basis' pore water pressure distribution	'Hydrostatic' pore water pressure distribution	'Interpolation' pore water pressure distribution
10C	6.29	6.03	6.30	5.61	5.21	5.96
11E	3.72	3.56	4.34	0.12	-1.25	2.13
11F(11D)	4.50	4.21	5.35	1.06	-0.14	2.94
13A	8.36	7.65	8.40	8.46	7.01	8.45
13E1	7.14	6.92	7.20	6.81	5.19	6.83
13E2	7.27	6.73	7.28	6.66	5.64	6.74

In Figure 79 are the results of the calculations of JAV with the 'hydrostatic' pore water pressure distribution given overtopping plotted with the results of the WBI calibration study. Furthermore, in Figure 80 are the results of the calculations of JAV with the 'interpolation' pore water pressure distribution given overtopping plotted with the results of the WBI calibration study. One can see that especially the two yellow diamond shapes on the left of the calibration line are shifted upwards and more to the right in Figure 80 in comparison with Figure 79. However, the horizontal differences between the results of JAV and the WBI calibration line are still large for both pore water pressure distributions given overtopping.

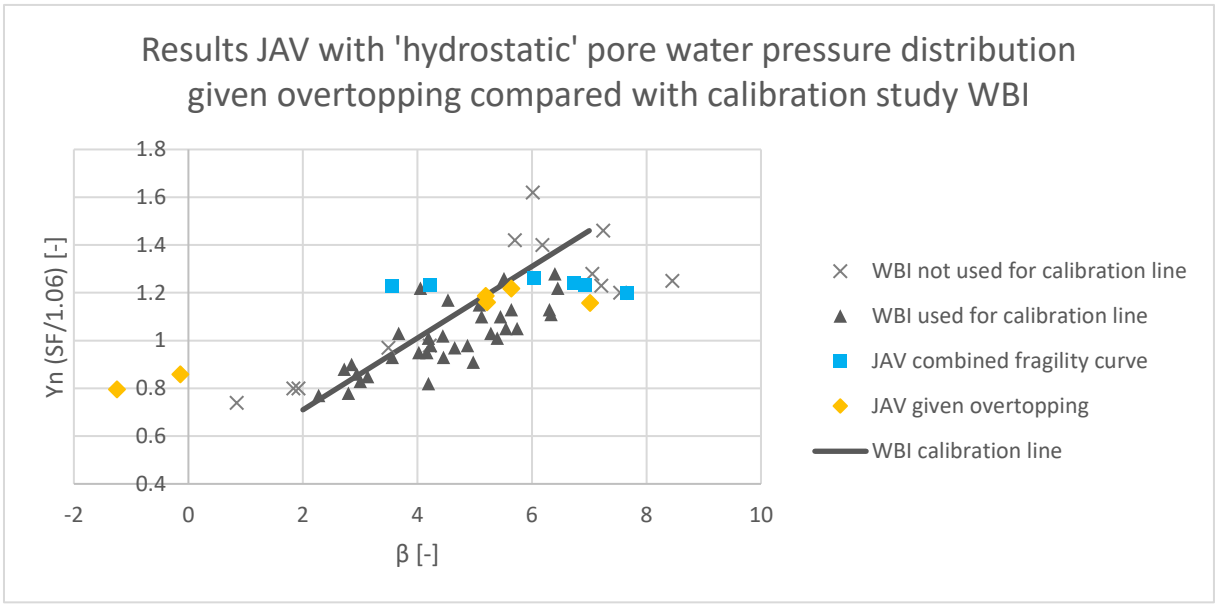

Figure 79: The results of the calculations of JAV with 'hydrostatic' pore water pressure distribution given overtopping compared with the calibration study of WBI. The vertical position of the results of JAV from the combined fragility curves (blue squares) are determined based on the semi-probabilistic results without overtopping

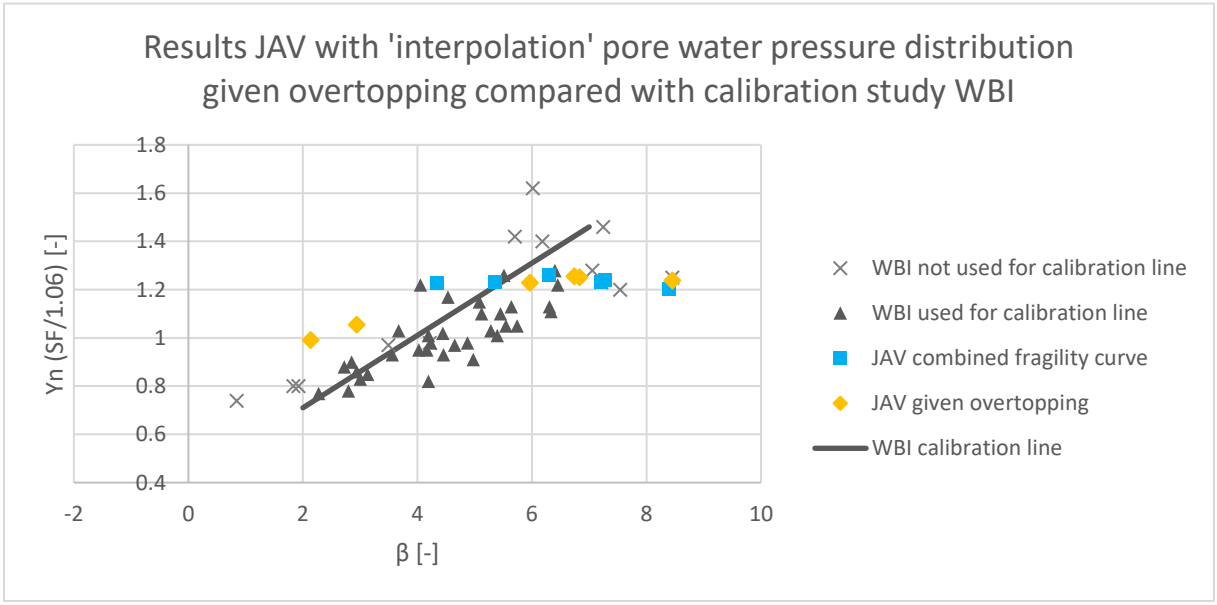

Figure 80: The results of the calculations of JAV with 'interpolation' pore water pressure distribution given overtopping compared with the calibration study of WBI. The vertical position of the results of JAV from the combined fragility curves (blue squares) are determined based on the semi-probabilistic results without overtopping

The sample standard deviations for the different pore water pressure distributions given overtopping are shown in Table 77. For every considered pore water pressure distribution given overtopping is the sample standard deviation larger than the sample standard deviation of the calibration study of 0.90 in terms of reliability index.

Table 77: Sample standard deviations for the different pore water pressure distributions given overtopping in terms of reliability index, when one assumes that the calibration line represents the sample mean of the reliability indexes

	'Basis' pore water pressure distribution	'Interpolation' pore water pressure distribution	'Hydrostatic' pore water pressure distribution
Sample standard deviation combined fragility curve [-]	1.98	1.87	1.70
Sample standard deviation given overtopping [-]	2.28	1.81	2.40

I. Results of the different combinations of the pore water pressure distribution plotted with the results of the WBI calibration study

In Figure 81 are the results of the calculations of JAV with combination 1, in Figure 82 with combination 2, in Figure 83 with combination 3 and in Figure 84 with combination 4 of the pore water pressure distribution given overtopping plotted with the results of the WBI calibration study.

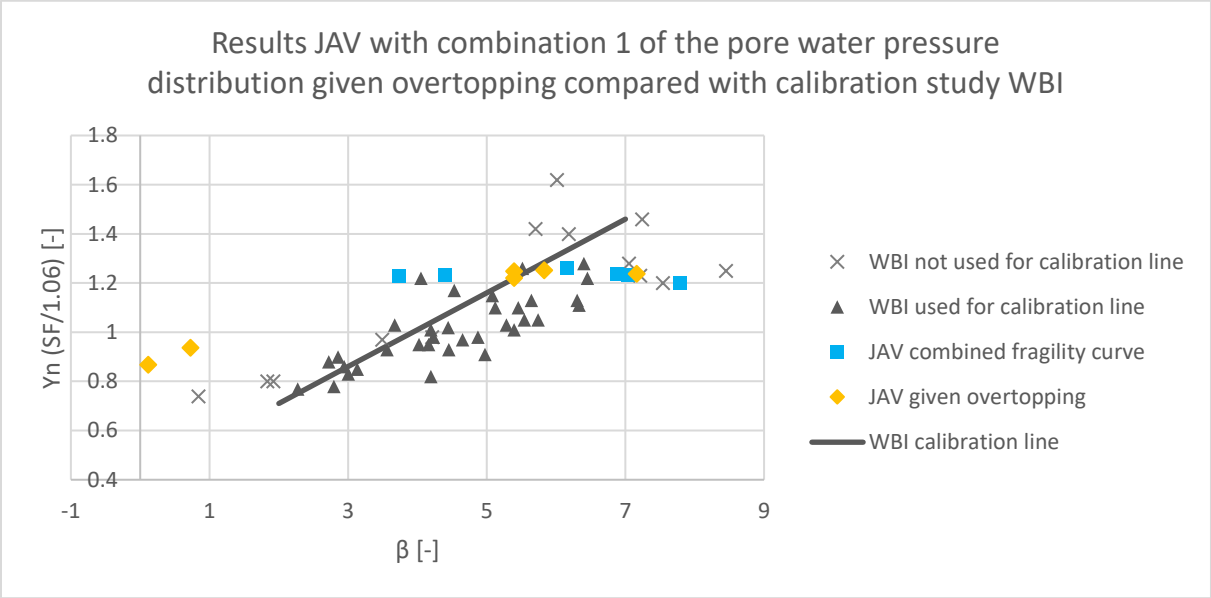

Figure 81: The results of the calculations of JAV with combination 1 of the pore water pressure distribution given overtopping compared with the calibration study of WBI. The vertical position of the results of JAV from the combined fragility curves (blue squares) are determined based on the semi-probabilistic results without overtopping

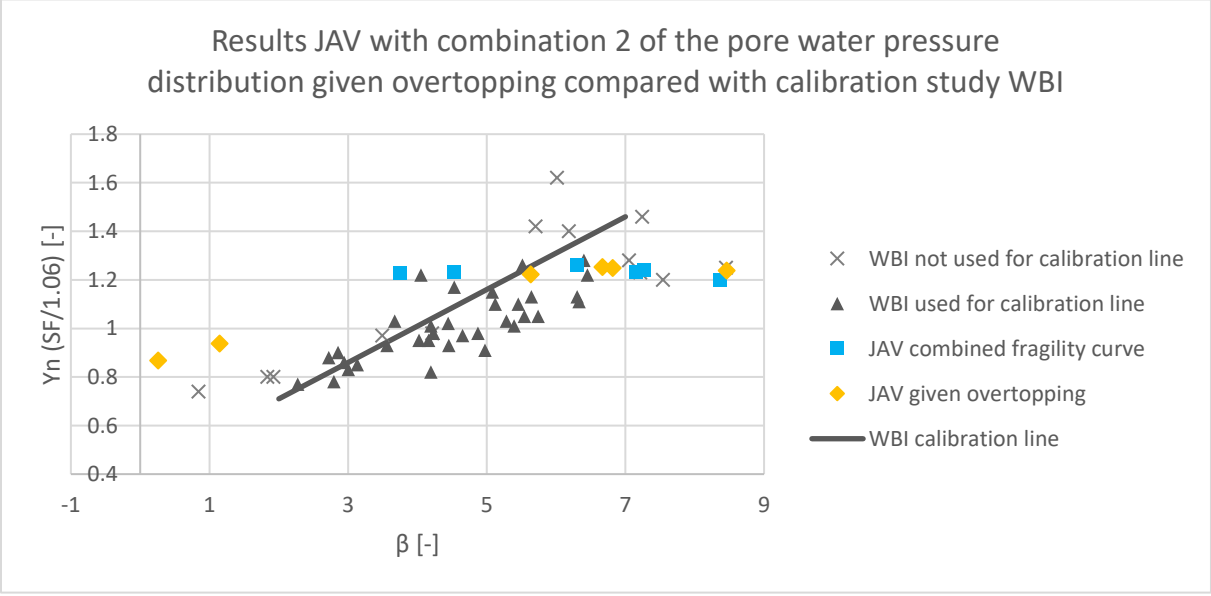

Figure 82: The results of the calculations of JAV with combination 2 of the pore water pressure distribution given overtopping compared with the calibration study of WBI. The vertical position of the results of JAV from the combined fragility curves (blue squares) are determined based on the semi-probabilistic results without overtopping

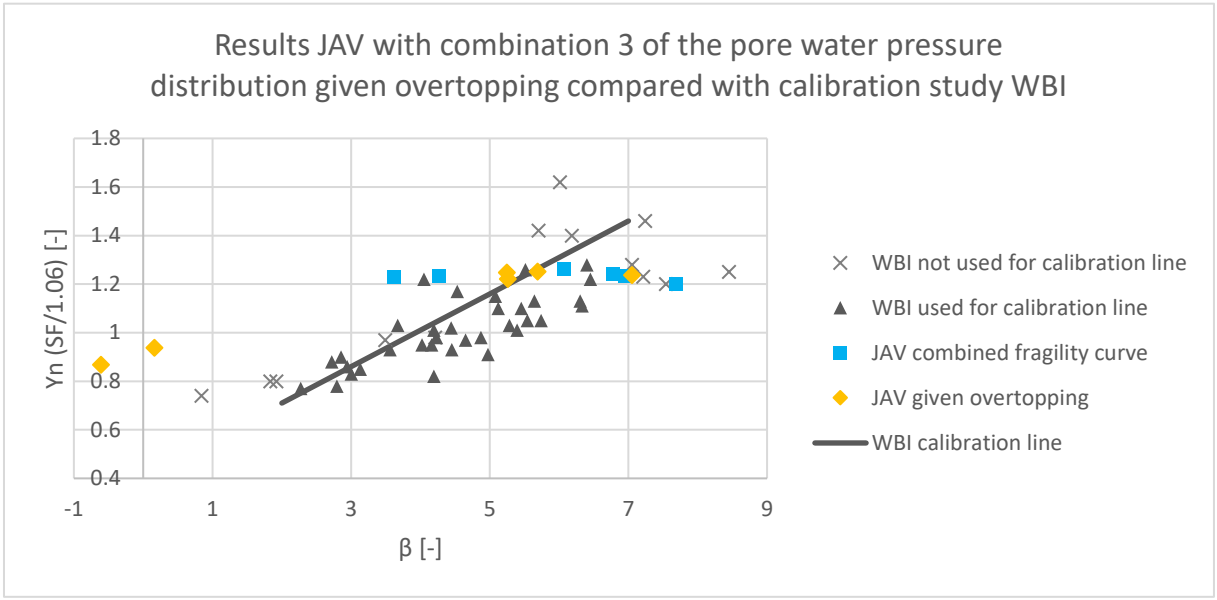

Figure 83: The results of the calculations of JAV with combination 3 of the pore water pressure distribution given overtopping compared with the calibration study of WBI. The vertical position of the results of JAV from the combined fragility curves (blue squares) are determined based on the semi-probabilistic results without overtopping

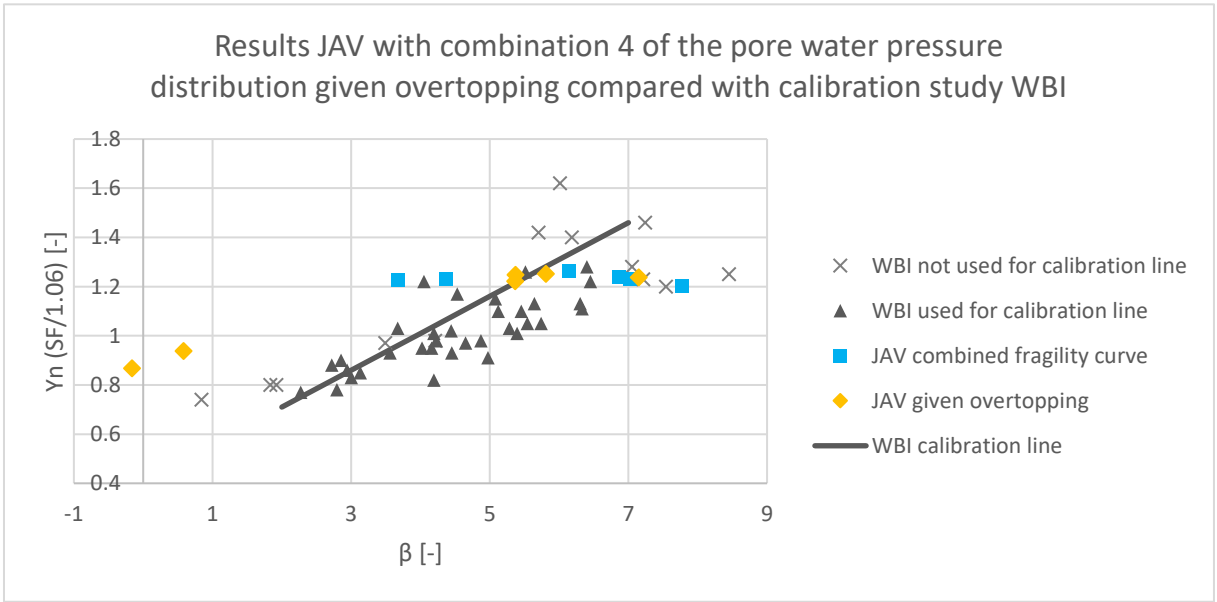

Figure 84: The results of the calculations of JAV with combination 4 of the pore water pressure distribution given overtopping compared with the calibration study of WBI. The vertical position of the results of JAV from the combined fragility curves (blue squares) are determined based on the semi-probabilistic results without overtopping

J. Results probabilistic calculations with a steepness of the inner slope of 1:3

The results of the probabilistic calculations with a steepness of the inner slope of 1:3 are given in this appendix. For every dike section are per water level the expected reliability index, coefficient of variation of the failure probability, 5% confidence bound of the reliability index and the difference between the expected reliability index and the 5% confidence bound of the reliability index given in the tables in this appendix. The coefficient of variation of the failure probability is specified as the standard deviation of the probability of failure divided by the probability of failure (Deltares, 2022). The 5% confidence bound of the reliability index is determined based on the failure probability and the coefficient of variation of the failure probability.

Besides, for every dike section are the fragility curves given. The fragility points, the fragility curve without overtopping, the fragility curve given overtopping, the combined fragility curve, the probability of exceedance of 1 l/s/m overtopping given the water level and the probability density function of the water level are given in the figures in this appendix. Furthermore, the reliability indexes are given per dike section.

The results of the probabilistic calculations with a steepness of the inner slope of 1:3 for dike section 10C are given in Table 78 and the fragility curves are shown in Figure 85.

Table 78: Reliability index probabilistic calculations with a steepness of the inner slope of 1:3 per water level for dike section 10C

Water level [m +NAP]	Traffic	Overtopping	Reliability index [-]	Coefficient of variation of the failure probability [-]	5% Confidence bound reliability index [-]	Reliability index - 5% confidence bound reliability index [-]
0.24	Yes	No	7.26	0.126	7.23	0.03
4.37	Yes	No	6.55	0.800	6.42	0.13
6.81	No	No	4.43	0.0949	4.40	0.03
6.66	No	No	4.57	0.101	4.54	0.03
6.96	No	No	4.20	0.0803	4.18	0.02
7.15	No	No	3.96	0.0778	3.93	0.03
6.66	No	Yes	0.262	0.0459	0.19	0.08
6.96	No	Yes	-0.231	0.0462	-0.35	0.12
6.21	No	Yes	0.366	0.0482	0.29	0.07
7.15	No	Yes	-0.369	0.0453	-0.50	0.13

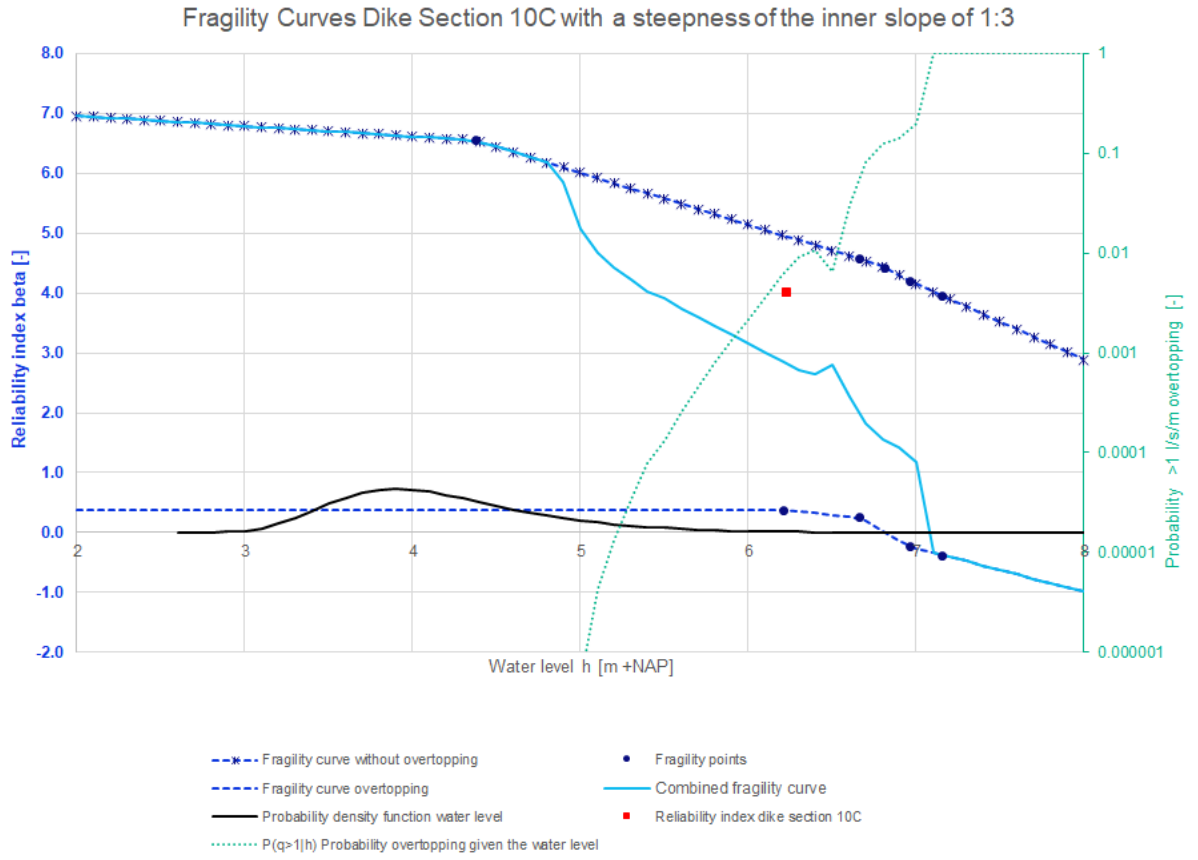

Figure 85: Fragility curves dike section 10C with a steepness of the inner slope of 1:3

The results of the probabilistic calculations with a steepness of the inner slope of 1:3 for dike section 11E are given in Table 79 and the fragility curves are shown in Figure 86.

Table 79: Reliability index probabilistic calculations with a steepness of the inner slope of 1:3 per water level for dike section 11E

Water level [m +NAP]	Traffic	Overtopping	Reliability index [-]	Coefficient of variation of the failure probability [-]	5% Confidence bound reliability index [-]	Reliability index - 5% confidence bound reliability index [-]
-0.04	Yes	No	7.20	0.117	7.17	0.03
2.39	Yes	No	7.23	0.149	7.20	0.03
3.47	Yes	No	6.40	0.362	6.33	0.07
6.77	No	No	4.15	0.0924	4.12	0.03
7.07	No	No	3.68	0.0903	3.64	0.04
6.77	No	Yes	-0.0804	0.0426	-0.17	0.09
7.07	No	Yes	-0.162	0.0499	-0.28	0.12
6.37	No	Yes	0.0923	0.0436	0.01	0.08

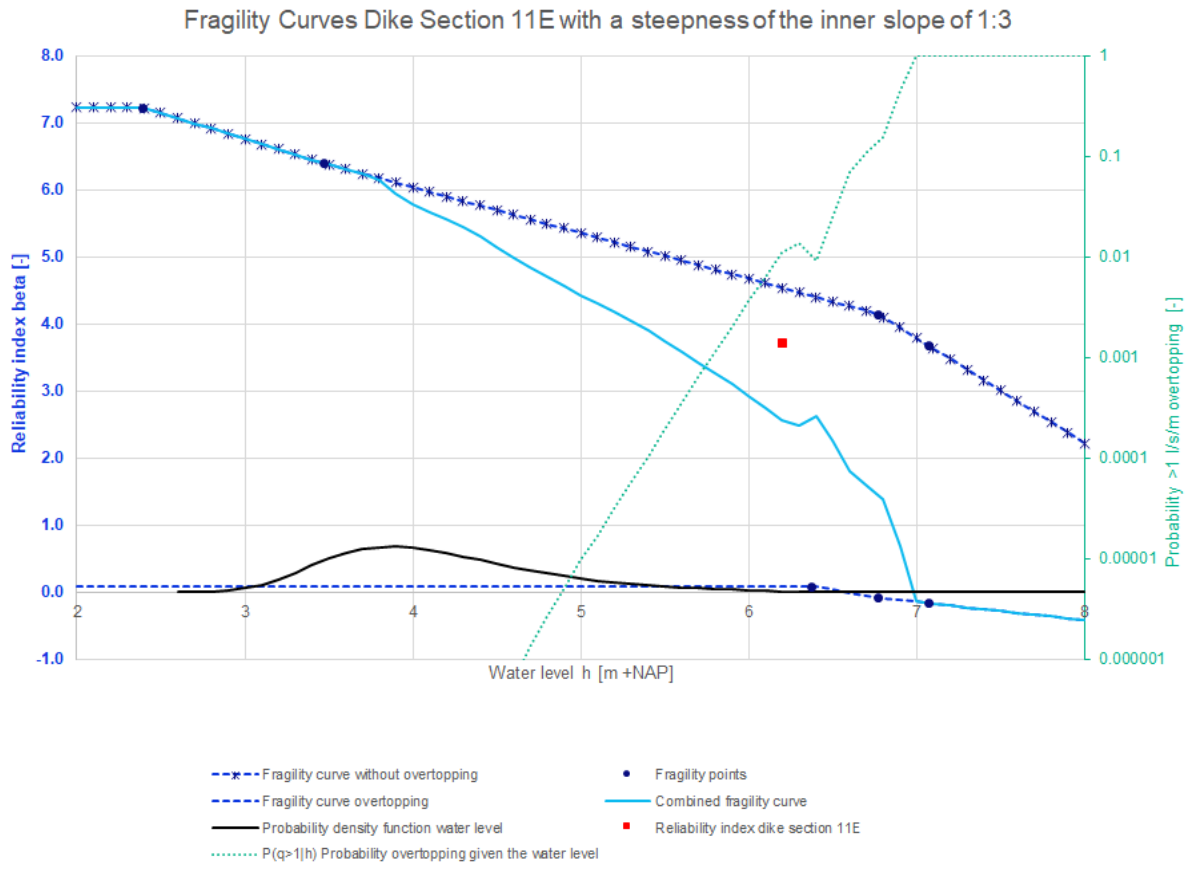

Figure 86: Fragility curves dike section 11E with a steepness of the inner slope of 1:3

The results of the probabilistic calculations with a steepness of the inner slope of 1:3 for dike section 11F(11D) are given in Table 80 and the fragility curves are shown in Figure 87.

Table 80: Reliability index probabilistic calculations with a steepness of the inner slope of 1:3 per water level for dike section 11F(11D)

Water level [m +NAP]	Traffic	Overtopping	Reliability index [-]	Coefficient of variation of the failure probability [-]	5% Confidence bound reliability index [-]	Reliability index - 5% confidence bound reliability index [-]
-0.04	Yes	No	6.88	0.175	6.85	0.03
2.63	Yes	No	6.94	0.129	6.92	0.02
5.24	Yes	No	4.73	0.108	4.70	0.03
6.79	No	No	3.75	0.0883	3.72	0.03
7.09	No	No	3.39	0.0817	3.36	0.03
6.79	No	Yes	-0.807	0.0500	-1.06	0.25
7.09	No	Yes	-0.965	0.0499	-1.29	0.32
6.38	No	Yes	-0.631	0.0500	-0.83	0.20

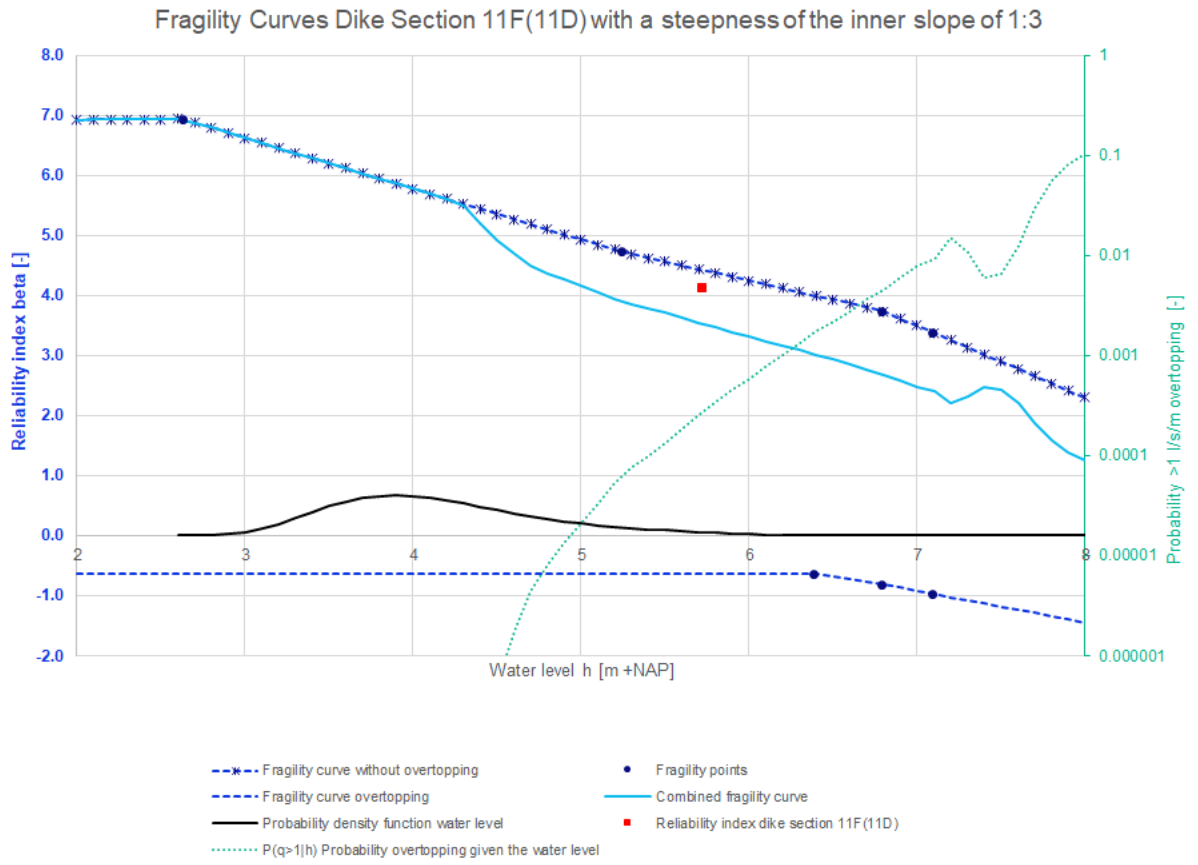

Figure 87: Fragility curves dike section 11F(11D) with a steepness of the inner slope of 1:3

The results of the probabilistic calculations with a steepness of the inner slope of 1:3 for dike section 13A are given in Table 81 and the fragility curves are shown in Figure 88.

Table 81: Reliability index probabilistic calculations with a steepness of the inner slope of 1:3 per water level for dike section 13A

Water level [m +NAP]	Traffic	Overtopping	Reliability index [-]	Coefficient of variation of the failure probability [-]	5% Confidence bound reliability index [-]	Reliability index - 5% confidence bound reliability index [-]
-0.30	Yes	No	7.43	0.572	7.34	0.09
0.87	Yes	No	7.66	0.737	7.56	0.10
2.07	Yes	No	7.25	0.554	7.16	0.09
6.26	No	No	4.99	0.145	4.95	0.04
6.56	No	No	4.65	0.209	4.59	0.06
6.26	No	Yes	-1.35	0.0174	-1.53	0.18
6.56	No	Yes	-1.61	0.0213	-2.06	0.45
5.66	No	Yes	-0.967	0.0146	-1.05	0.08

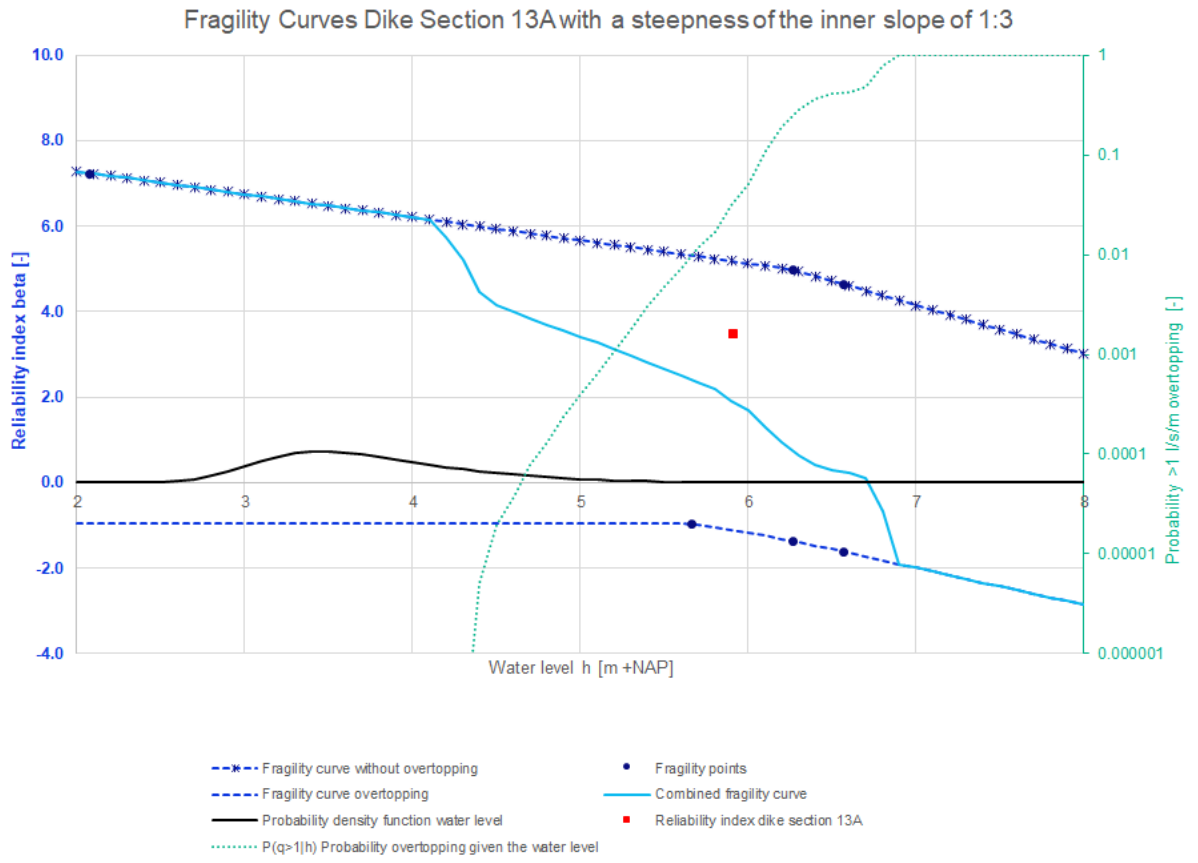

Figure 88: Fragility curves dike section 13A with a steepness of the inner slope of 1:3

The results of the probabilistic calculations with a steepness of the inner slope of 1:3 for dike section 13E1 are given in Table 82 and the fragility curves are shown in Figure 89.

Table 82: Reliability index probabilistic calculations with a steepness of the inner slope of 1:3 per water level for dike section 13E1

Water level [m +NAP]	Traffic	Overtopping	Reliability index [-]	Coefficient of variation of the failure probability [-]	5% Confidence bound reliability index [-]	Reliability index - 5% confidence bound reliability index [-]
-0.30	Yes	No	6.60	0.122	6.58	0.02
4.69	Yes	No	6.13	0.557	6.02	0.11
6.33	No	No	4.97	0.529	4.84	0.13
6.63	No	No	4.48	0.342	4.38	0.10
6.33	No	Yes	-0.174	0.0461	-0.28	0.11
6.63	No	Yes	-0.411	0.0476	-0.56	0.14
6.00	No	Yes	0.164	0.0500	0.07	0.09

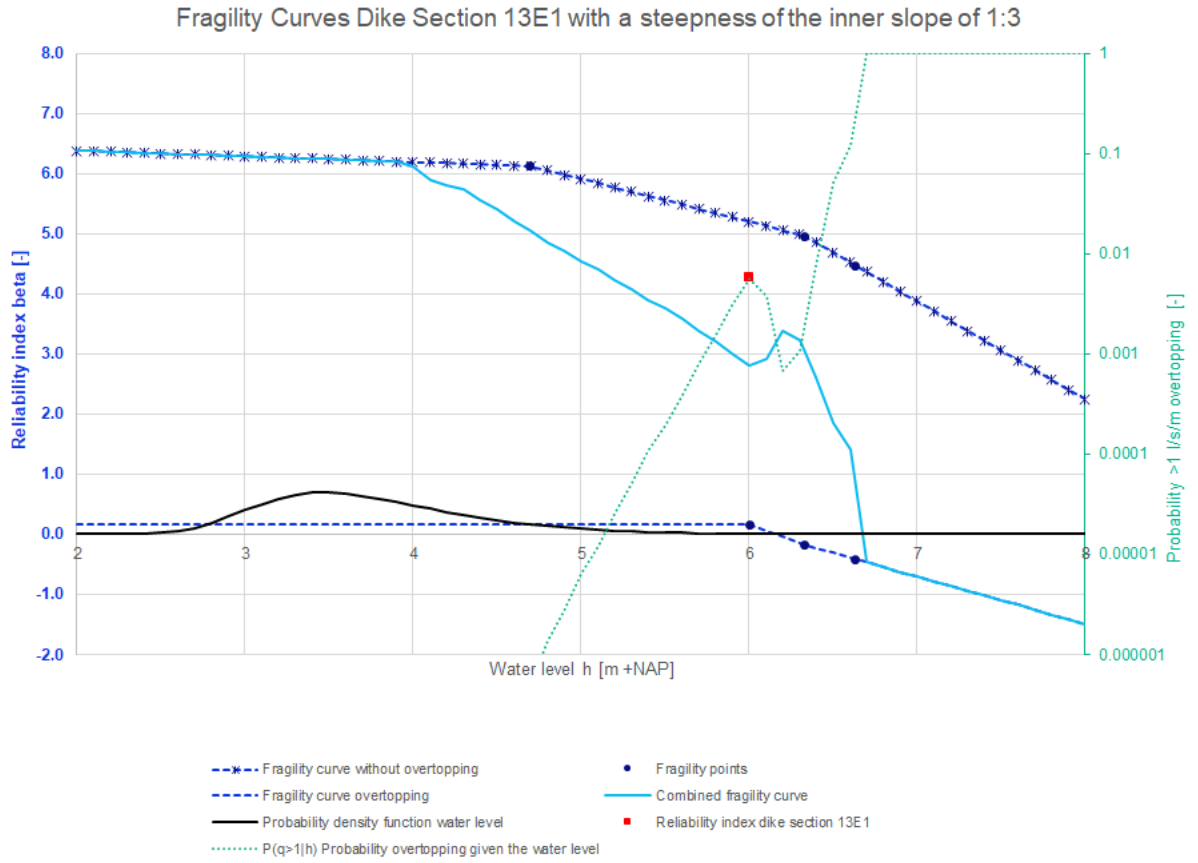

Figure 89: Fragility curves dike section 13E1 with a steepness of the inner slope of 1:3

The results of the probabilistic calculations with a steepness of the inner slope of 1:3 for dike section 13E2 are given in Table 83 and the fragility curves are shown in Figure 90.

Table 83: Reliability index probabilistic calculations with a steepness of the inner slope of 1:3 per water level for dike section 13E2

Water level [m +NAP]	Traffic	Overtopping	Reliability index [-]	Coefficient of variation of the failure probability [-]	5% Confidence bound reliability index [-]	Reliability index - 5% confidence bound reliability index [-]
-0.30	Yes	No	7.00	0.586	6.91	0.09
4.69	Yes	No	5.90	0.307	5.83	0.07
6.24	No	No	5.26	0.155	5.21	0.05
6.54	No	No	4.67	0.145	4.62	0.05
6.24	No	Yes	0.0431	0.0491	-0.06	0.10
6.54	No	Yes	-0.200	0.0500	-0.32	0.12
5.91	No	Yes	0.104	0.0500	0.01	0.10

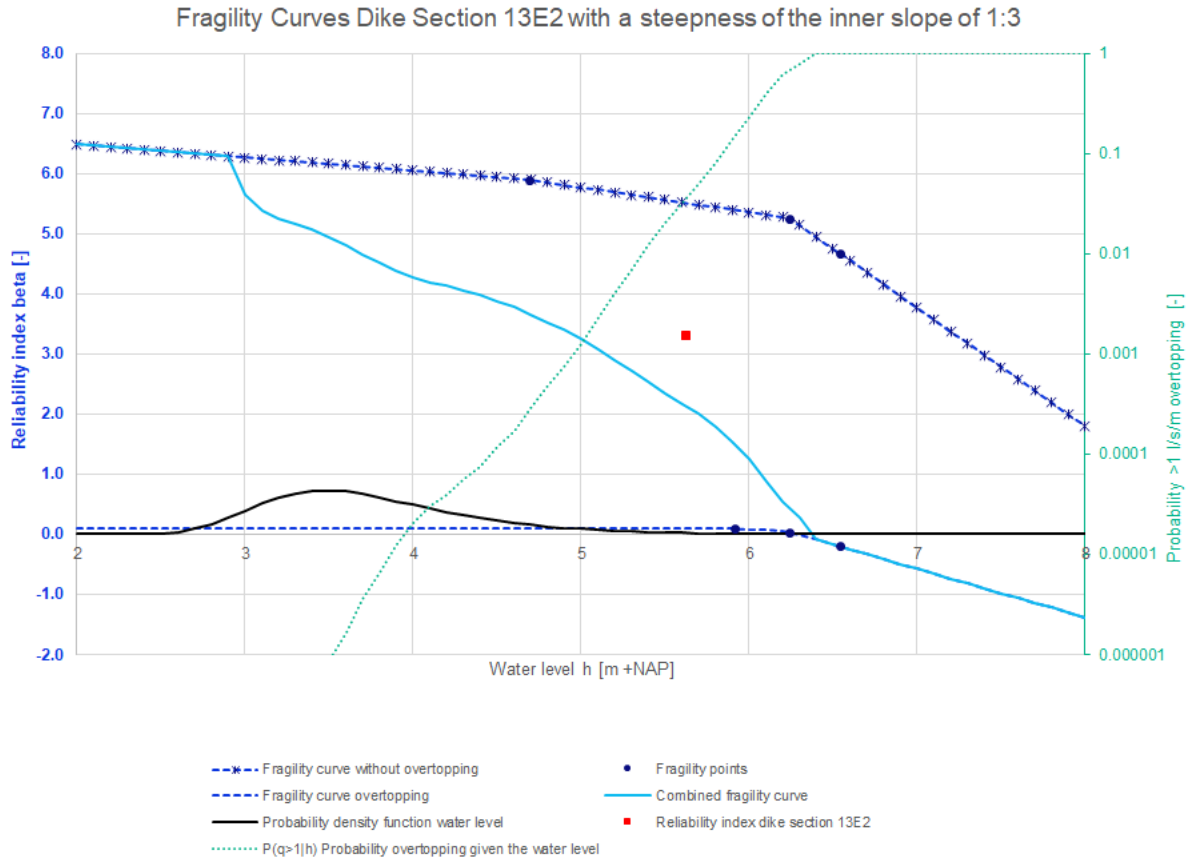

Figure 90: Fragility curves dike section 13E2 with a steepness of the inner slope of 1:3

The estimated reliability indexes based on the semi-probabilistic calculations with a steepness of the inner slope of 1:3 are given in Table 84. Furthermore, the reliability indexes of the probabilistic calculations with a steepness of the inner slope of 1:3 are shown in Table 85.

Table 84: Reliability index semi-probabilistic calculations with a steepness of the inner slope of 1:3

Dike section	Reliability index β without overtopping [-]	Reliability index β given overtopping [-]
10C	5.20	3.13
11E	5.04	3.05
11F(11D)	4.80	2.82
13A	4.85	2.66
13E1	5.52	2.58
13E2	5.59	2.57

Table 85: Reliability index probabilistic calculations with a steepness of the inner slope of 1:3

Dike section	Reliability index β combined fragility curve [-]	Reliability index β without overtopping [-]	Reliability index β given overtopping [-]
10C	4.01	5.72	0.37
11E	3.71	5.27	0.09
11F(11D)	4.14	4.92	-0.63
13A	3.49	5.93	-0.97
13E1	4.29	6.00	0.16
13E2	3.31	5.99	0.10

K. Results probabilistic calculations with a steepness of the inner slope of 1:3.5

The results of the probabilistic calculations with a steepness of the inner slope of 1:3.5 are given in this appendix. For every dike section are per water level the expected reliability index, coefficient of variation of the failure probability, 5% confidence bound of the reliability index and the difference between the expected reliability index and the 5% confidence bound of the reliability index given in the tables in this appendix. The coefficient of variation of the failure probability is specified as the standard deviation of the probability of failure divided by the probability of failure (Deltares, 2022). The 5% confidence bound of the reliability index is determined based on the failure probability and the coefficient of variation of the failure probability.

Besides, for every dike section are the fragility curves given. The fragility points, the fragility curve without overtopping, the fragility curve given overtopping, the combined fragility curve, the probability of exceedance of 1 l/s/m overtopping given the water level and the probability density function of the water level are given in the figures in this appendix. Furthermore, the reliability indexes are given per dike section, the results are plotted with the results of the WBI calibration study and the influence factors are shown.

The results of the probabilistic calculations with a steepness of the inner slope of 1:3.5 for dike section 10C are given in Table 86 and the fragility curves are shown in Figure 91.

Table 86: Reliability index probabilistic calculations with a steepness of the inner slope of 1:3.5 per water level for dike section 10C

Water level [m +NAP]	Traffic	Overtopping	Reliability index [-]	Coefficient of variation of the failure probability [-]	5% Confidence bound reliability index [-]	Reliability index - 5% confidence bound reliability index [-]
0.24	Yes	No	10.7	0.424	10.6	0.1
4.37	Yes	No	7.87	0.210	7.83	0.04
6.81	No	No	5.00	0.604	4.87	0.13
6.66	No	No	5.60	0.162	5.55	0.05
6.96	No	No	4.50	0.741	4.33	0.17
7.15	No	No	4.11	0.323	4.01	0.10
6.66	No	Yes	2.20	0.0579	2.16	0.04
6.96	No	Yes	2.03	0.0557	1.99	0.04
6.21	No	Yes	2.41	0.0679	2.37	0.04
7.15	No	Yes	1.94	0.0543	1.91	0.03

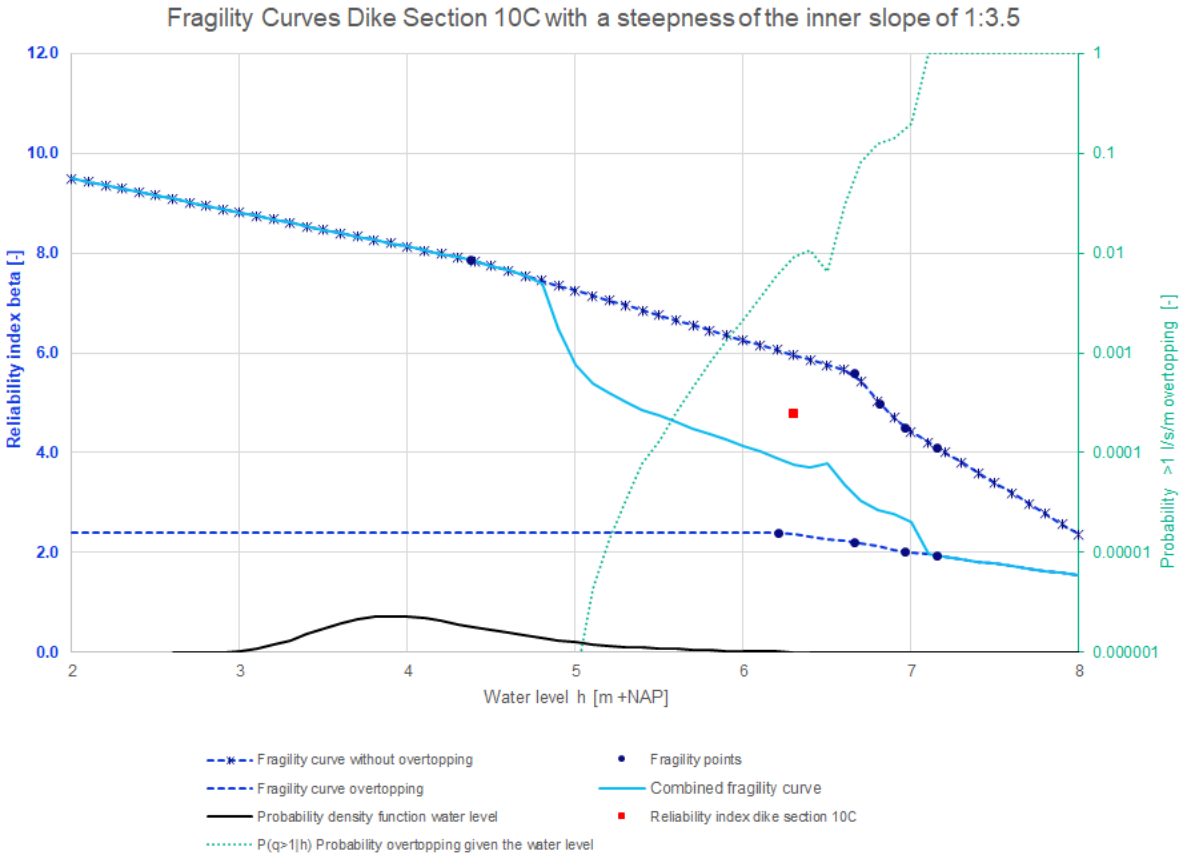

Figure 91: Fragility curves dike section 10C with a steepness of the inner slope of 1:3.5

The results of the probabilistic calculations with a steepness of the inner slope of 1:3.5 for dike section 11E are given in Table 87 and the fragility curves are shown in Figure 92.

Table 87: Reliability index probabilistic calculations with a steepness of the inner slope of 1:3.5 per water level for dike section 11E

Water level [m +NAP]	Traffic	Overtopping	Reliability index [-]	Coefficient of variation of the failure probability [-]	5% Confidence bound reliability index [-]	Reliability index - 5% confidence bound reliability index [-]
-0.04	Yes	No	8.33	0.316	8.28	0.05
2.39	Yes	No	8.24	0.333	8.18	0.06
3.47	Yes	No	7.11	0.113	7.09	0.02
6.77	No	No	4.99	0.187	4.93	0.06
7.07	No	No	4.63	0.155	4.59	0.04
7.30	No	No	4.35	0.143	4.30	0.05
6.77	No	Yes	1.37	0.05	1.33	0.04
7.07	No	Yes	1.16	0.05	1.11	0.05
6.37	No	Yes	1.72	0.101	1.64	0.08
7.30	No	Yes	1.07	0.05	1.02	0.05

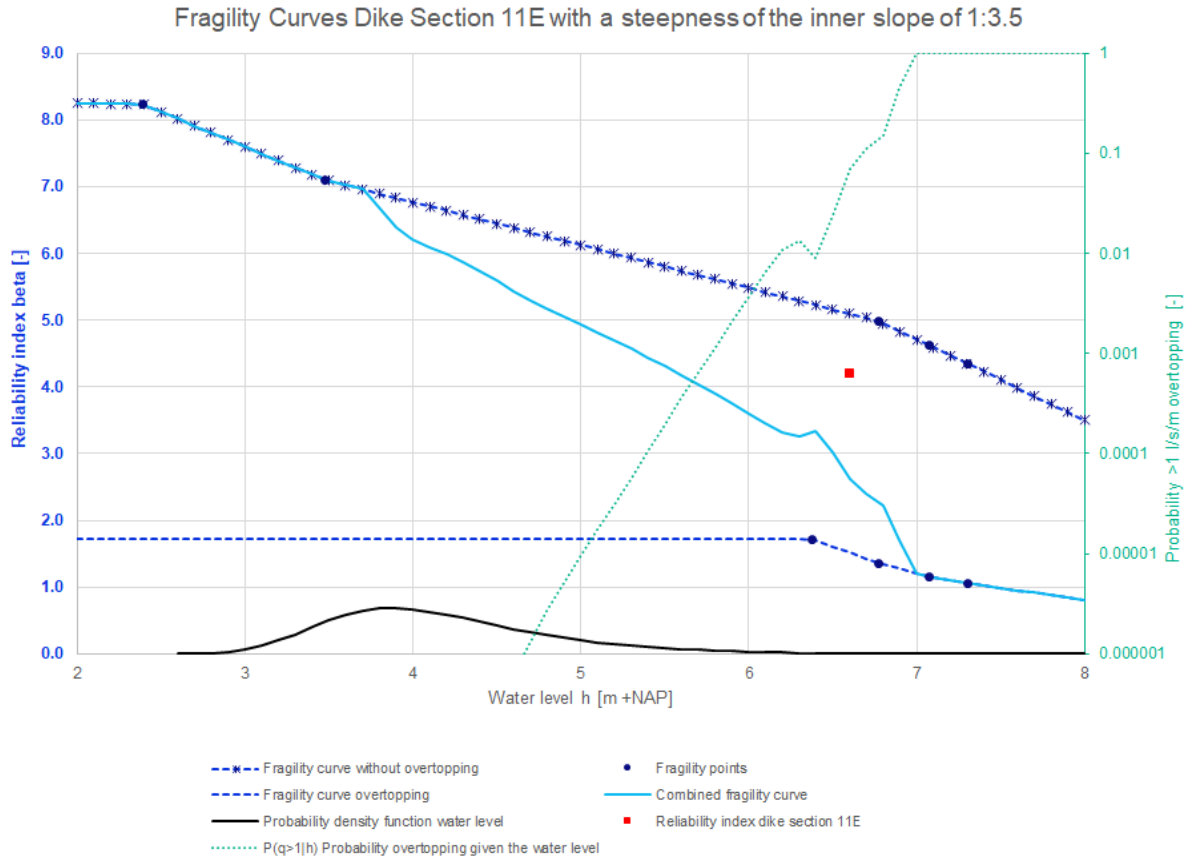

Figure 92: Fragility curves dike section 11E with a steepness of the inner slope of 1:3.5

The results of the probabilistic calculations with a steepness of the inner slope of 1:3.5 for dike section 11F(11D) are given in Table 88 and the fragility curves are shown in Figure 93.

Table 88: Reliability index probabilistic calculations with a steepness of the inner slope of 1:3.5 per water level for dike section 11F(11D)

Water level [m +NAP]	Traffic	Overtopping	Reliability index [-]	Coefficient of variation of the failure probability [-]	5% Confidence bound reliability index [-]	Reliability index - 5% confidence bound reliability index [-]
-0.04	Yes	No	8.84	0.308	8.79	0.05
2.63	Yes	No	8.82	0.305	8.78	0.04
5.24	Yes	No	5.98	0.130	5.95	0.03
6.79	No	No	5.09	0.111	5.06	0.03
7.09	No	No	4.75	0.102	4.72	0.03
6.79	No	Yes	1.31	0.05	1.27	0.04
7.09	No	Yes	1.14	0.05	1.09	0.05
6.38	No	Yes	1.56	0.05	1.52	0.04

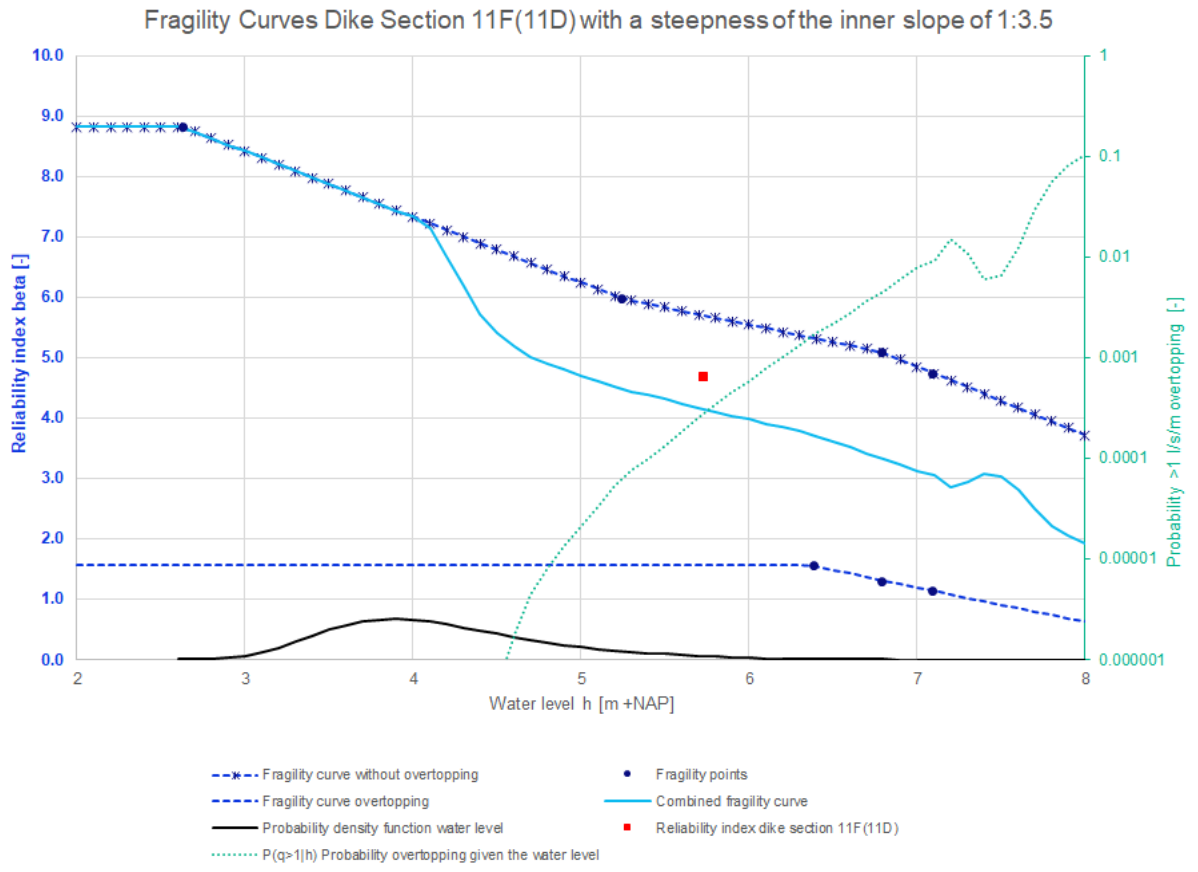

Figure 93: Fragility curves dike section 11F(11D) with a steepness of the inner slope of 1:3.5

The results of the probabilistic calculations with a steepness of the inner slope of 1:3.5 for dike section 13A are given in Table 89 and the fragility curves are shown in Figure 94.

Table 89: Reliability index probabilistic calculations with a steepness of the inner slope of 1:3.5 per water level for dike section 13A

Water level [m +NAP]	Traffic	Overtopping	Reliability index [-]	Coefficient of variation of the failure probability [-]	5% Confidence bound reliability index [-]	Reliability index - 5% confidence bound reliability index [-]
-0.30	Yes	No	13.3	0.496	13.3	0.0
0.87	Yes	No	12.8	0.310	12.8	0.0
2.07	Yes	No	11.8	0.326	11.8	0.0
6.26	No	No	6.03	0.175	5.99	0.04
6.56	No	No	5.70	0.117	5.67	0.03
6.26	No	Yes	0.982	0.0502	0.93	0.05
6.56	No	Yes	0.822	0.0500	0.76	0.06
5.66	No	Yes	1.25	0.0531	1.20	0.05

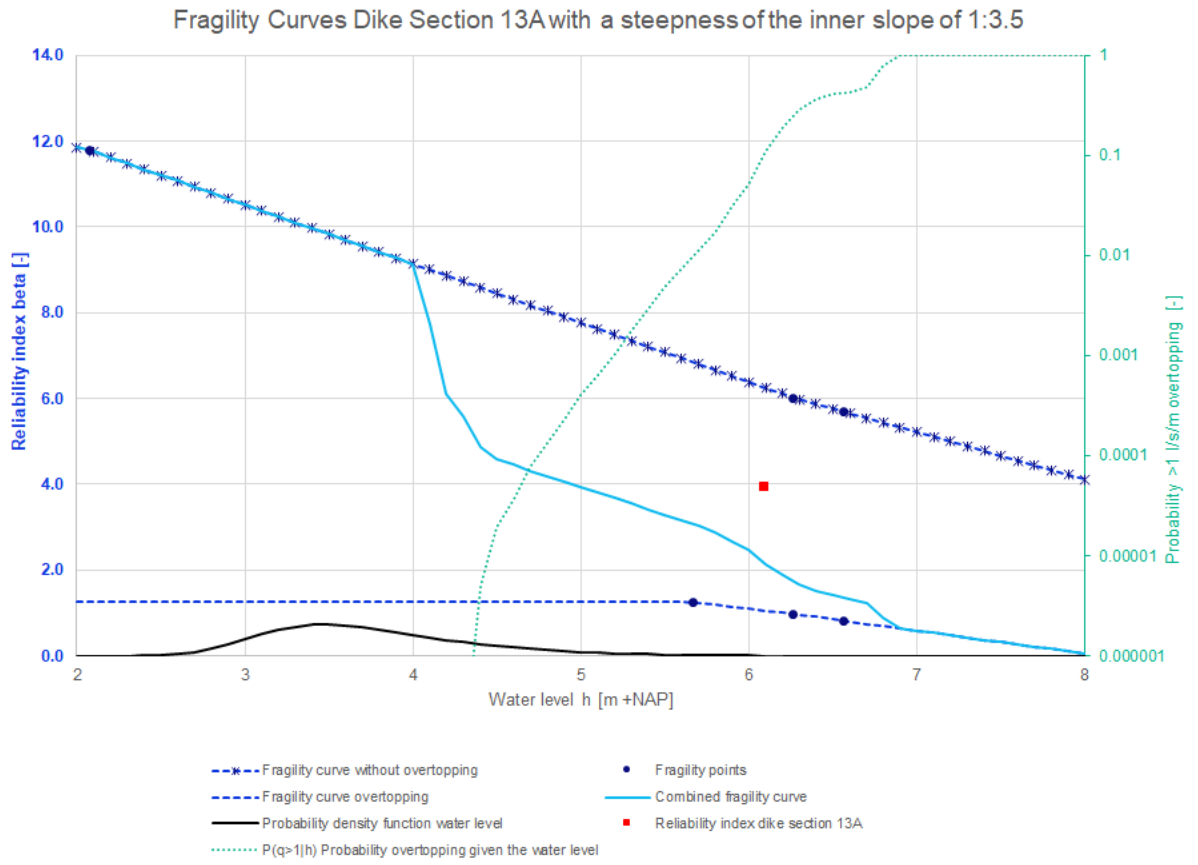

Figure 94: Fragility curves dike section 13A with a steepness of the inner slope of 1:3.5

The results of the probabilistic calculations with a steepness of the inner slope of 1:3.5 for dike section 13E1 are given in Table 90 and the fragility curves are shown in Figure 95.

Table 90: Reliability index probabilistic calculations with a steepness of the inner slope of 1:3.5 per water level for dike section 13E1

Water level [m +NAP]	Traffic	Overtopping	Reliability index [-]	Coefficient of variation of the failure probability [-]	5% Confidence bound reliability index [-]	Reliability index - 5% confidence bound reliability index [-]
-0.30	Yes	No	8.11	0.540	8.03	0.08
4.69	Yes	No	8.16	0.836	8.05	0.11
6.33	No	No	7.55	0.555	7.46	0.09
6.63	No	No	6.72	0.394	6.65	0.07
6.90	No	No	6.29	0.433	6.21	0.08
6.33	No	Yes	2.50	0.0801	2.46	0.04
6.63	No	Yes	2.17	0.0632	2.13	0.04
6.00	No	Yes	2.87	0.0911	2.82	0.05
6.90	No	Yes	1.85	0.0865	1.79	0.06

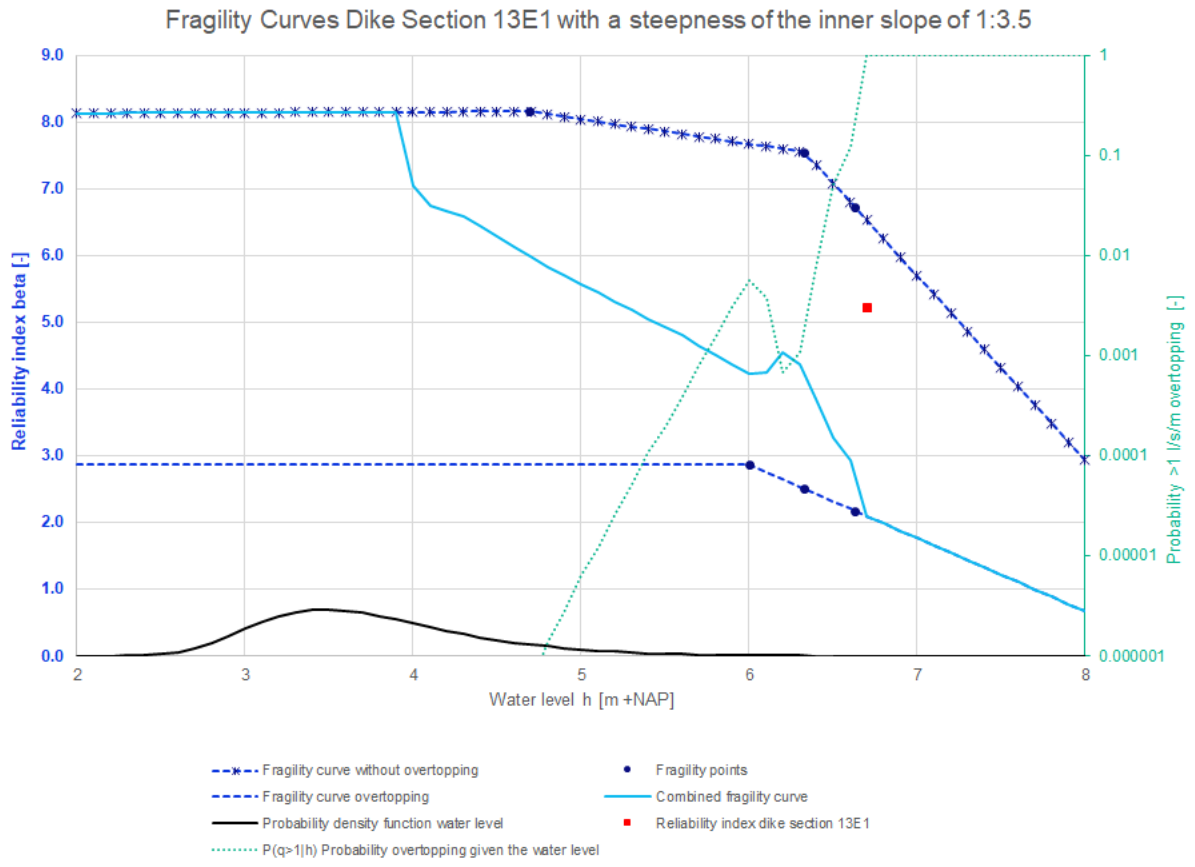

Figure 95: Fragility curves dike section 13E1 with a steepness of the inner slope of 1:3.5

The results of the probabilistic calculations with a steepness of the inner slope of 1:3.5 for dike section 13E2 are given in Table 91 and the fragility curves are shown in Figure 96.

Table 91: Reliability index probabilistic calculations with a steepness of the inner slope of 1:3.5 per water level for dike section 13E2

Water level [m +NAP]	Traffic	Overtopping	Reliability index [-]	Coefficient of variation of the failure probability [-]	5% Confidence bound reliability index [-]	Reliability index - 5% confidence bound reliability index [-]
-0.30	Yes	No	8.68	0.378	8.62	0.06
4.69	Yes	No	8.24	0.577	8.16	0.08
6.24	No	No	7.34	0.237	7.29	0.05
6.54	No	No	6.70	0.184	6.66	0.04
6.24	No	Yes	2.53	0.0706	2.49	0.04
6.54	No	Yes	2.26	0.0658	2.22	0.04
5.91	No	Yes	2.60	0.0812	2.55	0.05

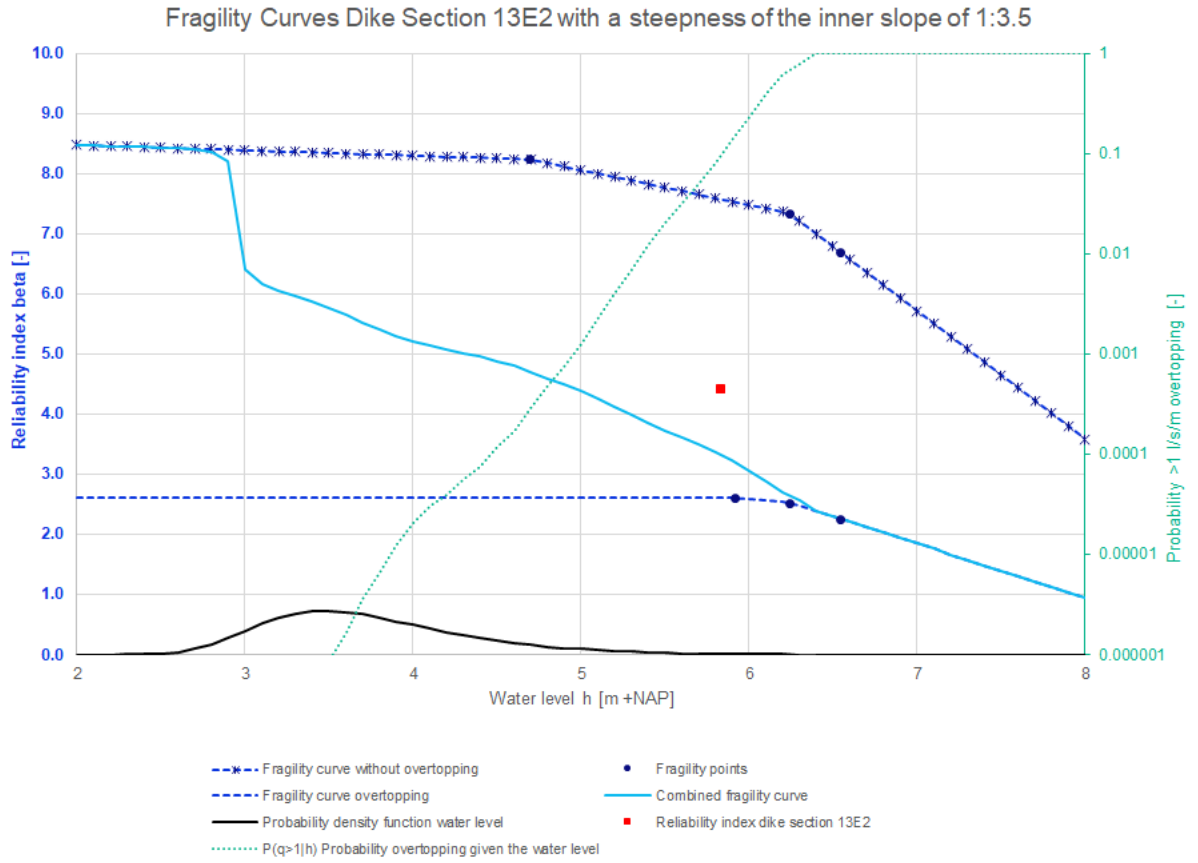

Figure 96: Fragility curves dike section 13E2 with a steepness of the inner slope of 1:3.5

The estimated reliability indexes based on the semi-probabilistic calculations with a steepness of the inner slope of 1:3.5 are given in Table 92. Furthermore, the reliability indexes of the probabilistic calculations with a steepness of the inner slope of 1:3.5 are shown in Table 93.

Table 92: Reliability index semi-probabilistic calculations with a steepness of the inner slope of 1:3.5

Dike section	Reliability index β without overtopping [-]	Reliability index β given overtopping [-]
10C	5.35	4.05
11E	5.34	3.82
11F(11D)	5.42	3.64
13A	4.98	3.34
13E1	5.46	3.34
13E2	5.59	3.71

Table 93: Reliability index probabilistic calculations with a steepness of the inner slope of 1:3.5

Dike section	Reliability index β combined fragility curve [-]	Reliability index β without overtopping [-]	Reliability index β given overtopping [-]
10C	4.80	6.40	2.41
11E	4.21	6.00	1.72
11F(11D)	4.68	6.09	1.56
13A	3.96	7.14	1.25
13E1	5.22	8.04	2.87
13E2	4.42	7.88	2.60

In Figure 97 are the results of JAV with an inner slope steepness of 1:3.5 plotted with the results of the WBI calibration study. In Figure 98 are the influence factors shown.

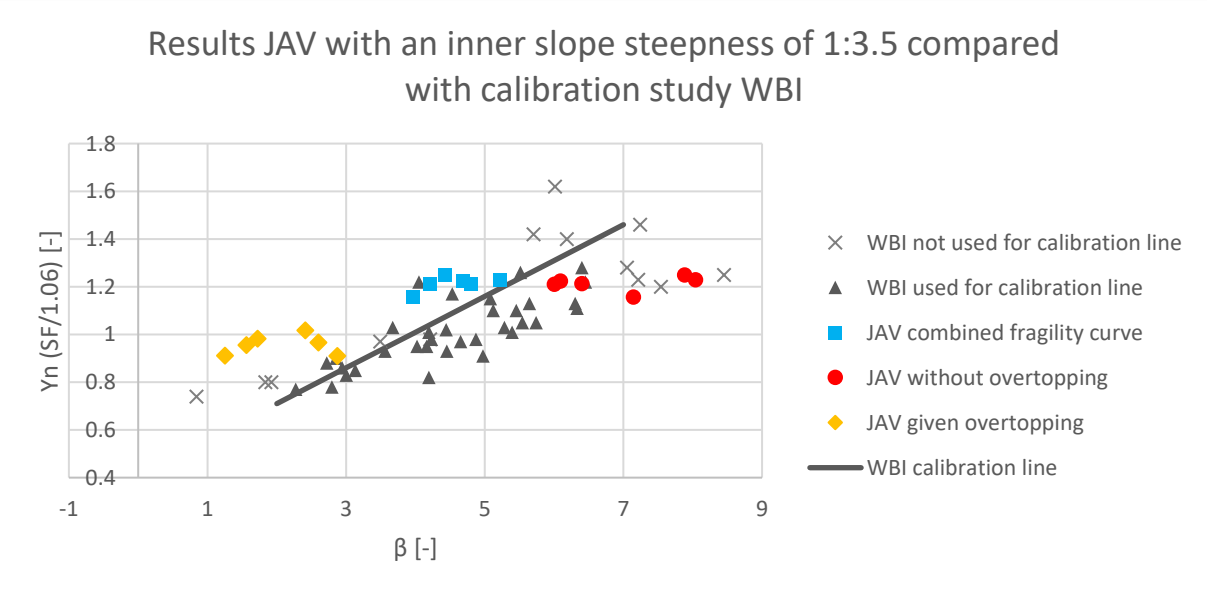

Figure 97: The results of the calculations of JAV with an inner slope steepness of 1:3.5 compared with the calibration study of WBI. The vertical position of the results of JAV from the combined fragility curves (blue squares) are determined based on the semi-probabilistic results without overtopping

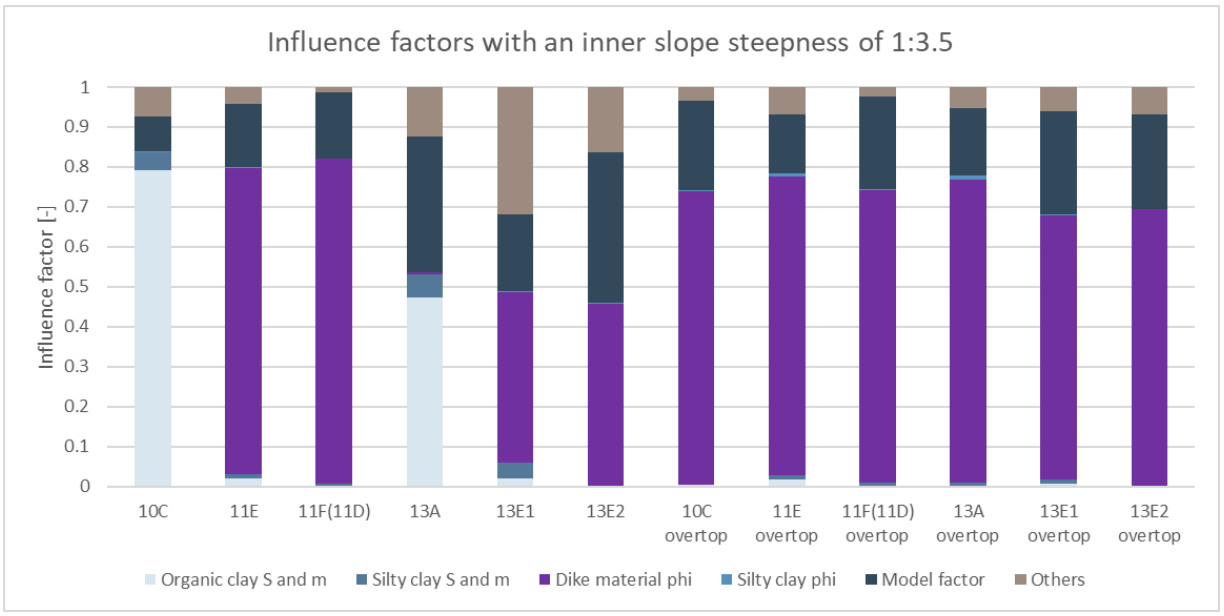

Figure 98: Influence factors with an inner slope steepness of 1:3.5 at WBN without overtopping and at the 1 l/s/m overtopping water level with overtopping

L. Results probabilistic calculations with a steepness of the inner slope of 1:4

The results of the probabilistic calculations with a steepness of the inner slope of 1:4 are given in this appendix. For every dike section are per water level the expected reliability index, coefficient of variation of the failure probability, 5% confidence bound of the reliability index and the difference between the expected reliability index and the 5% confidence bound of the reliability index given in the tables in this appendix. The coefficient of variation of the failure probability is specified as the standard deviation of the probability of failure divided by the probability of failure (Deltares, 2022). The 5% confidence bound of the reliability index is determined based on the failure probability and the coefficient of variation of the failure probability.

Besides, for every dike section are the fragility curves given. The fragility points, the fragility curve without overtopping, the fragility curve given overtopping, the combined fragility curve, the probability of exceedance of 1 l/s/m overtopping given the water level and the probability density function of the water level are given in the figures in this appendix. Furthermore, the reliability indexes are given per dike section, the results are plotted with the results of the WBI calibration study and the influence factors are shown.

The results of the probabilistic calculations with a steepness of the inner slope of 1:4 for dike section 10C are given in Table 94 and the fragility curves are shown in Figure 99.

Table 94: Reliability index probabilistic calculations with a steepness of the inner slope of 1:4 per water level for dike section 10C

Water level [m +NAP]	Traffic	Overtopping	Reliability index [-]	Coefficient of variation of the failure probability [-]	5% Confidence bound reliability index [-]	Reliability index - 5% confidence bound reliability index [-]
0.24	Yes	No	10.7	0.452	10.7	0.0
4.37	Yes	No	7.08	0.252	7.03	0.05
6.81	No	No	4.92	0.633	4.78	0.14
6.66	No	No	5.24	0.369	5.15	0.09
6.96	No	No	4.08	0.232	4.01	0.07
7.15	No	No	3.95	0.179	3.88	0.07
6.66	No	Yes	4.97	0.163	4.93	0.04
6.96	No	Yes	4.02	0.146	3.97	0.05
6.21	No	Yes	5.60	0.158	5.56	0.04
7.15	No	Yes	3.70	0.148	3.64	0.06

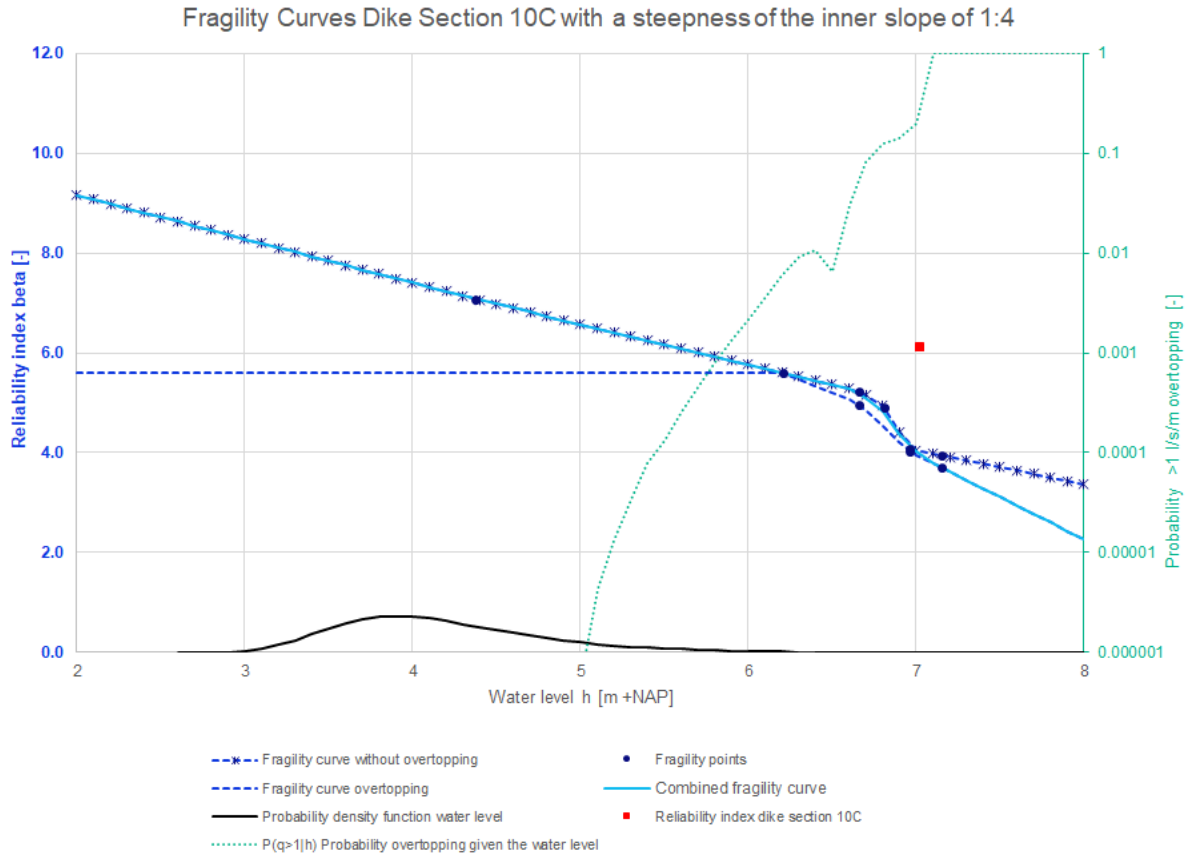

Figure 99: Fragility curves dike section 10C with a steepness of the inner slope of 1:4

The results of the probabilistic calculations with a steepness of the inner slope of 1:4 for dike section 11E are given in Table 95 and the fragility curves are shown in Figure 100.

Table 95: Reliability index probabilistic calculations with a steepness of the inner slope of 1:4 per water level for dike section 11E

Water level [m +NAP]	Traffic	Overtopping	Reliability index [-]	Coefficient of variation of the failure probability [-]	5% Confidence bound reliability index [-]	Reliability index - 5% confidence bound reliability index [-]
-0.04	Yes	No	9.78	0.155	9.76	0.02
2.39	Yes	No	9.73	0.636	9.66	0.07
3.47	Yes	No	8.52	0.417	8.46	0.06
6.77	No	No	6.42	0.645	6.31	0.11
7.07	No	No	6.06	0.777	5.92	0.14
6.77	No	Yes	3.64	0.0701	3.61	0.03
7.07	No	Yes	3.47	0.0740	3.44	0.03
6.37	No	Yes	3.87	0.0814	3.84	0.03

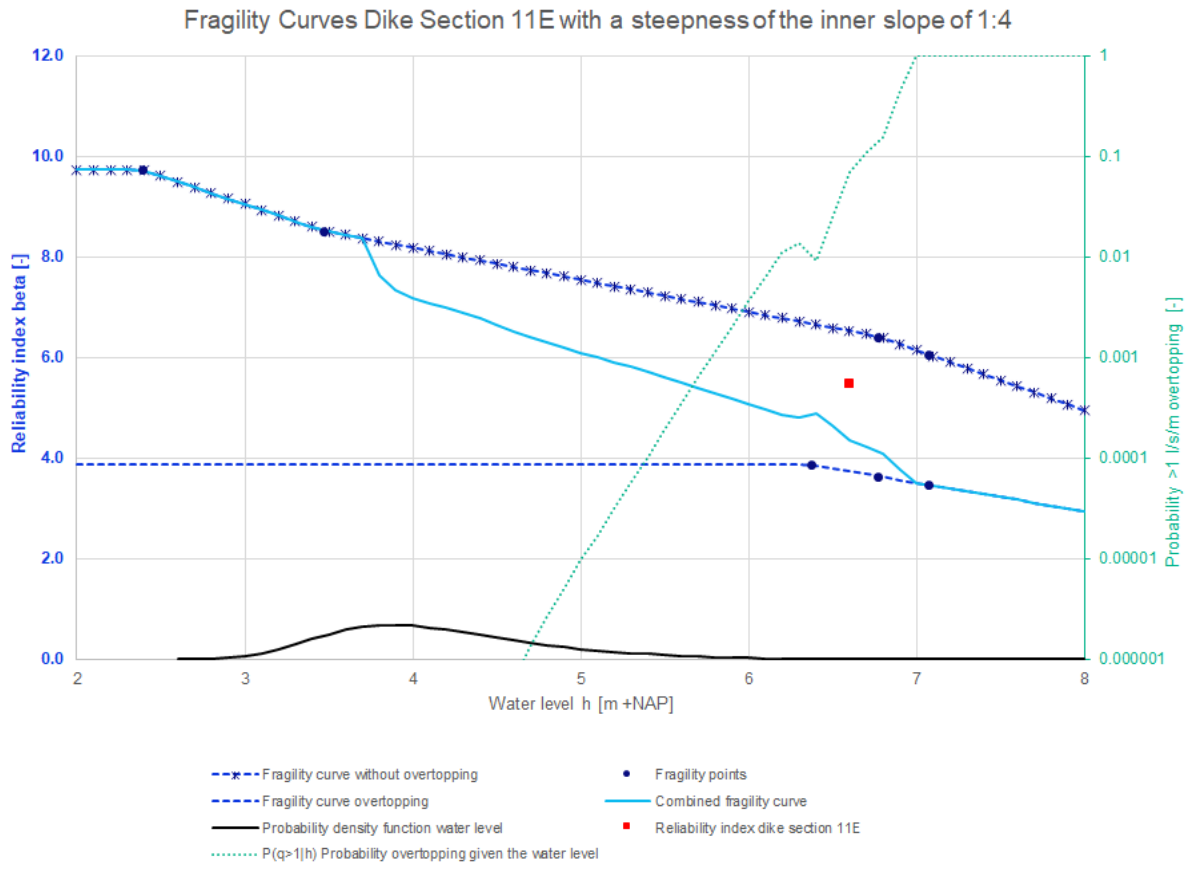

Figure 100: Fragility curves dike section 11E with a steepness of the inner slope of 1:4

The results of the probabilistic calculations with a steepness of the inner slope of 1:4 for dike section 11F(11D) are given in Table 96 and the fragility curves are shown in Figure 101.

Table 96: Reliability index probabilistic calculations with a steepness of the inner slope of 1:4 per water level for dike section 11F(11D)

Water level [m +NAP]	Traffic	Overtopping	Reliability index [-]	Coefficient of variation of the failure probability [-]	5% Confidence bound reliability index [-]	Reliability index - 5% confidence bound reliability index [-]
-0.04	Yes	No	9.90	0.200	9.87	0.03
2.63	Yes	No	10.2	0.694	10.1	0.1
5.24	Yes	No	7.18	0.457	7.10	0.08
6.79	No	No	6.23	0.143	6.20	0.03
7.09	No	No	5.91	0.142	5.88	0.03
6.79	No	Yes	3.05	0.0714	3.02	0.03
7.09	No	Yes	2.93	0.0744	2.89	0.04
6.38	No	Yes	3.13	0.074	3.09	0.04

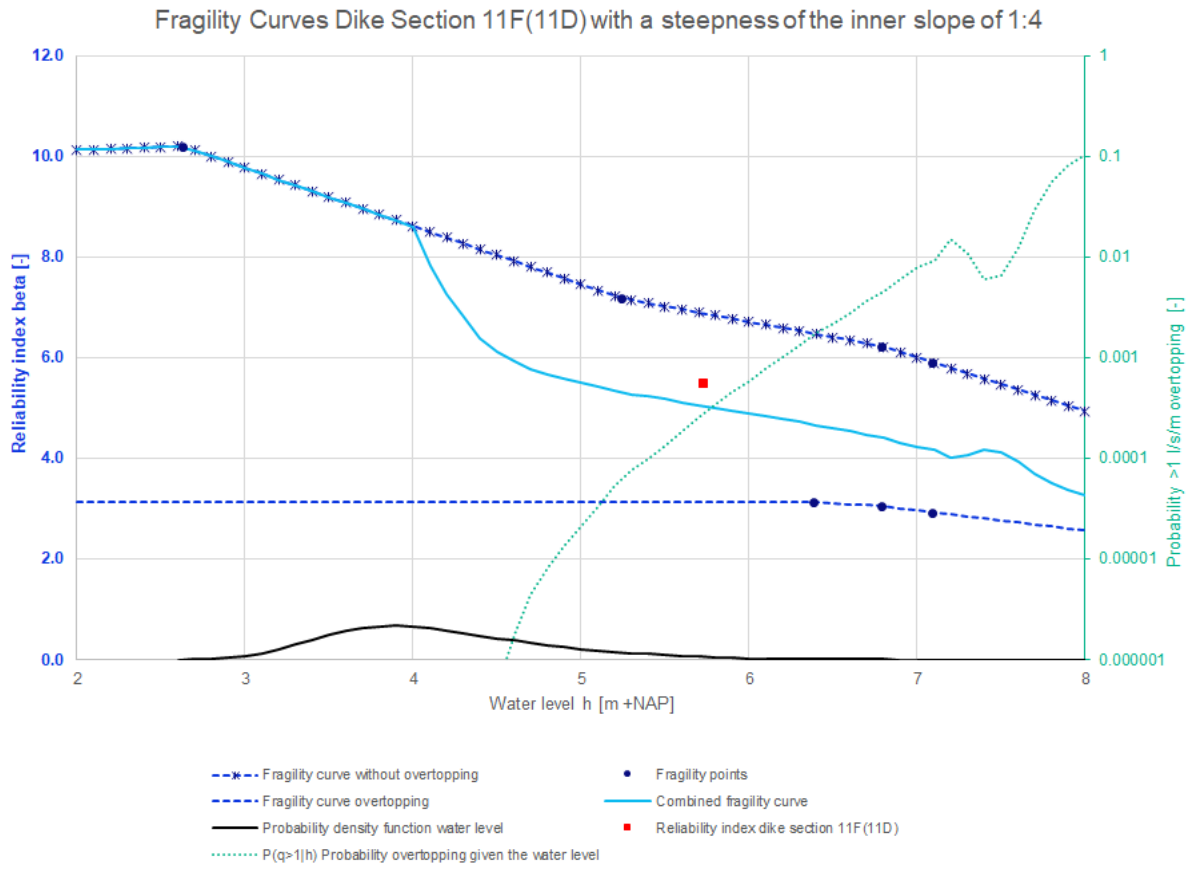

Figure 101: Fragility curves dike section 11F(11D) with a steepness of the inner slope of 1:4

The results of the probabilistic calculations with a steepness of the inner slope of 1:4 for dike section 13A are given in Table 97 and the fragility curves are shown in Figure 102.

Table 97: Reliability index probabilistic calculations with a steepness of the inner slope of 1:4 per water level for dike section 13A

Water level [m +NAP]	Traffic	Overtopping	Reliability index [-]	Coefficient of variation of the failure probability [-]	5% Confidence bound reliability index [-]	Reliability index - 5% confidence bound reliability index [-]
-0.30	Yes	No	13.7	0.288	13.7	0.0
0.87	Yes	No	13.1	0.972	13.0	0.1
2.07	Yes	No	11.7	0.419	11.7	0.0
6.26	No	No	6.66	0.122	6.63	0.03
6.56	No	No	6.23	0.314	6.16	0.07
6.26	No	Yes	2.89	0.0885	2.85	0.04
6.56	No	Yes	2.65	0.120	2.59	0.06
5.66	No	Yes	3.17	0.0837	3.13	0.04

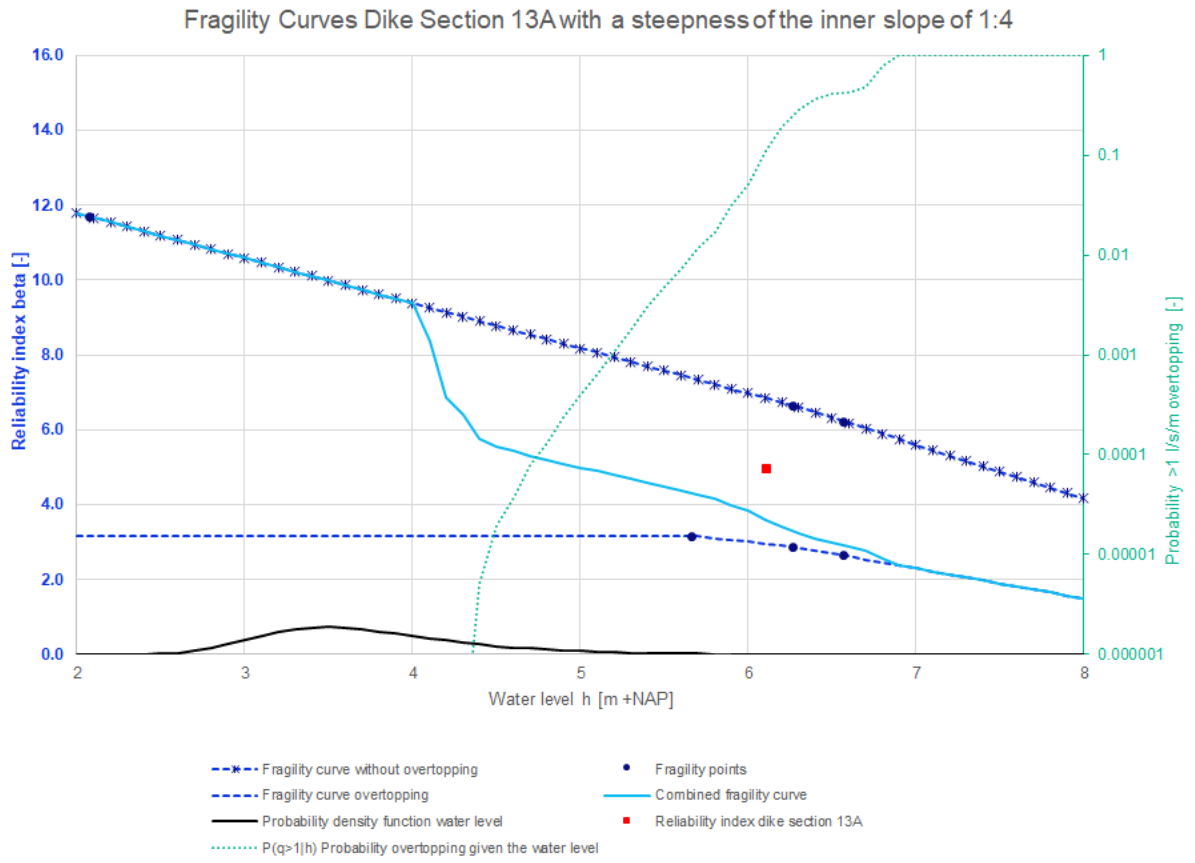

Figure 102: Fragility curves dike section 13A with a steepness of the inner slope of 1:4

The results of the probabilistic calculations with a steepness of the inner slope of 1:4 for dike section 13E1 are given in Table 98 and the fragility curves are shown in Figure 103.

Table 98: Reliability index probabilistic calculations with a steepness of the inner slope of 1:4 per water level for dike section 13E1

Water level [m +NAP]	Traffic	Overtopping	Reliability index [-]	Coefficient of variation of the failure probability [-]	5% Confidence bound reliability index [-]	Reliability index - 5% confidence bound reliability index [-]
-0.30	Yes	No	9.79	0.226	9.75	0.04
4.69	Yes	No	8.06	0.545	7.98	0.08
6.33	No	No	6.73	0.470	6.65	0.08
6.63	No	No	6.34	0.385	6.26	0.08
6.33	No	Yes	4.78	0.111	4.75	0.03
6.63	No	Yes	4.46	0.150	4.41	0.05
6.00	No	Yes	4.72	0.111	4.68	0.04

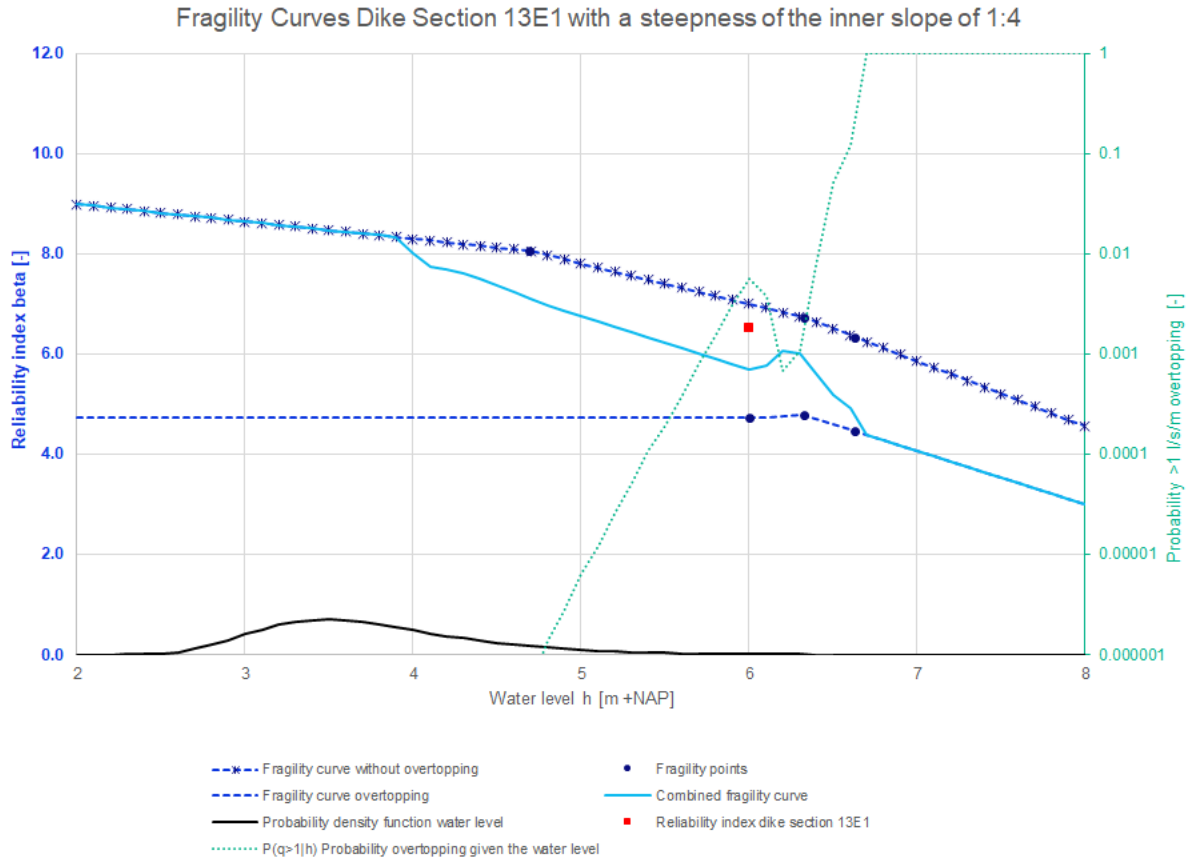

Figure 103: Fragility curves dike section 13E1 with a steepness of the inner slope of 1:4

The results of the probabilistic calculations with a steepness of the inner slope of 1:4 for dike section 13E2 are given in Table 99 and the fragility curves are shown in Figure 104.

Table 99: Reliability index probabilistic calculations with a steepness of the inner slope of 1:4 per water level for dike section 13E2

Water level [m +NAP]	Traffic	Overtopping	Reliability index [-]	Coefficient of variation of the failure probability [-]	5% Confidence bound reliability index [-]	Reliability index - 5% confidence bound reliability index [-]
-0.30	Yes	No	9.79	0.222	9.76	0.03
4.69	Yes	No	7.54	0.537	7.46	0.08
6.24	No	No	7.52	0.269	7.47	0.05
6.54	No	No	6.68	0.330	6.61	0.07
6.90	No	No	5.97	0.415	5.89	0.08
6.24	No	Yes	5.67	0.357	5.59	0.08
6.54	No	Yes	5.52	0.393	5.43	0.09
5.91	No	Yes	5.95	0.309	5.88	0.07
6.90	No	Yes	4.43	0.185	4.38	0.05

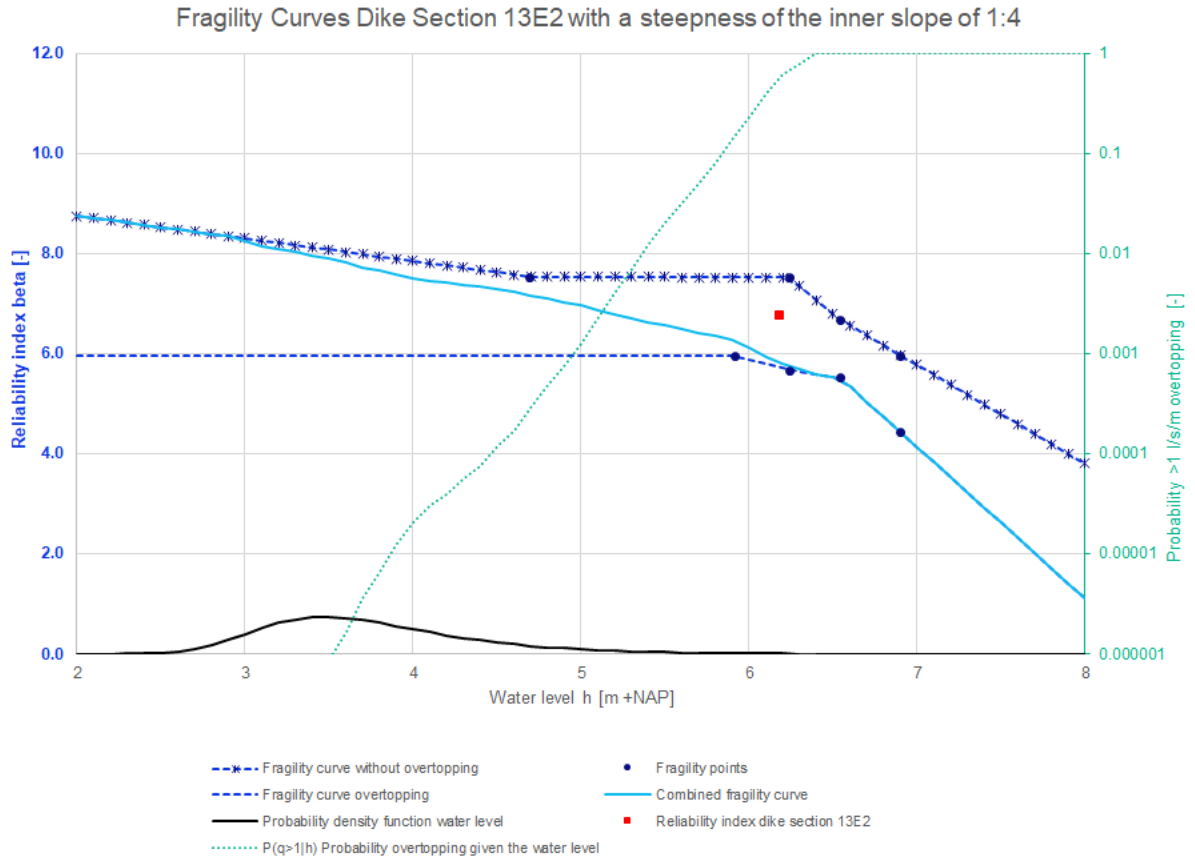

Figure 104: Fragility curves dike section 13E2 with a steepness of the inner slope of 1:4

The estimated reliability indexes based on the semi-probabilistic calculations with a steepness of the inner slope of 1:4 are given in Table 100. Furthermore, the reliability indexes of the probabilistic calculations with a steepness of the inner slope of 1:4 are shown in Table 101.

Table 100: Reliability index semi-probabilistic calculations with a steepness of the inner slope of 1:4

Dike section	Reliability index β without overtopping [-]	Reliability index β given overtopping [-]
10C	5.19	4.85
11E	5.61	4.80
11F(11D)	5.41	4.45
13A	5.02	4.15
13E1	5.42	4.39
13E2	5.47	4.40

Table 101: Reliability index probabilistic calculations with a steepness of the inner slope of 1:4

Dike section	Reliability index β combined fragility curve [-]	Reliability index β without overtopping [-]	Reliability index β given overtopping [-]
10C	6.13	6.19	5.60
11E	5.50	7.30	3.87
11F(11D)	5.48	7.16	3.13
13A	4.95	7.63	3.17
13E1	6.52	7.66	4.72
13E2	6.77	7.75	5.95

In Figure 105 are the results of JAV with an inner slope steepness of 1:4 plotted with the results of the WBI calibration study. In Figure 106 are the influence factors shown.

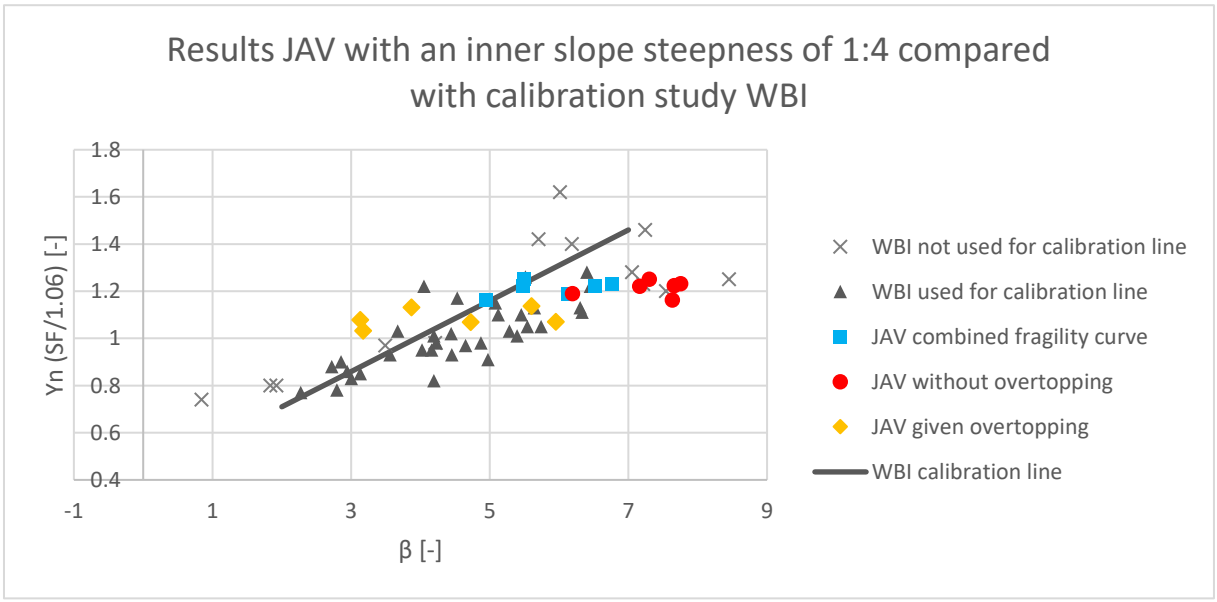

Figure 105: The results of the calculations of JAV with an inner slope steepness of 1:4 compared with the calibration study of WBI. The vertical position of the results of JAV from the combined fragility curves (blue squares) are determined based on the semi-probabilistic results without overtopping

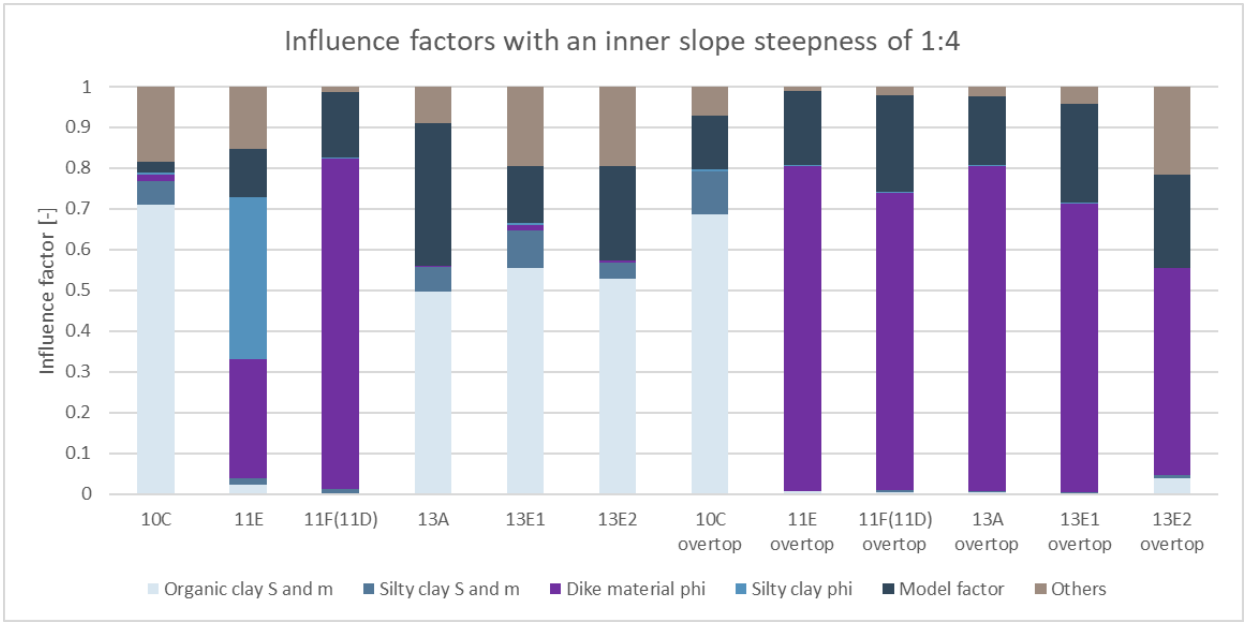

Figure 106: Influence factors with an inner slope steepness of 1:4 at WBN without overtopping and at the 1 l/s/m overtopping water level with overtopping

M. Results probabilistic calculations with a steepness of the inner slope of 1:4.5

The results of the probabilistic calculations with a steepness of the inner slope of 1:4.5 are given in this appendix. For every dike section are per water level the expected reliability index, coefficient of variation of the failure probability, 5% confidence bound of the reliability index and the difference between the expected reliability index and the 5% confidence bound of the reliability index given in the tables in this appendix. The coefficient of variation of the failure probability is specified as the standard deviation of the probability of failure divided by the probability of failure (Deltares, 2022). The 5% confidence bound of the reliability index is determined based on the failure probability and the coefficient of variation of the failure probability.

Besides, for every dike section are the fragility curves given. The fragility points, the fragility curve without overtopping, the fragility curve given overtopping, the combined fragility curve, the probability of exceedance of 1 l/s/m overtopping given the water level and the probability density function of the water level are given in the figures in this appendix. Furthermore, the reliability indexes are given per dike section, the results are plotted with the results of the WBI calibration study and the influence factors are shown.

The results of the probabilistic calculations with a steepness of the inner slope of 1:4.5 for dike section 10C are given in Table 102 and the fragility curves are shown in Figure 107.

Table 102: Reliability index probabilistic calculations with a steepness of the inner slope of 1:4.5 per water level for dike section 10C

Water level [m +NAP]	Traffic	Overtopping	Reliability index [-]	Coefficient of variation of the failure probability [-]	5% Confidence bound reliability index [-]	Reliability index - 5% confidence bound reliability index [-]
0.24	Yes	No	10.8	0.376	10.7	0.1
4.37	Yes	No	7.12	0.277	7.07	0.05
6.81	No	No	5.32	0.272	5.25	0.07
6.66	No	No	5.40	0.187	5.36	0.04
6.96	No	No	4.26	0.165	4.20	0.06
7.15	No	No	3.87	0.126	3.83	0.04
6.66	No	Yes	5.18	0.162	5.13	0.05
6.96	No	Yes	3.87	0.163	3.82	0.05
6.21	No	Yes	5.56	0.595	5.44	0.12
7.15	No	Yes	3.62	0.144	3.56	0.06

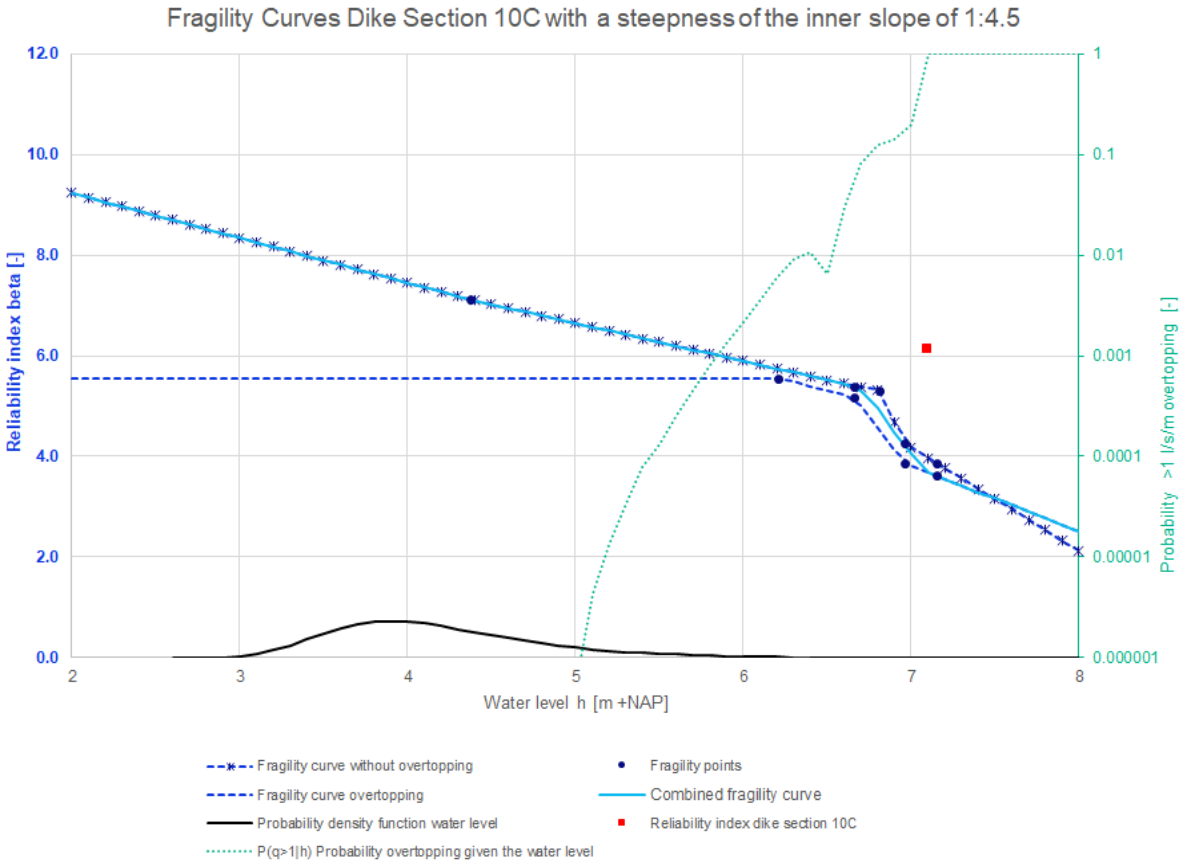

Figure 107: Fragility curves dike section 10C with a steepness of the inner slope of 1:4.5

The results of the probabilistic calculations with a steepness of the inner slope of 1:4.5 for dike section 11E are given in Table 103 and the fragility curves are shown in Figure 108.

Table 103: Reliability index probabilistic calculations with a steepness of the inner slope of 1:4.5 per water level for dike section 11E

Water level [m +NAP]	Traffic	Overtopping	Reliability index [-]	Coefficient of variation of the failure probability [-]	5% Confidence bound reliability index [-]	Reliability index - 5% confidence bound reliability index [-]
-0.04	Yes	No	11.0	0.181	11.0	0.0
2.39	Yes	No	11.3	0.923	11.2	0.1
3.47	Yes	No	9.42	0.607	9.35	0.07
6.77	No	No	7.76	0.768	7.65	0.11
7.07	No	No	6.78	0.158	6.75	0.03
7.30	No	No	6.48	0.147	6.45	0.03
6.77	No	Yes	4.74	0.0950	4.71	0.03
7.07	No	Yes	4.56	0.106	4.52	0.04
6.37	No	Yes	5.00	0.0990	4.97	0.03
7.30	No	Yes	4.40	0.106	4.36	0.04

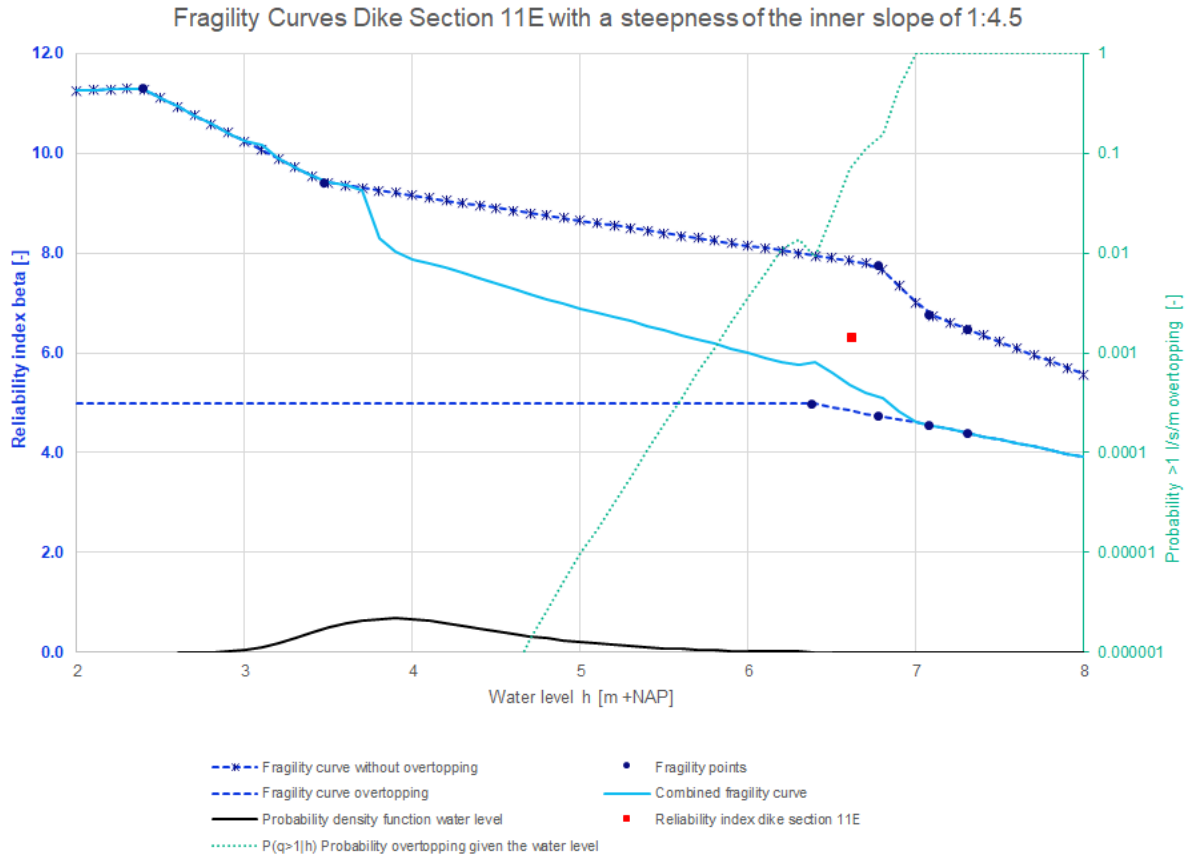

Figure 108: Fragility curves dike section 11E with a steepness of the inner slope of 1:4.5

The results of the probabilistic calculations with a steepness of the inner slope of 1:4.5 for dike section 11F(11D) are given in Table 104 and the fragility curves are shown in Figure 109.

Table 104: Reliability index probabilistic calculations with a steepness of the inner slope of 1:4.5 per water level for dike section 11F(11D)

Water level [m +NAP]	Traffic	Overtopping	Reliability index [-]	Coefficient of variation of the failure probability [-]	5% Confidence bound reliability index [-]	Reliability index - 5% confidence bound reliability index [-]
-0.04	Yes	No	22.6	0.716	22.6	0.0
2.63	Yes	No	15.0	0.569	15.0	0.0
5.24	Yes	No	9.13	0.416	9.07	0.06
6.79	No	No	7.31	0.187	7.27	0.04
7.09	No	No	7.09	0.165	7.05	0.04
6.79	No	Yes	4.30	0.338	4.20	0.10
7.09	No	Yes	4.25	0.101	4.22	0.03
6.38	No	Yes	4.69	0.0965	4.66	0.03

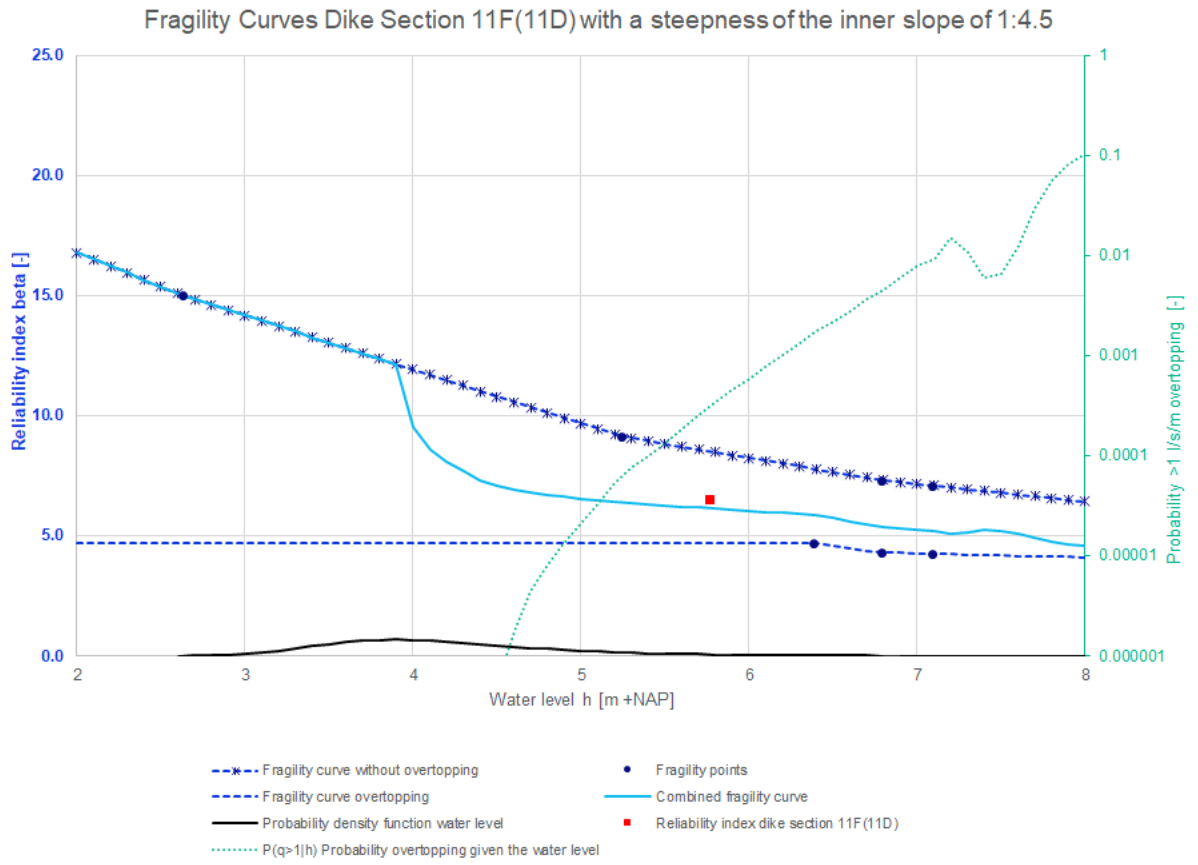

Figure 109: Fragility curves dike section 11F(11D) with a steepness of the inner slope of 1:4.5

The results of the probabilistic calculations with a steepness of the inner slope of 1:4.5 for dike section 13A are given in Table 105 and the fragility curves are shown in Figure 110.

Table 105: Reliability index probabilistic calculations with a steepness of the inner slope of 1:4.5 per water level for dike section 13A

Water level [m +NAP]	Traffic	Overtopping	Reliability index [-]	Coefficient of variation of the failure probability [-]	5% Confidence bound reliability index [-]	Reliability index - 5% confidence bound reliability index [-]
-0.30	Yes	No	13.9	0.593	13.9	0.0
0.87	Yes	No	13.1	0.688	13.0	0.1
2.07	Yes	No	11.3	0.814	11.2	0.1
6.26	No	No	6.99	0.306	6.93	0.06
6.56	No	No	6.62	0.460	6.53	0.09
6.26	No	Yes	5.81	0.215	5.76	0.05
6.56	No	Yes	5.57	0.594	5.45	0.12
5.66	No	Yes	6.13	0.200	6.08	0.05

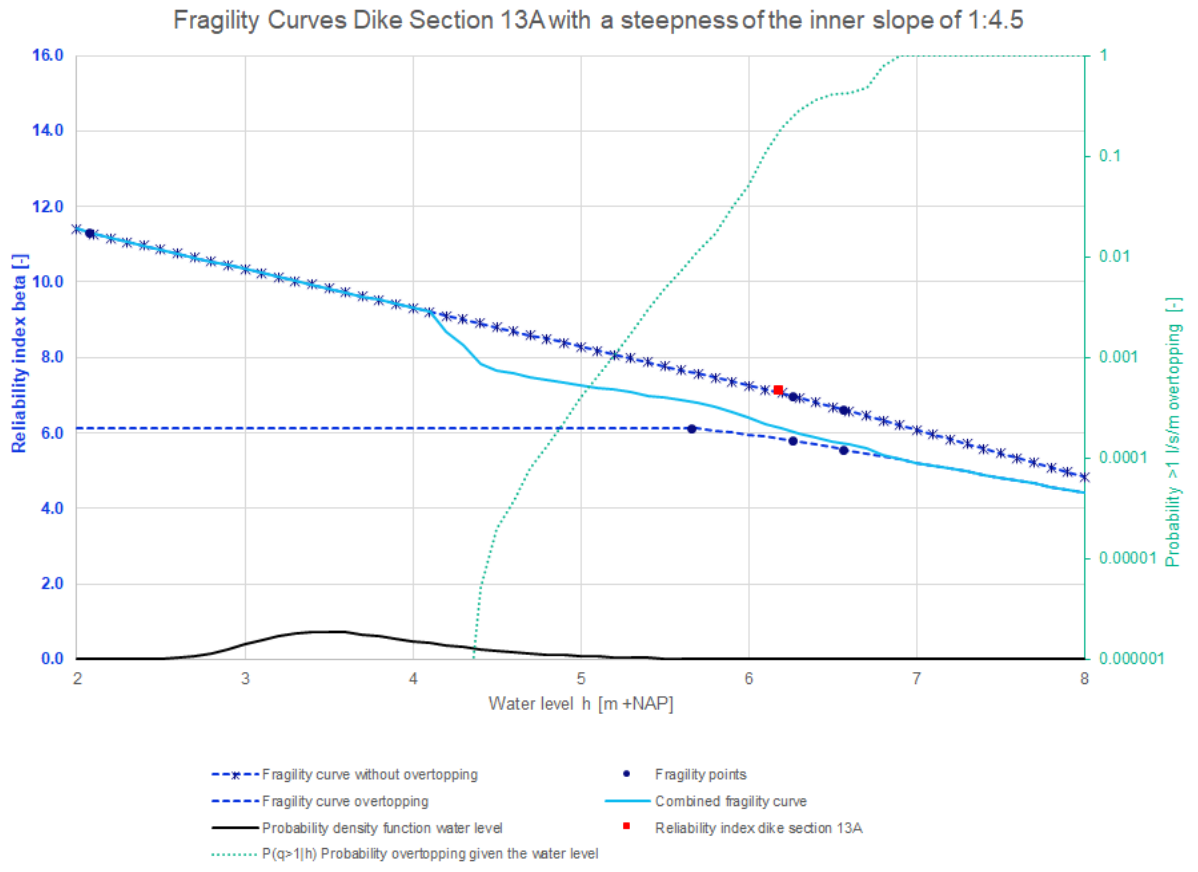

Figure 110: Fragility curves dike section 13A with a steepness of the inner slope of 1:4.5

The results of the probabilistic calculations with a steepness of the inner slope of 1:4.5 for dike section 13E1 are given in Table 106 and the fragility curves are shown in Figure 111.

Table 106: Reliability index probabilistic calculations with a steepness of the inner slope of 1:4.5 per water level for dike section 13E1

Water level [m +NAP]	Traffic	Overtopping	Reliability index [-]	Coefficient of variation of the failure probability [-]	5% Confidence bound reliability index [-]	Reliability index - 5% confidence bound reliability index [-]
-0.30	Yes	No	9.82	0.242	9.79	0.03
4.69	Yes	No	7.43	0.655	7.33	0.10
6.33	No	No	6.23	0.194	6.18	0.05
6.63	No	No	5.73	0.164	5.69	0.04
6.90	No	No	5.48	0.126	5.44	0.04
6.33	No	Yes	6.11	0.122	6.08	0.03
6.63	No	Yes	5.72	0.154	5.69	0.03
6.00	No	Yes	6.47	0.150	6.44	0.03
6.90	No	Yes	5.36	0.134	5.32	0.04

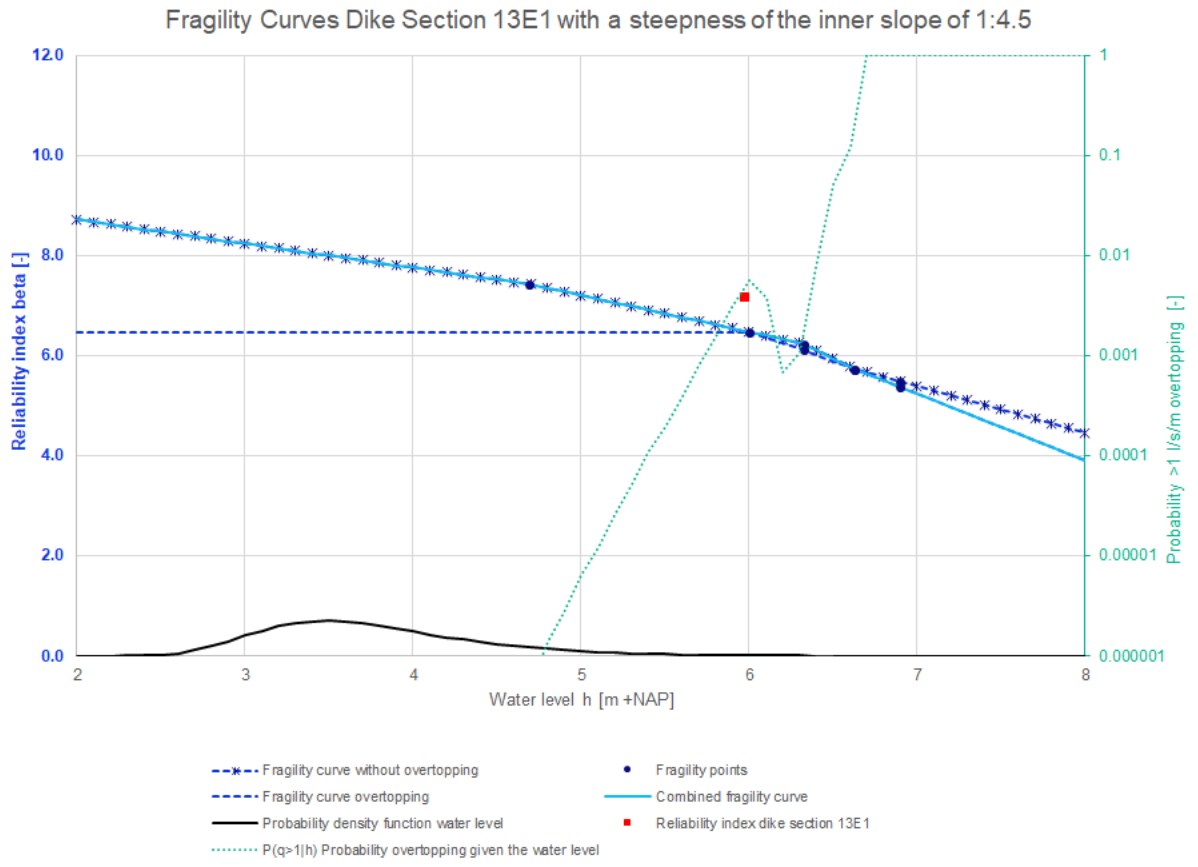

Figure 111: Fragility curves dike section 13E1 with a steepness of the inner slope of 1:4.5

The results of the probabilistic calculations with a steepness of the inner slope of 1:4.5 for dike section 13E2 are given in Table 107 and the fragility curves are shown in Figure 112.

Table 107: Reliability index probabilistic calculations with a steepness of the inner slope of 1:4.5 per water level for dike section 13E2

Water level [m +NAP]	Traffic	Overtopping	Reliability index [-]	Coefficient of variation of the failure probability [-]	5% Confidence bound reliability index [-]	Reliability index - 5% confidence bound reliability index [-]
-0.30	Yes	No	9.88	0.160	9.85	0.03
4.69	Yes	No	7.46	0.422	7.39	0.07
6.24	No	No	6.31	0.579	6.20	0.11
6.54	No	No	5.89	0.209	5.84	0.05
6.24	No	Yes	6.19	0.157	6.16	0.03
6.54	No	Yes	5.84	0.162	5.80	0.04
5.91	No	Yes	6.52	0.149	6.49	0.03

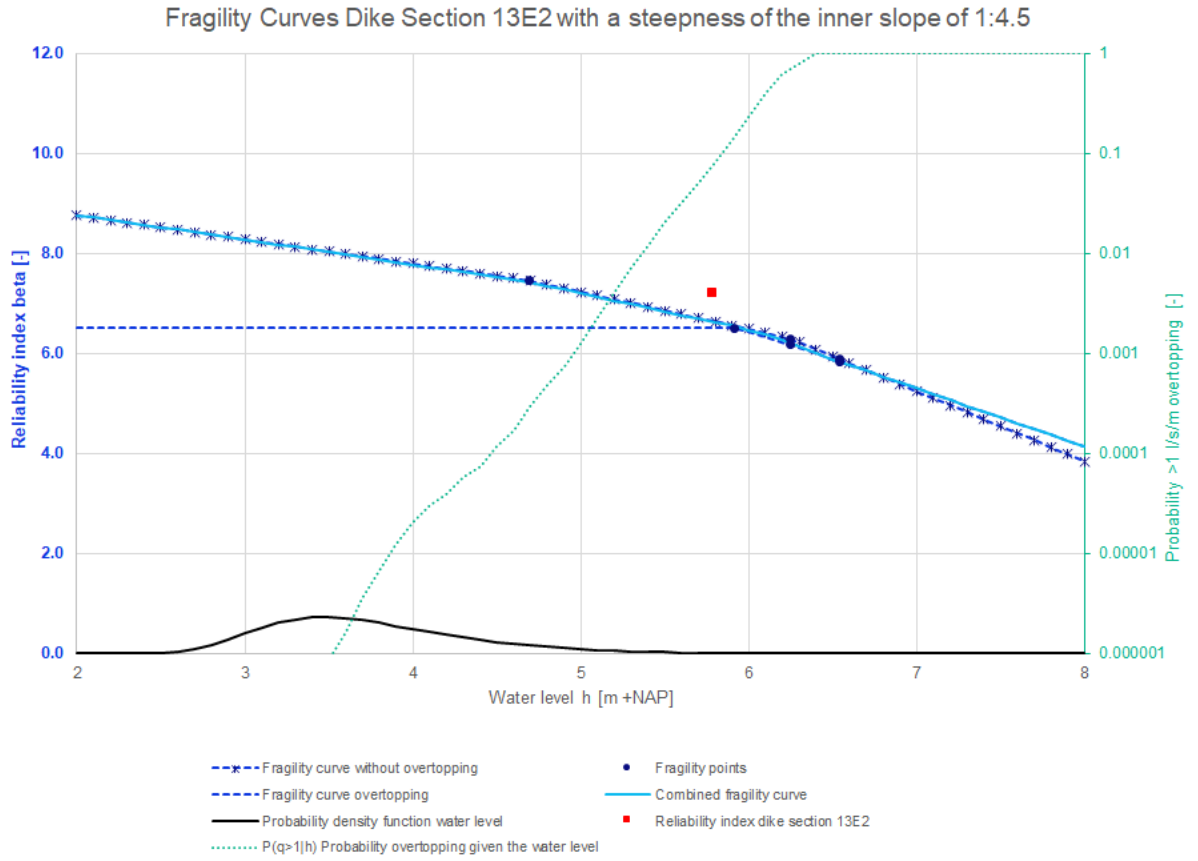

Figure 112: Fragility curves dike section 13E2 with a steepness of the inner slope of 1:4.5

The estimated reliability indexes based on the semi-probabilistic calculations with a steepness of the inner slope of 1:4.5 are given in Table 108. Furthermore, the reliability indexes of the probabilistic calculations with a steepness of the inner slope of 1:4.5 are shown in Table 109.

Table 108: Reliability index semi-probabilistic calculations with a steepness of the inner slope of 1:4.5

Dike section	Reliability index β without overtopping [-]	Reliability index β given overtopping [-]
10C	5.14	5.34
11E	5.90	5.44
11F(11D)	5.40	5.26
13A	5.10	4.92
13E1	5.41	5.57
13E2	5.47	5.61

Table 109: Reliability index probabilistic calculations with a steepness of the inner slope of 1:4.5

Dike section	Reliability index β combined fragility curve [-]	Reliability index β without overtopping [-]	Reliability index β given overtopping [-]
10C	6.16	6.25	5.56
11E	6.31	8.25	5.00
11F(11D)	6.49	8.29	4.69
13A	7.13	7.92	6.13
13E1	7.17	7.17	6.47
13E2	7.21	7.24	6.52

In Figure 113 are the results of JAV with an inner slope steepness of 1:4.5 plotted with the results of the WBI calibration study. In Figure 114 are the influence factors shown.

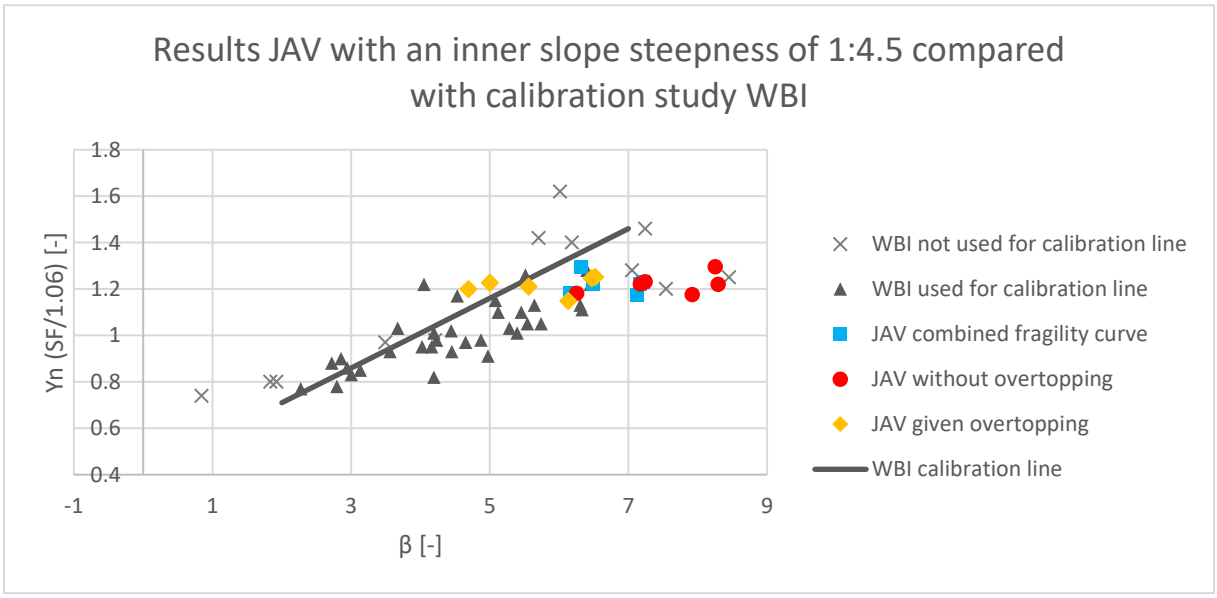

Figure 113: The results of the calculations of JAV with an inner slope steepness of 1:4.5 compared with the calibration study of WBI. The vertical position of the results of JAV from the combined fragility curves (blue squares) are determined based on the semi-probabilistic results without overtopping

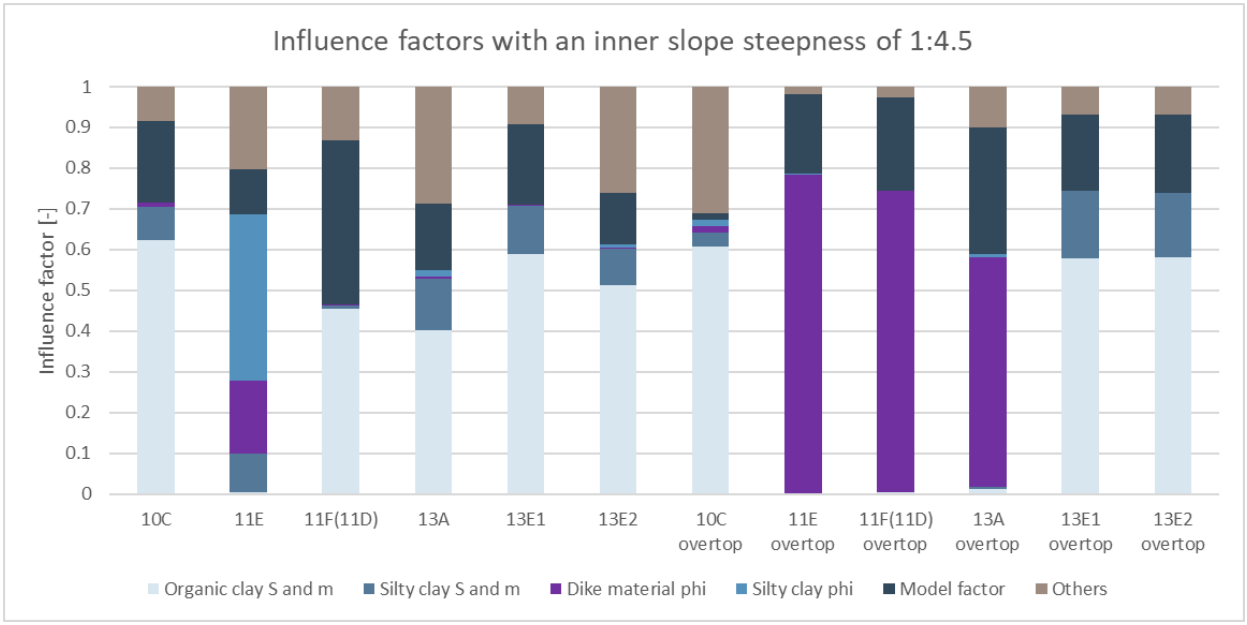

Figure 114: Influence factors with an inner slope steepness of 1:4.5 at WBN without overtopping and at the 1 l/s/m overtopping water level with overtopping

N. Results probabilistic calculations with a steepness of the inner slope of 1:5

The results of the probabilistic calculations with a steepness of the inner slope of 1:5 are given in this appendix. For every dike section are per water level the expected reliability index, coefficient of variation of the failure probability, 5% confidence bound of the reliability index and the difference between the expected reliability index and the 5% confidence bound of the reliability index given in the tables in this appendix. The coefficient of variation of the failure probability is specified as the standard deviation of the probability of failure divided by the probability of failure (Deltares, 2022). The 5% confidence bound of the reliability index is determined based on the failure probability and the coefficient of variation of the failure probability.

Besides, for every dike section are the fragility curves given. The fragility points, the fragility curve without overtopping, the fragility curve given overtopping, the combined fragility curve, the probability of exceedance of 1 l/s/m overtopping given the water level and the probability density function of the water level are given in the figures in this appendix. Furthermore, the reliability indexes are given per dike section.

The results of the probabilistic calculations with a steepness of the inner slope of 1:5 for dike section 10C are given in Table 110 and the fragility curves are shown in Figure 115.

Table 110: Reliability index probabilistic calculations with a steepness of the inner slope of 1:5 per water level for dike section 10C

Water level [m +NAP]	Traffic	Overtopping	Reliability index [-]	Coefficient of variation of the failure probability [-]	5% Confidence bound reliability index [-]	Reliability index - 5% confidence bound reliability index [-]
0.24	Yes	No	10.8	0.246	10.7	0.1
4.37	Yes	No	7.07	0.324	7.01	0.06
6.81	No	No	5.23	0.273	5.16	0.07
6.66	No	No	5.17	0.449	5.06	0.11
6.96	No	No	4.44	0.152	4.40	0.04
7.15	No	No	3.98	0.129	3.93	0.05
6.66	No	Yes	5.01	0.230	4.95	0.06
6.96	No	Yes	4.19	0.108	4.15	0.04
6.21	No	Yes	5.49	0.234	5.43	0.06
7.15	No	Yes	3.81	0.127	3.76	0.05

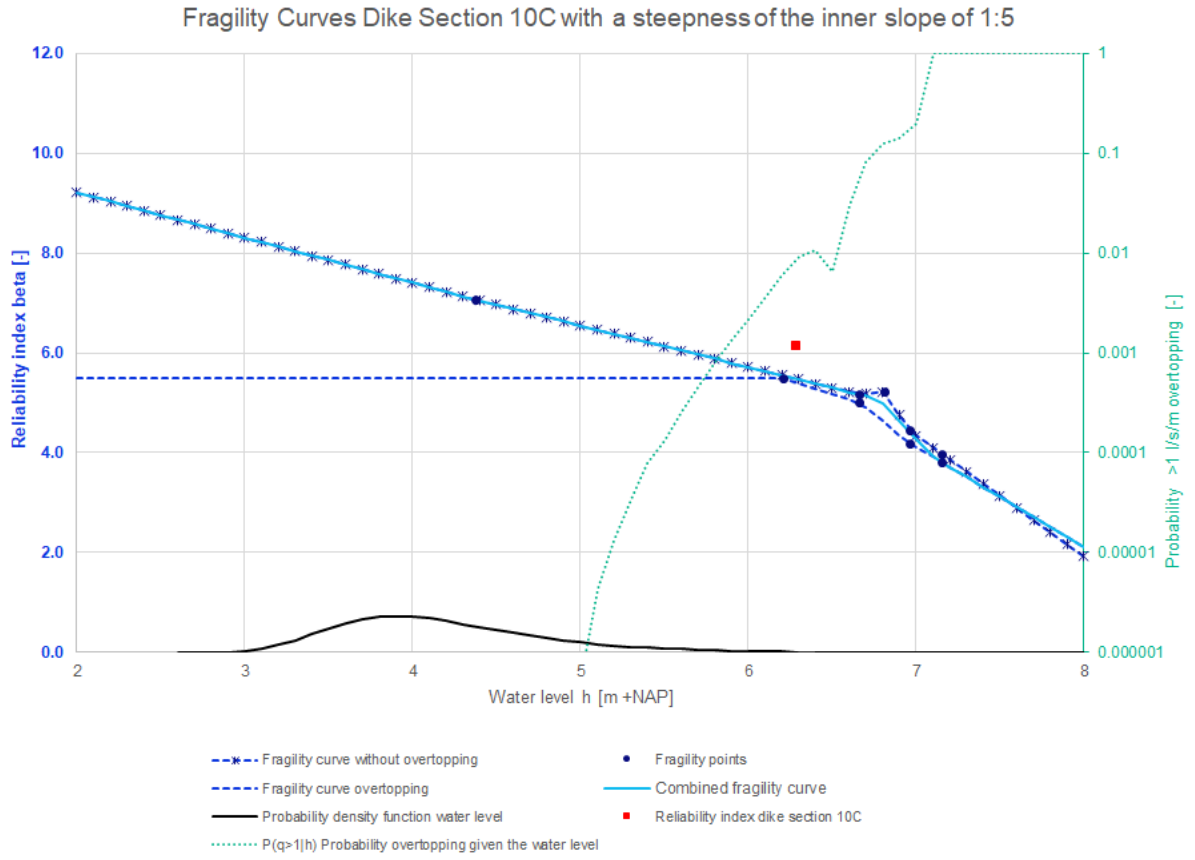

Figure 115: Fragility curves dike section 10C with a steepness of the inner slope of 1:5

The results of the probabilistic calculations with a steepness of the inner slope of 1:5 for dike section 11E are given in Table 111 and the fragility curves are shown in Figure 116.

Table 111: Reliability index probabilistic calculations with a steepness of the inner slope of 1:5 per water level for dike section 11E

Water level [m +NAP]	Traffic	Overtopping	Reliability index [-]	Coefficient of variation of the failure probability [-]	5% Confidence bound reliability index [-]	Reliability index - 5% confidence bound reliability index [-]
-0.04	Yes	No	12.8	0.954	12.7	0.1
2.39	Yes	No	13.1	0.693	13.0	0.1
3.47	Yes	No	11.6	0.515	11.5	0.1
6.77	No	No	7.92	0.322	7.87	0.05
7.07	No	No	7.59	0.305	7.53	0.06
7.30	No	No	7.34	0.216	7.30	0.04
6.77	No	Yes	6.21	0.251	6.16	0.05
7.07	No	Yes	6.01	0.231	5.96	0.05
6.37	No	Yes	6.51	0.287	6.45	0.06
7.30	No	Yes	5.80	0.259	5.74	0.06

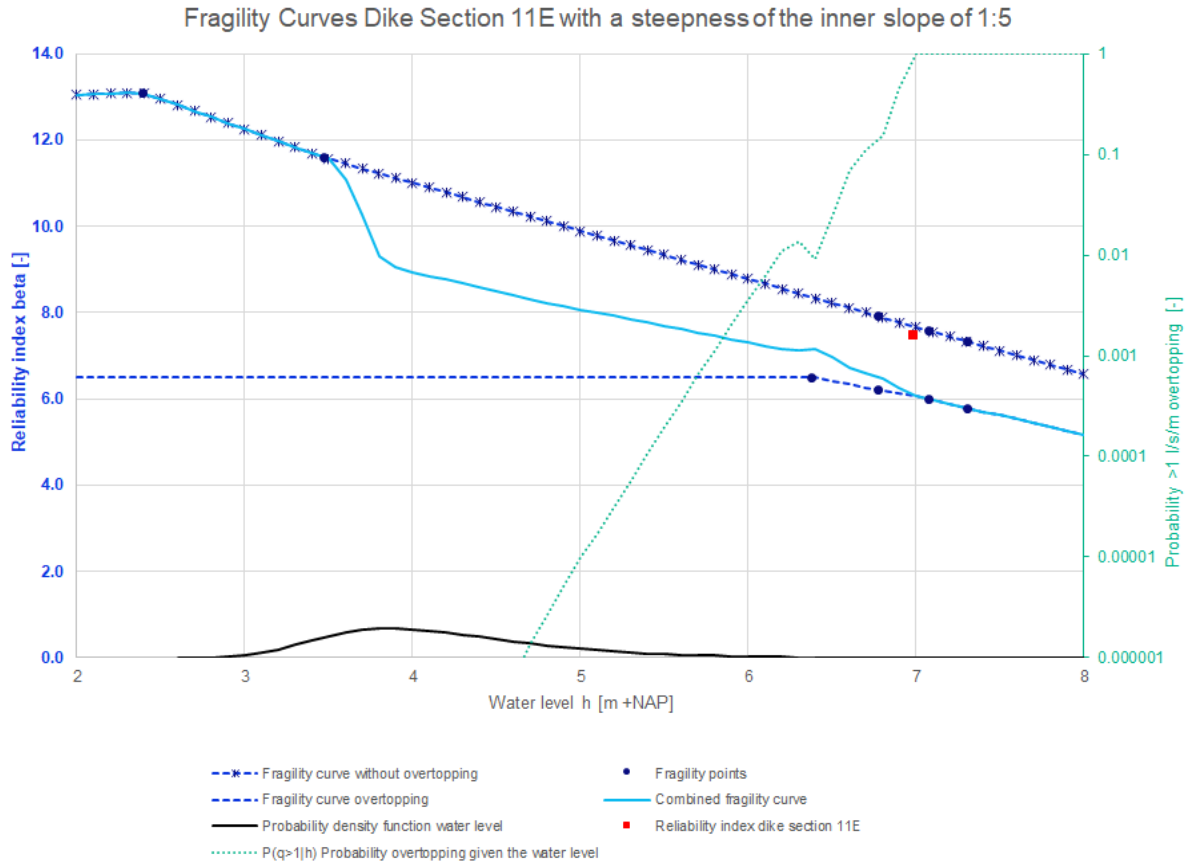

Figure 116: Fragility curves dike section 11E with a steepness of the inner slope of 1:5

The results of the probabilistic calculations with a steepness of the inner slope of 1:5 for dike section 11F(11D) are given in Table 112 and the fragility curves are shown in Figure 117.

Table 112: Reliability index probabilistic calculations with a steepness of the inner slope of 1:5 per water level for dike section 11F(11D)

Water level [m +NAP]	Traffic	Overtopping	Reliability index [-]	Coefficient of variation of the failure probability [-]	5% Confidence bound reliability index [-]	Reliability index - 5% confidence bound reliability index [-]
-0.04	Yes	No	20.9	0.999	20.9	0.0
2.63	Yes	No	14.9	0.554	14.9	0.0
5.24	Yes	No	8.75	0.288	8.71	0.04
6.79	No	No	7.25	0.244	7.20	0.05
7.09	No	No	7.09	0.212	7.05	0.04
6.79	No	Yes	5.80	0.0982	5.78	0.02
7.09	No	Yes	5.63	0.0927	5.60	0.03
6.38	No	Yes	5.89	0.134	5.86	0.03

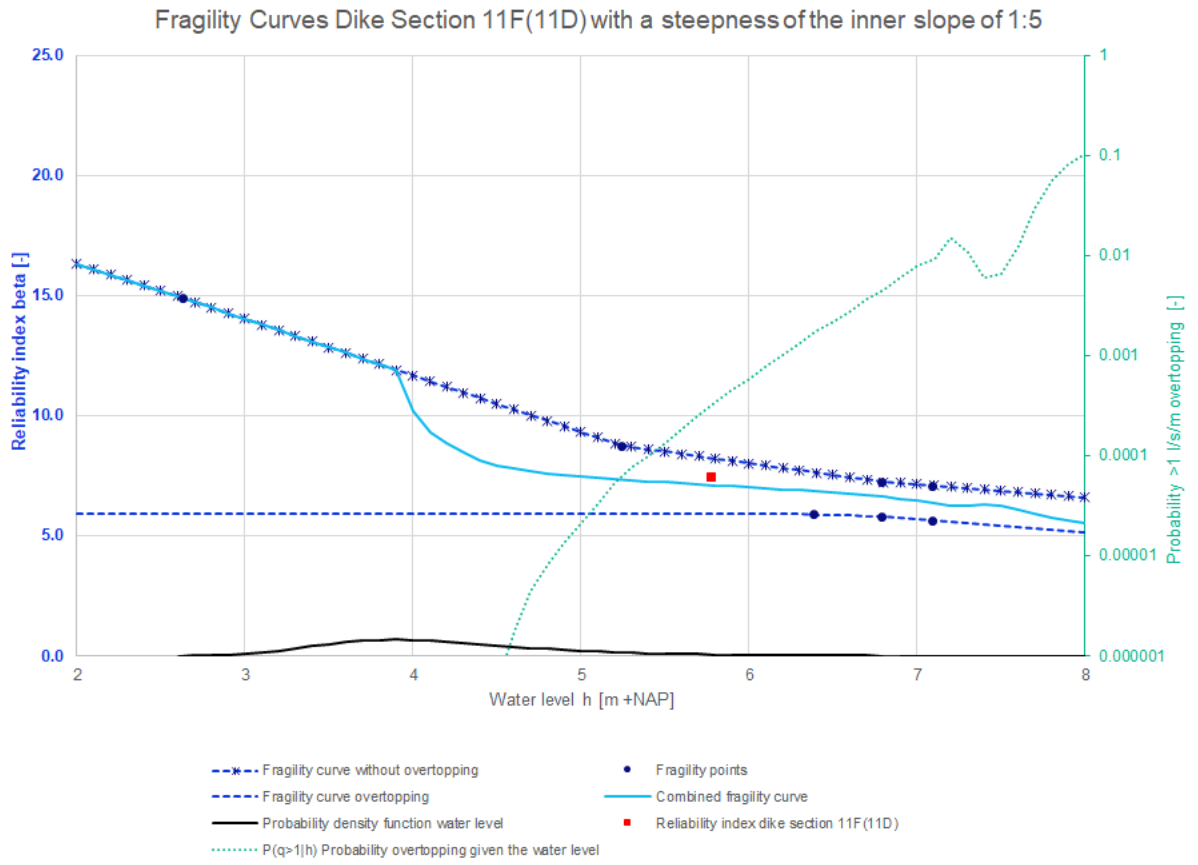

Figure 117: Fragility curves dike section 11F(11D) with a steepness of the inner slope of 1:5

The results of the probabilistic calculations with a steepness of the inner slope of 1:5 for dike section 13A are given in Table 113 and the fragility curves are shown in Figure 118.

Table 113: Reliability index probabilistic calculations with a steepness of the inner slope of 1:5 per water level for dike section 13A

Water level [m +NAP]	Traffic	Overtopping	Reliability index [-]	Coefficient of variation of the failure probability [-]	5% Confidence bound reliability index [-]	Reliability index - 5% confidence bound reliability index [-]
-0.30	Yes	No	13.7	0.376	13.7	0.0
0.87	Yes	No	12.9	0.643	12.8	0.1
2.07	Yes	No	11.4	0.681	11.3	0.1
6.26	No	No	7.44	0.139	7.41	0.03
6.56	No	No	7.16	0.132	7.13	0.03
6.26	No	Yes	7.03	0.348	6.97	0.06
6.56	No	Yes	6.82	0.342	6.75	0.07
5.66	No	Yes	8.22	0.296	8.17	0.05

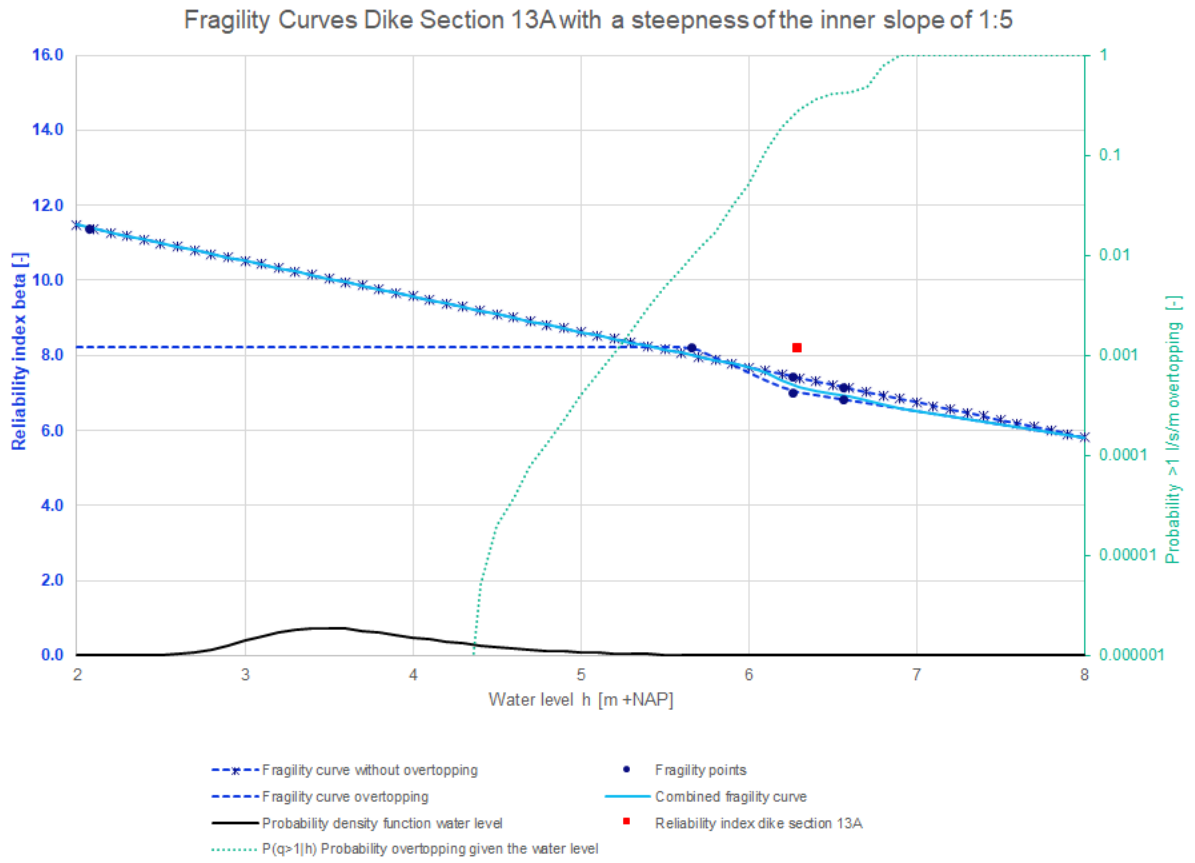

Figure 118: Fragility curves dike section 13A with a steepness of the inner slope of 1:5

The results of the probabilistic calculations with a steepness of the inner slope of 1:5 for dike section 13E1 are given in Table 114 and the fragility curves are shown in Figure 119.

Table 114: Reliability index probabilistic calculations with a steepness of the inner slope of 1:5 per water level for dike section 13E1

Water level [m +NAP]	Traffic	Overtopping	Reliability index [-]	Coefficient of variation of the failure probability [-]	5% Confidence bound reliability index [-]	Reliability index - 5% confidence bound reliability index [-]
-0.30	Yes	No	9.89	0.265	9.85	0.04
4.69	Yes	No	7.42	0.309	7.36	0.06
6.33	No	No	6.16	0.206	6.11	0.05
6.63	No	No	5.72	0.179	5.68	0.04
6.33	No	Yes	6.30	0.331	6.24	0.06
6.63	No	Yes	5.83	0.154	5.79	0.04
6.00	No	Yes	6.61	0.511	6.52	0.09

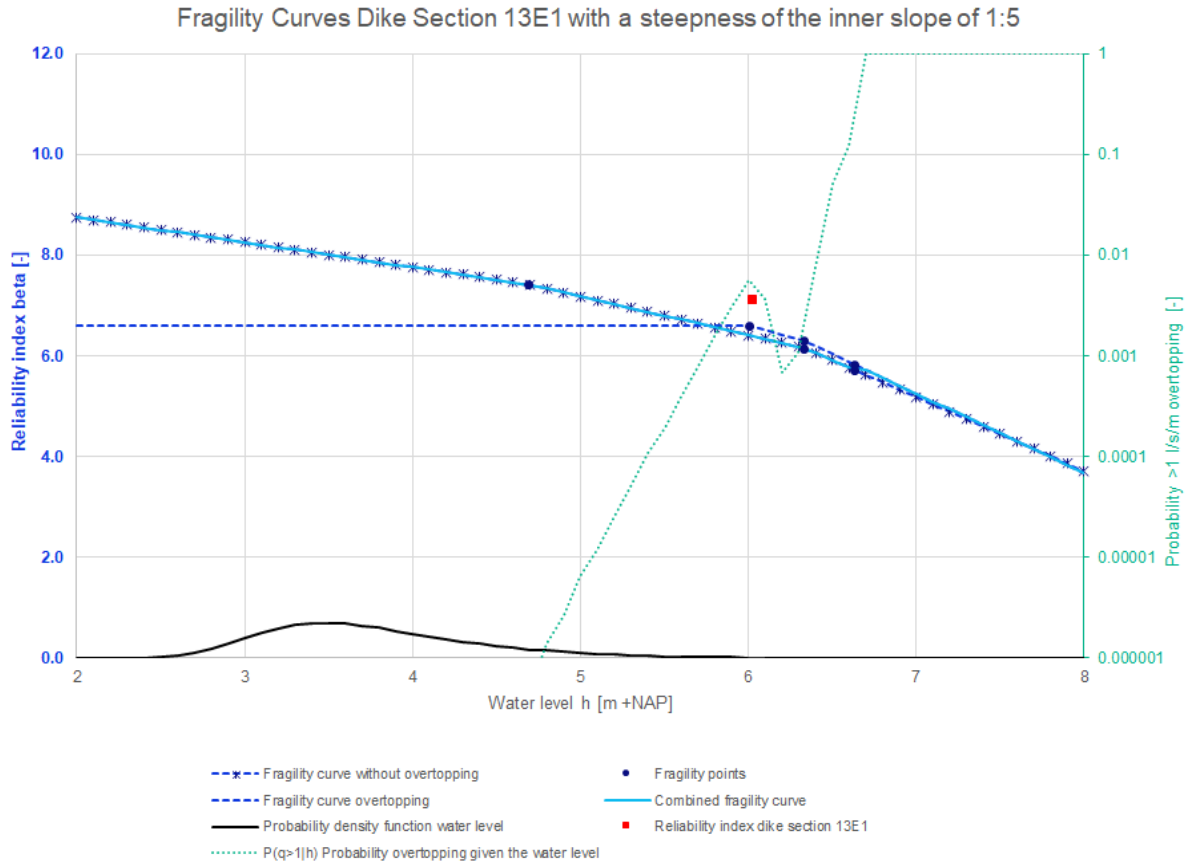

Figure 119: Fragility curves dike section 13E1 with a steepness of the inner slope of 1:5

The results of the probabilistic calculations with a steepness of the inner slope of 1:5 for dike section 13E2 are given in Table 115 and the fragility curves are shown in Figure 120.

Table 115: Reliability index probabilistic calculations with a steepness of the inner slope of 1:5 per water level for dike section 13E2

Water level [m +NAP]	Traffic	Overtopping	Reliability index [-]	Coefficient of variation of the failure probability [-]	5% Confidence bound reliability index [-]	Reliability index - 5% confidence bound reliability index [-]
-0.30	Yes	No	9.96	0.249	9.92	0.04
4.69	Yes	No	7.37	0.156	7.34	0.03
6.24	No	No	6.32	0.161	6.29	0.03
6.54	No	No	5.90	0.129	5.87	0.03
6.24	No	Yes	6.35	0.336	6.28	0.07
6.54	No	Yes	6.01	0.166	5.97	0.04
5.91	No	Yes	6.74	0.880	6.60	0.14

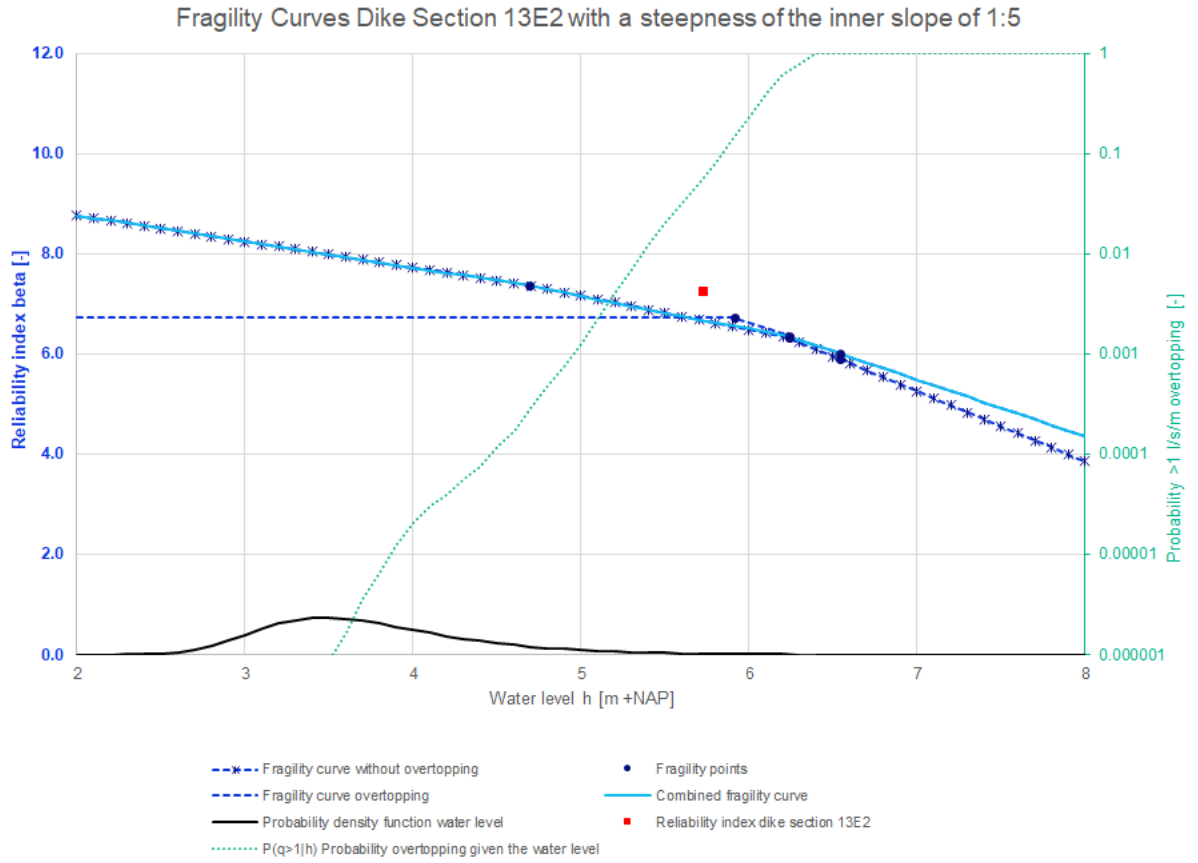

Figure 120: Fragility curves dike section 13E2 with a steepness of the inner slope of 1:5

The estimated reliability indexes based on the semi-probabilistic calculations with a steepness of the inner slope of 1:5 are given in Table 116. Furthermore, the reliability indexes of the probabilistic calculations with a steepness of the inner slope of 1:5 are shown in Table 117.

Table 116: Reliability index semi-probabilistic calculations with a steepness of the inner slope of 1:5

Dike section	Reliability index β without overtopping [-]	Reliability index β given overtopping [-]
10C	5.16	5.34
11E	6.27	6.39
11F(11D)	5.40	5.43
13A	5.20	5.42
13E1	5.42	5.56
13E2	5.49	5.59

Table 117: Reliability index probabilistic calculations with a steepness of the inner slope of 1:5

Dike section	Reliability index β combined fragility curve [-]	Reliability index β without overtopping [-]	Reliability index β given overtopping [-]
10C	6.16	6.19	5.49
11E	7.49	8.78	6.51
11F(11D)	7.45	8.22	5.89
13A	8.20	8.34	8.22
13E1	7.13	7.13	6.61
13E2	7.24	7.22	6.74

O. Results probabilistic calculations with different CoV

The results of the probabilistic calculations with different coefficients of variation are given in this appendix. For every dike section are per water level the expected reliability index, coefficient of variation of the failure probability, 5% confidence bound of the reliability index and the difference between the expected reliability index and the 5% confidence bound of the reliability index given in the tables in this appendix. The coefficient of variation of the failure probability is specified as the standard deviation of the probability of failure divided by the probability of failure (Deltares, 2022). The 5% confidence bound of the reliability index is determined based on the failure probability and the coefficient of variation of the failure probability.

Besides, for every dike section are the fragility curves given. The fragility points, the fragility curve without overtopping, the fragility curve given overtopping, the combined fragility curve, the probability of exceedance of 1 l/s/m overtopping given the water level and the probability density function of the water level are given in the figures in this appendix. Furthermore, the reliability indexes are given per dike section, the results are plotted with the results of the WBI calibration study and the influence factors are shown.

The results of the probabilistic calculations with different coefficients of variation for dike section 10C are given in Table 118 and the fragility curves are shown in Figure 121.

Table 118: Reliability index probabilistic calculations with different coefficients of variation per water level for dike section 10C

Water level [m +NAP]	Traffic	Overtopping	Reliability index [-]	Coefficient of variation of the failure probability [-]	5% Confidence bound reliability index [-]	Reliability index - 5% confidence bound reliability index [-]
0.24	Yes	No	7.02	0.214	6.98	0.04
4.37	Yes	No	5.27	0.141	5.23	0.04
6.81	No	No	4.10	0.147	4.04	0.06
6.66	No	No	4.28	0.169	4.23	0.05
6.96	No	No	3.66	0.0941	3.63	0.03
7.15	No	No	3.48	0.0746	3.44	0.04
6.66	No	Yes	4.14	0.127	4.10	0.04
6.96	No	Yes	3.52	0.102	3.48	0.04
6.21	No	Yes	4.32	0.236	4.25	0.07
7.15	No	Yes	3.33	0.0754	3.29	0.04

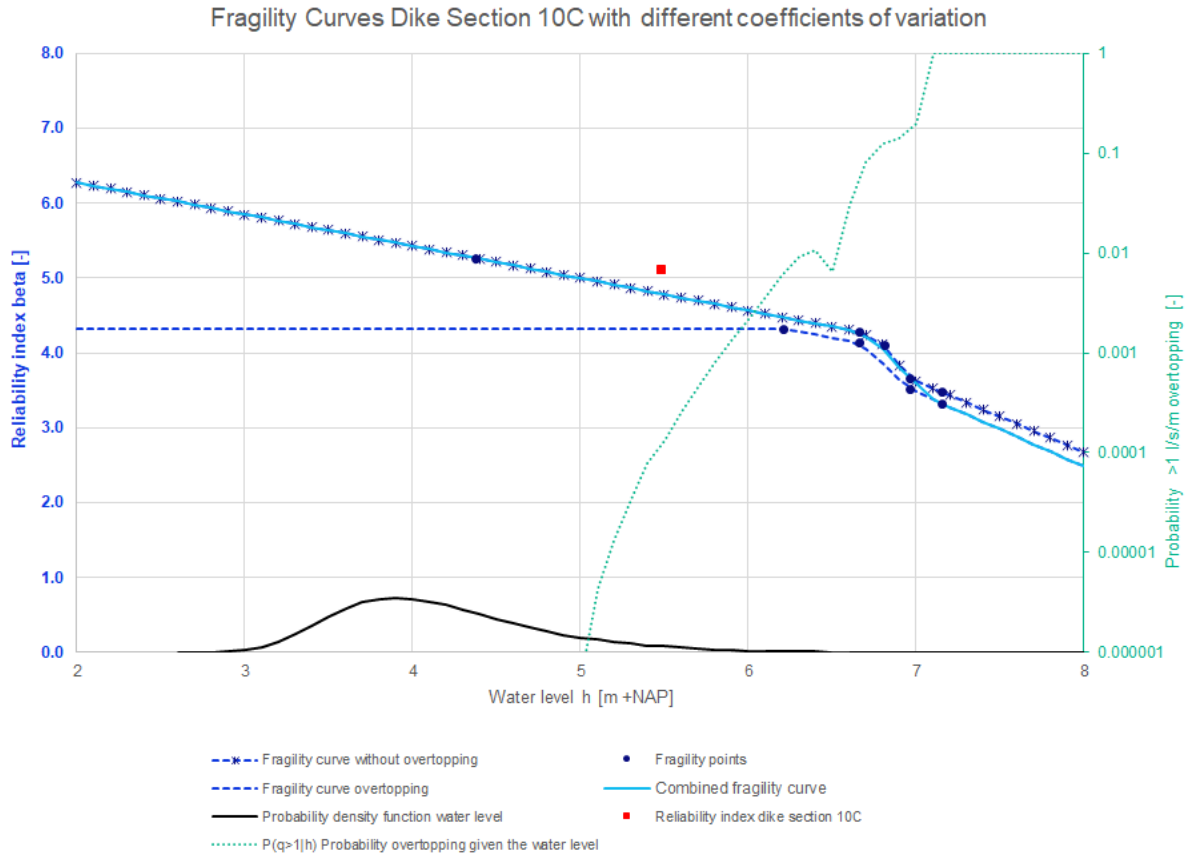

Figure 121: Fragility curves dike section 10C with different coefficients of variation

The results of the probabilistic calculations with different coefficients of variation for dike section 11E are given in Table 119 and the fragility curves are shown in Figure 122.

Table 119: Reliability index probabilistic calculations with different coefficients of variation per water level for dike section 11E

Water level [m +NAP]	Traffic	Overtopping	Reliability index [-]	Coefficient of variation of the failure probability [-]	5% Confidence bound reliability index [-]	Reliability index - 5% confidence bound reliability index [-]
-0.04	Yes	No	7.00	0.190	6.96	0.04
2.39	Yes	No	7.03	0.119	7.00	0.03
3.47	Yes	No	6.60	0.168	6.56	0.04
6.77	No	No	4.18	0.115	4.14	0.04
7.07	No	No	3.68	0.0860	3.65	0.03
6.77	No	Yes	-0.0991	0.0419	-0.19	0.09
7.07	No	Yes	-0.112	0.0493	-0.23	0.11
6.37	No	Yes	0.123	0.0440	0.04	0.08

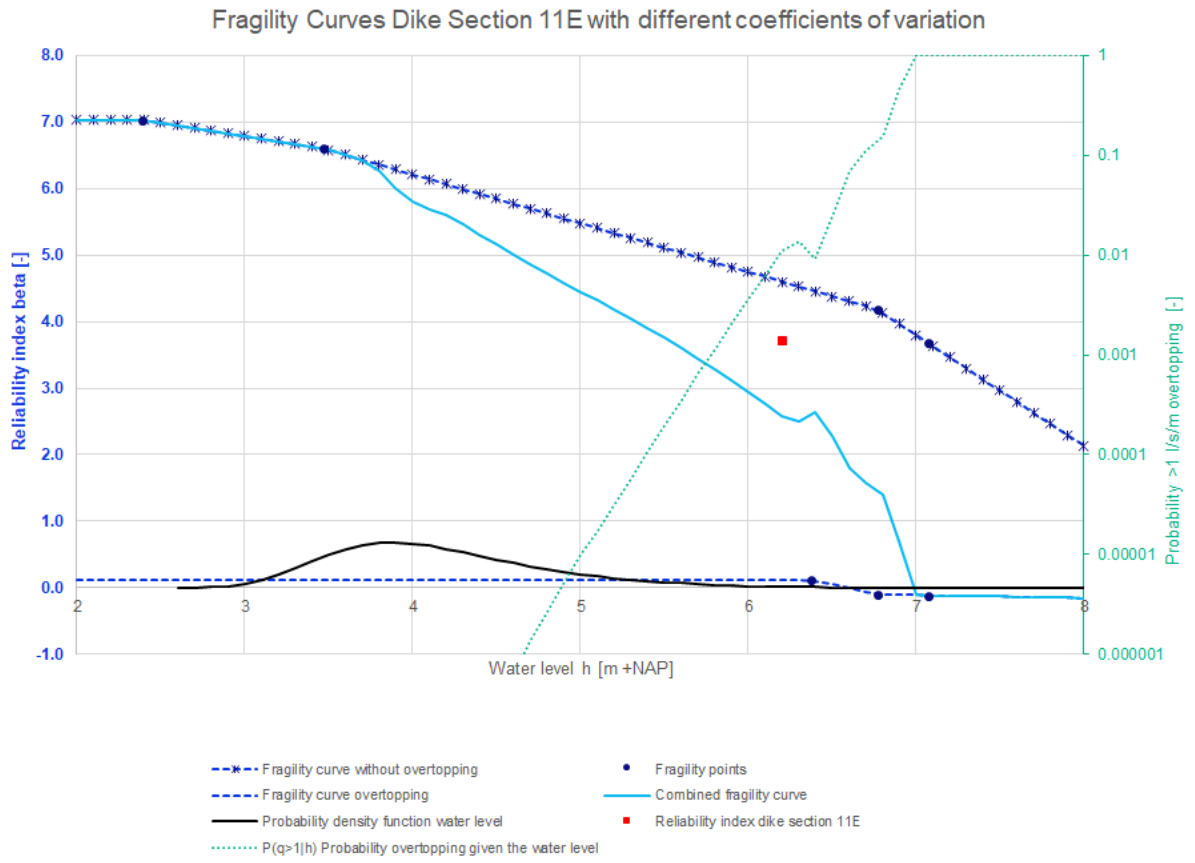

Figure 122: Fragility curves dike section 11E with different coefficients of variation

The results of the probabilistic calculations with different coefficients of variation for dike section 11F(11D) are given in Table 120 and the fragility curves are shown in Figure 123.

Table 120: Reliability index probabilistic calculations with different coefficients of variation per water level for dike section 11F(11D)

Water level [m +NAP]	Traffic	Overtopping	Reliability index [-]	Coefficient of variation of the failure probability [-]	5% Confidence bound reliability index [-]	Reliability index - 5% confidence bound reliability index [-]
-0.04	Yes	No	14.1	0.846	14.0	0.1
2.63	Yes	No	11.5	0.982	11.4	0.1
5.24	Yes	No	7.26	0.294	7.20	0.06
6.79	No	No	6.18	0.155	6.14	0.04
7.09	No	No	5.94	0.162	5.90	0.04
6.79	No	Yes	0.88	0.0499	0.82	0.06
7.09	No	Yes	0.766	0.0499	0.71	0.06
6.38	No	Yes	1.06	0.0559	1.00	0.06

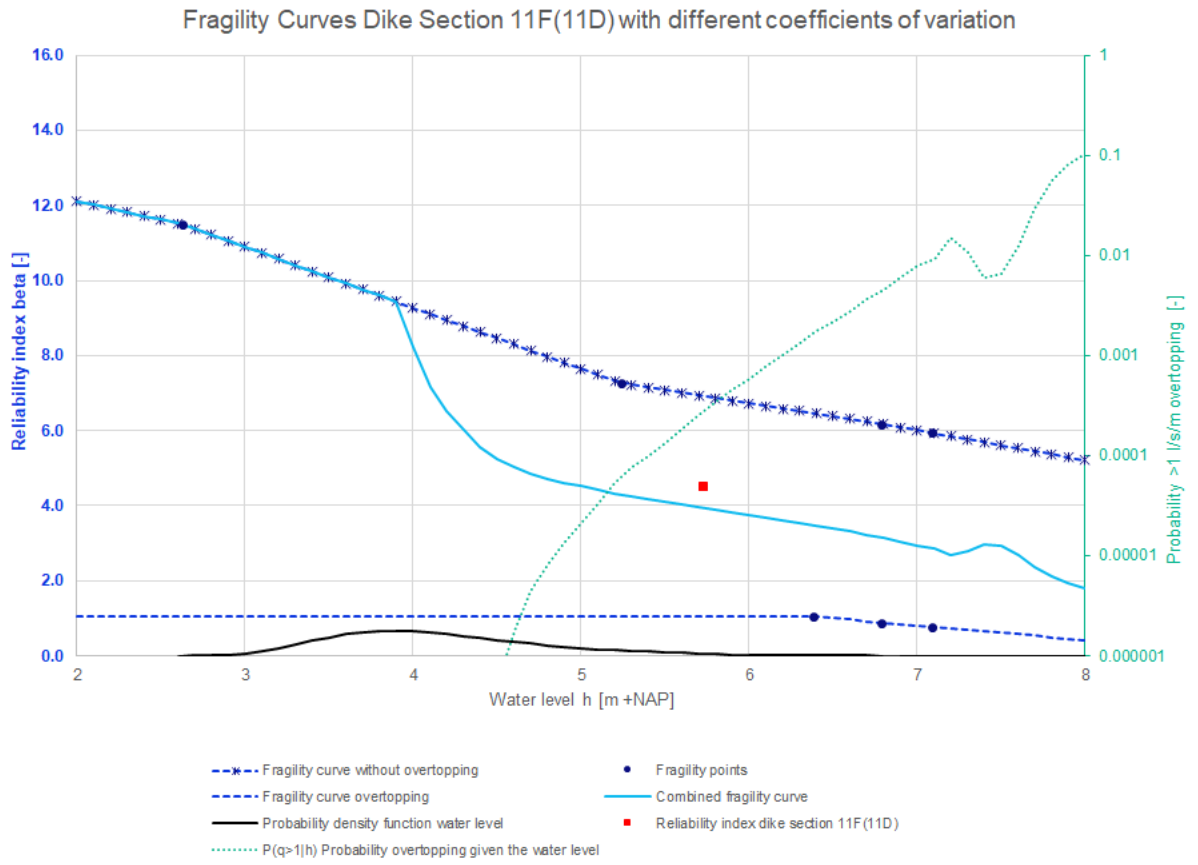

Figure 123: Fragility curves dike section 11F(11D) with different coefficients of variation

The results of the probabilistic calculations with different coefficients of variation for dike section 13A are given in Table 121 and the fragility curves are shown in Figure 124.

Table 121: Reliability index probabilistic calculations with different coefficients of variation per water level for dike section 13A

Water level [m +NAP]	Traffic	Overtopping	Reliability index [-]	Coefficient of variation of the failure probability [-]	5% Confidence bound reliability index [-]	Reliability index - 5% confidence bound reliability index [-]
-0.30	Yes	No	8.48	0.176	8.45	0.03
0.87	Yes	No	8.41	0.438	8.34	0.07
2.07	Yes	No	7.68	0.369	7.62	0.06
6.26	No	No	5.74	0.254	5.68	0.06
6.56	No	No	5.75	0.154	5.71	0.04
6.26	No	Yes	5.55	0.189	5.50	0.05
6.56	No	Yes	5.35	0.218	5.29	0.06
5.66	No	Yes	6.10	0.290	6.03	0.07

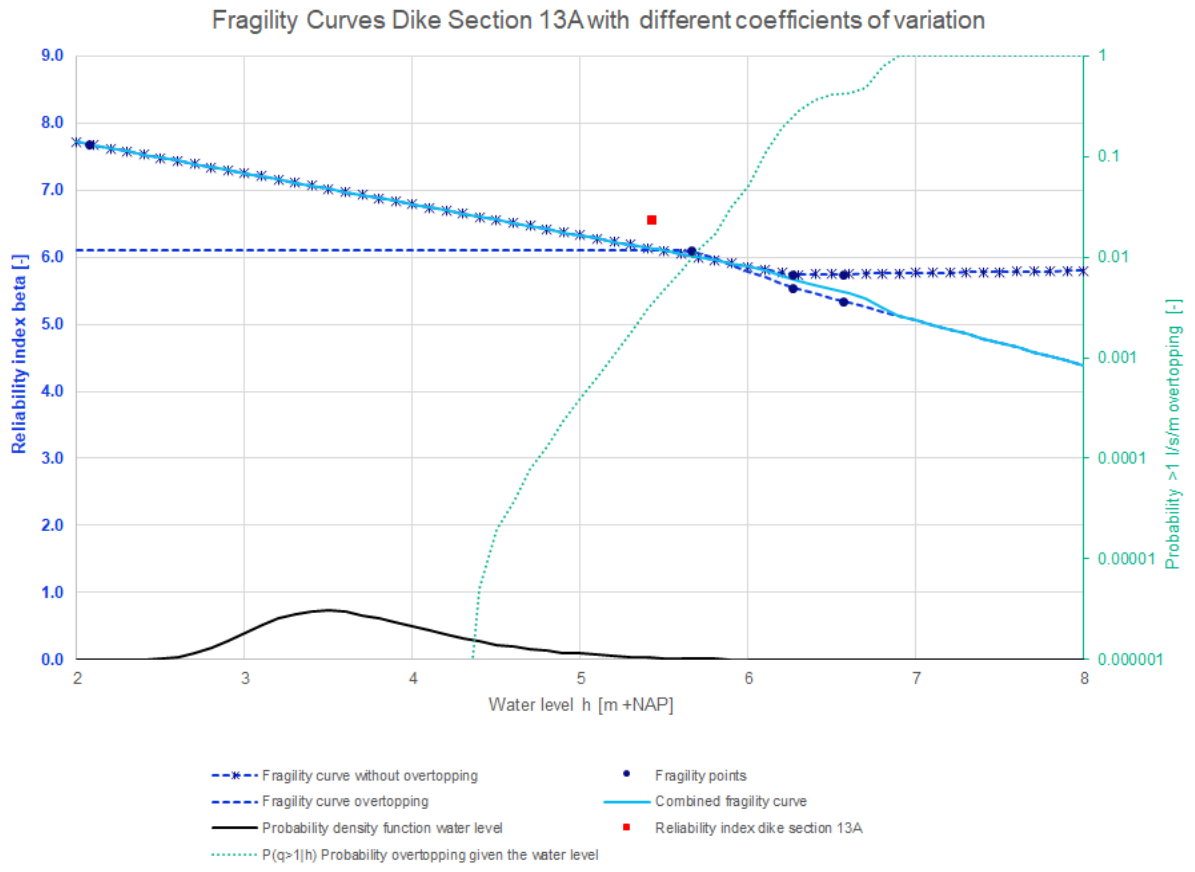

Figure 124: Fragility curves dike section 13A with different coefficients of variation

The results of the probabilistic calculations with different coefficients of variation for dike section 13E1 are given in Table 122 and the fragility curves are shown in Figure 125.

Table 122: Reliability index probabilistic calculations with different coefficients of variation per water level for dike section 13E1

Water level [m +NAP]	Traffic	Overtopping	Reliability index [-]	Coefficient of variation of the failure probability [-]	5% Confidence bound reliability index [-]	Reliability index - 5% confidence bound reliability index [-]
-0.30	Yes	No	6.73	0.175	6.69	0.04
4.69	Yes	No	5.40	0.126	5.37	0.03
6.33	No	No	4.93	0.255	4.86	0.07
6.63	No	No	4.75	0.262	4.67	0.08
6.33	No	Yes	4.73	0.324	4.64	0.09
6.63	No	Yes	4.47	0.219	4.41	0.06
6.00	No	Yes	5.16	0.232	5.10	0.06

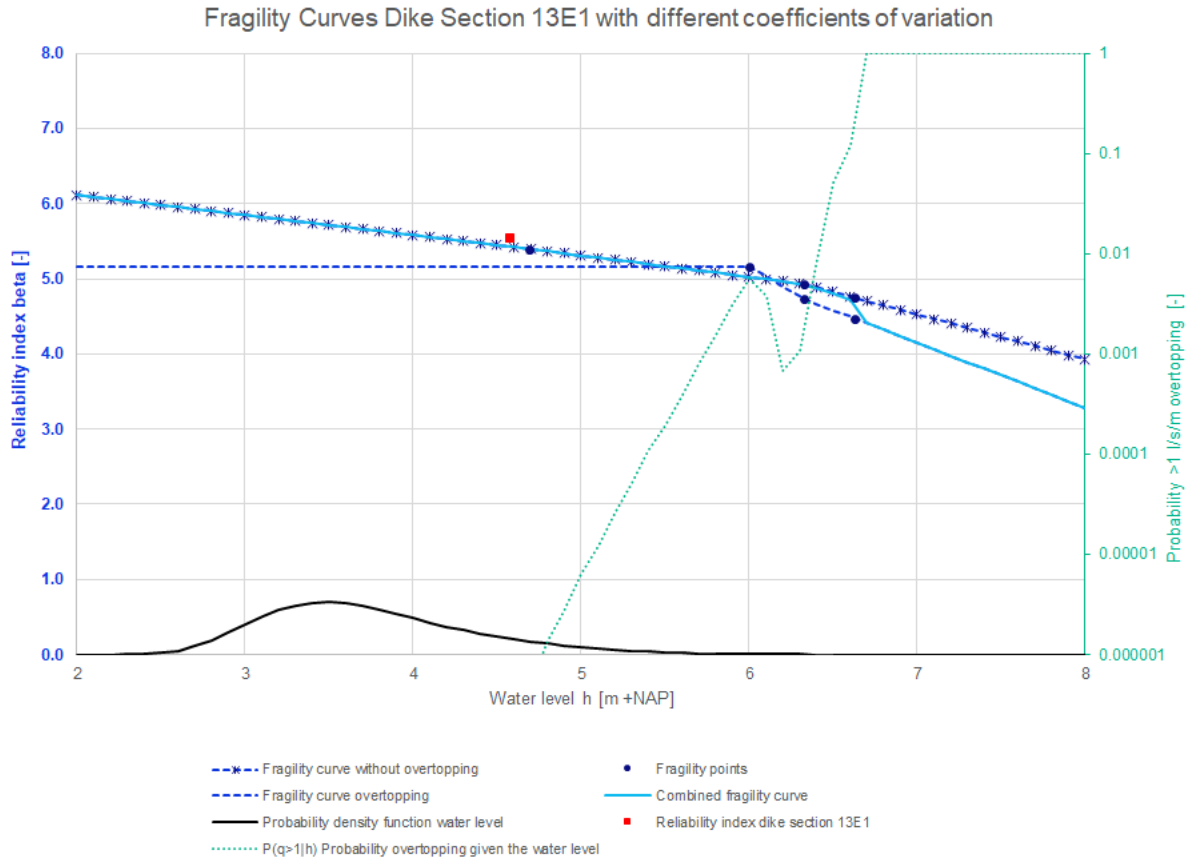

Figure 125: Fragility curves dike section 13E1 with different coefficients of variation

The results of the probabilistic calculations with different coefficients of variation for dike section 13E2 are given in Table 123 and the fragility curves are shown in Figure 126.

Table 123: Reliability index probabilistic calculations with different coefficients of variation per water level for dike section 13E2

Water level [m +NAP]	Traffic	Overtopping	Reliability index [-]	Coefficient of variation of the failure probability [-]	5% Confidence bound reliability index [-]	Reliability index - 5% confidence bound reliability index [-]
-0.30	Yes	No	6.59	0.116	6.56	0.03
4.69	Yes	No	5.36	0.0916	5.33	0.03
6.24	No	No	4.89	0.132	4.85	0.04
6.54	No	No	4.64	0.168	4.59	0.05
6.24	No	Yes	4.84	0.147	4.79	0.05
6.54	No	Yes	4.64	0.124	4.60	0.04
5.91	No	Yes	4.94	0.165	4.89	0.05

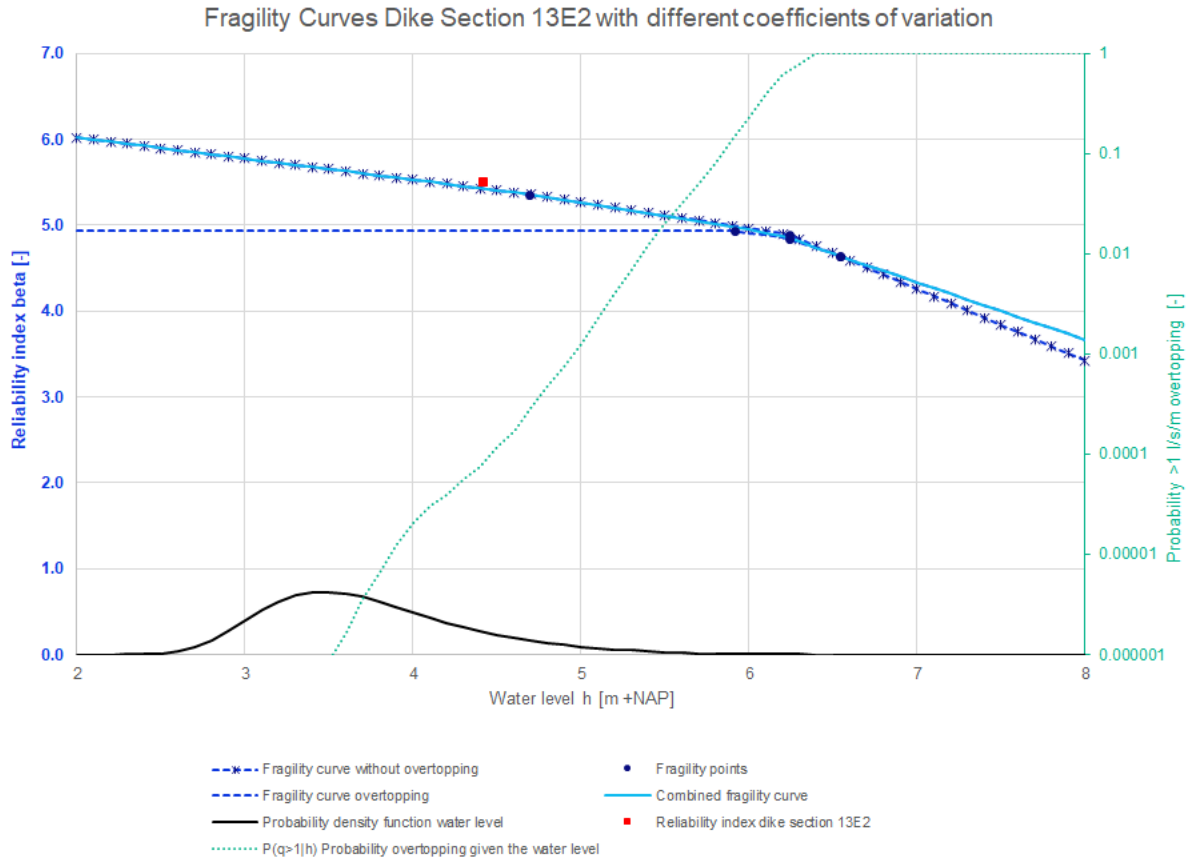

Figure 126: Fragility curves dike section 13E2 with different coefficients of variation

The estimated reliability indexes based on the semi-probabilistic calculations with different coefficients of variation are given in Table 124. Please note the estimated reliability indexes in Table 124 are the same as for the basis calculations in paragraph 4.1.1, because the design values are not changed. Furthermore, the reliability indexes of the probabilistic calculations with different coefficients of variation are shown in Table 125.

Table 124: Reliability index semi-probabilistic calculations with different coefficients of variation

Dike section	Reliability index β without overtopping [-]	Reliability index β given overtopping [-]
10C	5.68	5.41
11E	5.45	3.05
11F(11D)	5.48	3.52
13A	5.27	5.52
13E1	5.48	5.59
13E2	5.53	5.61

Table 125: Reliability index probabilistic calculations with different coefficients of variation

Dike section	Reliability index β combined fragility curve [-]	Reliability index β without overtopping [-]	Reliability index β given overtopping [-]
10C	5.12	5.12	4.32
11E	3.71	5.33	0.12
11F(11D)	4.50	7.16	1.06
13A	6.56	6.56	6.10
13E1	5.55	5.55	5.16
13E2	5.51	5.51	4.94

In Figure 127 are the results of JAV with different coefficients of variation plotted with the results of the WBI calibration study. In Figure 128 are the influence factors shown.

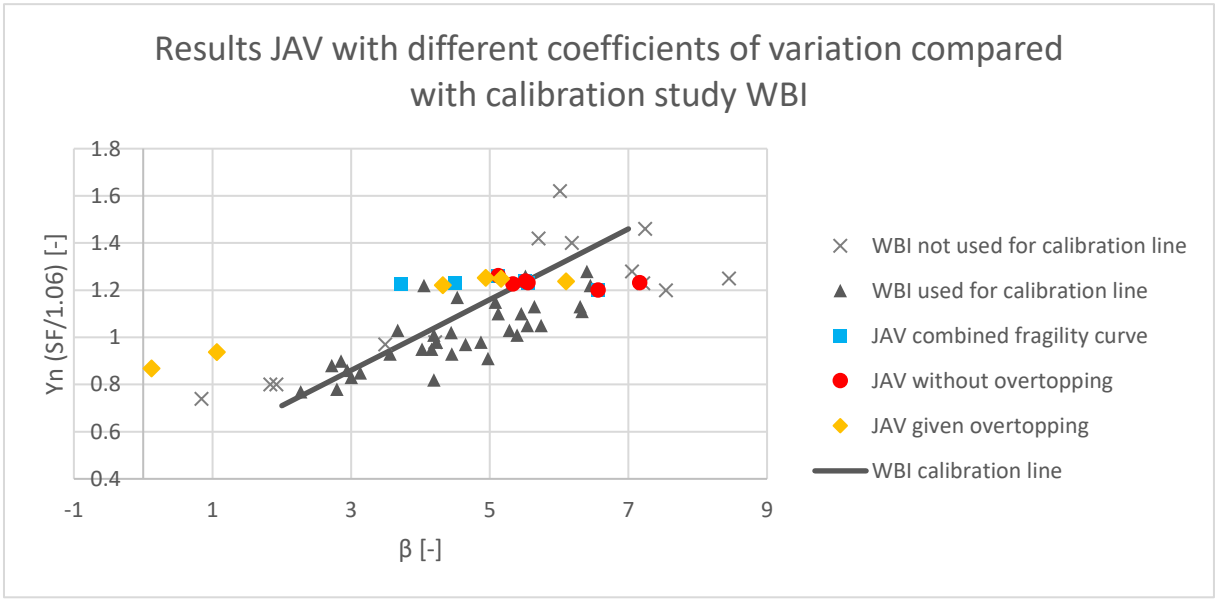

Figure 127: Results of JAV with different coefficients of variation compared with the calibration study of WBI. The vertical position of the results of JAV from the combined fragility curves (blue squares) are determined based on the semi-probabilistic results without overtopping

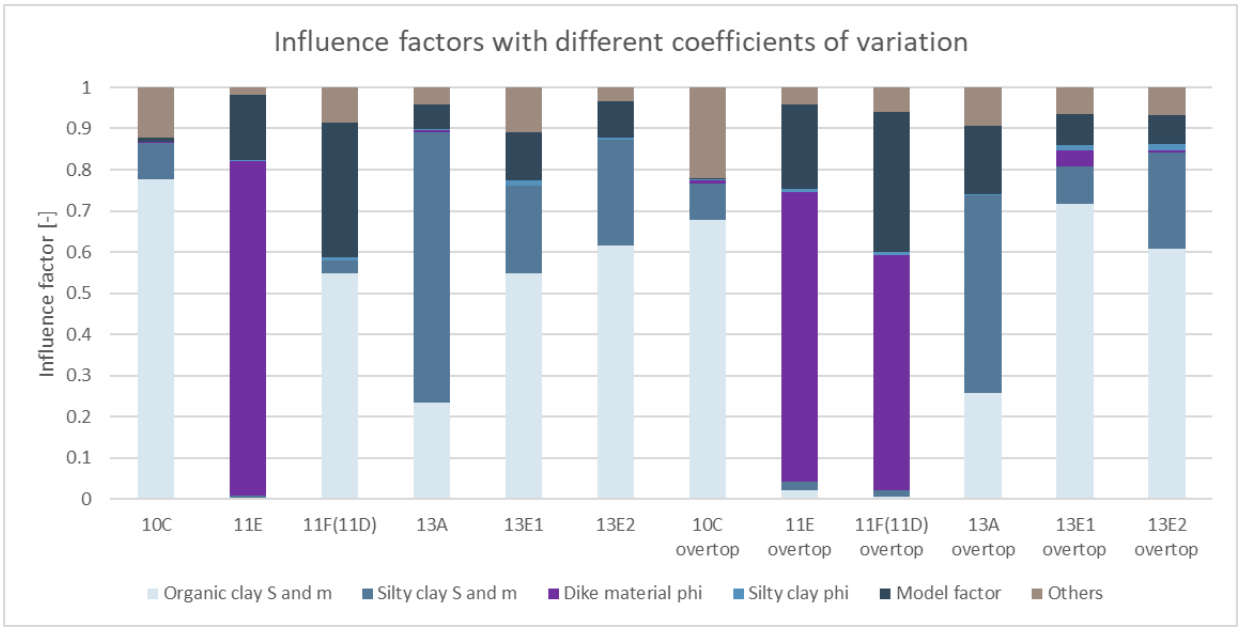

Figure 128: Influence factors with different coefficients of variation at WBN without overtopping and at the 1 l/s/m overtopping water level with overtopping